



DESIGN, SYNTHESIS AND EVALUATION OF ADVANCED POLYMERIC TAXANE FORMULATIONS

Benoit LOUAGE

Master of Science in Drug Development

Thesis submitted to obtain the degree of Doctor in Pharmaceutical Sciences

2017

Promotor:

Prof. Dr. Ir. Bruno G. De Geest

DEPARTMENT OF PHARMACEUTICS

The author and promotor give the authorization to consult and to copy parts of this thesis for personal use only. Any other use is limited by the Laws of Copyright, especially concerning the obligation to refer to the source whenever results are cited from this thesis.

Ghent, January 4th, 2017

The promotor

Prof. Dr. Ir. Bruno G. De Geest

The author

Benoit Louage

acknowledgements

This PhD could not have been realized without the consult and assistance of many people to whom I would like express my gratitude.

Faculty of Pharmaceutical Sciences 3rd floor, Ghent University

First of all, I would like to thank my promotor Prof. Bruno De Geest for providing me the opportunity to start a PhD. The broad, up-to-date and highly multidisciplinary scope of your research group allowed me to upgrade both my scientific knowledge and skills, as well as my resilience and perseverance. I could always rely on your full support and counsel throughout my thesis. I am thereby very grateful our collaboration has resulted in various quality papers.

Prof. Jean Paul Remon, Prof. Chris Vervaet and Prof. Thomas De Beer

Secretary and technical staff: Katharine Wullaert, Ilse Dupon and Christine Geldhof

Gratitude to Dr. Lutz Nuhn. The presented work could never have been accomplished without your meticulous chemical/analytical know-how and expert advice.

Thesis students

To present and former colleagues: Bart, Jana, Joke, Jurgen, Laurens, Lien, Lieselotte, Marijke, Maxim, Nane, Nils, Pieter-Jan, Ruben, Sabah, Simon, Wesley, Wouter and all the others from the third floor. Thanks for all the conversations and the laughter, for exchanging your ideas and opinions, both scientifically and beyond. You all contributed to providing an enjoyable working atmosphere defined by collaboration, helping each other out and learning from one another.

Department of Pharmaceutics, Ghent University

Prof. Serge Van Calenbergh

Dr. Martijn Risseeuw

Izet Karalic, Joren Guillaume and Fabian Hulpia

Department of Bioanalysis, Ghent University

Prof. Jan Van Bocxlaer

Sofie Vande Castele

Department of Organic Chemistry, Ghent University

Prof. Johan Winne, Prof. Richard Hoogenboom

Dr. Qilu Zhang, Dr. Lenny Voorhaar

Department of Radiation Oncology and Experimental Cancer Research, Ghent University

Prof. Olivier De Wever

Dr. Elly De Vlieghere

Vlaams Instituut voor Biotechnologie (VIB)

Prof. Bart Lambrecht

Kim Deswarte

Department of Pharmaceutics, Utrecht University

Prof. Wim Hennink

Dr. Yang Shi, Mies van Steenbergen

Departments of Bioengineering, Chemical and Petroleum Engineering, Surgery, Mechanical Engineering and Materials Science, and the McGowan Institute for Regenerative Medicine, University of Pittsburgh

Prof. Yadong Wang

Thank you Lana, my parents Martine and Claude, my brother Cédric, my sister-in-law Alien and the rest of my family. You have been extremely supportive throughout this period and always wondered what (on earth) I was doing all the time at the lab: 'something with cancer', yes, but what specifically? I am pleased to announce that I can now hand over this little piece of 'literature' in which you can read all about it :)

Finally, I would like to thank my friends from the Belgian, West-Flemish outskirts where I have my roots:

Pieter V. - aka Pito, Pieter B. - aka Boef, Dries - aka (Dr.) Dre, Liesbeth - aka Betje, Tomas - aka Duuj, Jasper – aka Del Cano and many others. We go back a long time, I appreciate you all simply for being who you are.

To all whom I still have forgotten to mention at this point, many thanks!

table of contents

abbreviations and symbols		1
aims and outline of thesis		7
PART I	general introduction	
chapter 1	chemotherapy and nanomedicine	13
chapter 2	taxanes	27
PART II	design of advanced taxane nanoformulations based on physical encapsulation	
chapter 3	poly(glycerol sebacate) nanoparticles for encapsulation of hydrophobic anti-cancer drugs	37
chapter 4	degradable ketal-based block copolymer nanoparticles for anti-cancer drug delivery: a systematic evaluation	55
PART III	design of advanced taxane-polymer conjugates	
chapter 5	well-defined polymer-paclitaxel prodrugs by a grafting-from-drug approach	99
chapter 6	micellar paclitaxel-initiated RAFT polymer conjugates with acid-sensitive behavior	131
chapter 7	active targeted docetaxel-polymer prodrug conjugates	167
PART IV	relevance, summary and general conclusions	
chapter 8	broader international context	207
chapter 9	summary and general conclusions	231
	samenvatting en algemene conclusies	237
curriculum vitae		243

abbreviations and symbols

ABC	accelerated blood clearance
ACUPA	S,S-2-(3-(5-amino-1-carboxypentyl)-ureido)-pentanedioic acid
ADC	antibody-drug conjugate
AF488	alexa fluor 488
AIBN	2, 2'-azoisobutyronitrile
APB	aspartic acid modified with 4-phenyl-butanol
API	active pharmaceutical ingredient
ARho	acryloxyethyl thiocarbamoyl rhodamine B
Asp	aspartate
ATRP	atom transfer radical polymerization
BBB	blood brain barrier
BSA	bovine serum albumin
Bz	benzyl
C	carbon
CAC	critical aggregation concentration
CRADA	cooperative research and development agreement
cRGD	cyclic arginine-glycine-aspartate peptide
CSA	camphor-10-sulfonic acid
CTA	chain transfer agent
Cy5-N ₃	cyanine5-azide
<i>D</i>	dispersity
Da	dalton
DAD	diode array detector
DAPI	4',6-diamidino-2-phenylindole
DAR	drug-antibody-ratio

DCM	dichloromethane
DEGA	di(ethylene glycol) acetal
DEGVE	di(ethylene glycol) vinyl ether
DHP	3,4-dihydro-2H-pyran-2-methanol
DIC (1)	differential interference contrast (1)
DIC (2)	<i>N,N'</i> -diisopropylcarbodiimide (2)
DLS	dynamic light scattering
DMA	<i>N,N'</i> -dimethylacrylamide
DMAc	<i>N,N'</i> -dimethylacetamide
DMAP	4-(dimethylamino)pyridine
DMDMA	2,2-dimethyl-1,3-dioxolane-4-yl)methyl acrylate
DMEM	Dulbecco's Modified Eagle Medium
DMF	<i>N,N'</i> -dimethylformamide
DMSO	dimethyl sulfoxide
DNA	deoxyribonucleic acid
DOX	doxorubicin
DP	degree of polymerization
DPA	2-(diisopropylamino)ethyl methacrylate
DTX	docetaxel
EE	encapsulation efficiency
EGFR	epidermal growth factor receptor
EPR	enhanced permeability and retention effect
ESI	electron spray ionization
EtOH	ethanol
FA	folic acid
FACS	flow cytometry
FBS	fetal bovine serum
FDA	Food and Drug Administration
FR	folate receptor
GC	gas chromatography

GEM	genetically engineered mouse
Glu	glutamate
gp60	glycoprotein 60
H ₂ O	water
HA	hyaluronic acid
HEA	hydroxyethyl acrylate
HMW	high molecular weight
HPMA	<i>N</i> -(2-hydroxypropyl)methacrylamide
HSA	human serum albumin
HTS	high-throughput screening
IC ₅₀	half maximal inhibitory concentration
IFP	interstitial fluid pressure
LA	lactic acid
Lac	lactate
LC (1)	liquid chromatography (1)
LC (2)	loading capacity (2)
LCST	lower critical solution temperature
LMW	low molecular weight
LRP1	low-density lipoprotein receptor-related protein 1
mAb	monoclonal antibody
MDR	multiple drug resistance
MeOH	methanol
MHA	6-maleimidohexanoic acid
MIP	maximum intensity projection
MMAE	monomethyl auristatin E
MMP	matrix metalloproteinase
M _n	number average molecular weight
MPC	2-(methacryloyloxy)ethyl phosphorylcholine
MPS	mononuclear phagocytic system
MRM	multiple reaction monitoring

MS	mass spectrometry
MTD	maximum tolerated dose
mTEGA	methoxy tri(ethylene glycol) acrylate
MTT	thiazolyl blue tetrazolium bromide
MW	molecular weight
MWCO	molecular weight cut off
N ₂	nitrogen gas
NaCl	sodium chloride
NCI	National Cancer Institute
NIPAM	<i>N</i> -isopropyl acrylamide
NMP	nitroxide-mediated polymerization
NMR	nuclear magnetic resonance
NSCLC	non-small cell lung cancer
OEG(M)A	oligo(ethylene glycol) (meth)acrylate
OH	hydroxyl
P ₂ O ₅	phosphorus pentoxide
PABTC	2-(butylthiocarbonothioylthio)propanoic acid
PBS	phosphate buffered saline
Pd	palladium
PDI	polydispersity
PDT	photodynamic therapy
PDX	patient-derived xenograft
PEG	poly(ethylene glycol)
PFP	pentafluorophenol
PFS	progression free survival
P-gp	P-glycoprotein
PGS	poly(glycerol sebacate)
PLA	poly(lactic acid)
PLGA	poly(lactic- <i>co</i> -glycolic acid)
PMMA	poly(methyl methacrylate)

POx	poly(2-oxazoline)
psi	pound-force per square inch
PSMA	prostate specific membrane antigen
PTX	paclitaxel
PVA	poly(vinyl alcohol)
QoL	quality of life
R18	octadecyl rhodamine B chloride
RAFT	reversible addition-fragmentation chain transfer
RES	reticulo-endothelial system
RGD	arginine-glycine-aspartate peptide
Rho	rhodamine
RID	refractive index detector
ROP	ring-opening polymerization
RP	reversed phase
RPMI	Roswell Park Memorial Institute
SEC	size exclusion chromatography
SIP	small immune protein
SMDC	small molecule-drug conjugate
SPARC	secreted protein acidic and rich in cysteine
SPPS	solid phase peptide synthesis
TCEP	tris(2-carboxyethyl)phosphine
TEA	triethylamine
TFA	trifluoroacetic acid
THP	tetrahydropyran
TIC	total ion chromatogram
TLC	thin layer chromatography
TMP	trimethyl phosphite
TOF	time-of-flight
UPLC	ultra performance liquid chromatography
UV-VIS	ultraviolet-visible spectroscopy

VEGF(R)	vascular endothelial growth factor (receptor)
XRD	X-ray diffraction
Z-Ave	Z-Average hydrodynamic diameter

aims and outline of thesis

aims of thesis

Today toxic side-reactions of taxane chemotherapy still severely affect patient quality of life (QoL). Abraxane and Genexol-PM have been able to significantly lower or even exclude side-effects caused by the toxic surfactants such as Cremophor EL and polysorbate 80 used in Taxol and Taxotere, respectively. However, the manifested intrinsic systemic toxicity of taxanes (e.g. neutropenia and neuropathy) remains a major issue and shows that further exploration of alternative formulations is required for pursuing more efficient and safer taxane administration. Polymer-based drug formulations are attractive systems due to the chemical versatility and low-cost of polymeric carrier material compared to biotechnological carriers such as solubilizing proteins (e.g. albumin) and monoclonal antibodies (mAbs). As physical entrapment and chemical conjugation have already shown great promise in the development of advanced polymeric drug formulations, the overall aim of this thesis was to design, synthesize and evaluate new taxane platforms based on these two formulation strategies.

With respect to physical encapsulation, two types of polymeric carriers will be evaluated. As a first system we aimed to explore the potential of poly(glycerol sebacate) (PGS). This polymer has established biodegradable and biocompatible properties which can be an important asset for future regulatory approval. As this polymer is insoluble in water, the aim is to devise a formulation strategy based on solvent displacement. The second system, a block copolymer micelle system with stimuli-responsive behavior, was aimed for physical drug encapsulation. The goal was for the latter polymer to degrade and disassemble into fully water-soluble derivatives under acidic conditions as encountered in the tumor-microenvironment, endosomes and lysosomes. In this way, entrapped drug could be released in a more selective fashion and the corresponding polymer degradation products cleared more swiftly from the body (i.e. by renal excretion). The strategy for achieving this objective involved introduction of

acid-sensitive ketal-moieties pending on the amphiphilic block copolymer backbone. Subsequently, an extensive *in vitro* analysis of both platforms should allow to assess whether or not the suggested systems have potential as hydrophobic drug delivery vehicles.

Literature reports that, in the bloodstream, physically encapsulated drugs can diffuse out of the carrier vehicle. This could still induce systemic toxicity, irrespective of bioresponsive behavior and/or low critical aggregation concentration (CAC) of the carrier system. Though this cannot be generalized and should be evaluated for each system separately, this dissertation also wanted to provide an alternative taxane formulation platform which could allow for less susceptibility to systemic burst release. Chemical conjugation of drug to a polymer is a fitting rationale in this regard. Taxane-polymer conjugates currently in clinical trial are typically synthesized through post-modification of high molecular weight polymer with taxanes. However, the relatively high dispersity of these polymers (i.e. poly(glutamic acid), polyHPMA) does not allow for obtaining well-defined drug-polymer conjugates and might also put challenges in acquiring high drug loadings with minimal batch-to-batch variation. The latter however can be of crucial importance when aiming for regulatory approval and might be resolved when a polymer chain is grafted onto taxanes. The goal was to investigate whether this reversed approach is feasible with advanced polymerization techniques, to examine the chemical versatility of this approach and to evaluate the overall drug delivery performance.

outline of thesis

PART I – Chapter 1 provides a concise overview of the current issues of conventional chemotherapy and describes the opportunities for nanomedicine strategies to improve the efficacy of anti-cancer drugs. A description of the different assets of nanomedicines for altering pharmacokinetics and biodistribution by passive/active targeting and bioresponsive drug release is provided.

Chapter 2 describes the history and early development of taxanes (i.e. paclitaxel (Taxol) and docetaxel (Taxotere)). Both the discovery and the historic evolution in manufacturing strategies of taxanes are covered. Additionally, the biological mechanism of action of taxanes is described. Next, the physicochemical background of the commercial formulations Taxol and Taxotere is described, along with their clinical translation and related toxicity issues.

PART II – Chapter 3 reports on the formulation of polymeric nanoparticles based on PGS. A straightforward solvent displacement method was developed and key physicochemical properties in aqueous medium were evaluated including nanoparticle size, dispersity, colloidal stability and CAC. Next, nanoprecipitation of an organic phase containing both PGS and hydrophobic dye/paclitaxel (PTX) was investigated to obtain loaded nanoparticles by solvent displacement. Fluorescent dye- and PTX-loaded PGS nanoparticles were subsequently used for *in vitro* uptake and cytotoxicity studies, respectively.

Chapter 4 describes the synthesis of acid-degradable block copolymers based on hydroxyethyl acrylate (HEA) and ketal-based (2,2-dimethyl-1,3-dioxolane-4-yl)methyl acrylate (DMDMA) by reversible addition-fragmentation chain transfer (RAFT) polymerization. Using a macroCTA (macro chain transfer agent) approach, the main focus of this study was to systematically examine the influence of hydrophobic block design on self-assembly behavior (i.e. CAC, colloidal stability and degradation), drug loading and *in vitro* biological performance by varying the DMDMA content in the hydrophobic block. Solvent displacement was applied to physically encapsulate a hydrophobic fluorescent dye and PTX. In this way, we systematically evaluated the potential of these block copolymers for their use as nanocarrier for hydrophobic anti-cancer drugs.

PART III – Chapter 5 investigates a novel design approach for paclitaxel-polymer prodrug conjugates by conjugation of PTX to a CTA and subsequent RAFT polymerization of hydrophilic *N,N*-dimethylacrylamide (DMA). As PTX and pDMA can serve as hydrophobic and hydrophilic segment respectively, amphiphilic properties (self-assembly, CAC and aqueous stability) were examined. Furthermore, the possibility for post-polymerization modification of the opposite polymer chain end was explored with a fluorescent dye. Finally, uptake of the PTX-polymer prodrug conjugate and effective delivery of PTX to cancer cells was evaluated *in vitro*.

Chapter 6 reports on “second-generation” PTX-polymer conjugates, by implementing two types of acid-sensitive acetal-linkers in the synthesis strategy reported in Chapter 5. Both the first- and second-generation PTX-polymer conjugates were compared in terms of polymer composition and characteristics, self-assembly behavior, *in vitro* drug release and cytotoxicity.

Chapter 7 describes the synthesis of a polymeric prodrug conjugate of docetaxel (DTX), inspired by the synthetic approach described for PTX in Chapter 5. Additionally, a high-affinity small molecule ligand for prostate-specific membrane antigen (PSMA) was synthesized and modified with a maleimide moiety to be further used for post-modification of the DTX-polymer prodrug conjugate. *In vitro* cellular uptake of the PSMA-targeted DTX-polymer prodrug conjugate was evaluated by flow cytometry (FACS) using a human, PSMA-positive prostate cancer cell line and compared to a non-targeted DTX-polymer prodrug control conjugate.

PART IV - Chapter 8 positions this doctoral dissertation within a broader international context by providing an up-to-date overview of the taxane formulations which are either approved or currently residing in clinical trial. First, the two approved PTX formulations alternative to Taxol (i.e. Abraxane and Genexol-PM) are described in detail in terms of synthesis, formulation and clinical evaluation. Next, a series of pioneering advanced taxane formulations are highlighted which are currently being evaluated in clinical trials. Additionally, two other platforms are described which are considered somewhat outside the nanomedicine field (i.e. antibody-drug conjugates (ADCs) and small molecule-drug conjugates (SMDCs)), as the latter have also been explored for improving the delivery of taxanes and other chemotherapeutic drugs. Finally, a critical view on the current limited clinical availability of nanomedicines including taxane formulations is described, along with important considerations and suggestions for future improvement of clinical translation of not only advanced taxane formulations, but anti-cancer medicines in general.

Chapter 9 provides a summary of the aforementioned topics, along with general conclusions that can be drawn from the obtained results of this doctoral dissertation. In addition, suggestions are brought forward for future exploration, evaluation and optimization of the developed systems, in particular for the grafting-from-drug approach.

PART I

GENERAL INTRODUCTION

chapter 1

chemotherapy and nanomedicine

Benoit Louage,^a Olivier De Wever,^b Wim E. Hennink,^c Bruno G De Geest^a

^a Laboratory of Pharmaceutical Technology, Department of Pharmaceutics,
Ghent University, Ottergemsesteenweg 460, 9000 Ghent, Belgium

^b Department of Radiation Oncology and Experimental Cancer Research,
Ghent University and Ghent University Hospital, De Pintelaan 185, 9000 Ghent, Belgium

^c Department of Pharmaceutics, Utrecht Institute for Pharmaceutical Sciences,
Utrecht University, Universiteitsweg 99, 3584CG Utrecht, The Netherlands

Journal of Controlled Release 2017

1 chemotherapy

Cancer is a major cause of death worldwide, only exceeded by cardiovascular diseases.^[1,2] Surgery and radiotherapy are effective and valuable treatment modalities for solid, well-localized tumors, but less suitable for treatment of metastatic cancer.^[1] For the latter, small molecule chemotherapy is the current choice of treatment, as systemic circulation upon intravenous administration allows for drugs to distribute throughout the body and thus the likeliness of reaching metastatic sites is enhanced.^[3,4]

Several small molecule anti-neoplastic compounds targeting highly proliferative cells have already been identified half a century ago. Today however, the use of these compounds is often hampered by a low therapeutic index.^[5] **Table 1** summarizes the most common types of antineoplastic agents used in clinical setting. Although chemotherapeutic drugs exhibit substantial toxicity towards cancer cells as the latter exhibit high proliferation rates, healthy tissues featured by fast cell proliferation (e.g. hair follicles, bone marrow, gastrointestinal tract) are equally affected, thereby causing uncomfortable and sometimes life threatening side-effects.^[6] These side-effects often have to be addressed by additional (pre)medication.^[7] Due to the aspecific distribution of chemotherapeutic drugs throughout the body, relatively high doses need to be administered (e.g. 175 mg/m² Taxol in combination with carboplatin for treatment of advanced non-small cell lung cancer (NSCLC)) in order to achieve sufficient drug levels at the tumor site.^[8] However, increasing dose is limited to a certain extent, as high systemic exposure further increases toxicity and severely reduces the quality of life (QoL) of patients.^[9]

Another issue arises from a pharmaceutical point of view. It is estimated that approximately one third of potent small molecule anti-cancer drugs are rather hydrophobic and thus have limited solubility in aqueous medium.^[10] This in particular holds true for the taxanes paclitaxel (PTX) and docetaxel (DTX) (**Figure 1**) and hence poses major challenges towards pharmaceutical formulation of these drugs.^[11,12] This issue prompted the pharmaceutical industry to identify effective solubilizing excipients and concurrently triggered intensive research towards more advanced anti-cancer formulations capable of delivering drugs in a more effective, safer and patient-friendly fashion.^[13,14]

Table 1. Classification of commonly used antineoplastic agents.^[15–18]

drug class	mechanism of action	examples	indications
alkylating agents	impair cell function by forming covalent bonds on important molecules (e.g. proteins, DNA, RNA)	cisplatin, carboplatin, chlorambucil, cyclophosphamide	ovarian, breast, testicular and bladder cancer, (non)-hodgkin lymphoma, leukemia
anti-metabolites	structural analogues of naturally occurring metabolites involved in DNA and RNA synthesis	5-fluorouracil, methotrexate, gemcitabine, mercaptopurine	gastric, colorectal, head, neck, lung, breast, ovarian and pancreatic cancer, osteosarcoma, leukemia, non-hodgkin lymphoma
antitumor antibiotics	intercalate DNA at specific sequences, creating free radicals which cause strand breakage	bleomycin, anthracyclines (doxorubicin, epirubicin)	breast, gastric, testicular, ovarian and thyroid cancer, (non)-hodgkin lymphoma, leukemia, neuroblastoma, squamous cell carcinoma
topoisomerase inhibitors	interfere with enzymes responsible for uncoiling of DNA during replication	irinotecan, etoposide, camptothecin, SN-38	colorectal and testicular cancer, small cell lung cancer
tubulin-binding drugs	taxanes block microtubule disassembly vinca alkaloids prevent microtubule formation	taxanes (PTX, DTX) vinca alkaloids (vincristine, vinorelbine)	breast, prostate, ovarian, and pancreatic cancer, NSCLC, leukemia, adenocarcinoma, AIDS-related Kaposi sarcoma
mechanistic target of rapamycin (mTOR) inhibitors	interfere with mTOR, a protein kinase involved in cellular metabolism, growth and proliferation	everolimus, temsirolimus	breast, pancreatic and lung cancer, renal cell carcinoma

Abbreviations: DNA, deoxyribonucleic acid; RNA, ribonucleic acid; SN-38, 7-ethyl-10-hydroxycamptothecin; PTX, paclitaxel; DTX, docetaxel; AIDS, acquired immune deficiency syndrome.

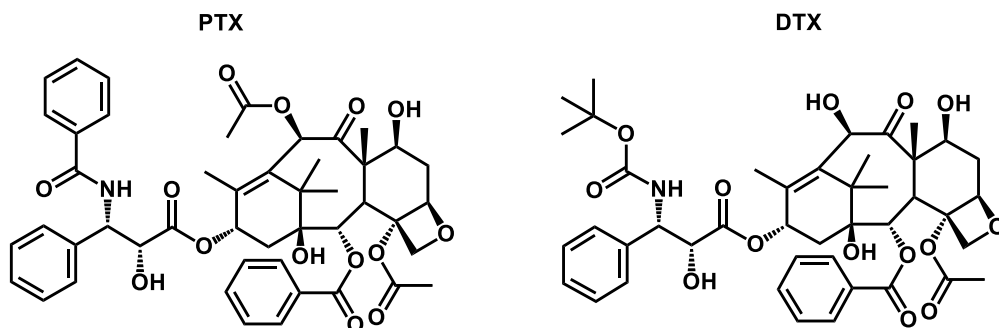


Figure 1. Chemical structures of PTX and DTX.

2 nanomedicine

The knowledge of cancer biology and etiology has expanded substantially over the past few decades.^[19,20] Not only has this led to novel classes of small molecule anti-cancer therapeutics (e.g. molecularly targeted drugs), this improved understanding also provided a means to optimize the efficacy of conventional anti-cancer drugs. In view of increasing the therapeutic index of conventional, FDA-approved chemotherapeutics, great efforts have been put in the field of nanomedicine.^[21–23] Initially investigated by merely liposomal formulations (e.g. Doxil, an FDA-approved liposomal formulation of doxorubicin),^[24] similar endeavors have now also been developed using various other types of versatile, biocompatible polymeric nanomaterials such as dendrimers, polyerosomes, block copolymer micelles, polymer-drug conjugates and antibody-drug conjugates (**Figure 2**).^[25–31]

2.1 assets

Several arguments are in favor of nanomedicines for enhancing the therapeutic efficacy of extremely hydrophobic chemotherapeutics such as taxanes. First of all, physical encapsulation or chemical conjugation of taxanes into amphiphilic nanostructures can significantly enhance drug solubility and the carrier vehicle can serve as a protective shield against chemical and biochemical degradation.^[32,33] Second, hydrophobic compounds, solubilized by conventional surfactants (e.g. PTX is solubilized with Cremophor EL in Taxol and DTX is solubilized with Tween 80 in Taxotere) are susceptible to premature burst release into the bloodstream by supramolecular dissociation of the surfactant and/or by fast passive drug diffusion and subsequent interaction with plasma proteins.^[34] Chemical conjugation or strong non-covalent interaction between drug and polymeric carrier can be crucial techniques for circumventing systemic drug release and hence side-effects.^[35–37] Third, fast renal clearance

of small molecule anti-cancer drugs can be avoided as drug-associated nanocarriers with size ≥ 5 nm do not easily pass the small fenestrae in renal vasculature.^[38-40] The latter can drastically prolong drug half-life. Numerous *in vivo* studies indeed report on altered pharmacokinetic profiling of physically encapsulated and chemically conjugated nanomedicine drugs, compared to the corresponding free drugs.^[41-43] Fourth, it is known that nanocarriers passively distribute throughout the body in a heterogeneous manner. Nanomaterials tend to accumulate in tissues with highly fenestrated vasculature.^[44-47] This phenomenon can be exploited to provide a more selective delivery of drugs into tumors whether or not in combination with additional active targeting strategies. Passive and active targeting will be discussed into more detail in section 2.2. Fifth, polymeric carriers can be chemically designed to trigger a response towards specific internal or external stimuli (e.g. change in pH, enzymes, redox, ultrasound, light). These bio- or stimuli-responsive properties can further enhance the selectivity and control in delivering anti-cancer agents and hence increase their therapeutic index.^[48-50] Finally, nanomedicines can significantly alter the route of cellular drug uptake and hence limit drug resistance. Hydrophobic small molecule drugs typically enter (tumor) cells by passive diffusion. Nanoparticles on the other hand are predominantly taken up by endocytosis, a mechanism which can be stimulated even more by active targeting strategies (section 2.2.2).^[51,52] Altering the route of uptake can inherently change intracellular drug localization and concentration. While gradual uptake by passive diffusion only leads to modest cellular drug concentrations, endocytosis of nanocarriers allows for delivering a high amount of drug cargo within a short period of time.^[53] The resulting high intracellular drug concentrations can hence saturate efflux, mediated by cytosolic multiple drug resistance (MDR) proteins such as to P-glycoproteins (P-gp).^[54] This can be of great importance for improving the efficacy of chemotherapeutic agents for which drug resistance has been reported.

2.2 altering pharmacokinetics and biodistribution

2.2.1 passive targeting

On a cellular level, cancer can be characterized by several aberrations in normal processes (e.g. proliferation, metabolism, ...).^[19,20] These malfunctions translate into tumors with physiological properties significantly different from healthy tissue. Nanomedicines enable the exploitation of these anomalies for tumor targeting by the so called enhanced permeability and retention effect (EPR).^[46,55,56] Blood vessels in solid tumors are often highly fenestrated due to aberrant angiogenesis. This results in endothelial gaps between 100 – 780 nm in size through which nanocarriers can easily extravasate into the interstitial fluid.^[4,57,58] The lymphatic drainage of

the latter is often impaired in tumors. This allows nanocarriers to reside longer in proximity of malignant tissues (Figure 3). The FDA-approved formulation Doxil and the majority of the nanomedicines currently in clinical trials (e.g. Table 2 for taxane-based nanomedicines) rely on this passive targeting, mediated by the EPR effect.^[59]

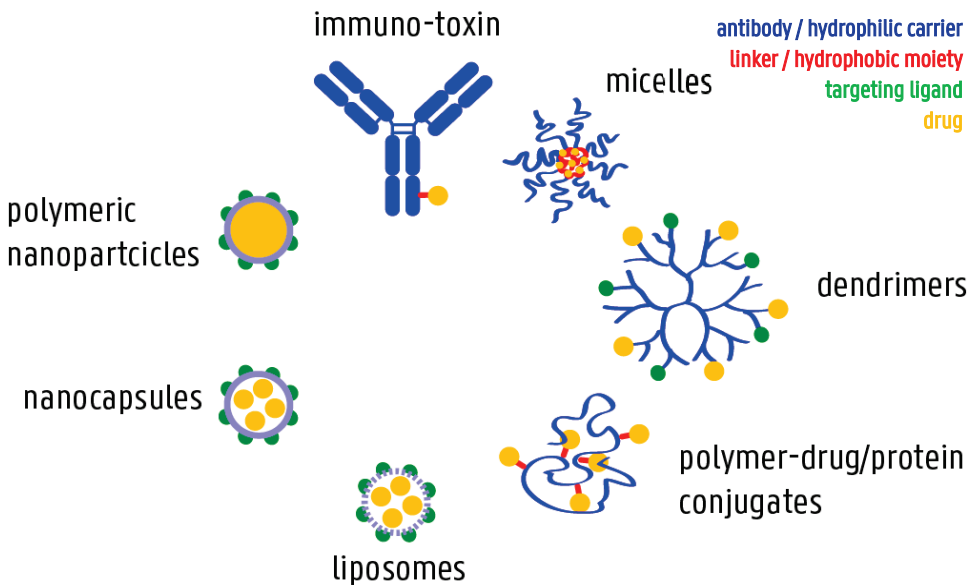


Figure 2. Overview of prominent nanomedicines.

In order to achieve significant passive targeting, it is crucial for nanomaterials to possess long blood circulation half-lives.^[60] This sets up challenges as the latter is a very complex biological matrix, containing several substances (e.g. enzymes, antibodies) which can induce systemic drug clearance. A key player in causing these phenomena is the reticulo-endothelial system (RES), also called the mononuclear phagocytic system (MPS).^[61] Certain plasma proteins, called opsonins, interact with non-endogenous materials. This renders them immunogenic and allows recognition by macrophages in liver (Kupffer cells), lymph nodes and spleen. This accelerated clearance can be avoided by decorating the surface of the nanocarriers with a hydrophilic corona (e.g. poly(ethylene glycol) (PEG)).^[62] It is also known that larger materials (> 200 nm) are more likely to be affected by MPS, irrespective of surface chemistry.^[63,64] The optimal size to benefit from the EPR effect should be evaluated for each system, as it involves finding the right balance between prolonging circulation time (increased size) and tumor penetrating capacity (decreased size).^[65,66]

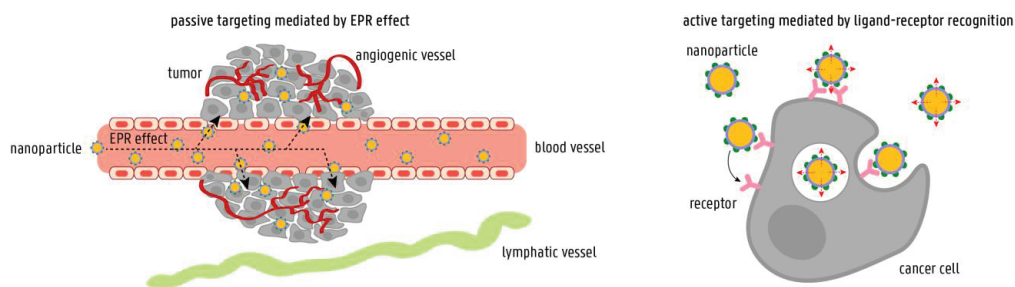


Figure 3. Illustration of passive (EPR-mediated) and active targeting.

2.2.2 active targeting

Active targeting is a promising tool to further enhance the delivery of nanomedicines and hence broaden the therapeutic window. As mentioned before, MDR can be overcome as active targeted anti-cancer nanomedicines are known to be taken up by receptor-mediated endocytosis. The resulting high intracellular drug concentrations are less susceptible to P-gp-mediated cytosolic efflux.^[67] Additionally, in many cases active targeting results in internalization and subcellular trafficking of drug loaded nanoparticles close to the target site. The latter can be exploited for drugs which cannot spontaneously pass cellular membranes (e.g. nucleic acid-based drugs).^[68]

Active targeting involves decoration of the carrier vehicle with high-affinity ligands which can be recognized by receptors or antigens, specifically overexpressed in the targeted tissues (**Figure 3**).^[69] A wide range of receptors have been evaluated, either for direct targeting of tumor cells (e.g. CD44 receptor,^[70–76] folate receptors (FRs),^[77–79] transferrin receptors,^[80,81] prostate specific membrane antigen (PSMA),^[82,83] epidermal growth factor receptors (EGFRs)^[84,85] and/or targeting of tumor-associated vasculature (e.g. α V β 3 integrins,^[86] PSMA,^[87] glycoprotein 60 (gp60)).^[88] Several types of targeting ligands have been used including proteins (e.g. transferrin and albumin for targeting transferrin receptors and gp60, respectively),^[88,89] monoclonal antibodies and their fragments (e.g. for EGFRs targeting),^[69,90] polysaccharides (e.g. hyaluronic acid (HA) for CD44 receptor targeting),^[91–94] peptides (e.g. cyclic arginine-glycine-aspartate peptide (cRGD) for α V β 3 integrin targeting),^[95–98] aptamers (e.g. A10 for PSMA targeting)^[99,100] and small molecules (e.g. folic acid (FA) for FRs targeting).^[77,101–103]

However, active targeting is not without risk. Additional functionalization can alter the physicochemical properties of the carrier vehicle.^[104] This can in turn significantly influence the *in vivo* behavior. As these ligands are not always hydrophilic (e.g. FA), high densities onto the surface of the vehicle can result in colloidal instability and aggregation. Furthermore, stealth properties can be jeopardized when the hydrophilic domains of the carrier are covered up to a high extent by more hydrophobic ligands which can lead to higher RES-mediated clearance.^[105,106]

Indeed, preclinical evaluation of PSMA-targeted, DTX-loaded nanoparticles, developed by Langer and co-workers, demonstrated that an average 200 PSMA-ligands per nanoparticle resulted in the best *in vivo* outcome, even though up to 1000 molecules could be decorated per nanoparticle.^[82] Finding this optimal degree of functionalization to obtain active targeting and to maintain *in vivo* stability has proven to be challenging and partly explains the lacking clinical translation of active targeted nanomedicines (Chapter 8).^[69,107] Recent literature also reports that active targeting can be both time- and dose-dependent. Effective active targeting has been demonstrated shortly after intravenous injection, whilst over longer periods of time, passive targeting can predominate.^[108] Additionally, active targeting has shown to be more efficient at lower doses. When nanomedicines are administered at high doses, passive targeting can prevail.^[109] These findings should be taken into account for future evaluation of active targeted nanomedicines.

2.2.3 stimuli-responsive release

Systemic drug exposure and side-effects can be further restricted by triggering a release under specific conditions. These triggers can be either external or internal.^[110] Examples of external stimuli include ultraviolet or near-infrared light which are often used within the field of photodynamic therapy (PDT).^[111] Other examples are ultrasound and magnetic forces which will not be further discussed. This dissertation focuses on the use of internal triggers. For instance, various nanocarrier systems reported in literature rely on change in pH for inducing drug release.^[112–117] Due to the high metabolic rate of tumors, the tumor microenvironment is slightly more acidic (i.e. pH 6.5) than the physiological level (i.e. pH 7.4). Additionally, endo- and lysosomal vesicles are characterized by higher acidity (i.e. pH 5.5 - 5).^[118,119] Furthermore, the expression of certain enzymes is often upregulated in cancerous tissue (e.g. matrix metalloproteinases (MMPs), cathepsin B).^[120,121] Also, certain tumors which are low in oxygen and nutrient levels are often rich in reductive agents.^[122] All these features can be exploited for bio-responsive release of anti-cancer drugs by designing acid-sensitive, enzyme-sensitive and redox-sensitive carrier systems, respectively.

A variety of acid-sensitive (e.g. ketals, acetals, hydrazones, oximes, orthoesters), enzyme-sensitive (e.g. peptide sequences, esters), base (esters, carbonate esters) and redox-sensitive (e.g. disulfides) functionalities have been exploited to design responsive nanomedicines (**Figure 4**).^[123–132] With regard to stimuli-responsive polymeric micelles, these functionalities can be introduced inside the hydrophobic core either by using functionalized monomers or by post-modification.^[133–135] The stimulus will trigger degradation of the hydrophobic core into

hydrophilic moieties, resulting in complete disassembly and release of encapsulated drug.^[136] Additionally, for cross-linked systems (e.g. cross-linked block copolymer micelles, nanogels) stimuli-responsive cross-linkers can be used, allowing full degradation of the nanovehicle into hydrophilic degradation products which can be cleared from the body by renal filtration.^[137,138] For polymer-drug conjugates, the goal is to covalently bind drug and polymer through a responsive linker, allowing for tumor-specific, oxidative/reductive, enzyme- or pH-triggered cleavage and avoiding systemic premature burst release.^[139] Importantly, as several stimuli are not highly tumor-specific (e.g. low pH in endo- and lysosomes, enzymes such as esterases, ...), combinations with active targeting should be considered to maximize the therapeutic benefit.^[140]

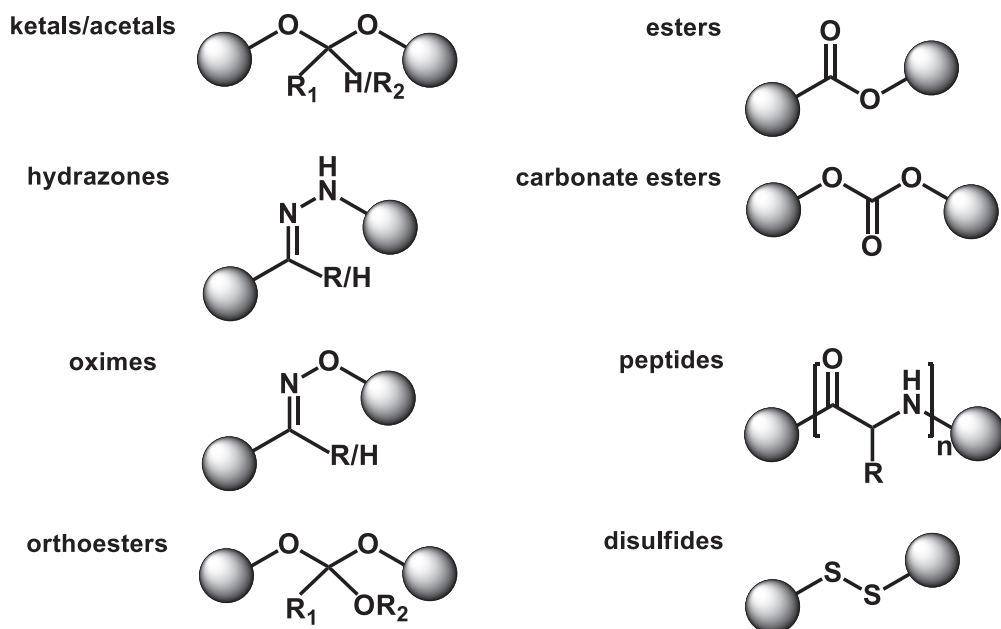


Figure 4. Overview of bio-responsive linker chemistries.

3 references

- [1] E. Perez-Herrero, A. Fernandez-Medarde, *Eur. J. Pharm. Biopharm.* **2015**, *93*, 52–79.
- [2] R. L. Siegel, K. D. Miller, A. Jemal, *CA Cancer J. Clin.* **2016**, *66*, 7–30.
- [3] L. A. Torre, R. L. Siegel, E. M. Ward, A. Jemal, *Cancer Epidemiol. Biomarkers Prev.* **2016**, *25*, 16–27.
- [4] A. Wicki, D. Witzigmann, V. Balasubramanian, J. Huwyler, *J. Control. Release* **2015**, *200*, 138–157.
- [5] R. Panchagnula, *Int. J. Pharm.* **1998**, *172*, 1–15.
- [6] D. Sampath, C. M. Discafani, F. Loganzo, C. Beyer, H. Liu, X. Z. Tan, S. Musto, T. Annable, P. Gallagher, C. Rios, et al., *Mol. Cancer Ther.* **2003**, *2*, 873–884.
- [7] S. Koudelka, J. Turanek, *J. Control. Release* **2012**, *163*, 322–334.
- [8] D. H. Johnson, D. M. Paul, K. R. Hande, Y. Shyr, C. Blanke, B. Murphy, M. Lewis, R. F. DeVore, *J. Clin. Oncol.* **1996**, *14*, 2054–2060.
- [9] S. Patricia Egusquiguire, M. Igartua, R. Maria Hernandez, J. Luis Pedraz, *Clin. Transl. Oncol.* **2012**, *14*, 83–93.
- [10] P. Lee, R. Zhang, V. Li, X. Liu, R. W. Y. Sun, C.-M. Che, K. K. Y. Wong, *Int. J. Nanomedicine* **2012**.
- [11] H. B. Chen, C. Khemtong, X. L. Yang, X. L. Chang, J. M. Gao, *Drug Discov. Today* **2011**, *16*, 354–360.
- [12] P. L. Soo, M. Dunne, J. Liu, C. Allen, in *Nanotechnol. Drug Deliv.*, Springer New York, New York, NY, **2009**, pp. 349–383.
- [13] F. Greco, M. J. Vicent, *Adv. Drug Deliv. Rev.* **2009**, *61*, 1203–1213.
- [14] E. Miele, G. P. Spinelli, F. Tomao, S. Tomao, *Int. J. Nanomedicine* **2009**, *4*, 99–105.
- [15] R. Jones, *Medicine (Baltimore)* **2016**, *44*, 25–29.
- [16] M. J. Lind, *Medicine (Baltimore)* **2016**, *44*, 20–24.
- [17] “A to Z List of Cancer Drugs,” can be found under <https://www.cancer.gov/about-cancer/treatment/drugs>, **2016**.
- [18] “Targeted Treatments for a Type of Pancreatic Cancer: Rapamycin and Other mTOR Inhibitors,” can be found under <https://www.cancer.gov/research/progress/discovery/mTOR-inhibitors>, **2014**.
- [19] D. Hanahan, R. A. Weinberg, *Cell* **2011**, *144*, 646–674.
- [20] N. N. Pavlova, C. B. Thompson, *Cell Metab.* **2016**, *23*, 27–47.
- [21] S. Svenson, *Curr. Opin. Solid State Mater. Sci.* **2012**, *16*, 287–294.
- [22] L. Y. Rizzo, B. Theek, G. Storm, F. Kiessling, T. Lammers, *Curr. Opin. Biotechnol.* **2013**, *24*, 1159–1166.
- [23] B. Y. S. Kim, J. T. Rutka, W. C. W. Chan, *N. Engl. J. Med.* **2010**, *363*, 2434–2443.
- [24] Y. (Chezy) Barenholz, *J. Control. Release* **2012**, *160*, 117–134.
- [25] D. Peer, J. M. Karp, S. Hong, O. C. Farokhzad, R. Margalit, R. Langer, *Nat. Nanotechnol.* **2007**, *2*, 751–760.
- [26] N. Kamaly, Z. Y. Xiao, P. M. Valencia, A. F. Radovic-Moreno, O. C. Farokhzad, *Chem. Soc. Rev.* **2012**, *41*, 2971–3010.
- [27] C. Oerlemans, W. Bult, M. Bos, G. Storm, J. F. W. Nijsen, W. E. Hennink, *Pharm. Res.* **2010**, *27*, 2569–2589.
- [28] H. Riechelmann, A. Sauter, W. Golze, G. Hanft, C. Schroen, K. Hoermann, T. Erhardt, S. Gronau, *Oral Oncol.* **2008**, *44*, 823–829.
- [29] S. Eetezadi, S. N. Ekdawi, C. Allen, *Adv. Drug Deliv. Rev.* **2015**, *91*, 7–22.
- [30] C. Deng, Y. J. Jiang, R. Cheng, F. H. Meng, Z. Y. Zhong, *Nano Today* **2012**, *7*, 467–480.
- [31] R. Haag, *Angew. Chem. Int. Ed. Engl.* **2004**, *43*, 278–282.
- [32] M. Beck-Broichsitter, J. Nicolas, P. Couvreur, *Nanoscale* **2015**, *7*, 9215–9221.
- [33] R. Wang, P. S. Billone, W. M. Mullett, *J. Nanomater.* **2013**, *2013*, 12.
- [34] L. Feng, R. J. Mumper, *Cancer Lett.* **2013**, *334*, 157–175.
- [35] C. Li, S. Wallace, *Adv. Drug Deliv. Rev.* **2008**, *60*, 886–898.
- [36] Y. Shi, M. J. van Steenberg, E. A. Teunissen, L. Novo, S. Gradmann, M. Baldus, C. F. van Nostrum, W. E. Hennink, *Biomacromolecules* **2013**, *14*, 1826–1837.
- [37] Y. Shi, R. van der Meel, B. Theek, E. O. Blenke, E. H. E. Pieters, M. Fens, J. Ehling, R. M. Schiffelers, G. Storm, C. F. van Nostrum, et al., *ACS Nano* **2015**, *9*, 3740–3752.
- [38] N. Larson, H. Ghandehari, *Chem. Mater.* **2012**, *24*, 840–853.
- [39] H. Sarin, *J. Angiogenes. Res.* **2010**, *2*, 1–19.
- [40] N. Bertrand, J. C. Leroux, *J. Control. Release* **2012**, *161*, 152–163.

- [41] L. Zhang, F. X. Gu, J. M. Chan, A. Z. Wang, R. S. Langer, O. C. Farokhzad, *Clin. Pharmacol. Ther.* **2008**, *83*, 761–769.
- [42] G. S. Kwon, K. Kataoka, *Adv. Drug Deliv. Rev.* **1995**, *16*, 295–309.
- [43] R. Duncan, *Adv. Drug Deliv. Rev.* **2009**, *61*, 1131–1148.
- [44] O. C. Farokhzad, R. Langer, *ACS Nano* **2009**, *3*, 16–20.
- [45] P. Burgess, P. B. Hutt, O. C. Farokhzad, R. Langer, S. Minick, S. Zale, *Nat. Biotechnol.* **2010**, *28*, 1267–1271.
- [46] J. Fang, H. Nakamura, H. Maeda, *Adv. Drug Deliv. Rev.* **2011**, *63*, 136–151.
- [47] V. Torchilin, *Adv. Drug Deliv. Rev.* **2011**, *63*, 131–135.
- [48] S. S. Linton, S. G. Sherwood, K. C. Drews, M. Kester, *Wiley Interdiscip. Rev. Nanomed. Nanobiotechnol.* **2016**, *8*, 208–222.
- [49] A. E. Smith, X. W. Xu, C. L. McCormick, *Prog. Polym. Sci.* **2010**, *35*, 45–93.
- [50] E. Fleige, M. A. Quadir, R. Haag, *Adv. Drug Deliv. Rev.* **2012**, *64*, 866–884.
- [51] I. Canton, G. Battaglia, *Chem. Soc. Rev.* **2012**, *41*, 2718–2739.
- [52] T.-G. Iversen, T. Skotland, K. Sandvig, *Nano Today* **2011**, *6*, 176–185.
- [53] H. Hillaireau, P. Couvreur, *Cell. Mol. Life Sci.* **2009**, *66*, 2873–2896.
- [54] M. M. Gottesman, T. Fojo, S. E. Bates, *Nat. Rev. Cancer* **2002**, *2*, 48–58.
- [55] M. E. Davis, Z. Chen, D. M. Shin, *Nat. Rev. Drug Discov.* **2008**, *7*, 771–782.
- [56] H. Maeda, J. Wu, T. Sawa, Y. Matsumura, K. Hori, *J. Control. Release* **2000**, *65*, 271–284.
- [57] S. K. Hobbs, W. L. Monsky, F. Yuan, W. G. Roberts, L. Griffith, V. P. Torchilin, R. K. Jain, *Proc. Natl. Acad. Sci.* **1998**, *95*, 4607–4612.
- [58] P. P. Deshpande, S. Biswas, V. P. Torchilin, *Nanomedicine* **2013**, *8*, 1509–1528.
- [59] R. K. Jain, T. Stylianopoulos, *Nat. Rev. Clin. Oncol.* **2010**, *7*, 653–664.
- [60] S.-D. Li, L. Huang, *Mol. Pharm.* **2008**, *5*, 496–504.
- [61] V. P. Chauhan, R. K. Jain, *Nat. Mater.* **2013**, *12*, 958–962.
- [62] K. Knop, R. Hoogenboom, D. Fischer, U. S. Schubert, *Angew. Chem. Int. Ed. Engl.* **2010**, *49*, 6288–6308.
- [63] M. H. Stenzel, *Chem. Comm.* **2008**, *30*, 3486–3503.
- [64] F. Alexis, E. Pridgen, L. K. Molnar, O. C. Farokhzad, *Mol. Pharm.* **2008**, *5*, 505–515.
- [65] T. Lammers, W. E. Hennink, G. Storm, *Br. J. Cancer* **2008**, *99*, 392–397.
- [66] H. Cabral, Y. Matsumoto, K. Mizuno, Q. Chen, M. Murakami, M. Kimura, Y. Terada, M. R. Kano, K. Miyazono, M. Uesaka, et al., *Nat. Nanotechnol.* **2011**, *6*, 815–823.
- [67] D. Kim, Z. G. Gao, E. S. Lee, Y. H. Bae, *Mol. Pharm.* **2009**, *6*, 1353–1362.
- [68] U. Lachelt, E. Wagner, *Chem. Rev.* **2015**, *115*, 11043–11078.
- [69] R. van der Meel, L. J. Vehmeijer, R. J. Kok, G. Storm, E. V van Gaal, *Adv. Drug Deliv. Rev.* **2013**, *65*, 1284–1298.
- [70] V. M. Platt, F. C. Szoka Jr., *Mol. Pharm.* **2008**, *5*, 474–486.
- [71] K. Lessan, D. J. Aguiar, T. Oegema, L. Siebenson, A. P. N. Skubitz, *Am. J. Pathol.* **1999**, *154*, 1525–1537.
- [72] M. P. Ween, M. K. Oehler, C. Ricciardelli, *Int. J. Mol. Sci.* **2011**, *12*, 1009–1029.
- [73] C. Underhill, *J. Cell Sci.* **1992**, *103*, 293–298.
- [74] S. Misra, P. Heldin, V. C. Hascall, N. K. Karamanos, S. S. Skandalis, R. R. Markwald, S. Ghatak, *FEBS J.* **2011**, *278*, 1429–1443.
- [75] R. E. Eliaz, F. C. Szoka, *Cancer Res.* **2001**, *61*, 2592–2601.
- [76] H. Ponta, L. Sherman, P. A. Herrlich, *Nat. Rev. Mol. Cell Biol.* **2003**, *4*, 33–45.
- [77] Y. Lu, P. S. Low, *Adv. Drug Deliv. Rev.* **2012**, *64*, 342–352.
- [78] J. Sudimack, R. J. Lee, *Adv. Drug Deliv. Rev.* **2000**, *41*, 147–162.
- [79] J. Eliezar, W. Scarano, N. R. B. Boase, K. J. Thurecht, M. H. Stenzel, *Biomacromolecules* **2015**, *16*, 515–523.
- [80] M. E. Davis, J. E. Zuckerman, C. H. Choi, D. Seligson, A. Tolcher, C. A. Alabi, Y. Yen, J. D. Heidel, A. Ribas, *Nature* **2010**, *464*, 1067–1070.
- [81] S. Tortorella, T. C. Karagiannis, *Curr. Drug Deliv.* **2014**, *11*, 427–443.
- [82] J. Hrkach, D. Von Hoff, M. M. Ali, E. Andrianova, J. Auer, T. Campbell, D. De Witt, M. Figa, M. Figueiredo, A. Horhota, et al., *Sci. Transl. Med.* **2012**, *4*, 128–139.
- [83] C. Zhu, A. Bandekar, M. Sempkowski, S. R. Banerjee, M. G. Pomper, F. Bruchertseifer, A. Morgenstern, S. Sofou, *Mol. Cancer Ther.* **2016**, *15*, 106–113.
- [84] M. Creixell, A. C. Bohorquez, M. Torres-Lugo, C. Rinaldi, *ACS Nano* **2011**, *5*, 7124–7129.

- [85] C. Mamot, R. Ritschard, A. Wicki, G. Stehle, T. Dieterle, L. Bubendorf, C. Hilker, S. Deuster, R. Herrmann, C. Rochlitz, *Lancet Oncol.* **2012**, *13*, 1234–1241.
- [86] N. Graf, D. R. Bielenberg, N. Kolishetti, C. Muus, J. Banyard, O. C. Farokhzad, S. J. Lippard, *ACS Nano* **2012**, *6*, 4530–4539.
- [87] M. C. Haffner, J. Laimer, A. Chau, G. Schäfer, P. Obrist, A. Brunner, I. E. Kronberger, K. Laimer, B. Gurel, J.-B. Koller, *Mod. Pathol.* **2012**, *25*, 1079–1085.
- [88] D. A. Yardley, *J. Control. Release* **2013**, *170*, 365–372.
- [89] M. S. Muthu, R. V. Kutty, Z. Luo, J. Xie, S. S. Feng, *Biomaterials* **2015**, *39*, 234–248.
- [90] S. Oliveira, R. Heukers, J. Soronkom, R. J. Kok, P. M. van Bergen En Henegouwen, *J. Control. Release* **2013**, *172*, 607–617.
- [91] H. Lee, K. Lee, T. G. Park, *Bioconjug. Chem.* **2008**, *19*, 1319–1325.
- [92] G. Journo-Gersfeld, D. Kapp, Y. Shamay, J. Kopecek, A. David, *Pharm. Res.* **2012**, *29*, 1121–1133.
- [93] T. Fernandes Stefanello, A. Szapak-Jankowska, F. Appaix, B. Louage, L. Hamard, B. G. De Geest, B. van der Sanden, C. V. Nakamura, R. Auzely-Velty, *Acta Biomater.* **2014**, *10*, 4750–4758.
- [94] K. K. Upadhyay, J. F. Le Meins, A. Misra, P. Voisin, V. Bouchaud, E. Ibarboure, C. Schatz, S. Lecommandoux, *Biomacromolecules* **2009**, *10*, 2802–2808.
- [95] C. Deng, X. Chen, J. Sun, T. Lu, W. Wang, X. Jing, *J. Polym. Sci. Part A Polym. Chem.* **2007**, *45*, 3218–3230.
- [96] A. Eldar-Boock, K. Miller, J. Sanchis, R. Lupu, M. J. Vicent, R. Satchi-Fainaro, *Biomaterials* **2011**, *32*, 3862–74.
- [97] P. R. Patel, R. C. Kiser, Y. Y. Lu, E. Fong, W. C. Ho, D. A. Tirrell, R. H. Grubbs, *Biomacromolecules* **2012**, *13*, 2546–2553.
- [98] Z. Zhang, Y. Lai, L. Yu, J. Ding, *Biomaterials* **2010**, *31*, 7873–7882.
- [99] V. Bagalkot, O. C. Farokhzad, R. Langer, S. Jon, *Angew. Chem. Int. Ed. Engl.* **2006**, *45*, 8149–8152.
- [100] O. C. Farokhzad, J. Cheng, B. A. Teplý, I. Sherifi, S. Jon, P. W. Kantoff, J. P. Richie, R. Langer, *Proc. Natl. Acad. Sci.* **2006**, *103*, 6315–6320.
- [101] Y. Zhong, F. Meng, C. Deng, Z. Zhong, *Biomacromolecules* **2014**, *15*, 1955–1969.
- [102] Y. G. Assaraf, C. P. Leamon, J. A. Reddy, *Drug Resist. Updat.* **2014**, *17*, 89–95.
- [103] A. R. Hilgenbrink, P. S. Low, *J. Pharm. Sci.* **2005**, *94*, 2135–2146.
- [104] P. M. Valencia, M. H. Hanewich-Hollatz, W. Gao, F. Karim, R. Langer, R. Karnik, O. C. Farokhzad, *Biomaterials* **2011**, *32*, 6226–6233.
- [105] S. Bhattacharyya, R. D. Singh, R. Pagano, J. D. Robertson, R. Bhattacharya, P. Mukherjee, *Angew. Chem. Int. Ed. Engl.* **2012**, *51*, 1563–1567.
- [106] S. Bhattacharyya, R. Bhattacharya, S. Curley, M. A. McNiven, P. Mukherjee, *Proc. Natl. Acad. Sci.* **2010**, *107*, 14541–14546.
- [107] M. Elsabahy, K. L. Wooley, *Chem. Soc. Rev.* **2012**, *41*, 2545–61.
- [108] S. Kunjachan, R. Pola, F. Gremse, B. Theek, J. Ehling, D. Moeckel, B. Hermans-Sachweh, M. Pechar, K. Ulbrich, W. E. Hennink, *Nano Lett.* **2014**, *14*, 972–981.
- [109] R. Singh, M. Norret, M. J. House, Y. Galabura, M. Bradshaw, D. Ho, R. C. Woodward, T. G. S. Pierre, I. Luzinov, N. M. Smith, *Small* **2016**, *12*, 351–359.
- [110] G. Gaucher, M. H. Dufresne, V. P. Sant, N. Kang, D. Maysinger, J. C. Leroux, *J. Control. Release* **2005**, *109*, 169–188.
- [111] R. Tong, D. S. Kohane, in *Annu. Rev. Pharmacol. Toxicol.*, **2016**, pp. 41–57.
- [112] I. Lee, M. Park, Y. Kim, O. Hwang, G. Khang, D. Lee, *Int. J. Pharm.* **2013**, *448*, 259–266.
- [113] M. J. Heffernan, N. Murthy, *Bioconjug. Chem.* **2005**, *16*, 1340–1342.
- [114] J. Liu, Y. Huang, A. Kumar, A. Tan, S. Jin, A. Mozhi, X.-J. Liang, *Biotechnol. Adv.* **2014**, *32*, 693–710.
- [115] A. E. Felber, M. H. Dufresne, J. C. Leroux, *Adv. Drug Deliv. Rev.* **2012**, *64*, 979–992.
- [116] R. De Coen, N. Vanparijs, M. D. Risseeuw, L. Lybaert, B. Louage, S. De Koker, V. Kumar, J. Grooten, L. Taylor, N. Ayres, et al., *Biomacromolecules* **2016**, *17*, 2479–2488.
- [117] L. Nuhn, N. Vanparijs, A. De Beuckelaer, L. Lybaert, G. Verstraete, K. Deswarte, S. Lienenklaus, N. M. Shukla, A. C. Salyer, B. N. Lambrecht, et al., *Proc. Natl. Acad. Sci.* **2016**, *113*, 8098–8103.
- [118] K. Ulbrich, V. Subr, *Adv. Drug Deliv. Rev.* **2004**, *56*, 1023–1050.
- [119] S. Binauld, M. H. Stenzel, *Chem. Comm.* **2013**, *49*, 2082–2102.
- [120] L. Liang, S.-W. Lin, W. Dai, J.-K. Lu, T.-Y. Yang, Y. Xiang, Y. Zhang, R.-T. Li, Q. Zhang, *J. Control. Release* **2012**, *160*, 618–629.
- [121] L. Zhu, T. Wang, F. Perche, A. Taigind, V. P. Torchilin, *Proc. Natl. Acad. Sci.* **2013**, *110*, 17047–17052.
- [122] A. W. Jackson, D. A. Fulton, *Polym. Chem.* **2013**, *4*, 31–45.

- [123] H. T. T. Duong, C. P. Marquis, M. Whittaker, T. P. Davis, C. Boyer, *Macromolecules* **2011**, *44*, 8008–8019.
- [124] F. Meng, W. E. Hennink, Z. Zhong, *Biomaterials* **2009**, *30*, 2180–2198.
- [125] J. Z. Du, Y. Q. Tang, A. L. Lewis, S. P. Armes, *J. Am. Chem. Soc.* **2005**, *127*, 17982–17983.
- [126] Q. L. Zhang, N. Vanparijs, B. Louage, B. G. De Geest, R. Hoogenboom, *Polym. Chem.* **2014**, *5*, 1140–1144.
- [127] D. W. Zhang, H. Zhang, J. Nie, J. Yang, *Polym. Int.* **2010**, *59*, 967–974.
- [128] R. A. Shenoi, J. K. Narayanannair, J. L. Hamilton, B. F. L. Lai, S. Horte, R. K. Kainthan, J. P. Varghese, K. G. Rajeev, M. Manoharan, J. N. Kizhakkedathu, *J. Am. Chem. Soc.* **2012**, *134*, 14945–14957.
- [129] Z. Shatsberg, X. Zhang, P. Ofek, S. Malhotra, A. Krivitsky, A. Scomparin, G. Tiram, M. Calderon, R. Haag, R. Satchi-Fainaro, *J. Control. Release* **2016**, *239*, 159–168.
- [130] B. Louage, Q. Zhang, N. Vanparijs, L. Voorhaar, S. Vande Castele, Y. Shi, W. E. Hennink, J. Van Bocxlaer, R. Hoogenboom, B. G. De Geest, *Biomacromolecules* **2015**, *16*, 336–50.
- [131] Q. Zhang, Z. Hou, B. Louage, D. Zhou, N. Vanparijs, B. G. De Geest, R. Hoogenboom, *Angew. Chem. Int. Ed. Engl.* **2015**, *127*, 11029–11033.
- [132] S. Kasmi, B. Louage, L. Nuhn, A. Van Driessche, J. Van Deun, I. Karalic, M. Risseeuw, S. Van Calenbergh, R. Hoogenboom, R. De Rycke, et al., *Biomacromolecules* **2016**, *17*, 119–127.
- [133] A. Gregory, M. H. Stenzel, *Prog. Polym. Sci.* **2012**, *37*, 38–105.
- [134] C. Boyer, V. Bulmus, T. P. Davis, V. Ladmiral, J. Liu, S. Perrier, *Chem. Rev.* **2009**, *109*, 5402–36.
- [135] M. I. Gibson, E. Froehlich, H.-A. Klok, *J. Polym. Sci. Part A Polym. Chem.* **2009**, *47*, 4332–4345.
- [136] R. Tong, L. Tang, L. Ma, C. Tu, R. Baumgartner, J. Cheng, *Chem. Soc. Rev.* **2014**, *43*, 6982–7012.
- [137] V. T. Huynh, S. Binauld, P. L. de Souza, M. H. Stenzel, *Chem. Mater.* **2012**, *24*, 3197–3211.
- [138] M. Longmire, P. L. Choyke, H. Kobayashi, *Nanomedicine* **2008**, *3*, 703–717.
- [139] R. Tong, J. Cheng, *Angew. Chem. Int. Ed. Engl.* **2008**, *47*, 4830–4834.
- [140] R. Cheng, F. Meng, C. Deng, Z. Zhong, *Nano Today* **2015**, *10*, 656–670.

chapter 2

taxanes

Benoit Louage,^a Olivier De Wever,^b Wim E. Hennink,^c Bruno G De Geest^a

^a Laboratory of Pharmaceutical Technology, Department of Pharmaceutics,
Ghent University, Ottergemsesteenweg 460, 9000 Ghent, Belgium

^b Department of Radiation Oncology and Experimental Cancer Research,
Ghent University and Ghent University Hospital, De Pintelaan 185, 9000 Ghent, Belgium

^c Department of Pharmaceutics, Utrecht Institute for Pharmaceutical Sciences,
Utrecht University, Universiteitsweg 99, 3584CG Utrecht, The Netherlands

Journal of Controlled Release 2017

1 history

In 1962, a plant screening operation was organized by the US National Cancer Institute. It was found that an extract of the bark of *Taxus brevifolia* (or Pacific yew) exerted cytotoxicity *in vitro* against the human KB cancer cell line. Initially, only modest anti-cancer activity was detected *in vivo*, therefore the discovery initially did not receive overall positive response. In the 1970s, the complete structure elucidation of the active compound (i.e. paclitaxel (PTX)) was performed along with more extensive *in vivo* studies. Contrarily, the latter showed very promising results. The subsequent discovery of the mechanism of action (section 3) fueled the scientific interest even further which eventually led to clinical translation of PTX.^[1] Phase I and II trials started in 1984 and 1985, respectively. The first report on clinical anti-cancer activity against ovarian cancer was published in 1989. Few years later, similar positive results were obtained for breast cancer treatment with PTX and in 1992, Bristol-Myers Squibb got FDA-approval for Taxol (formulation details are described in section 4) for treatment of ovarian, breast and NSCLC.^[2,3]

The scarcity of PTX triggered the exploration towards alternative, renewable sources (section 2). In 1981, a collaboration started between the pharmaceutical company Rhône-Poulenc Rorer Inc. and the Institut de Chimie des Substances Naturelles. In 1986, this collaboration resulted in the discovery of the semisynthetic analogue docetaxel (DTX).^[4] DTX exhibited widespread *in vitro* and *in vivo* activity with at least similar potency compared to PTX.^[5] Due to the regenerative capacity of the source (i.e. needles), DTX experienced swift clinical development.^[6] In 1992, Rhône-Poulenc Rorer Inc. and the National Cancer Institute (NCI) signed a cooperative research and development agreement (CRADA) to seek approval for Taxotere (formulation details are described in section 4).^[7] Phase I and II trials started in 1992 and 1993, respectively.^[8,9] Substantial single agent activity was observed in treatment of breast, ovarian and NSCLC.^[10] In 1996, DTX was granted accelerated approval for second-line treatment of breast cancer.^[11]

2 production

PTX can be extracted from the bark of Pacific yew trees, but only in very low yields (i.e. 0.01 %). Approximately 2500 trees need to be harvested to obtain 1 kg of PTX.^[12] Additionally, these trees are characterized by a very slow growth rate, impeding large scale cultivation. This led to a supply crisis for clinical phase III trials of Taxol in the 1990s and urged the pharmaceutical industry to search for alternative production methods.^[13] Extensive research was conducted in finding protocols for the total synthesis of PTX.^[14-18] Even though methods

have been developed and described in literature, none of these, however, appeared to be viable on an industrial scale. The most successful strategy which eventually resolved the PTX supply crisis involved a semisynthetic approach out of 10-deacetyl baccatin III.^[2] The latter is a precursor which can be extracted out of renewable sources (i.e. needles) of a broader spectrum of yew tree varieties with faster growth rates (e.g. European yew (*Taxus baccata*)).^[19,20] This approach also led to the discovery and development of DTX (section.1). Novel biotechnological approaches including production from fungal endophytes and plant cell cultures are currently gaining interest as well. Semisynthesis of DTX and PTX from 10-deacetyl baccatin III, obtained from either yew trees or plant cell cultures, are the most commonly applied strategies for the commercial supply of taxanes. Extensive efforts are currently being devoted to achieving higher yields, lowering the production costs and improving the environmental sustainability.^[21]

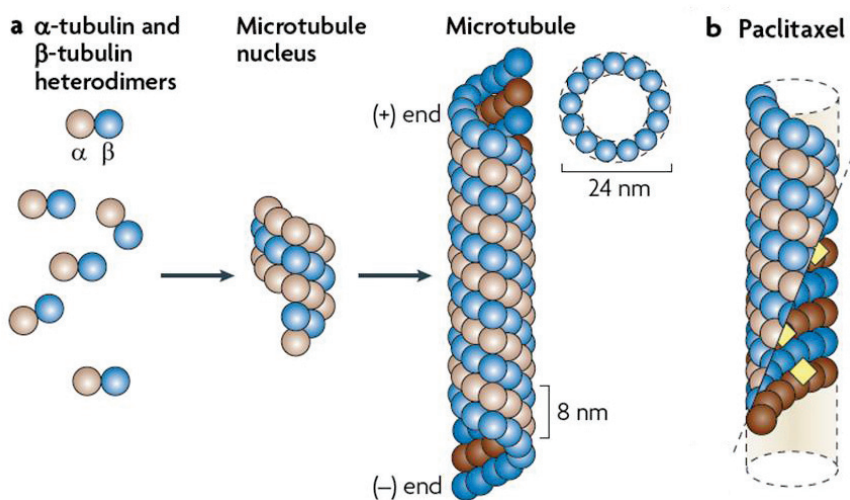


Figure 1. (a) composition, size and structural organization of microtubules, (b) microtubule binding site of PTX (DTX shares the same binding site).^[22]

3 mechanism of action

Taxanes are known for their interaction with microtubules.^[22] These hollow cylindrical macromolecular structures are built out of 13 longitudinal protofilaments composed of tubulin, a dimeric protein containing an α - and a β -subunit (**Figure 1a**).^[23] Microtubules are important building blocks of the cytoskeleton and play pivotal roles in various dynamic processes including cell migration, organelle movement and spindle formation during mitosis.

The latter renders microtubules an attractive drugable target, as the proportion of cells in active cell cycle phase is substantially higher in tumor tissue than in normal tissues. Taxanes bind to the inner surface of microtubules, specifically through interaction with the β -tubulin subunit and thereby promote both their formation and their stabilization (**Figure 1b**).^[24] DTX possesses a 2-fold higher microtubule binding affinity compared to PTX.^[25] The latter partly explains the lower dose of DTX required for obtaining similar *in vitro* and *in vivo* anti-cancer effects (section 4). This stabilization thus prevents depolymerization of microtubules from occurring as during normal mitosis, but instead arrests cells in the late G2/M-phase which eventually leads to apoptotic cell death.

4 taxane solubilization: Taxol and Taxotere

Despite their high potency in cancer treatment, taxanes are used only to a modest extent in clinic today. The hydrophobic structure of PTX, discovered in the 1970s, already highlighted that taxanes possess extremely low water-solubility. For example, it was found that the solubility of PTX in water is below 0.3 $\mu\text{g}/\text{mL}$. Thus, finding a suitable pharmaceutical formulation was challenging for Bristol-Myers Squibb. The company developed a formulation of PTX composed of a 50:50 ethanol:Cremophor EL mixture and commercialized it under the brand name Taxol.^[26] In clinic, often 175 mg/m^2 of PTX is administered by intravenous infusion every 3 weeks.^[27] This formulation is diluted into an iso-osmotic solution (e.g. 5 % dextrose) which is subsequently administered by intravenous infusion over a time course of several hours.^[28] Taxol has been FDA-approved for treatment of several cancers including NSCLC, AIDS-related Kaposi sarcoma, ovarian and breast cancer.^[29]

Even though slightly more hydrophilic, DTX also exhibits very limited water-solubility. For this reason, Rhône-Poulenc Rorer Inc. (now Sanofi) formulated DTX in a 50:50 ethanol:polysorbate 80 mixture and commercialized it under the brand name Taxotere.^[5] A DTX dose of 100 mg/m^2 is often administered upon dilution, every 3 weeks within 1 - 2 hours of intravenous infusion.^[27] In phase III trials, Taxotere has shown both similar and superior efficacy compared to Taxol (e.g. in platinum combination therapy for treatment of ovarian cancer and as single agent for treatment of anthracycline-resistant metastatic breast cancer, respectively).^[30-33] Neutropenia was often more abundant in DTX treatment but generally, less neuropathy was observed than with PTX.^[30] Taxotere is currently FDA-approved for treatment of adenocarcinoma, squamous cell carcinoma of head and neck, NSCLC, breast and prostate cancer.^[34]

However, the surfactants of both Taxol (i.e. Cremophor EL, a pegylated derivative of castor oil) and Taxotere (i.e. polysorbate 80, an ester of pegylated sorbitan with oleic acid) cause serious hypersensitivity reactions in patients, even within minutes during infusion.^[35-41] Therefore, patients undergoing therapy with Taxol or Taxotere have to be pretreated with antihistamines and/or corticosteroids to temper severe, possibly fatal allergic reaction. Polysorbate 80 in particular can also induce fluid retention and often requires additional treatment with diuretics.^[37] This has somewhat hampered extensive use of Taxol and Taxotere in clinic, but also instigated scientific interest for developing alternative taxane formulations using more biocompatible excipients in order to administer taxanes in a safer fashion.

5 references

- [1] D. G. Kingston, *J. Nat. Prod.* **2000**, *63*, 726–734.
- [2] D. G. I. Kingston, *Phytochemistry* **2007**, *68*, 1844–1854.
- [3] “Taxol® (NSC 125973),” can be found under https://dtp.cancer.gov/timeline/flash/success_stories/52_taxol.htm, **2016**.
- [4] F. Lavelle, F. Gueritte-Voegelein, D. Guenard, *Bull. Cancer* **1993**, *80*, 326–338.
- [5] M. C. Bissery, G. Nohynek, G. J. Sanderink, F. Lavelle, *Anticancer Drugs* **1995**, *6*, 339–355–368.
- [6] J. Verweij, M. Clavel, B. Chevalier, *Ann. Oncol.* **1994**, *5*, 495–505.
- [7] E. Blume, *J. Natl. Cancer Inst.* **1992**, *84*, 673.
- [8] R. Pazdur, R. A. Newman, B. M. Newman, A. Fuentes, J. Benvenuto, B. Bready, D. Moore Jr., I. Jaiyesimi, F. Vreeland, M. M. Bayssas, et al., *J. Natl. Cancer Inst.* **1992**, *84*, 1781–1788.
- [9] A. D. Seidman, C. Hudis, J. P. A. Crown, C. Balmaceda, D. Lebwohl, V. Currie, T. Gilewski, T. Hakes, M. Robles, K. Klem, in *Proc. Am. Soc. Clin. Oncol.*, **1993**, p. 63.
- [10] A. T. van Oosterom, D. Schrijvers, *Anticancer Drugs* **1995**, *6*, 356–368.
- [11] R. Dagher, J. Johnson, G. Williams, P. Keegan, R. Pazdur, *J. Natl. Cancer Inst.* **2004**, *96*, 1500–1509.
- [12] G. M. Cragg, K. M. Snader, *Cancer Cells* **1991**, *3*, 233–235.
- [13] D. Guenard, F. Gueritte-Voegelein, P. Potier, *Acc. Chem. Res.* **1993**, *26*, 160–167.
- [14] R. A. Holton, R. R. Juo, H. B. Kim, A. D. Williams, S. Harusawa, R. E. Lowenthal, S. Yogai, *J. Am. Chem. Soc.* **1988**, *110*, 6558–6560.
- [15] W. F. Berkowitz, A. S. Amarasekara, J. J. Perumattam, *J. Org. Chem.* **1987**, *52*, 1119–1124.
- [16] J. Lin, M. M. Nikaido, G. Clark, *J. Org. Chem.* **1987**, *52*, 3745–3752.
- [17] P. A. Wender, D. B. Rawlins, *Tetrahedron* **1992**, *48*, 7033–7048.
- [18] L. Ettouati, A. Ahond, C. Poupat, P. Potier, *Tetrahedron* **1991**, *47*, 9823–9838.
- [19] D. G. Kingston, *Pharmacol. Ther.* **1991**, *52*, 1–34.
- [20] V. Senilh, S. Blechert, M. Colin, D. Guenard, F. Picot, P. Potier, P. Varenne, *J. Nat. Prod.* **1984**, *47*, 131–137.
- [21] S. Soliman, Y. Tang, *Biotechnol. Bioeng.* **2015**, *112*, 229–235.
- [22] C. Dumontet, M. A. Jordan, *Nat. Rev. Drug Discov.* **2010**, *9*, 790–803.
- [23] I. Arnal, R. H. Wade, *Curr. Biol.* **1995**, *5*, 900–908.
- [24] S. Rao, L. He, S. Chakravarty, I. Ojima, G. A. Orr, S. B. Horwitz, *J. Biol. Chem.* **1999**, *274*, 37990–37994.
- [25] J. F. Diaz, J. M. Andreu, *Biochemistry* **1993**, *32*, 2747–2755.
- [26] A. Sparreboom, O. VanTellingen, W. J. Nooijen, J. H. Beijnen, *Cancer Res.* **1996**, *56*, 2112–2115.
- [27] S. E. Jones, J. Erban, B. Overmoyer, G. T. Budd, L. Hutchins, E. Lower, L. Laufman, S. Sundaram, W. J. Urba, K. I. Pritchard, et al., *J. Clin. Oncol.* **2005**, *23*, 5542–5551.
- [28] P. H. Wiernik, E. L. Schwartz, J. J. Strauman, J. P. Dutcher, R. B. Lipton, E. Paietta, *Cancer Res.* **1987**, *47*, 2486–2493.
- [29] “Paclitaxel,” can be found under <https://www.cancer.gov/about-cancer/treatment/drugs/paclitaxel>, **2016**.
- [30] P. A. Vasey, G. C. Jayson, A. Gordon, H. Gabra, R. Coleman, R. Atkinson, D. Parkin, J. Paul, A. Hay, S. B. Kaye, *J. Natl. Cancer Inst.* **2004**, *96*, 1682–1691.
- [31] S. B. Kaye, M. Piccart, M. Aapro, P. Francis, J. Kavanagh, *Eur. J. Cancer* **1997**, *33*, 2167–2170.
- [32] E. Saloustros, D. Mavroudis, V. Georgoulas, *Expert Opin. Pharmacother.* **2008**, *9*, 2603–2616.
- [33] T. Vu, S. Ellard, C. H. Speers, S. C. Taylor, M. L. de Lemos, F. Hu, K. Kuik, I. A. Olivotto, *Ann. Oncol.* **2008**, *19*, 461–464.
- [34] “Docetaxel,” can be found under <https://www.cancer.gov/about-cancer/treatment/drugs/docetaxel>, **2016**.
- [35] H. Gelderblom, J. Verweij, K. Nooter, A. Sparreboom, *Eur. J. Cancer* **2001**, *37*, 1590–1598.
- [36] E. K. Rowinsky, E. A. Eisenhauer, V. Chaudry, S. G. Arbuck, R. C. Donehower, *Semin. Oncol.* **1993**, *20*, 1–15.
- [37] A. J. ten Tije, J. Verweij, W. J. Loos, A. Sparreboom, *Clin. Pharmacokinet.* **2003**, *42*, 665–685.
- [38] L. B. Norris, Z. P. Qureshi, P. B. Bookstaver, D. W. Raisch, O. Sartor, H. Chen, F. Chen, C. L. Bennett, *Community Oncol.* **2010**, *7*, 425–428.

- [39] Z. Weiszhar, J. Czucz, C. Revesz, L. Rosivall, J. Szebeni, Z. Rozsnyay, *Eur. J. Pharm. Sci.* **2012**, *45*, 492–498.
- [40] M. J. Hawkins, P. Soon-Shiong, N. Desai, *Adv. Drug Deliv. Rev.* **2008**, *60*, 876–885.
- [41] J. Wanders, D. Schrijvers, U. Brunsch, M. Gore, J. Verweij, A. Hanauske, H. Franklin, M. Roelvink, M. Bayssas, S. B. Kaye, in *Proc. Am. Soc. Clin. Oncol.*, **1993**, p. 73.

PART II

DESIGN OF ADVANCED TAXANE NANOFORMULATIONS BASED ON PHYSICAL ENCAPSULATION

chapter 3

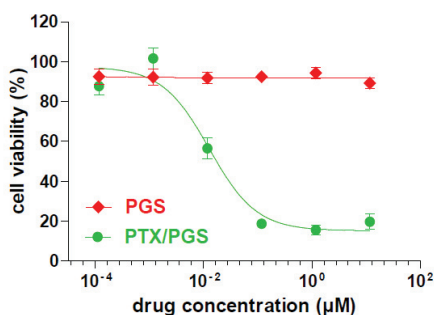
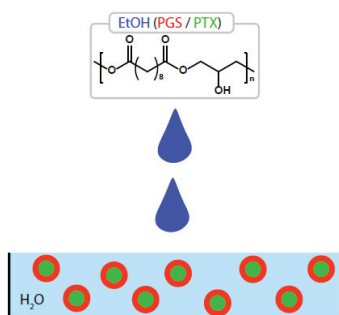
poly(glycerol sebacate) nanoparticles for encapsulation of hydrophobic anti-cancer drugs

Benoit Louage,^a Liesa Tack,^a Yadong Wang,^b Bruno G. De Geest^a

^a Laboratory of Pharmaceutical Technology, Department of Pharmaceutics,
Ghent University, Ottergemsesteenweg 460, 9000 Ghent, Belgium

^b Departments of Bioengineering, Chemical and Petroleum Engineering, Surgery, Mechanical Engineering and
Materials Science, and the McGowan Institute for Regenerative Medicine,
3700 O'Hara Street, 411 Benedum Hall, Pittsburgh, PA 15261, USA

Polymer Chemistry 2017, DOI: 10.1039/C6PY02192A



abstract

Physical encapsulation of hydrophobic compounds into nanocarriers which are stable in aqueous medium is of high interest as it can increase solubilization of the drug, lower its toxicity, control its pharmacokinetic profile and thus overall improve the therapeutic efficacy. To increase solubilization of a drug in aqueous medium, the carrier should contain hydrophobic domains which can form non-covalent interactions with hydrophobic drug molecules. Besides liposomes, polymers have been widely acknowledged as promising nanocarriers. In this paper, we report on the formulation of poly(glycerol sebacate) (PGS), an inexpensive, water insoluble but biodegradable and biocompatible polymer, into nanocarriers for hydrophobic drugs. Mixing of alcoholic PGS solutions with water (i.e. solvent displacement) produced a fine and highly stable dispersion with a size which can be controlled by the PGS concentration and solvent to water ratio. These dispersions were used for the encapsulation of hydrophobic compounds such as a fluorescent dye and two drugs known for their anti-mitotic activity (i.e. paclitaxel (PTX) and flubendazole (FLU)). These formulations were then evaluated *in vitro*.

1 introduction

Up to now, patients receiving chemotherapy still experience aggravating side-effects (i.e. hypersensitivity, hair loss, nausea, higher susceptibility for diseases due to impaired immune function, etc.).^[1] Non-specific drug activity and toxic solubilizing agents present in the anti-cancer drug formulations can cause these adverse effects.^[2-5] These issues have triggered research over the past 20 years towards advanced delivery systems for chemotherapeutic drugs to minimize these side-effects of chemotherapy. Nanomedicine is considered to be one of the most promising strategies to achieve this goal.^[6-8] One key feature of nanocarriers is the possibility of improving drug selectivity by the so-called enhanced permeability and retention (EPR) effect.^[9-11] This passive targeting mechanism involves accumulation of nanoparticles in tumor tissue due to poor endothelial connections in neoplastic blood vessels and impaired lymphatic drainage. Secondly, aqueous solubility of hydrophobic anti-cancer drugs (e.g. paclitaxel (PTX) and flubendazole (FLU)) can be significantly improved by physical or chemical incorporation into a nanoparticle.^[12,13]

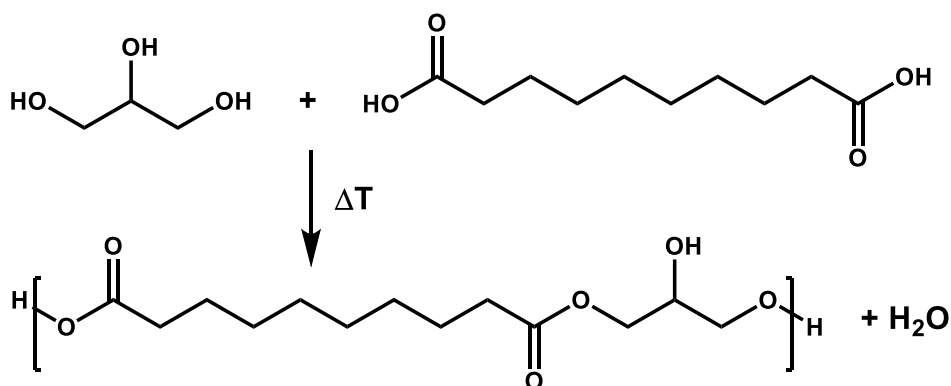


Figure 1. Synthesis of poly(glycerol sebacate) by polycondensation between glycerol and sebacic acid under heating and reduced pressure. The structure is an idealized form as branching occurs involving the middle hydroxyl group of glycerol in the polycondensation reaction.

Polymers are a critical player in the field of nanomedicines.^[14-23] Besides affording drug encapsulation, another crucial requirement for the polymer is to be biocompatible, as excipients are known to cause severe side-effects (i.e. Cremophor EL). Poly(glycerol sebacate) (PGS) is a polyester formed by polycondensation of glycerol and sebacic acid (**Figure 1**), resulting in a viscous polymer with moderate molecular weight. So far, PGS has been used for subsequent treatment under high vacuum and heating to produce a crosslinked elastomeric material.^[24] Attractive aspects of PGS are its biodegradability owing to the abundant presence of esters bonds and the fact that

both glycerol and sebacic acid are inexpensive and endogenous components present in the human body.^[25] Moreover, materials made from glycerol and sebacic acid have been approved by FDA for use in medical applications.^[26] Literature shows that PGS elastomers show excellent biocompatibility *in vitro* and *in vivo*.^[27] Due to its established biocompatibility and interesting mechanical properties, PGS elastomers have already proven to be a useful biomaterial, especially in the field of regenerative medicine.^[27-29] Despite these attractive properties the use of non-crosslinked PGS as drug nanocarrier has been overlooked, to the best of our knowledge.

Though the pending hydroxyl groups contribute to a hydrophilic nature on the polymer surface, PGS is not water-soluble, suggesting that the polymer also exhibits hydrophobic behaviour in aqueous medium which can be suitable for both self-assembly behaviour and physical encapsulation of hydrophobic drugs. These features raise the potential of PGS to produce nanoparticles for hydrophobic anti-cancer drugs.

2 results and discussion

Unlike the widespread poly(lactic-co-glycolic acid) (PLGA) which is still regarded as one of the gold standards for hydrophobic drug encapsulation, PGS can be readily dissolved in ethanol (EtOH) up to a fairly high concentration (at least 100 mg/mL). **Figure S1** shows the size exclusion chromatography (SEC) elugram of PGS, along with its average molecular weight (M_n) and polydispersity (\mathcal{D}). Stable PGS nanoparticle suspensions were obtained using a straightforward solvent displacement method (pictures of PGS nanoparticles formulated in H₂O and physiological glucose solution (i.e. dextrose 5 %) are shown in **Figure S2 - S3**, respectively). Briefly, a concentrated PGS solution in EtOH was diluted into deionized water (H₂O) under simple stirring, without the need for high shear homogenization or ultrasonication. Instantaneously, a fine dispersion was formed which is ascribed to the so-called ouzo effect.^[30] This effect involves a series of interfacial phenomena and recently, Couvreur and co-workers proposed for PLGA-based particles that organic solvents with high water affinity lead to smaller nanoparticles than solvents with a lower water affinity.^[31] As PLGA is not soluble in ethanol, this solvent was not included in their study. Here the use of ethanol for PGS nanoparticles formulation is a strong asset as it avoids work up of the nanoparticles by dialysis to remove organic solvent due to the biocompatible nature of ethanol. Importantly, we also noticed that stable dispersions could be obtained in the absence of any surfactant.

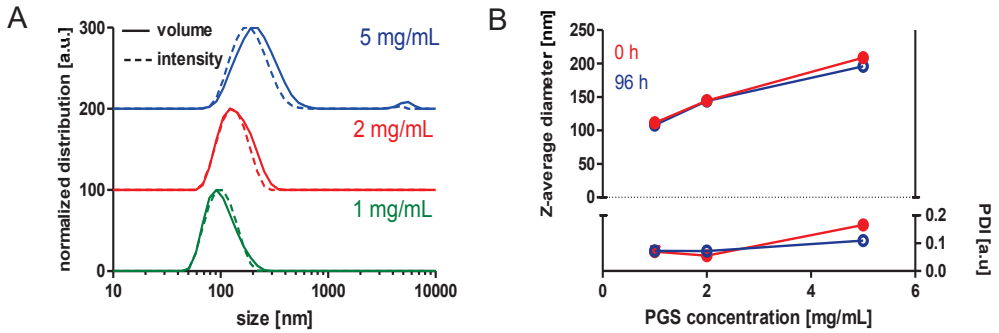


Figure 2. Particle size distribution (A), PDI and Z-average after 0 h and 96 h (B) of PGS nanoparticles formulated by solvent displacement from EtOH into deionized H₂O (n = 4).

Dynamic light scattering (DLS) was used to determine nanoparticle size, polydispersity (PDI) and colloidal stability over time under static conditions. PGS stock solutions in EtOH (10, 20 and 50 mg/mL) were prepared and 1 mL stock solution was subsequently formulated into 10 mL of H₂O. The DLS data in **Figure 2A** show that particle size depends on PGS concentration. Indeed, increasing PGS concentrations leads to larger nanoparticles with Z-average diameters of 111.6 ± 0.9 , 144.4 ± 0.3 and 208.6 ± 2.4 nm (n = 4), for a PGS concentration of 1, 2 and 5 mg/mL, respectively. Overall, PDIs were found to be low (i.e. < 0.2). Furthermore, all the nanoparticles suspensions exhibited excellent stability over time with no detectable alteration in nanoparticle size and PDI within a timeframe of 96 hours (**Figure 2B**).

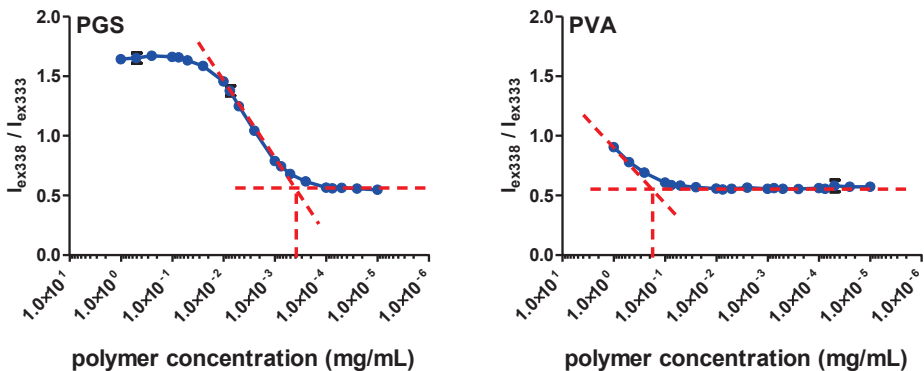


Figure 3. Excitation intensity ratio of pyrene at 338 nm (I_{ex338}) and 333 nm (I_{ex333}) as function of PGS or PVA concentration (n = 3).

To test if hydrophobic interaction was the main driving force for the formation of nanoparticles, we measured the critical aggregation concentration (CAC) of PGS by plotting the ratio of the excitation intensity at 338 and 333 nm of the hydrophobic dye pyrene versus the concentration of PGS in aqueous medium. These experiments show that pyrene becomes accommodated within the hydrophobic environment at PGS concentrations as low as $0.4 \pm 0.1 \mu\text{g/mL}$ ($n = 3$) (**Figure 3**). This value is roughly 500-fold lower as compared to the measured CAC of poly(vinyl alcohol) (PVA) (i.e. $200 \pm 8 \mu\text{g/mL}$ ($n = 3$), a commonly used emulsion stabilizer in several pharmaceutical formulations such as PLGA.^[32]

The low CAC of PGS motivated us at exploring the potential of these nanoparticles for encapsulation of hydrophobic drugs and subsequent intracellular drug delivery. For this purpose, we loaded the PGS nanoparticles with a hydrophobic fluorescent dye (i.e. Cy5-N₃) by co-dissolution of Cy5-N₃ and PGS in EtOH prior to solvent displacement in H₂O. Note that nanoparticles were prepared at a PGS concentration of 5 mg/mL as this appeared to be optimal for drug encapsulation (*vide infra*). Precipitated, non-encapsulated dye was removed by filtration (0.450 μm). SKOV-3 human ovarian carcinoma cells were pulsed with different concentrations of Cy5-N₃-labelled PGS nanoparticles and their cellular uptake was analysed by flow cytometry (FACS). As a control, we prepared an equally concentrated Cy5-N₃ solution in EtOH in the absence of PGS, followed by solvent displacement in H₂O and membrane filtration. The flow cytometry histograms, shown in **Figure 4A**, clearly indicate a dose-dependent uptake of both encapsulated and freely soluble dye. However, the mean fluorescence values of cells pulsed with Cy5-N₃-labelled PGS nanoparticles are dramatically higher than those of cells pulsed with non-encapsulated dye. These findings demonstrate that formulation of a hydrophobic dye in PGS nanoparticles increases its aqueous compatibility and hence leads to much higher cellular association. We attribute this to the ability of the hydrophobic interior of the PGS nanoparticles to accommodate hydrophobic compounds which otherwise precipitate from solution. Confocal microscopy was subsequently used to investigate the intracellular fate of the nanoparticles. **Figure 4B** shows that the Cy5-N₃-labelled PGS nanoparticles are inside the SKOV-3 cells and not merely adhering to the cell membrane. Counterstaining of the intracellular acidic vesicles (i.e. endosomes and lysosomes) with LysoTracker (**Figure 4C**) yields significant co-localization between the LysoTracker channel and the Cy5-N₃ channel, suggesting that PGS nanoparticles are predominantly internalized by endocytosis, as would be expected for particles within this size range.

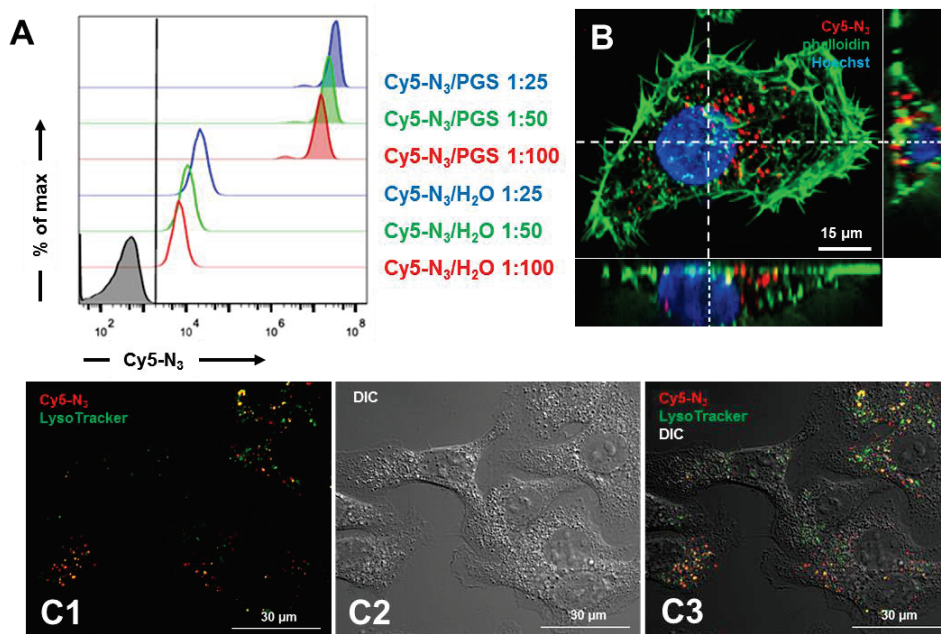


Figure 4. (A) Flow cytometry histograms obtained from SKOV-3 cells pulsed with different concentrations of Cy5-N₃ formulated in PGS nanoparticles or in H₂O. (B) Confocal microscopy image (maximum intensity projection (MIP) + orthogonal planes) of SKOV-3 cells pulsed with Cy5-N₃-labelled PGS nanoparticles (red fluorescence). Cell membrane was stained in green with phalloidin-AlexaFluor488 (note that when not permeabilizing the cell membrane with Triton-X, phalloidin behaves as a membrane staining rather than an actin staining). Cell nuclei were stained in blue with Hoechst. (C) Confocal and differential interference contrast (DIC) images of SKOV-3 cells pulsed with Cy5-N₃-labelled PGS nanoparticles (red) and counter-stained with LysoTracker (green). Co-localization is observed as a yellow/orange signal. Note that the dark/bright dots on the DIC image are not lysosomes/endosomes by lipid bodies.

Next, we aimed at exploiting the capacity of the PGS nanoparticles to accommodate hydrophobic drugs. For this purpose, PTX was formulated using a similar protocol as for the formulation of Cy5-N₃-labelled PGS nanoparticles. Paclitaxel has a very low solubility in water and will therefore be largely distributed within the PGS phase. We measured by LC-MS the solubility of PTX in a 10% ethanol in water solution to be only 4.5 μg/mL. By altering the concentrations of PGS and PTX in EtOH, the solvent displacement procedure was optimized for formulation in both H₂O and dextrose 5%. When the formulation contained 5 mg/mL PGS and 0.5 mg/mL PTX, drug precipitation was not observed neither macroscopically (i.e. by visual inspection: **Figure S2 - S3**), nor microscopically (i.e. by optical microscopy: **Figure SA1** or by DLS: **Figure 6** and **Figure S4**). By contrast, PTX similarly diluted from EtOH into deionized H₂O resulted in macroscopic precipitation as confirmed by both optical microscopy (**Figure S2 - S3**) and DLS (**Figure SA2 - SB**). DLS of the PGS/PTX nanoparticles yielded a similar Z-average diameter and low PDI as

compared to the unloaded 5 mg/mL PGS nanoparticles both in H₂O (**Figure 2A** and **Figure 6**) and in dextrose 5 % (**Figure S4**). Additionally, Z-average diameter and PDI remained constant for at least 2 days. This implies that no further work-up would be required. Additionally, when formulated in dextrose 5 %, the obtained formulation could directly be added to an infusion bag as the presence of 10 % of ethanol is not hampering the medical use of the formulation.

To investigate whether indeed PTX is encapsulated within the PGS nanoparticles in amorphous form and not present as PTX nanocrystals stabilized by PGS polymers, we performed X-ray diffraction (XRD). The diffractograms shown in **Figure 7** give clear proof of the highly crystalline nature of PTX and the semi-crystalline nature of PGS as bulk gel material. Upon nanoparticle formation, the crystallinity of PGS is reduced as the peak intensity at 20 is strongly reduced and the peak intensity at 5 is almost fully abolished. The diffractogram of the PGS/PTX nanoparticles on its turn also shows reduced peak intensity of the PGS-related peaks but also does not show any PTX-related peaks. This suggests that PTX is present in amorphous state, likely being molecularly dissolved within the matrix of the PGS nanoparticles. To further explore the potential of the PGS nanoparticles we also attempted the formulation of flubendazole (FLU, **Figure S5**). FLU is an anti-helminthic drug with extremely poor solubility in aqueous medium and with moderate solubility in DMSO and formic acid. Interestingly, FLU has recently been found to exhibit an anti-mitotic effect which suggests its potential use as anti-cancer drug.^[13] Contrary to PTX, FLU-loaded nanoparticles were formulated by solvent displacement from DMSO into water, which required a dialysis period of 3 days to remove the DMSO. This procedure yielded nanoparticles with similar size as PTX/PGS nanoparticles.

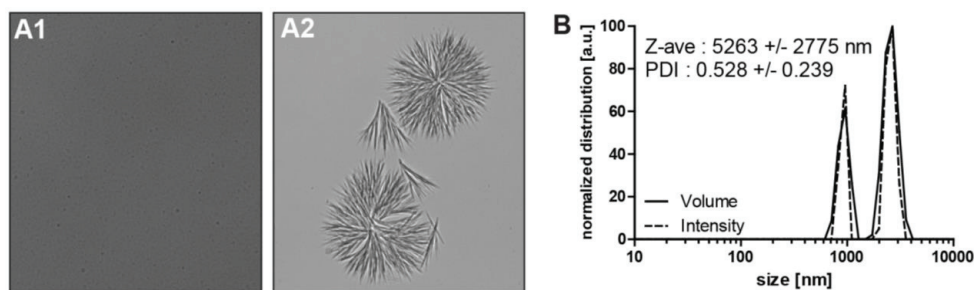


Figure 5. Optical microscopy images of PTX formulated in PGS (**A1**) and diluted from EtOH into H₂O (**A2**). (**B**) Size distribution measured by DLS of PTX diluted from EtOH into H₂O.

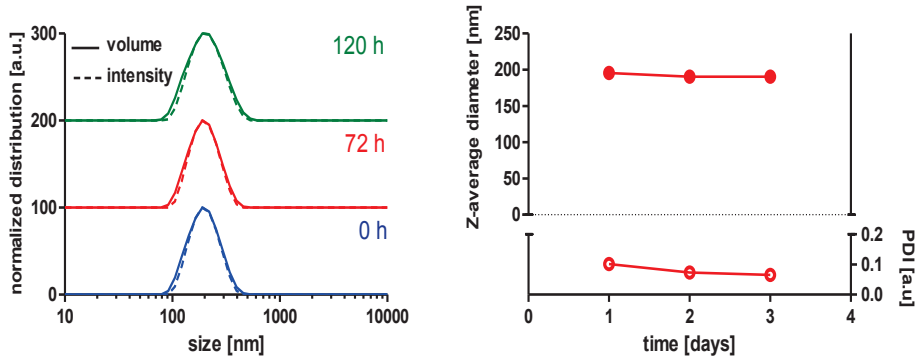


Figure 6. DLS size distribution (A), Z-average diameter and PDI over 3 days (B) of PGS/PTX nanoparticles in H₂O.

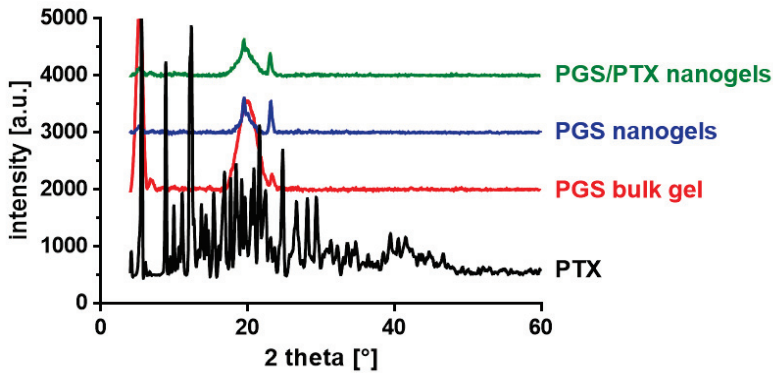


Figure 7. X-ray diffractograms of PTX, PGS and PGS/PTX formulations.

Finally, *in vitro* cytotoxicity of the developed PTX/PGS and FLU/PGS formulations were evaluated on SKOV-3 cells by MTT assay, along with the cytocompatibility of unloaded PGS nanoparticles. Two commercial PTX formulations (i.e. Abraxane and Genexol-PM) were included for comparison. Abraxane is a PTX formulation solubilized and stabilized by albumin, whilst Genexol-PM consists of PTX-loaded polymeric micelles based on monomethoxy poly(ethylene glycol)-*block*-poly(D,L-lactide) (mPEG-*b*-P_{D,L}LA). SKOV-3 cells were incubated for 72 hours to evaluate the *in vitro* cytotoxic effect of PTX. **Figure 8** shows that the PTX/PGS formulation induces similar *in vitro* cytotoxicity compared to Abraxane and Genexol-PM at equal PTX dosing, whilst PGS itself does not exert intrinsic cytotoxic effects, as expected. Even a lower IC₅₀-value was observed for the PTX/PGS formulation (**Table 1**). Cell viability can be decreased to less than 20%, indicating that PTX can be released out of the PGS nanoparticles

and can exert its anti-mitotic effect. The release of PTX could occur both in the cell culture medium and after cellular uptake. Release of PTX in culture medium would most probably be due to passive diffusion out of the nanoparticles and not because of particle disintegration, considering even at a PTX dose of 0.1 $\mu\text{g}/\text{mL}$, the corresponding PGS concentration (i.e. 1 $\mu\text{g}/\text{mL}$) is still above the CAC of PGS (i.e. $0.4 \pm 0.1 \mu\text{g}/\text{mL}$ PGS). Additionally, a significant drop in cell viability was induced by the FLU/PGS formulation as. The lower IC_{50} -value is most likely attributed to the lower intrinsic potency of FLU compared to PTX.

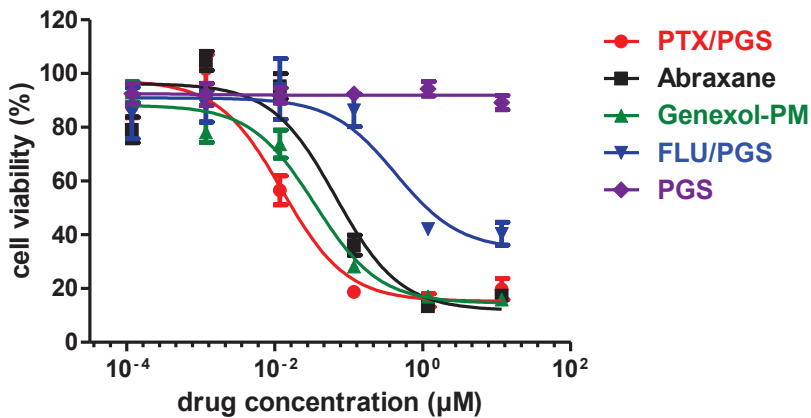


Figure 8. Cell viability measured by MTT assay of SKOV-3 cell treated with unloaded PGS nanoparticles, PTX/PGS and FLU/PGS nanoparticles, Abraxane and Genexol-PM. *The PGS data points refer to the concentration of PGS present at the respective PTX/FLU concentrations (i.e. in the developed PTX/PGS and FLU/PGS formulation, the PGS concentration (in $\mu\text{g}/\text{mL}$) is 10-fold higher than the PTX and FLU concentration) (n = 6).

Table 1. IC_{50} -values of PGS and PTX formulations. (n = 6)

formulation	IC_{50} [nM]
PGS	/
PTX/PGS	13
Abraxane	67
Genexol-PM	35
FLU/PGS	433

3 conclusions

We have shown that PGS is capable of forming well-defined nanoparticles by a very simple solvent displacement method. The produced PGS nanoparticle dispersion is colloidally stable in aqueous medium for prolonged periods of time and a low CAC implies that the formed nanoparticles are unlikely to rapidly disassemble upon dilution. We demonstrated *in vitro* that a hydrophobic fluorescent dye is efficiently endocytosed by cells when loaded into PGS nanoparticles. Finally, a sufficient amount of PTX and FLU could be physically encapsulated into the PGS nanoparticles. MTT assay confirmed the expected intrinsic cytocompatibility of PGS nanoparticle itself, whilst high cytotoxicity was observed for PTX- and FLU-loaded PGS nanoparticles. These data stimulate further exploration to assess whether PGS nanoparticles could serve as a nanomedicine platform for physical encapsulation of hydrophobic drugs.

4 experimental

4.1 materials

Chemicals were purchased from Sigma-Aldrich unless mentioned otherwise. PGS was synthesized as previously reported.²⁷ SEC analysis in dimethylacetamide (DMAc) revealed a M_n of 4.6 kDa Da and a D of 3.7. Cy5-N₃ was obtained from Lumiprobe. Enzyme-free cell dissociation buffer, Dulbecco's modified Eagle medium (DMEM), foetal bovine serum (FBS), L-glutamine, sodium pyruvate, penicillin, streptomycin, Hoechst, Alexa Fluor 488 Phalloidin and LysoTracker Red were obtained from Thermofisher. SKOV-3 cells were supplied by ATCC. Paclitaxel (PTX) was purchased from LC Laboratories.

4.2 nanoparticle formulation

Formulation of the PGS nanoparticles was carried out by a solvent displacement technique. Briefly, 1 mL of PGS stock solution in EtOH (10, 20 or 50 mg/mL) was added dropwise to 10 mL of H₂O under stirring. Nanoparticle size, polydispersity and colloidal stability was analysed by dynamic light scattering (DLS). Measurements were performed at 37 °C on a Zetasizer Nano S (Malvern).

4.3 critical aggregation concentration (CAC)

Following a described protocol, the CAC of PGS nanoparticles was determined by fluorescence spectrometry using pyrene as a fluorescent probe.^[23] First, 2.5 mL serial dilutions of PGS nanoparticles in H₂O were prepared with PGS concentrations ranging from 1×10^{-6} to 1 mg/mL. Second, a 3.6 mg/mL (1.8×10^{-2} M) stock solution of pyrene in acetone was prepared and kept on ice to prevent evaporation of the acetone. Next, 10 μ L of this solution was diluted to 1 mL acetone and kept on ice. To each dilution, 8.3 μ L of the latter pyrene solution was added under stirring leading to a pyrene concentration of 6.0×10^{-7} M. Similarly, the CAC of poly(vinyl alcohol) (PVA) was determined for comparison. Fluorescence excitation spectra were recorded at 20 °C on a Cary Eclipse fluorescence spectrophotometer (Agilent Technologies) equipped with a Varian Cary Temperature Controller. The CAC was quantified based on the change in excitation intensity ratio at 338 and 333 nm with varying concentration.

4.4 x-ray diffraction

X-ray diffractograms were recorded on a Bruker D8 diffractometer.

4.5 cell culture

SKOV-3 (human ovarian cancer cell line) cells were cultured in DMEM, supplemented with 10% FBS, 2 mM L-glutamine, 1 mM sodium pyruvate, and antibiotics (50 units/mL penicillin and 50 μ g/mL streptomycin). Cells were incubated at 37 °C in a controlled, sterile environment of 95 % relative humidity and 5 % CO₂. SKOV-3 cells were used for all cell experiments.

4.6 hydrophobic dye encapsulation

Cy5-N₃-loaded PGS nanoparticles were prepared by co-dissolution in EtOH of Cy5-N₃ (0.2 mg/mL) and PGS (50 mg/mL), followed by solvent displacement in H₂O as described above. Using a similar protocol, a Cy5-N₃ solution in EtOH (0.2 mg/mL) was formulated in 10 mL of H₂O and used as control for further *in vitro* cellular uptake experiments. All samples were filtered (0.450 μ m) before use to remove precipitated dye.

4.7 FACS

SKOV-3 cells were seeded into 24-well titer plates (250 000 cells per well, suspended in 1 mL of culture medium) and incubated overnight. Next 10, 20 or 40 μL of Cy5-N₃-labelled PGS nanoparticle/control was added to the cells followed by 24 hours of incubation to allow cellular uptake. After incubation, wells were aspirated and detached. Cell suspensions were centrifuged (350 g, 7 min, 4 °C). Finally, supernatant was aspirated and the cell pellets were suspended into 350 μL of PBS and kept on ice to maintain cell integrity. FACS was performed on a BD Accuri C6 (BD Biosciences). Data were processed by FlowJo software.

4.8 confocal microscopy

First, a Hoechst stock solution of 1 mg/mL was prepared in dimethyl sulfoxide (DMSO). Alexa Fluor 488 Phalloidin was dissolved in 1.5 mL of methanol to obtain a stock concentration of 6.6 μM . Of these stock solutions, 6 and 35 μL were added to 1.4 mL of PBS supplemented with 1% bovine serum albumin (BSA), respectively. The commercial LysoTracker Red 1 mM stock solution was diluted in culture medium to a working concentration of 60 nM. SKOV-3 cells were plated out on Willco-Dish glass bottom dishes (5 000 cells, suspended in 200 μL of culture medium) and incubated overnight. Next, 5 μL of Cy5-N₃-labelled PGS nanoparticle was added, followed by 24 hours of incubation. Hoechst and Alexa Fluor 488 Phalloidin staining was carried out on fixed cells. In summary, culture medium was aspirated and cells were washed with PBS. Next, 200 μL of 2 % paraformaldehyde was added and allowed to fixate for 15 min. After aspiration and washing, 200 μL of Hoechst-Alexa Fluor 488 Phalloidin working solution was added and incubated for 40 min at room temperature. Finally, the samples were washed with PBS. Further, staining with LysoTracker Red was performed on live cells. Briefly, culture medium was aspirated and cells were washed twice with PBS. Next, 200 μL of LysoTracker Red working solution was added and allowed to incubate for 1.5 h before performing confocal microscopy. Confocal microscopy was carried out on a Leica DMI6000 B inverted microscope equipped with an oil immersion objective (Leica, 63 \times , NA 1.40) and attached to an Andor DSD2 confocal scanner. Images were processed with the ImageJ software package.

4.9 hydrophobic drug encapsulation

PTX/PGS nanoparticles were prepared by co-dissolution of PTX (5 mg/mL) and PGS (50 mg/mL) in EtOH, followed by solvent displacement in H₂O as described earlier.

FLU/PGS nanoparticles were prepared by co-dissolution of FLU (5 mg/mL) and PGS (50 mg/mL) in DMSO, followed by solvent displacement in H₂O as described earlier. The formulation was subsequently dialyzed against H₂O for 3 days (MWCO 3.5 kDa) to remove organic solvent.

4.10 *in vitro* cytotoxicity

MTT assay was performed as previously described.^[23] Dilution series of unloaded PGS nanoparticles were prepared (concentrations ranging from 5×10^{-3} to 5 mg/mL). PTX/PGS and FLU/PGS nanoparticles were diluted (concentrations ranging from 5×10^{-5} to 50 μ g/mL) along with two control nanoparticle formulations: Abraxane (Celgene) and Genexol-PM (Samyang Biopharmaceuticals). The MTT stock solution was prepared by dissolving 100 mg MTT in 20 mL of PBS and subsequent membrane filtration (0.220 μ m). Before use, MTT stock solution was 5-fold diluted with culture medium. Briefly, SKOV-3 cells were seeded into 96-well titer plates (10 000 cells per well, suspended in 200 μ L of culture medium) and incubated overnight. Next, 50 μ L of sample, DMSO (positive control = 0% viability) or H₂O (negative control = 100% viability) was added to the cells followed by 72 hours of incubation. Cells were washed with PBS, 100 μ L MTT working solution was added and incubated for 2.5 hours. Finally, the formed purple formazan crystals were dissolved in 50 μ L of DMSO. Absorbance was determined at 590 nm using an EnVision Multilabel plate reader. The absorbance of the positive control was used as blank and therefore subtracted from all values.

5 references

- [1] R. Jones, *Medicine (Baltimore)* **2016**, *44*, 25–29.
- [2] H. Gelderblom, J. Verweij, K. Nooter, A. Sparreboom, *Eur. J. Cancer* **2001**, *37*, 1590–1598.
- [3] L. B. Norris, Z. P. Qureshi, P. B. Bookstaver, D. W. Raisch, O. Sartor, H. Chen, F. Chen, C. L. Bennett, *Community Oncol.* **2010**, *7*, 425–428.
- [4] A. J. ten Tije, J. Verweij, W. J. Loos, A. Sparreboom, *Clin. Pharmacokinet.* **2003**, *42*, 665–685.
- [5] Z. Weiszhar, J. Czucz, C. Revesz, L. Rosivall, J. Szebeni, Z. Rozsnyay, *Eur. J. Pharm. Sci.* **2012**, *45*, 492–498.
- [6] C. A. Schutz, L. Juillerat-Jeaneret, H. Mueller, I. Lynch, M. Riediker, *Nanomedicine* **2013**, *8*, 449–467.
- [7] R. Wang, P. S. Billone, W. M. Mullett, *J. Nanomater.* **2013**, *2013*, 12.
- [8] S. Svenson, *Curr. Opin. Solid State Mater. Sci.* **2012**, *16*, 287–294.
- [9] J. Fang, H. Nakamura, H. Maeda, *Adv. Drug Deliv. Rev.* **2011**, *63*, 136–151.
- [10] H. Maeda, J. Wu, T. Sawa, Y. Matsumura, K. Hori, *J. Control. Release* **2000**, *65*, 271–284.
- [11] R. K. Jain, T. Stylianopoulos, *Nat. Rev. Clin. Oncol.* **2010**, *7*, 653–664.
- [12] Y. Shi, M. J. van Steenberg, E. A. Teunissen, L. Novo, S. Gradmann, M. Baldus, C. F. van Nostrum, W. E. Hennink, *Biomacromolecules* **2013**, *14*, 1826–1837.
- [13] P. A. Spagnuolo, J. Hu, R. Hurren, X. Wang, M. Gronda, M. A. Sukhai, A. Di Meo, J. Boss, I. Ashali, R. B. Zavareh, et al., *Blood* **2010**, *115*, 4824–4833.
- [14] A. E. Smith, X. W. Xu, C. L. McCormick, *Prog. Polym. Sci.* **2010**, *35*, 45–93.
- [15] S. Binauld, M. H. Stenzel, *Chem. Comm.* **2013**, *49*, 2082–2102.
- [16] K. Ulbrich, K. Hola, V. Subr, A. Bakandritsos, J. Tucek, R. Zboril, *Chem. Rev.* **2016**, *116*, 5338–5431.
- [17] K. Miyata, R. J. Christie, K. Kataoka, *React. Funct. Polym.* **2011**, *71*, 227–234.
- [18] R. Haag, *Angew. Chem. Int. Ed. Engl.* **2004**, *43*, 278–282.
- [19] R. De Coen, N. Vanparijs, M. D. Risseeuw, L. Lybaert, B. Louage, S. De Koker, V. Kumar, J. Grooten, L. Taylor, N. Ayres, et al., *Biomacromolecules* **2016**, *17*, 2479–2488.
- [20] B. Louage, L. Nuhn, M. D. Risseeuw, N. Vanparijs, R. De Coen, I. Karalic, S. Van Calenbergh, B. G. De Geest, *Angew. Chem. Int. Ed. Engl.* **2016**, *55*, 11791–11796.
- [21] L. Nuhn, N. Vanparijs, A. De Beuckelaer, L. Lybaert, G. Verstraete, K. Deswarte, S. Lienenklaus, N. M. Shukla, A. C. Salyer, B. N. Lambrecht, et al., *Proc. Natl. Acad. Sci.* **2016**, *113*, 8098–8103.
- [22] S. Kasmi, B. Louage, L. Nuhn, A. Van Driessche, J. Van Deun, I. Karalic, M. Risseeuw, S. Van Calenbergh, R. Hoogenboom, R. De Rycke, et al., *Biomacromolecules* **2016**, *17*, 119–127.
- [23] B. Louage, Q. Zhang, N. Vanparijs, L. Voorhaar, S. Vande Castele, Y. Shi, W. E. Hennink, J. Van Bocxlaer, R. Hoogenboom, B. G. De Geest, *Biomacromolecules* **2015**, *16*, 336–50.
- [24] Y. Li, W. D. Cook, C. Moorhoff, W.-C. Huang, Q.-Z. Chen, *Polym. Int.* **2013**, *62*, 534–547.
- [25] S.-L. Liang, X.-Y. Yang, X.-Y. Fang, W. D. Cook, G. A. Thouas, Q.-Z. Chen, *Biomaterials* **2011**, *32*, 8486–8496.
- [26] A. Patel, A. K. Gaharwar, G. Iviglia, H. Zhang, S. Mukundan, S. M. Mihaila, D. Demarchi, A. Khademhosseini, *Biomaterials* **2013**, *34*, 3970–3983.
- [27] Y. D. Wang, G. A. Ameer, B. J. Sheppard, R. Langer, *Nat. Biotechnol.* **2002**, *20*, 602–606.
- [28] Q.-Z. Chen, A. Bismarck, U. Hansen, S. Junaid, M. Q. Tran, S. E. Harding, N. N. Ali, A. R. Boccaccini, *Biomaterials* **2008**, *29*, 47–57.
- [29] R. Rai, M. Tallawi, A. Grigore, A. R. Boccaccini, *Prog. Polym. Sci.* **2012**, *37*, 1051–1078.
- [30] S. A. Vitale, J. L. Katz, *Langmuir* **2003**, *19*, 4105–4110.
- [31] M. Beck-Broichsitter, J. Nicolas, P. Couvreur, *Nanoscale* **2015**, *7*, 9215–9221.
- [32] C. Perez, A. Sanchez, D. Putnam, D. Ting, R. Langer, M. J. Alonso, *J. Control. Release* **2001**, *75*, 211–224.

6 supporting info

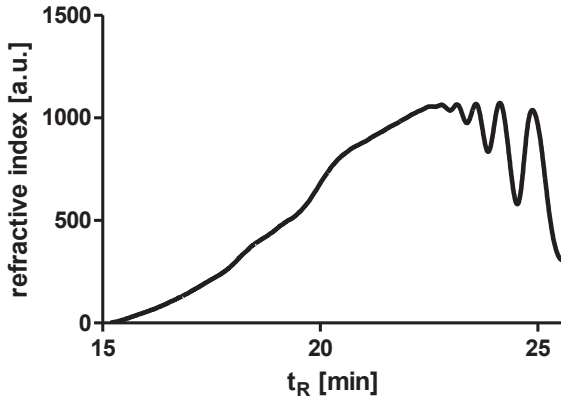


Figure S1. Size exclusion chromatography (SEC)-elugram of PGS.

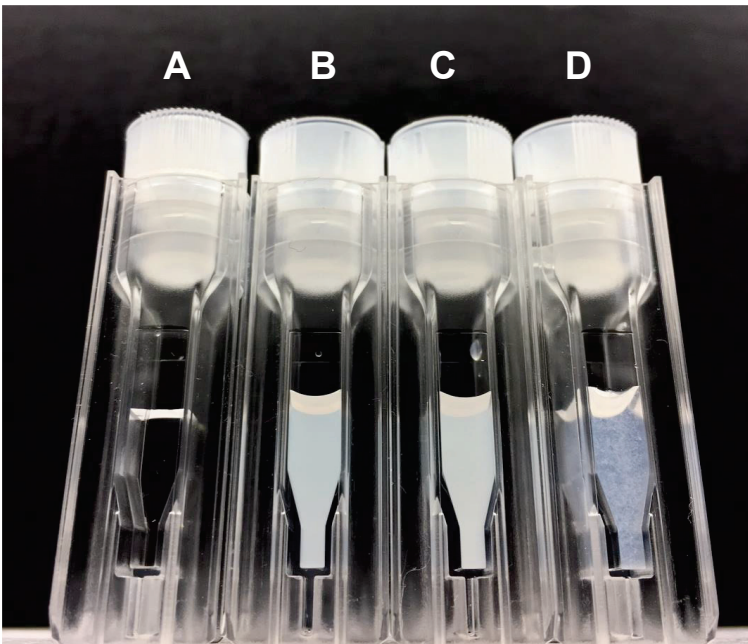


Figure S2. Digital photographs PGS nanoparticles (B), PTX/PGS nanoparticles (C) and pure PTX formulated in H₂O (D), compared with pure H₂O (A).

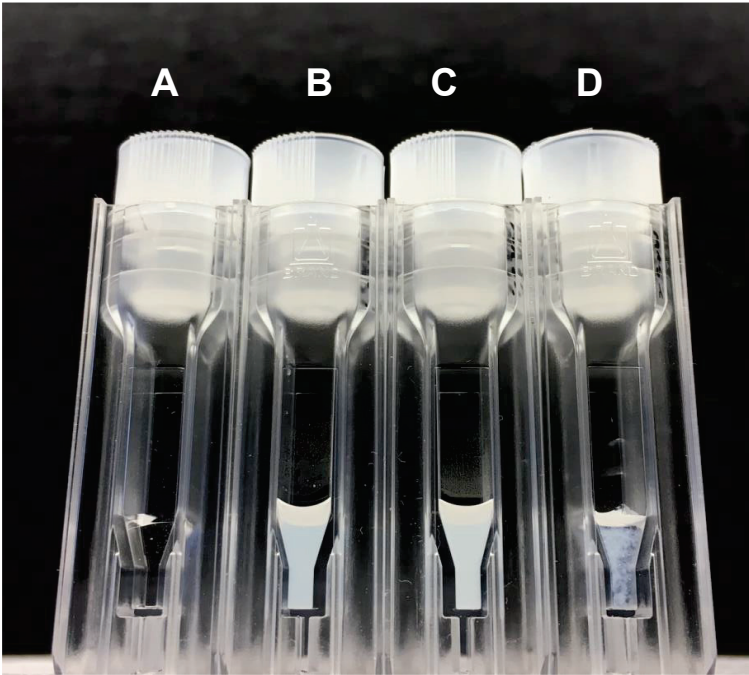


Figure S3. Digital photographs PGS nanoparticles (B), PTX/PGS nanoparticles (C) and pure PTX formulated in physiological glucose solution (i.e. dextrose 5 %) (D), compared with pure dextrose 5 % (A).

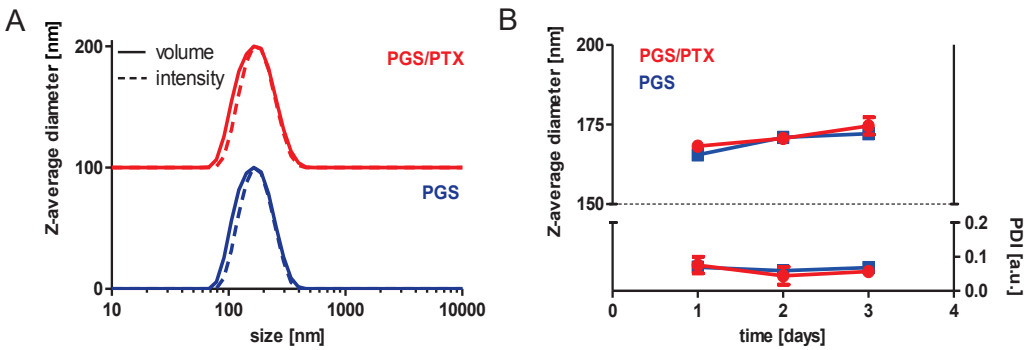


Figure S4. Size (A) and 48-hour stability (B) of PGS and PGS/PTX nanoparticles in dextrose 5 %, measured by DLS at 25 °C.

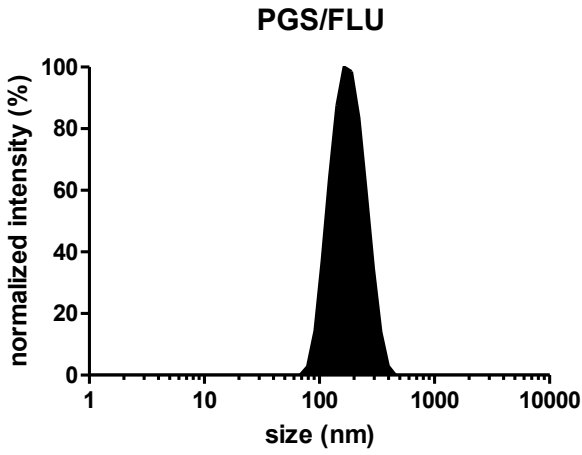


Figure S5. Size distribution (intensity) of PGS/FLU nanoparticles measured by DLS.

chapter 4

degradable ketal-based block copolymer nanoparticles for anti-cancer drug delivery: a systematic evaluation

Benoit Louage,^a Qilu Zhang,^b Nane Vanparijs,^a Lenny Voorhaar,^b Sofie Vande Castele,^c Yang Shi,^d Wim E. Hennink,^d
Jan Van Bocxlaer,^c Richard Hoogenboom,^b Bruno G. De Geest^a

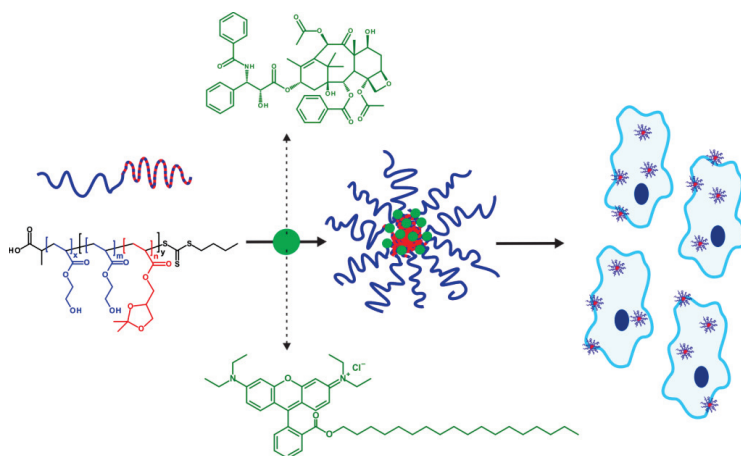
^a Laboratory of Pharmaceutical Technology, Department of Pharmaceutics,
Ghent University, Ottergemsesteenweg 460, 9000 Ghent, Belgium

^b Supramolecular Chemistry Group, Department of Organic and Macromolecular Chemistry, Ghent University,
Krijgslaan 281 S4, 9000 Ghent, Belgium

^c Department of Bioanalysis,
Ghent University, Ottergemsesteenweg 460, 9000 Ghent, Belgium

^d Department of Pharmaceutics, Utrecht Institute for Pharmaceutical Sciences,
Utrecht University, Universiteitsweg 99, 3584CG Utrecht, The Netherlands

Biomacromolecules 2015, 16 (1), 336-50



abstract

Low solubility of potent (anti-cancer) drugs is a major driving force for the development of non-cytotoxic, stimuli-responsive nanocarriers, including systems based on amphiphilic block copolymers. In this regard, we investigated the potential of block copolymers based on 2-hydroxyethyl acrylate (HEA) and the acid-sensitive ketal-containing monomer ([2,2-dimethyl-1,3-dioxolane-4-yl)methyl acrylate (DMDMA) to form responsive drug nanocarriers. Block copolymers were successfully synthesized by sequential reversible addition-fragmentation chain transfer (RAFT) polymerization, in which we combined a hydrophilic poly(HEA)_x block with a (responsive) hydrophobic poly(HEA_m-*co*-DMDMA_n)_y copolymer block. The DMDMA content of the hydrophobic block was systematically varied to investigate the influence of polymer design on physico-chemical properties and *in vitro* biological performance. We found that a DMDMA content higher than 11 mol% is required for self-assembly behavior in aqueous medium. All particles showed colloidal stability in PBS at 37 °C for at least 4 days, with sizes ranging from 23 to 338 nm, proportional to the block copolymer DMDMA content. Under acidic conditions, the nanoparticles decomposed into soluble unimers, of which the decomposition rate was inversely proportional to the block copolymer DMDMA content. Flow cytometry and confocal microscopy showed dose-dependent, active *in vitro* cellular uptake of the particles loaded with hydrophobic octadecyl rhodamine B chloride (R18). The block copolymers showed no intrinsic *in vitro* cytotoxicity whilst loaded with paclitaxel (PTX) a significant decrease in cell viability was observed comparable or better than the two commercial PTX nanoformulations Abraxane and Genexol-PM at equal PTX dose. This systematic approach evaluated and showed the potential of these block copolymers as nanocarriers for hydrophobic drugs.

1 introduction

Even though anti-neoplastic compounds with remarkable potential were already discovered half a century ago, poor solubility in aqueous medium still hampers widespread clinical use.^{[1],[2]} With a solubility of merely 0.3 µg/mL, paclitaxel (PTX) in particular is considered as extremely hydrophobic.^[3] PTX is an important anti-cancer drug, known for inhibiting cell replication by blocking microtubuli depolymerization during the late G2/M phase of the cell cycle. It has shown activity against several cancer types including ovarian, lung, breast, bladder, neck and AIDS-related Kaposi's sarcoma.^{[4],[5]} The clinically used PTX formulation, i.e. Taxol, involves a 50:50 ethanol:Cremophor EL co-solvent mixture to enhance PTX solubility and allow systemic administration of a therapeutic relevant dose. However, severe side effects including anaphylactoid hypersensitivity reactions, hyperlipidaemia, abnormal lipoprotein patterns, aggregation of erythrocytes and peripheral neuropathy have been associated with Cremophor EL upon intravenous administration.^[6] To avoid hypersensitivity, patients are pretreated with corticosteroids and antihistamines which in turn further complicates therapy and quality of life.^[7]

Poor solubility and non-specific pharmacodynamics of conventional chemotherapeutics have strongly contributed to an exponentially growing interest for advanced chemotherapy through nanoscale drug delivery systems.^{[8],[9]} Important assets have been ascribed to nanomedicines.^{[10],[11]} First, the use of alternative carriers can eliminate toxicity of excipients. Second, due to leaky vasculature and impaired lymphatic drainage, solid tumors have the tendency to retain nanoparticles especially when their size is between 10 and 200 nm.^[12] This so-called enhanced permeability and retention (EPR) effect, along with prolonged circulation time, induced by the stealth corona on the surface of the nanoparticles as well as by reduced renal clearance, can lower the effective dose.^{[13],[14]} Third, drug solubility can dramatically be increased by encapsulation into hydrophobic compartments of nanovehicles. These assets have partly been confirmed in the clinic for Abraxane, an FDA-approved 130 nm albumin stabilized (crystalline) paclitaxel formulation which is administered intravenously.^[15] Compared to Taxol, it has reduced systemic toxicity and increased efficacy against several cancer types.^[16] However, the manufacturing of nanocarriers containing recombinant proteins (i.e. human serum albumin in case of Abraxane) remains a costly process.^[17]

Table 1. Block copolymer anti-cancer drug delivery systems in clinical trial.

formulation	block polymer type	diameter	drug	progress
Genexol-PM	mPEG-PDLLA	< 50 nm	PTX	phase II ^a
NK-105	PEG-PAPB	85 nm	PTX	phase II
NK-012	PEG-PGlu-SN-38 conjugate	20 nm	SN-38	phase II
NK-911	PEG-PAsp-DOX conjugate	40 nm	DOX	phase II
NC-6004	PEG-PGlu	30 nm	cisplatin	phase I/II
NC-4016	PEG-PGlu	40 nm	oxaliplatin	phase I
BIND-014	PEG-PDLLA/PEG-PLGA	100 nm	docetaxel	phase I
SP-1049C	Pluronic L61, F127	30 nm	DOX	phase III

Abbreviations: PDLLA, poly(D,L-lactide); PAPB, poly(aspartic acid) modified with 4-phenyl-butanol; PGlu, poly(glutamic acid); PAsp, poly(aspartic acid); PLGA, poly(D,L-lactic-co-glycolic acid); PTX, paclitaxel; SN-83, 7-ethyl-10-hydroxy-camptothecin; DOX, doxorubicin

^a Approved in South Korea in 2007.

Fully synthetic supramolecular polymeric nanostructures form a sound alternative for controlled drug delivery.^[18] In particular nanoparticles composed of amphiphilic block copolymers (e.g. micelles, nanospheres and polymerosomes) have attracted increasing attention owing to their unique features such as small size, high water-solubility, stability in the blood stream and high drug loading capacity and their general *in vitro* and *in vivo* tolerance.^{[19],[20],[21]} In addition, amphiphilic block copolymers can be tailored in terms of responsiveness to stimuli such as temperature, pH, enzymes, oxidation/reduction etc... , allowing straightforward formulation strategies, selective drug release upon cellular uptake and degradation in a biological medium.^{[22],[23],[24],[25],[26]} Finally, the opportunity to engineer drug nanocarriers with targeting moieties enables active tumor targeting which can be crucial in treating metastatic cancer.^{[27],[28]}

Amphiphilic block copolymers can be solid candidates for anti-cancer drug delivery, as several types already made it into clinical trials (**Table 1**).^{[29],[30],[31],[32],[33]} Due to the promising potential of this technology, elaborate research has been conducted the last decade to further fine-tune block copolymer properties. In this way, various pH- and temperature responsive block copolymer systems have been reported in literature.^{[34],[35],[36],[37]} The most widely described temperature-responsive polymeric systems are based on poly(*N*-isopropyl acrylamide) (PNIPAM), poly(oligo(ethylene glycol) (meth)acrylate) (OEG(M)A) or poly(2-oxazoline) (POx) which exhibit a lower

critical solution temperature (LCST) within the physiological relevant range in aqueous medium.^{[38],[39],[40],[41]} Reversible pH-sensitive systems have been developed using functional moieties of which the hydrophobicity is altered by protonation and deprotonation (e.g. tertiary amino groups).^[42] In this way, Armes and co-workers reported on pH-sensitive vesicles based on a 2-(methacryloyloxy)ethyl phosphorylcholine (MPC) and 2-(diisopropylamino)ethyl methacrylate (DPA) diblock copolymer.^[42] This system forms vesicles at pH > 6 and dissolves at lower pH values due to protonation of DPA, inducing a fast release of payload. A possible risk, however, of such reversible systems is bioaccumulation as re-self-assembly can occur when the polymers exit acidic organelles (i.e. endosomes and lysosomes). This can be circumvented by using functional groups which irreversibly switch into hydrophilic moieties under acidic conditions. Next to imines, hydrazides, hydrazones, orthoesters and oximes, ketals are of particular interest due to their non-cytotoxic nature.^{[43],[44],[45],[46],[47],[48]} Several pH-sensitive ketal-based polymeric structures have been reported (e.g. micelles and microparticles).^{[49],[50]} The irreversible hydrolysis of ketals at pH < 5 allows endosomal (pH 4 – 5.5) degradation and drug release. Furthermore, irreversible hydrolysis leads to fully soluble polymeric degradation products which should afford better (renal) clearance from the body.^[51]

Reversible addition-fragmentation chain transfer (RAFT) polymerization has proven to be a powerful technique for the preparation of well-defined amphiphilic block copolymers.^{[52],[53],[54]} Compared to other controlled radical polymerizations (CRP) such as nitroxide-mediated polymerization (NMP) and atom transfer radical polymerization (ATRP), RAFT polymerization excels in its versatility.^{[55],[56],[57]} A wide variety of (functional) monomers can be prepared by RAFT polymerization in different solvents under mild reaction conditions. Finally, the technique's high end-group fidelity at reasonably high conversion (80 %) offers the opportunity for pre- and post-functionalization, e.g. with cell receptor specific targeting ligands and proteins.^{[58],[59],[60]} Recently, we have reported on the RAFT copolymerization of (2,2-dimethyl-1,3-dioxolane-4-yl)methyl acrylate (DMDMA), a monomer containing a ketal functional group, with either methoxy tri(ethylene glycol) acrylate (mTEGA) or 2-hydroxyethyl acrylate (HEA).^{[61],[62]} These copolymers proved to exhibit LCST behavior which can be tailored by varying the DMDMA feed ratio. The copolymers degraded into fully soluble unimers under acidic conditions and furthermore showed promising *in vitro* cytocompatibility. When using HEA as co-monomer, a significantly faster degradation rate was witnessed. This can be ascribed to the higher exposure of the DMDMA units to the acidic aqueous medium in copolymers with HEA, whereas DMDMA units are more shielded from exposure to the aqueous environment in copolymers with the more bulky mTEGA monomer.

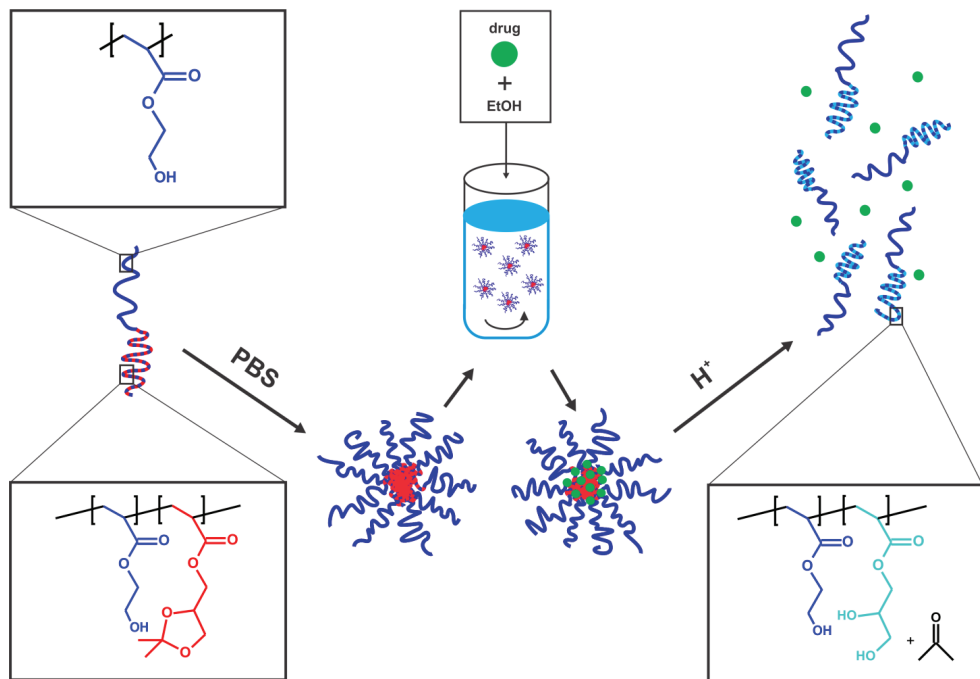


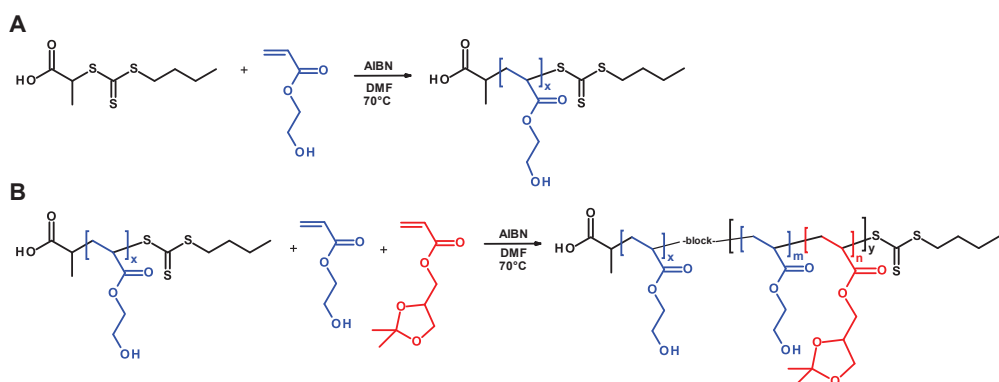
Figure 1. Self-assembly behavior, loading strategy (solvent displacement) and acid-triggered degradation of responsive poly(HEA)_x-*b*-poly(HEA_m-*co*-DMDMA_n)_y block copolymer drug nanocarriers.

In this paper we report on the synthesis of responsive acid-degradable block copolymers based on HEA and DMDMA by RAFT polymerization, using a macroCTA (macro chain transfer agent) approach, to exploit the faster degradation of these copolymers.^[63] The general block copolymer structure consists of a hydrophilic poly(HEA)_x block and a (responsive) hydrophobic poly(HEA_m-*co*-DMDMA_n)_y block, as shown in **Figure 1**. The main focus of this study was to systematically examine the influence of polymer design on self-assembly behavior, physico-chemical properties (critical aggregation concentration (CAC), colloidal stability and pH-responsive behavior), drug loading properties and *in vitro* biological performance by varying the DMDMA content of the hydrophobic block. The applied loading strategy (solvent displacement) is shown in **Figure 1**, along with the rationale for acidic DMDMA hydrolysis. The latter involves the change of the hydrophobic ketal functional group into a hydrophilic glycerol moiety inducing supramolecular disassembly and release of payload, as the hydrophobic block gradually turns hydrophilic. In this way, we systematically evaluated the potential of these block copolymers for their use as nanocarrier for PTX as hydrophobic anti-cancer drug.

2 results and discussion

2.1 synthesis poly(HEA)_x macroCTA

Amphiphilic block copolymers were prepared by sequential RAFT polymerization, starting with the synthesis of poly(2-hydroxyethylacrylate) (poly(HEA)_x). This polymer serves as hydrophilic polymer block and is subsequently used as macroCTA for chain extension with a second responsive block consisting of both HEA as hydrophilic monomer and DMDMA as hydrophobic acid-degradable ketal monomer (**Scheme 1A**). Synthesis of poly(HEA)_x was terminated at 70 % conversion as determined by GC. SEC analysis in DMA showed a number average molecular weight (M_n) of 12.8 kDa and a dispersity (\mathcal{D}) of 1.11. No significant low or high molecular weight shoulders could be observed on the SEC trace (**Figure S1**), indicating the formation of a well-defined polymer. The latter is necessary for further use as macroCTA for subsequent block copolymerization.



Scheme 1. Synthesis of **(A)** poly(HEA)_x macroCTA and **(B)** poly(HEA)_x-*b*-poly(HEA_m-*co*-DMDMA_n)_y. HEA and DMDMA are depicted in blue and red, respectively.

2.2 synthesis and characterization poly(HEA)_x-*b*-poly(HEA_m-*co*-DMDMA_n)_y

To allow for a systematic investigation on how the HEA:DMDMA feed ratio of the second block influences the structural block copolymer composition and properties, we used an automated synthesis robot. The advantage of this approach is, next to the obviously improved time efficiency, the reduced inter-experiment variability as well as the ability to automatically withdraw samples during the polymerizations to study their kinetics. The poly(HEA)_x macroCTA was used as hydrophilic block to which five different HEA:DMDMA molar feed ratios (40:10, 30:20, 25:25, 20:30, 10:40) were added to form a hydrophobic, responsive second block (**Scheme 1B**). In addition to triple

precipitation, the polymers were further purified by extensive dialysis to remove any residual solvent and monomer, as the latter two can influence *in vitro* cell culture experiments. Note that we did not synthesize block copolymers with a fully DMDMA-based hydrophobic block as preliminary experiments showed such block copolymers to form macroscopic aggregates in aqueous medium.

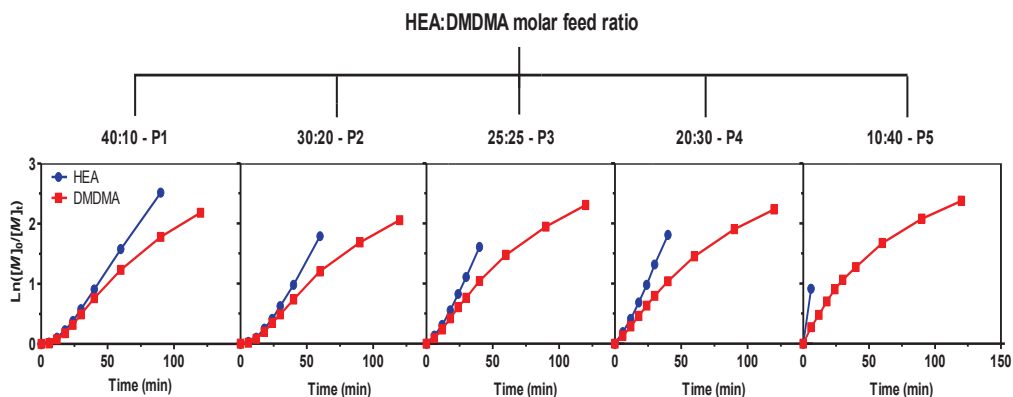


Figure 2. First order kinetic plots for the copolymerization of HEA (blue) and DMDMA (red) using the poly(HEA)_x macroCTA resulting in poly(HEA)_x-*b*-poly(HEA)_m-*c*c-DMDMA_n)_y.

Kinetic samples of the copolymerization reactions were analyzed by GC and SEC (SEC traces are shown in **Figure S2**) to determine the evolution of monomer conversion and the resulting polymer molar mass (distribution) in time. Initially, a linear increase of $\text{Ln}([M]_0/[M]_t)$ as function of reaction time is observed for both HEA and DMDMA (**Figure 2**). After nearly complete consumption of HEA, the polymerization rate for DMDMA decreases indicating that the HEA chain end is more reactive towards DMDMA than the DMDMA chain end. The lower reactivity of DMDMA might be related to its bulkier side chain. The copolymerization behavior of HEA and DMDMA was also evaluated by determination of the reactivity ratios by non-linear least square fitting of the incorporated HEA mol fraction (f_{HEA}) versus the theoretical HEA mol fraction (F_{HEA}) using the Contour software.^[71] As the copolymerization with 10:40 HEA:DMDMA ratio was so fast that only one data point for HEA was obtained at $\text{Ln}([M]_0/[M]_t)$ corresponding to 60% conversion, this copolymerization was not included in the fit. Furthermore, to exclude effects of equilibration of the RAFT polymerization process, f_{HEA} was determined at ~30 % conversion of HEA based on the GC kinetic data. The resulting reactivity ratios are $r_{\text{HEA}} = 1.07 \pm 0.09$ and $r_{\text{DMDMA}} = 0.62 \pm 0.07$, whereby it should be noted that these values are rough estimates as they are only based on four data points ($F_{\text{HEA}} = 0.4, 0.5, 0.6$ and 0.8 with $f_{\text{HEA}} = 0.472, 0.557,$

0.650 and 0.822, respectively). These reactivity ratios imply that the composition of the poly(HEA_m-*c*o-DMDMA_n)_y block gradually changes from being HEA rich to being DMDMA rich. This is schematically illustrated based on the calculated monomer distributions for the synthesized block copolymers by regression analysis of the GC kinetics (Figure 3). Furthermore, SEC analysis shows a linear increase of M_n with conversion and a narrow \mathcal{D} indicating good control over the polymerization (Figure 4). The composition of the different block copolymers is listed in Table 2. For each block copolymer, a clear similarity is observed between the overall DMDMA composition when calculated from GC and ¹H-NMR spectroscopy data. ¹H-NMR spectra with peak integrations are shown in Figure S3 → S7 for P1 → P5.

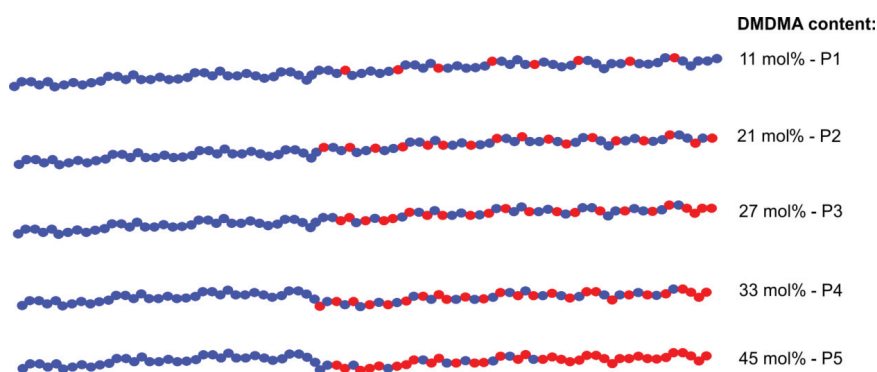


Figure 3. Average monomer distributions, calculated by regression analysis of the conversion versus time data, for the synthesized poly(HEA)_x-*b*-poly(HEA_m-*c*o-DMDMA_n)_y block copolymers. The blue and red dots represent HEA and DMDMA, respectively.

Table 2. Compositional data for the synthesized polymers.

polymer	[HEA] ₀	conversion	[HEA] ₀	conversion	[DMDMA] ₀	conversion	mol%	mol%	M_n	\mathcal{D}
	[CTA]	HEA (%) ^a	[mCTA]	HEA (%) ^a	[mCTA]	DMDMA (%) ^a	DMDMA ^b	DMDMA ^c		
	hydrophilic block		responsive block							
mCTA [*]	50	70	-	-	-	-	-	-	12.8	1.11
P1	50	70	40	100	10	89	11	12	26.6	1.22
P2	50	70	30	100	20	87	21	24	24.7	1.20
P3	50	70	25	100	25	90	27	27	26.2	1.21
P4	50	70	20	100	30	89	33	32	25.7	1.20
P5	50	70	10	100	40	91	45	39	24.3	1.20

^a Calculated by GC using DMF as internal standard. ^b Overall DMDMA composition calculated by GC. ^c Overall DMDMA composition determined by ¹H-NMR spectroscopy. ^d Analyzed by SEC. ^{*} mCTA = macroCTA

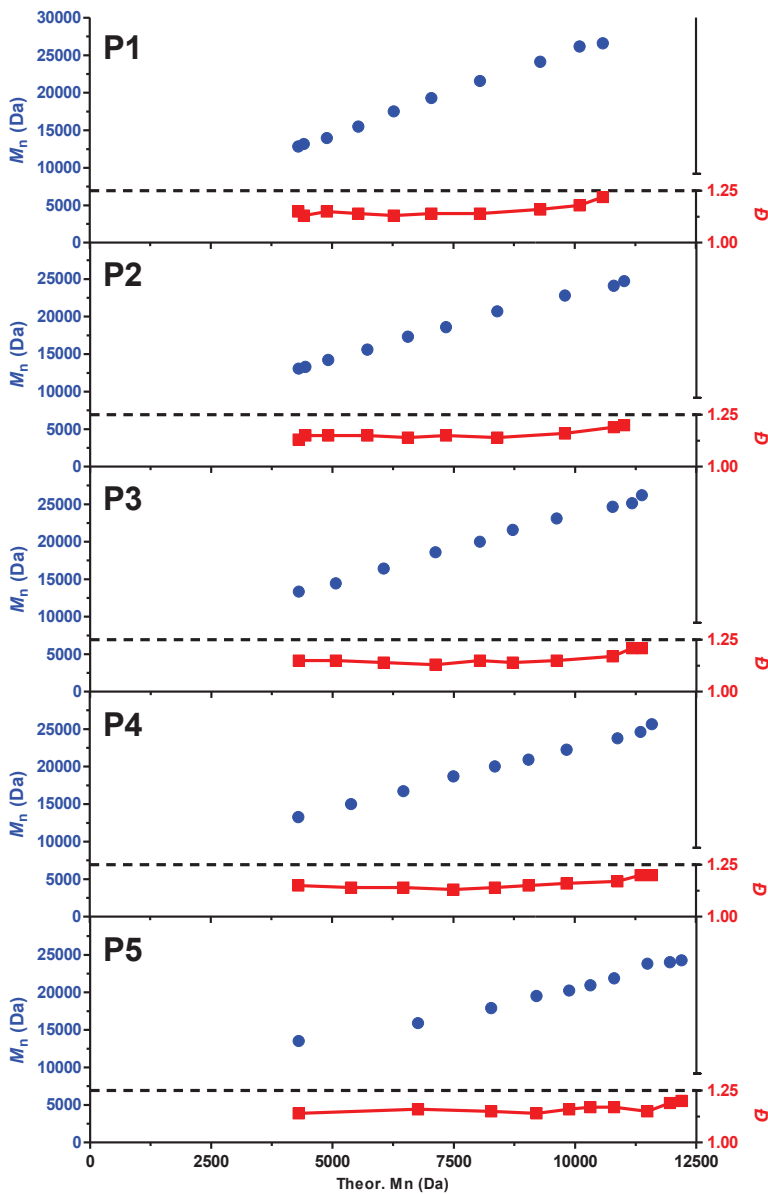


Figure 4. M_n and D (determined by SEC) plots as function of theoretical M_n (based on GC) for the kinetic study for the synthesis of poly(HEA)_x-*b*-poly(HEA_m-*c*-DMDMA_n)_y.

2.3 self-assembly and temperature-responsive behavior in aqueous medium

To investigate the influence of the DMDMA content on the self-assembly behavior and temperature-responsive properties, the block copolymers were dispersed (concentration 5 mg/mL) in cold phosphate buffered saline (PBS, pH 7.4, 150 mM NaCl) and subsequently measured by dynamic light scattering (DLS) at different temperatures (5, 20 and 37 °C). Normalized intensity and corresponding volume size distribution histograms of the particles, measured at increasing temperatures (5, 20 and 37 °C), are shown in **Figure 5A**. The corresponding Z-Average hydrodynamic diameter and polydispersity (PDI) are plotted in **Figure 5B** as function of temperature and the DMDMA content of the poly(HEA)_x-*b*-poly(HEA_m-*c**o*-DMDMA_n)_y block copolymers (**Table 2**). A bimodal intensity size distribution is observed for the block copolymer with the lowest DMDMA content (i.e. 11 mol%, P1). The highest intensity is observed for a distribution with a size around 4 nm, representing soluble unimers. Furthermore, loose aggregates (60 – 300 nm) are detected, as often observed for thermoresponsive polymers.^{[72],[73],[74]} However, the fraction of aggregates for P1 is limited, as the latter is not observed in the corresponding the volume size distribution of P1 (**Figure 5A**). The graphs show that the DMDMA content drastically affects the particle size. A larger particle diameter is measured with increasing DMDMA content. P2 , P3 and P4 (containing 21, 27 and 33 mol% DMDMA, respectively) likely form micelles, whereas P5 (45 mol% DMDMA) forms larger assemblies. This trend is in line with the expectations as in aqueous medium, hydrophobic molecules are more likely to interact mutually than with water instead, therefore generating larger assemblies.

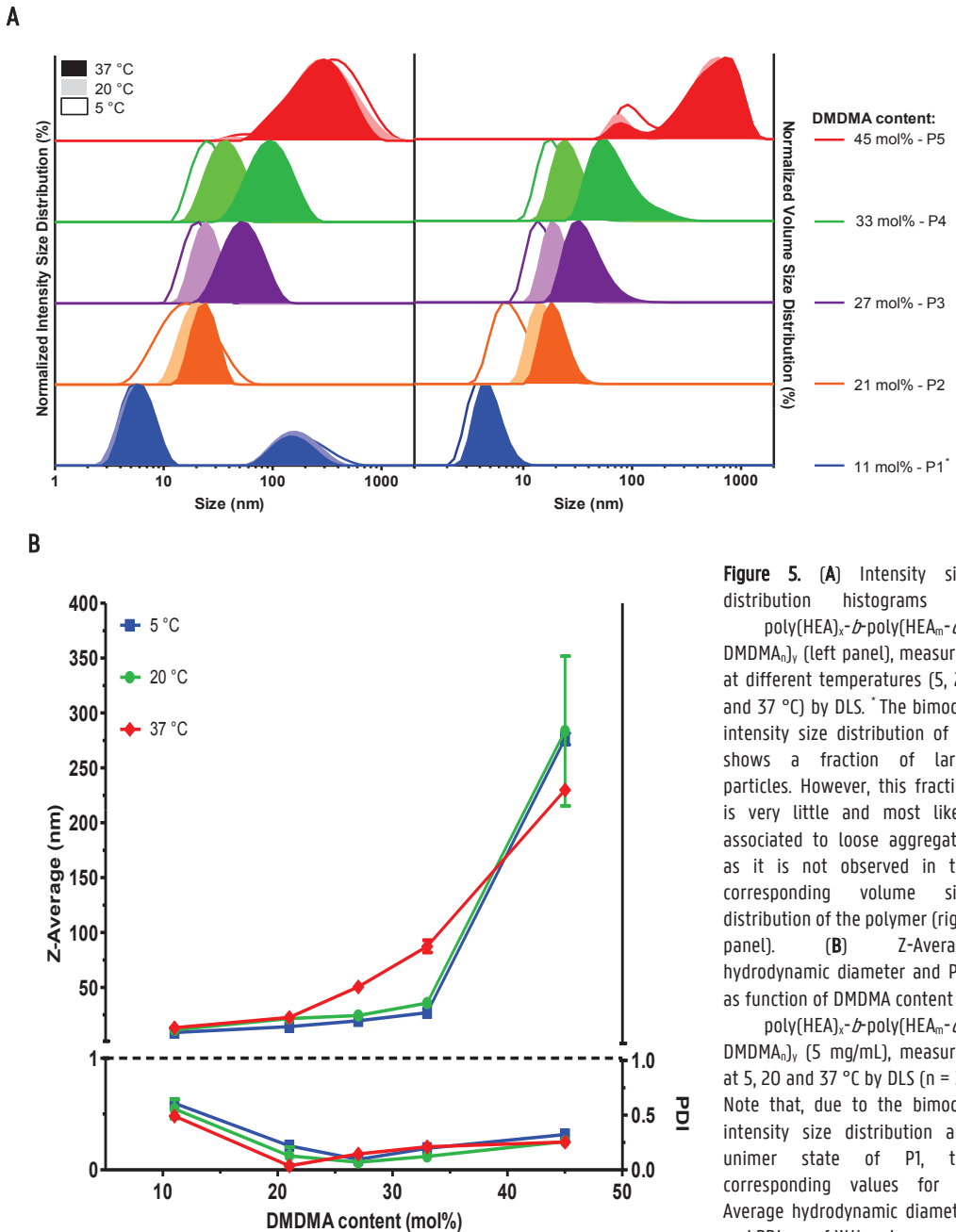


Figure 5. (A) Intensity size distribution histograms of poly(HEA)_x-*b*-poly(HEA_m-*co*-DMDMA_n)_y (left panel), measured at different temperatures (5, 20 and 37 °C) by DLS. The bimodal intensity size distribution of P1 shows a fraction of large particles. However, this fraction is very little and most likely associated to loose aggregates as it is not observed in the corresponding volume size distribution of the polymer (right panel). (B) Z-Average hydrodynamic diameter and PDI as function of DMDMA content of poly(HEA)_x-*b*-poly(HEA_m-*co*-DMDMA_n)_y (5 mg/mL), measured at 5, 20 and 37 °C by DLS (n = 3). Note that, due to the bimodal intensity size distribution and unimer state of P1, the corresponding values for Z-Average hydrodynamic diameter and PDI are of little relevance.

The block copolymers with 21, 27 and 33 mol% DMDMA (P2, P3 and P4, respectively) show an increase in particle size upon increasing temperature, indicating the temperature-responsive behavior of these polymers. This influence of temperature was not unexpected, as our previously reported poly(mTEGA_m-*co*-DMDMA_n)_y and poly(HEA_m-*co*-DMDMA_n)_y copolymers exhibited similar LCST behavior.^{[61],[62]} On the other hand, temperature exerted minimal effect on the block copolymers with the lowest (11 mol%, P1) and highest (45 mol%, P5) DMDMA content which form either mainly soluble unimers (P1) or larger aggregates (P5), respectively, with constant size irrespective of temperature. Note that the observed trends in particle size are not due to time-dependent aggregation as the nanoparticle size remained constant over at least 4 days as shown further on in this paper (Figure 7). The values for Z-Average hydrodynamic diameter and PDI against temperature are summarized for all block copolymers in Table 3. Note that a relatively low PDI is observed for all samples except for P1, due to its bimodal intensity size distribution.

2.4 critical aggregation concentration (CAC)

To compare the minimally required polymer concentration in aqueous medium for self-assembly of the different block copolymers, the excitation intensity ratio of pyrene at 338 nm (I_3) and 333 nm (I_1) was plotted versus the concentration of poly(HEA)_x-*b*-poly(HEA_m-*co*-DMDMA_n)_y in PBS at 20 °C (Figure 6A). The subsequent calculated CACs are shown in Table 3 and Figure 6B (see Figure S8 for CAC fitting parameters of each block copolymer individually). The CAC of the block copolymers decreased from 241 to 10 µg/mL with increasing DMDMA content from 11 (P1) to 45 (P5) mol%. Increasing hydrophobicity contributes to lowering of CAC because of more pronounced hydrophobic interactions. The observation that P1 does show a relatively high CAC although DLS does not show extensive particle formation (Figure 5A and 7), indicates that the presence of DMDMA does allow for a certain extent of hydrophobic interaction between pyrene and P1, possibly related to hydrophobic interactions occurring within the unimers or the loose aggregates. Similar observations were made by others, e.g. Hennink and co-workers observed that addition of PTX from ethanol to an aqueous solution containing a temperature-responsive polymer below its phase transition temperature did not lead to immediate precipitation of PTX.^[4] This behavior was ascribed to hydrophobic interaction between PTX and hydrophobic repeating units in the polymer backbone.

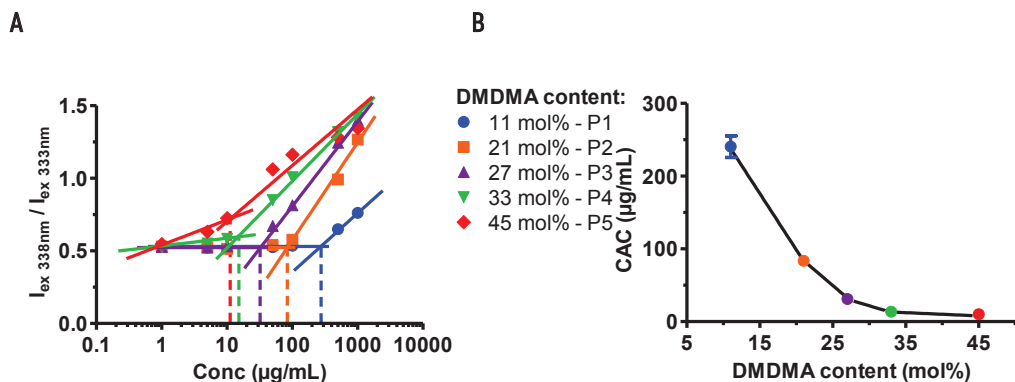


Figure 6. (A) Intensity ratio of pyrene at 338 nm (I_3) and 333 nm (I_1) as function of poly(HEA) $_x$ -*b*-poly(HEA $_m$ -*co*-DMDMA $_n$) $_y$ concentration, determined by fluorescence spectrophotometry at 20 °C ($n = 2$). (B) CAC of poly(HEA) $_x$ -*b*-poly(HEA $_m$ -*co*-DMDMA $_n$) $_y$ at 20 °C as function of DMDMA content ($n = 2$).

Table 3. Supramolecular characteristics of synthesized block copolymers.

polymer	mol% DMDMA ^a	5 °C		20 °C		37 °C		CAC (µg/mL) ^c
		Z-Average	PDI ^b	Z-Average	PDI ^b	Z-Average	PDI ^b	
		(nm) ^b		(nm) ^b		(nm) ^b		
P1	11	8.9 ± 0.4	0.61 ± 0.02	11.4 ± 1.8	0.56 ± 0.09	13.4 ± 1.0	0.49 ± 0.04	241 ± 15
P2	21	14.4 ± 0.1	0.22 ± 0.01	21.7 ± 3.4	0.13 ± 0.08	23.3 ± 0.5	0.05 ± 0.01	84 ± 4
P3	27	19.6 ± 0.6	0.10 ± 0.03	24.4 ± 1.2	0.07 ± 0.04	52.7 ± 0.1	0.16 ± 0.01	31 ± 1
P4	33	27.0 ± 0.8	0.20 ± 0.01	35.8 ± 5.0	0.12 ± 0.01	100.4 ± 0.6	0.24 ± 0.01	14 ± 1
P5	45	276.5 ± 5.3	0.32 ± 0.03	283.6 ± 68.2	0.26 ± 0.03	337.7 ± 6.1	0.23 ± 0.05	10 ± 1

^a Overall DMDMA composition based on GC data. ^b Numeric values for Z-Average hydrodynamic diameter and PDI of poly(HEA) $_x$ -*b*-poly(HEA $_m$ -*co*-DMDMA $_n$) $_y$, measured at 5, 20 and 37 °C ($n = 3$) by DLS. ^c CAC at 20 °C ($n = 2$).

2.5 *in vitro* stability and pH-responsive behavior

At first, we aimed at investigating the colloidal stability of the block copolymer assemblies at pH 7.4 and gaining proof-of-concept for the acidic hydrolysis of the DMDMA repeating units (**Figure 1**). To examine whether the poly(HEA)_x-*b*-poly(HEA_m-*co*-DMDMA_n)_y nanoparticles are stable when dispersed in PBS or show aggregation over time, the block copolymer assemblies in PBS (see **section 2.3**) were measured over 4 days at 37 °C by DLS. Measurements were performed in triplicate. As shown in **Figure 7**, all nanoparticles remained stable at pH 7.4 for at least 4 days. Particle stability at physiological pH is essential to avoid premature drug release before the nanoparticles are internalized by cells.

On day 4, HCl was added to obtain a HCl concentration of 100 mM (pH 1). To examine the effect on the potential acidic hydrolysis of the ketal groups in the block copolymer side chains, the Z-Average hydrodynamic diameter, light scattering intensity and size volume distribution profiles were monitored by DLS. As shown in **Figure 7**, all block copolymer dispersions, except the block copolymer with 11 mol% DMDMA (P1), exhibit a gradual decrease in Z-Average diameter, light scattering intensity and volume size distribution. The reason that this is not observed for P1 can be ascribed to the unimer state of this polymer which won't be affected by hydrolysis of its ketal moieties. The reason that often a bimodal distribution emerges during degradation is likely to be attributed to the inherent dynamic nature of block copolymer micelles, especially when their thermodynamic equilibrium is shifting due to hydrolysis of the DMDMA repeating units. The general decrease in size and scattering intensity suggests that in acidic medium, hydrolysis of the ketal groups effectively leads to decomposition of the block copolymer nanoparticles into soluble unimers. The latter is confirmed by ¹H-NMR spectroscopy (**Figure 8**) showing complete absence of the ketal groups for the block copolymer with 21 mol% DMDMA (P2) after hydrolysis. Similar observations were done for the block copolymer with 45 mol% DMDMA (P5) (**Figure S9**). Interestingly, from the evolution of the Z-average diameter and the scattering intensity as function of time, one can observe that the rate of hydrolysis depends on the DMDMA content, with hydrolysis being significantly slower as the hydrophobic poly(HEA_m-*co*-DMDMA_n)_y copolymer block contains more DMDMA repeating units and *gradient* structure. This slower hydrolysis can be ascribed to the stronger hydrophobic interactions within the polymers with higher DMDMA content, leading to stronger dehydration of the hydrophobic core domains and thereby decreased contact with HCl. Furthermore, a larger extent of DMDMA units needs to be hydrolyzed for the more hydrophobic block copolymers to render them hydrophilic enough for disassembly of the self-assembled structures.

2.6 *in vitro* cellular uptake

Next, we investigated the potential of the block copolymers for intracellular delivery of a hydrophobic payload. For this purpose we used the SKOV-3 human ovarian cancer cell line. Block copolymer nanoparticles were loaded with octadecyl rhodamine B chloride (R18), a fluorescent dye suitable for staining embedded hydrophobic moieties (**Figure S10**).^[75] The encapsulation was performed by adding a R18 stock solution in ethanol to a block copolymer dispersion (10 mg/mL) in PBS at a 1:10 volume ratio under stirring. R18 in pure PBS was used as a control. Subsequently, cellular uptake of the samples was assessed by flow cytometry (FACS) and confocal microscopy.

Flow cytometry shows a dose-dependent increase in fluorescence (**Figure 9A**) and percentage of rhodamine positive cells (**Figure 9B**) for all poly(HEA)_x-*b*-poly(HEA_m-*co*-DMDMA_n)_y nanoparticles, whereas no difference is observed between blank cells and cells pulsed with R18 in PBS. The latter indicates that the hydrophobic dye needs to be encapsulated in order to be internalized by cells. Earlier in this paper it was already shown that a 5 mg/mL dispersion in PBS of the block copolymer with 11 mol% DMDMA (P1) mainly consisted out of soluble unimers. This in turn explains why the R18-labeled formulation of P1 shows significantly lower cellular uptake compared to the other block copolymer formulations at the same concentration.

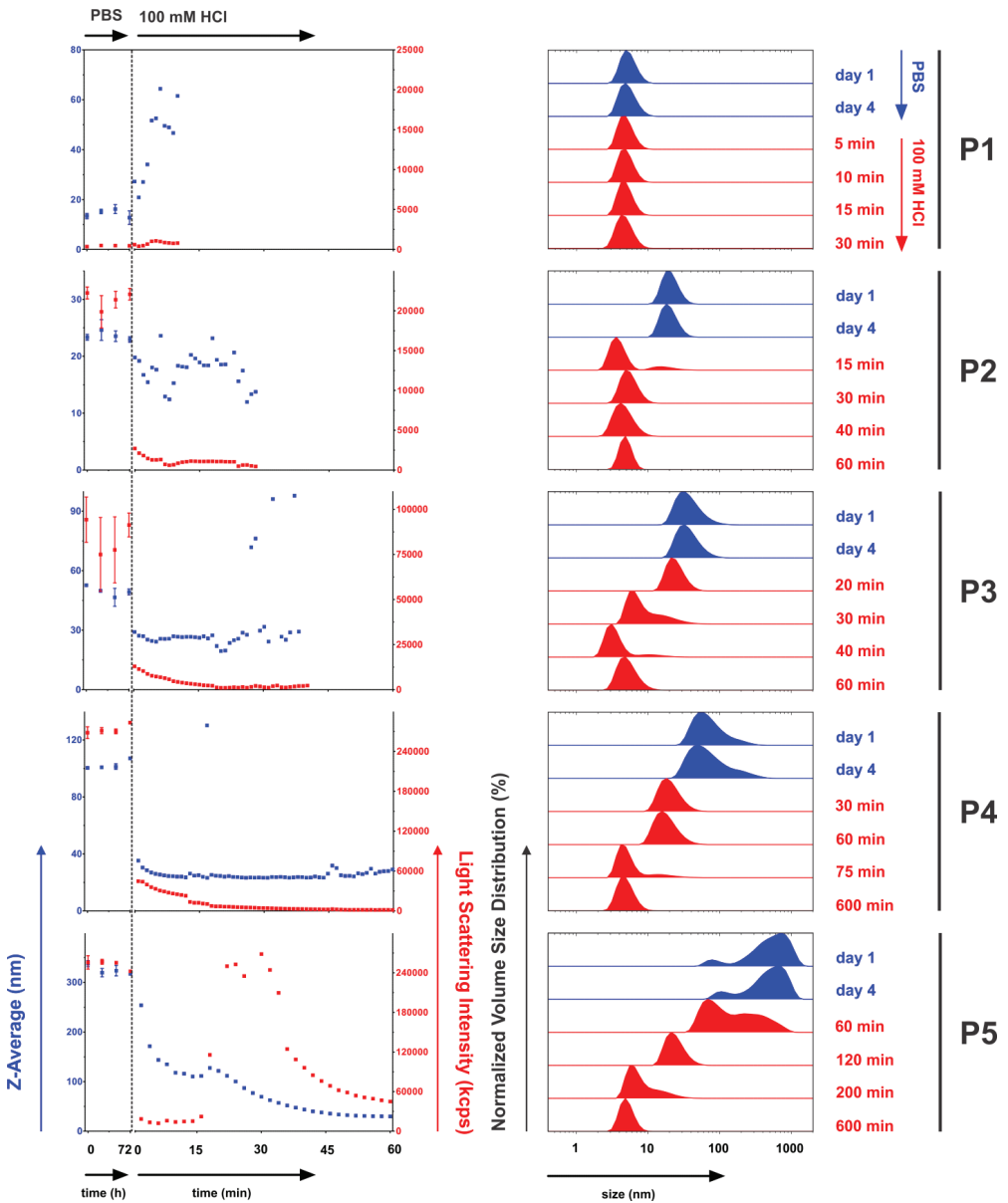


Figure 7. (Left panels) Z-Average diameter and light scattering intensity of the block copolymers as function of time, measured at 37 °C by DLS. The block copolymers were measured over 4 days in PBS ($n = 3$) after which HCl was added to obtain a HCl concentration of 100 mM (pH 1). (Right panels) Corresponding volume distribution histograms.

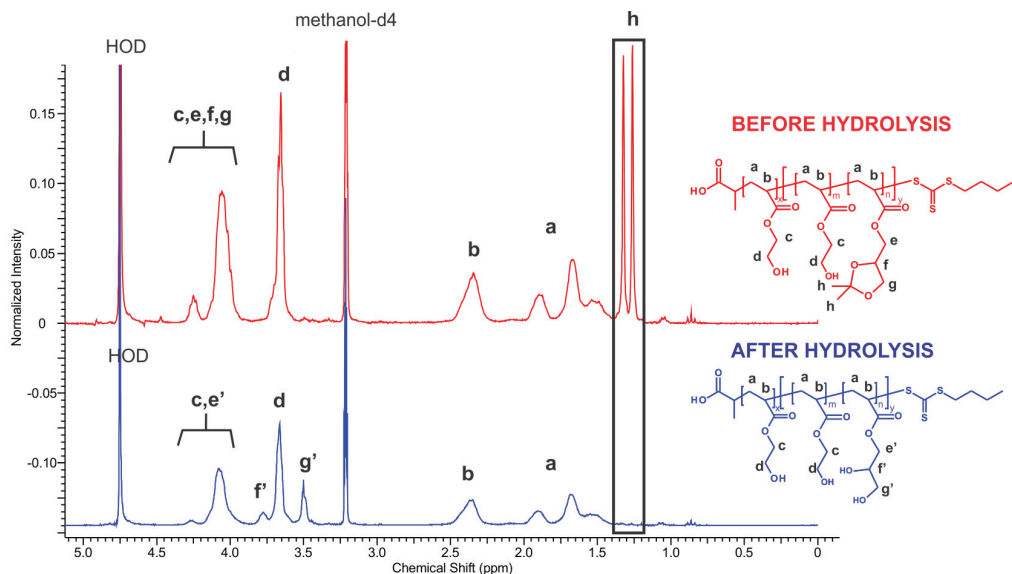


Figure 8. $^1\text{H-NMR}$ spectrum of P2 (21 mol% DMDMA) before (red) and after (blue) hydrolysis. Note the absence of the ketal functional group after hydrolysis.

Confocal microscopy was used to investigate the intracellular fate of the block copolymer nanoparticles in more detail. In particular confocal microscopy allows distinguishing between internalized and cell membrane bound nanoparticles. Fixed SKOV-3 cells were pulsed with Hoechst and Alexa Fluor 647 Phalloidin to stain the cell nuclei and the actin filaments, respectively. As shown in maximized intensity projections (MIPs) (**Figure 10**), cellular uptake of R18-loaded particles (depicted in red) is observed for all block copolymers except P1. The latter was similar to the blank which is in line with previous experiments showing absence of particle formation for this block copolymer. To further elucidate the intracellular fate of the observed nanoparticles, live SKOV-3 cells were stained with LysoTracker Deep Red. This is a fluorescent acidotropic probe, selectively accumulating in acidic organelles of live cells, e.g. endosomes and lysosomes. Presence of fluorescent nanoparticles in these organelles is confirmed by colocalization between red and green fluorescence (**Figure 11**), suggesting active intracellular uptake of the nanoparticles.^[76]

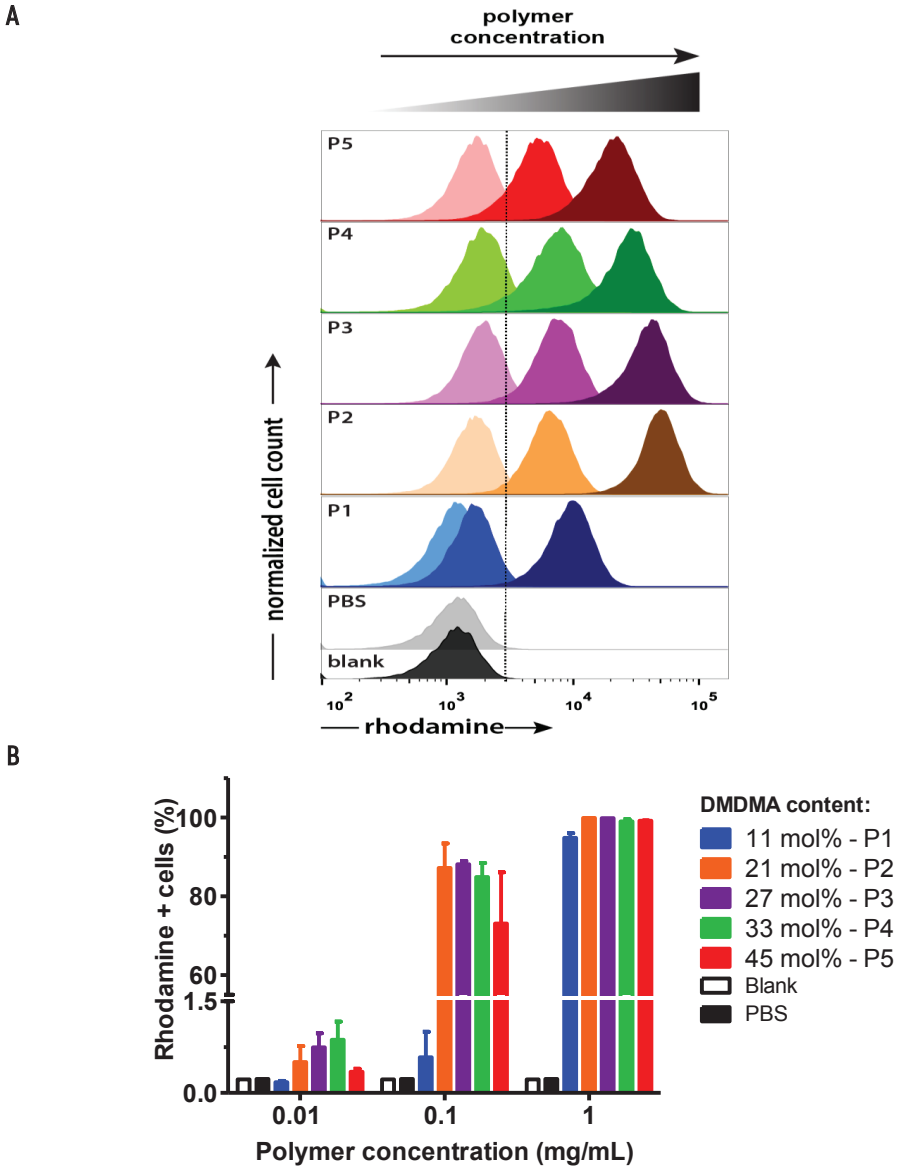


Figure 9. (A) Histograms of SKOV-3 cells, incubated for 24 hours with 0.01, 0.1 and 1 mg/mL of R18-loaded poly(HEA)_x-*b*-poly(HEA_m-*co*-DMDMA_n)_y. (B) Corresponding percentage rhodamine + cells ($n = 2$).

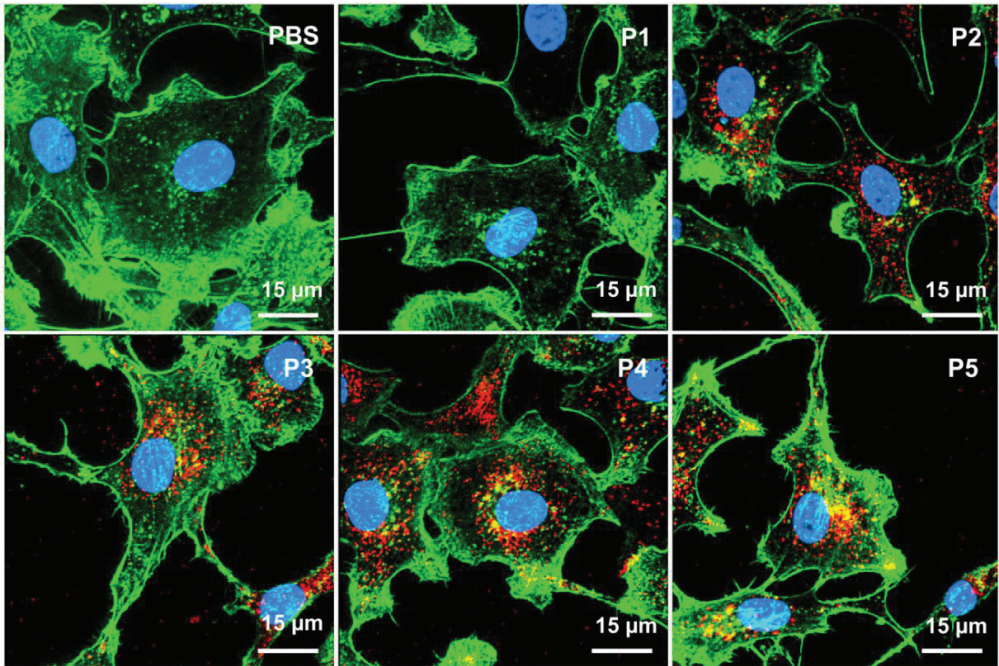


Figure 10. Maximized intensity projections (MIPs) of SKOV-3 cells, incubated for 24 hours with R18-loaded poly(HEA)_x-*b*-poly(HEA_m-*co*-DMDMA_n)_y (red). Cell nuclei and actin filaments are depicted in blue and green, respectively. Note that the Alexa Fluor 647 Phalloidin staining was performed without permeabilizing the cells to obtain a more selective staining of actin neighboring the cell membrane.

2.7 drug loading

To further explore the potential of the poly(HEA)_x-*b*-poly(HEA_m-*co*-DMDMA_n)_y block copolymers for intracellular delivery of hydrophobic drugs, we used PTX as hydrophobic anti-cancer drug. Similar to R18 encapsulation, PTX-loading was performed by addition of a PTX solution in ethanol (5 mg/mL) to a block copolymer dispersion (10 mg/mL) with a 1:10 volume ratio. Unloaded drug can easily be eliminated by membrane filtration as PTX precipitates in aqueous medium due to its limited solubility (0.3 μg/mL).

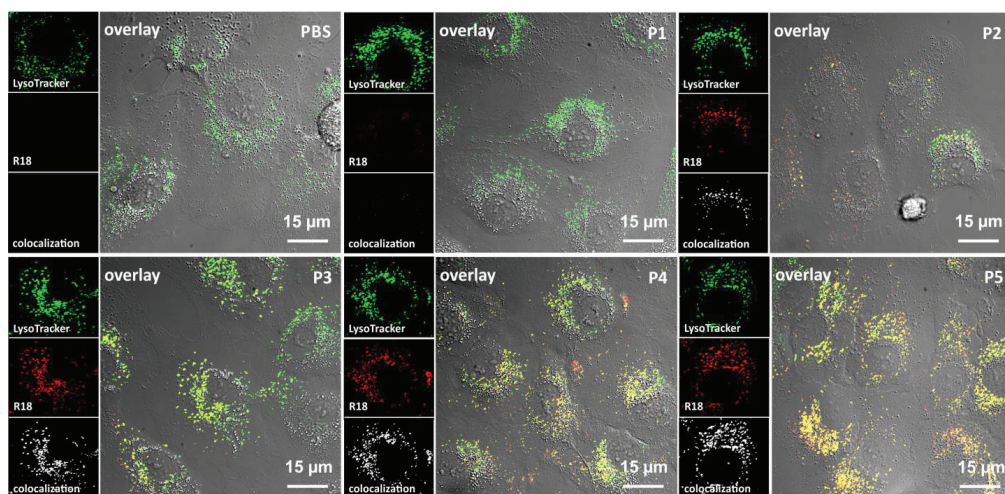


Figure 11. Confocal microscopy images of SKOV-3 cells, incubated for 24 hours with R18-loaded poly(HEA)_x-*b*-poly(HEA_m-*co*-DMDMA_n)_y (red). LysoTracker Deep Red was used for acidic organelle staining (green; note that this color was assigned for the sake of clarity and to allow rhodamine being assigned the red color). Colocalization of nanoparticles with these organelles (white) was analyzed using the colocalization function in the Imaris software package. Right panel: overlay of R18-loaded nanoparticles and acidic organelles with the corresponding differential interference contrast (DIC) image. The observed yellow color in the overlay panel also indicates colocalization.

The concentration of PTX in the samples after filtration was measured by LC-MS. As shown in **Figure 12A**, 4 out of 5 block copolymers solubilized significantly higher amounts of PTX than pure water. The block copolymer with 11 mol% DMDMA (P1) was not able to encapsulate PTX, fully in line with the observations of the previous DLS, CAC and FACS experiments. The almost identical structural composition of the block copolymers with 27 (P3) and 33 (P4) mol% DMDMA (**Figure 3**) probably results in comparable interaction with PTX and therefore similar PTX solubility. Nanoparticles of the block copolymer with 45 mol% DMDMA (P5) did not encapsulate higher concentrations of PTX compared to block copolymers with 27 (P3) or 33 (P4) mol% DMDMA. This can be explained based on the size distribution histograms of the block copolymer at 20 °C (**Figure 5A**). This shows that a significant amount of particles is larger than 450 nm which could have been removed during membrane filtration (0.450 μm). A similar trend is observed in **Figure 12B** for the calculated encapsulation efficiencies (EE) and loading capacities (LC), defined in **section 4.9**. DLS analysis of the PTX-loaded block copolymer nanoparticles showed no significant change in size compared to empty nanoparticles (data not shown).

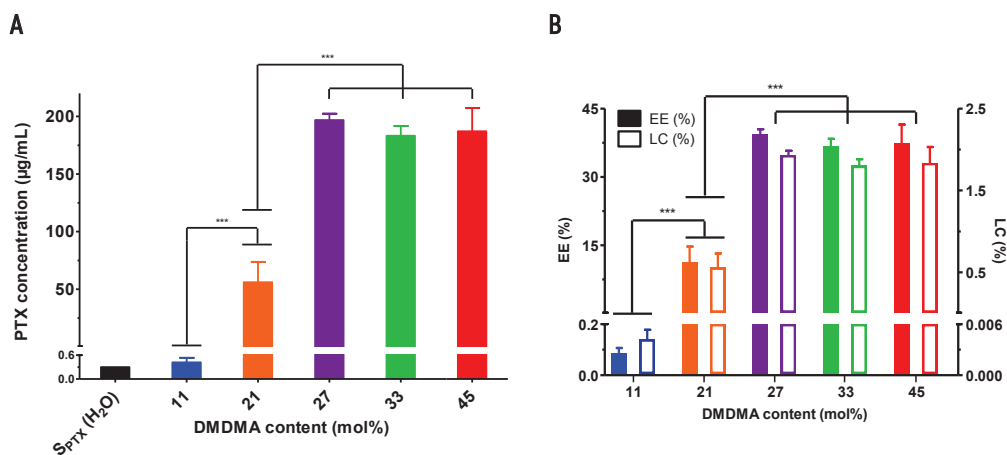


Figure 12. (A) Concentration of PTX, encapsulated by poly(HEA)_x-*b*-poly(HEA_m-*co*-DMDMA_n)_y, measured by LC-MS (n = 5). (B) Calculated encapsulation efficiency (EE) and loading capacity (LC) of PTX-loaded poly(HEA)_x-*b*-poly(HEA_m-*co*-DMDMA_n)_y. *** Student's *t*-test: *p* < 0.001.

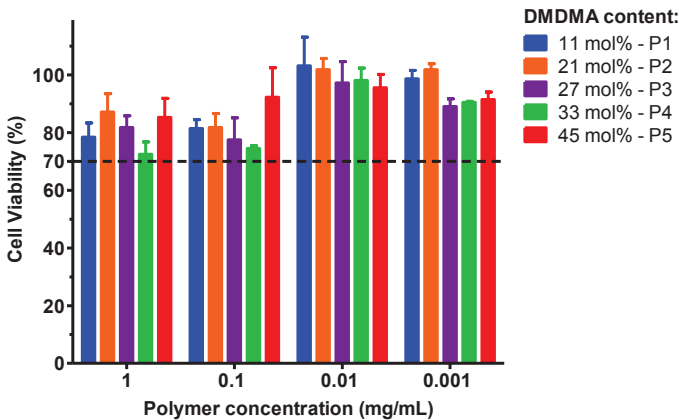
2.8 *in vitro* cytotoxicity

The *in vitro* cytotoxicity of empty and paclitaxel loaded poly(HEA)_x-*b*-poly(HEA_m-*co*-DMDMA_n)_y nanoparticles was evaluated on SKOV-3 cells *via* MTT assay. Abraxane and Genexol-PM were included for comparison. Abraxane is a formulation of albumin stabilized PTX nanocrystals, whilst Genexol-PM consists of PTX-loaded polymeric micelles based on monomethoxy poly(ethylene glycol)-*block*-poly(D,L-lactide) (mPEG-*b*-PDLLA).^[77] An incubation period of 72 hours was used to evaluate the known inhibitory effect of PTX on (cancer) cell proliferation. According to ISO 10993-5, cell viability below 70 % in comparison to negative control indicates cytotoxicity.

As shown in **Figure 13A**, no significant intrinsic cytotoxic effect can be ascribed to any of the block copolymers at concentrations up to 1 mg/mL. The formation of acetone (**Figure 1**) upon hydrolysis of the ketal moieties does not seem to affect the cell viability. This suggests that the synthesized block copolymers are cytocompatible, at least within the presently applied experimental setting. Significant *in vitro* cytotoxicity was observed for block copolymer formulations with PTX concentrations ranging from 0.01 to 10 µg/mL (**Figure 13B**). The cytotoxic effect was comparable or, in the case of PTX concentrations of 0.1 and 0.01 µg/mL, more potent than Abraxane and Genexol-PM. Based on the determined CACs, the PTX formulations prepared from the block polymers with a DMDMA content > 11 mol% (**section 2.4**) were below their CAC at a PTX concentration of 0.1 µg/mL. The

formulation prepared from the 11 mol% DMDMA block copolymer (P1) was below CAC at a PTX concentration of 0.01 $\mu\text{g/mL}$. Note that for the latter formulation, PTX concentrations of 10 and 1 $\mu\text{g/mL}$ could not be obtained. Taking CAC into account, along with the *in vitro* stability of the nanoparticles (section 2.5), the cytotoxic effect will likely be due to a combination of PTX which is efficiently solubilized in culture medium and PTX which is released after endocytosis by degradation of the DMDMA units. Future research will aim at elucidating the pH-induced release of the drug inside the complex intracellular medium and its relative contribution on PTX-induced cytotoxicity.

A



B

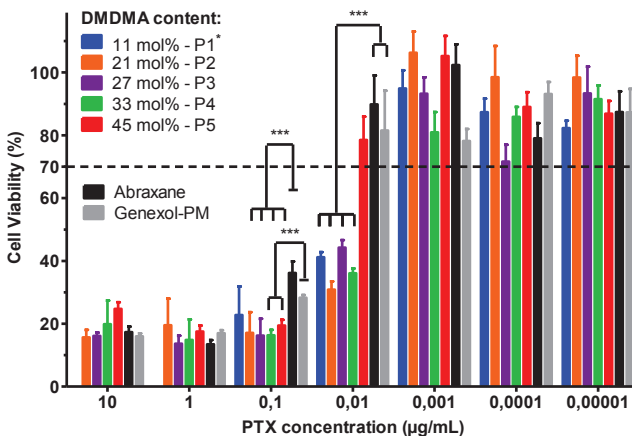


Figure 13. (A) *In vitro* cytotoxicity of unloaded poly(HEA)_x-*b*-poly(HEA_m-*c*o-DMDMA_n)_y on SKOV-3 cells after 72 hours of incubation (n = 3). (B) *In vitro* cytotoxicity of PTX-loaded poly(HEA)_x-*b*-poly(HEA_m-*c*o-DMDMA_n)_y on SKOV-3 cells after 72 hours of incubation (n = 3). Abraxane and Genexol-PM were used as control. * PTX well concentrations of 10 and 1 $\mu\text{g/mL}$ could not be obtained for P1. *** Student's *t*-test: $p < 0.001$.

3 conclusions

Well-defined responsive poly(HEA)_x-*b*-poly(HEA_m-*co*-DMDMA_n)_y block copolymers were synthesized with good control by sequential RAFT polymerization. Kinetic studies revealed that the reactivity ratios for the HEA:DMDMA copolymerization of the second block are $r_{\text{HEA}} = 1.07 \pm 0.09$ and $r_{\text{DMDMA}} = 0.62 \pm 0.07$. We have shown that the DMDMA content strongly influences aqueous self-assembly behavior, CAC and stimuli-responsive properties. A content of > 11 mol% DMDMA is required to afford the formation of nanoparticles in aqueous medium. All particles proved to be stable in PBS at 37 °C for at least 4 days and turned fully water-soluble upon acid-triggered hydrolysis. This should allow the polymers to be cleared from the body by renal filtration. Active cellular uptake was observed *in vitro* by flow cytometry and confocal microscopy. PTX could be loaded into the nanoparticles by solvent displacement, increasing PTX solubility in water by a factor of up to 650. Of these formulations, *in vitro* cytotoxicity comparable or better than 2 commercial PTX nanoformulations was observed, whilst empty particles did not induce any significant cytotoxic effect.

Due to these promising preliminary *in vitro* results, our current investigations aim at further exploring ketal-based systems for the design of anti-cancer drug nanocarriers which could, owing to their small size (i.e. the most promising systems in this paper had a Z-Average hydrodynamic diameter around 20, 50 and 100 nm, respectively), penetrate deep into poorly vascularized metastatic tumor tissue. We will for example consider cross-linking strategies to further lower the CAC. Additionally, we aim in the future at engineering the nanoparticle surface with ligands which afford active targeting of receptors which are overexpressed by ovarian cancer cells, such as the folate receptor alpha (FR_α) and CD44 receptor.^{[78],[79],[80],[81]}

4 experimental

4.1 materials

All chemicals were purchased from Sigma Aldrich unless mentioned otherwise. The RAFT agent 2-(butylthiocarbonothioylthio)propanoic acid (PABTC) and monomer (2,2-dimethyl-1,3-dioxolane-4-yl)methyl acrylate (DMDMA) were synthesized according to literature.^{[64],[65]} Octadecyl Rhodamine B Chloride (R18), enzyme-free Cell Dissociation Buffer, Dulbecco's Modified Eagle Medium (DMEM), fetal bovine serum (FBS), L-glutamine, sodium pyruvate, penicillin, streptomycin, Hoechst, Alexa Fluor 647 Phalloidin and LysoTracker Deep Red were

obtained from Invitrogen. SKOV-3 cells were supplied by ATCC. Paclitaxel (PTX) was purchased from LC Laboratories.

4.2 synthesis poly(HEA)_x macroCTA

The macroCTA was synthesized by RAFT homopolymerization of 2-hydroxyethyl acrylate (HEA). PABTC (2 mmol, 0.476 g), 2, 2'-azoisobutyronitrile (AIBN) (0.2 mmol, 0.033 g) and HEA (100 mmol, 11.612 g) were dissolved in *N,N*-dimethylformamide (DMF) to obtain a monomer concentration of 2 M and a monomer:CTA:initiator molar ratio of 50:1:0.1. The solution was bubbled with argon for 15 minutes. The reaction was performed at 70 °C under inert atmosphere and the monomer conversion was monitored by gas chromatography (GC). The homopolymer was isolated by triple precipitation in cold (5 °C) diethyl ether and subsequently dried under high vacuum at room temperature. The homopolymer was analyzed by size exclusion chromatography (SEC).

GC-samples were prepared by diluting 20 µL of polymerization mixture with 980 µL of methanol. GC was conducted on a 7890A system from Agilent Technologies equipped with an Agilent J&W Advanced Capillary GC column (30 m, 0.320 mm, and 0.25 µm). Injector and detector temperatures were kept constant at 250 and 280 °C, respectively. The column was initially set at 50 °C, followed by two heating stages: from 50 °C to 100 °C with a rate of 20 °C /min and from 100 °C to 300 °C with a rate of 40 °C /min, and then held at this temperature for 0.5 minutes. Injections were performed with an Agilent Technologies 7693 auto sampler. Detection was done with a flame ionization detector. Conversion was determined based on the integration of monomer peaks using DMF as internal standard.

SEC was carried out on an Agilent 1260 system, equipped with a 1260 ISO-pump, a 1260 diode array detector (DAD) and a 1260 refractive index detector (RID). Measurements were performed in DMA containing 50 mM LiCl at 50°C, using a flow rate of 0.593 mL/min. A guard column and two PL gel 5 µm mixed-D columns were used in series, calibrated with poly(methyl methacrylate) standards.

4.3 synthesis and characterization poly(HEA)_x-*b*-poly(HEA_m-*co*-DMDMA_n)_y

The block copolymers were synthesized by RAFT copolymerization of HEA and DMDMA using the poly(HEA)_x macroCTA described in **section 4.2**. A total of five block copolymers were synthesized for which the HEA:DMDMA molar feed ratio was 40:10, 30:20, 25:25, 20:30 and 10:40, respectively. All polymerizations were conducted within the same experimental setup using a Chemspeed ASW2000 automated synthesizer equipped with 16 parallel

reactors of 13 mL, a Huber Petite Fleur thermostat for heating/cooling, a Huber Ministat 125 for reflux and a Vacuubrand PC 3000 vacuum pump.^[66]

Stock solutions (336.5 mg/mL macroCTA in DMF and 4.7 mg/mL AIBN in DMF) and monomers (HEA and DMDMA, neat) were bubbled with argon for 30 minutes before being introduced into the robot system and then kept under argon atmosphere. The hood of the automated synthesizer was continuously flushed with nitrogen and the reactors were flushed with argon to ensure an inert atmosphere. Prior to the polymerizations, the reactors were deoxygenated through ten vacuum-argon cycles. Stock solutions and monomers were transferred into the reactors using the liquid handling robot of the automated synthesizer. Each reactor eventually contained poly(HEA)_x macroCTA (0.12 mmol, 0.514 g), AIBN (0.012 mmol, 2 mg) and 6 mmol of total monomer, dissolved in DMF to obtain a total monomer concentration of 1.8 M. The molar monomer_{total}:CTA:initiator ratio was 50:1:0.1. The reactions were run simultaneously at 70 °C. During the polymerizations, 50 µL samples were taken at preset time intervals for GC- and SEC-analysis. After the reactions, the block copolymers were purified by triple precipitation in cold diethyl ether and subsequent vacuum drying. Finally, all block copolymers were dialyzed (MWCO 3.5 kDa) for 4 days against water at 5 °C and recollected after freeze-drying.

The block copolymers were analyzed by SEC and ¹H-NMR spectroscopy. ¹H-NMR spectra were recorded on a Bruker 300 MHz FT-NMR spectrometer using chloroform-d or methanol-d₄ as solvent.

4.4 self-assembly and temperature-responsive behavior in aqueous medium

Supramolecular and temperature-responsive self-assembly behavior in PBS was evaluated by dynamic light scattering (DLS). The block copolymers of poly(HEA)_x-*b*-poly(HEA_m-*c*-DMDMA)_y (5 mg/mL) were sonicated for 15 minutes in cold (5 °C) PBS to induce faster dispersion compared to sonication at room temperature. After sonication, the samples were kept on ice overnight to allow complete dispersion. Next, the samples were filtered (0.450 µm) and measured at different temperatures (5, 20 and 37 °C). Measurements were carried out on a Zetasizer Nano S (Malvern).

4.5 critical aggregation concentration (CAC)

Similar to a described protocol, the CACs of poly(HEA)_x-*b*-poly(HEA_m-*co*-DMDMA_n)_y were determined by fluorescence microscopy using pyrene as a fluorescent probe.^{[67],[68]} First, 2.5 mL polymer dispersions in PBS were made according to **section 4.4** with concentrations ranging from 0.001 to 1 mg/mL. Secondly, a 3.6 mg/mL (1.8×10^{-2} M) stock solution of pyrene in acetone was prepared and kept on ice to prevent evaporation of the acetone. Next, 10 μ L of this solution was diluted to 1 mL acetone and kept on ice. To each polymer dispersion, 8.3 μ L of the latter pyrene solution was added under stirring leading to a pyrene concentration of 6.0×10^{-7} M. Fluorescence excitation spectra were collected at 20 °C on a Cary Eclipse fluorescence spectrophotometer (Agilent Technologies) equipped with a Varian Cary Temperature Controller. The CAC was quantified based on the change in excitation intensity ratio at 338 and 333 nm with varying concentration.

4.6 *in vitro* stability and pH-responsive behavior

Dispersions (5 mg/mL) of poly(HEA)_x-*b*-poly(HEA_m-*co*-DMDMA_n)_y were prepared as described in **section 4.4**. DLS measurements were conducted over 4 days at 37 °C. On day 4, HCl was added under vigorous stirring to obtain a HCl concentration of 100 mM (pH 1). Subsequently, size and light scattering intensity was monitored by DLS. After 7 hours incubation at 37 °C, a sample was taken from the acidic polymer dispersion and subsequently freeze-dried. The freeze-dried product was analyzed by ¹H-NMR spectroscopy, using methanol-d₄ as solvent.

4.7 cell culture

SKOV-3 (human ovarian cancer cell line) cells were cultured in DMEM, supplemented with 10% FBS, 2 mM L-glutamine, 1 mM sodium pyruvate and antibiotics (50 units/mL penicillin and 50 μ g/mL streptomycin). Cells were incubated at 37 °C in a controlled, sterile environment of 95% relative humidity and 5% CO₂. SKOV-3 cells were used for all cell experiments.

4.8 *in vitro* cellular uptake

4.8.1 encapsulation octadecyl rhodamine B chloride (R18)

A hydrophobic fluorescent dye (R18) was loaded into the nanoparticles using a solvent displacement technique. First, a 10 mg/mL stock solution of R18 in ethanol was prepared and kept on ice. Subsequently, 5 μ L of this solution was diluted to 1 mL ethanol and kept on ice. Next, 1 mL of poly(HEA)_x-*b*-poly(HEA_m-*co*-DMDMA_n)_y dispersions (10 mg/mL) were prepared in cold PBS according to **section 4.4**. Under stirring, 100 μ L of the R18 working solution was added to 1 mL of block copolymer dispersion. Formulations were stabilized overnight at room temperature with open lid to allow evaporation of the ethanol. Finally, excess dye was removed by membrane filtration (0.450 μ m). Dilutions of 1 and 0.1 mg/mL block copolymer were prepared in PBS. In a similar way a PBS control sample was prepared by adding 100 μ L of R18 working solution to 1 mL of pure PBS under stirring, followed by overnight incubation at room temperature. Precipitated dye was removed by filtration.

4.8.2 FACS

SKOV-3 cells were seeded into 24-well titer plates (250 000 cells per well, suspended in 0.9 mL of culture medium) and incubated overnight to allow cell sedimentation and subsequent adhesion to the bottom of the wells. Next, 100 μ L of R18-labeled poly(HEA)_x-*b*-poly(HEA_m-*co*-DMDMA_n)_y (0.1, 1 or 10 mg/mL)/PBS control (**section 4.8.1**) was added to the cells (polymer concentration in well: 0.01, 0.1 or 1 mg/mL), followed by 24 hours of incubation to allow cellular uptake. After incubation, the wells were aspirated and washed with 1 mL of PBS. After subsequent aspiration of the wells, 500 μ L of Cell Dissociation Buffer was added to the cells. The cells were completely detached from the wells after 15 minutes of incubation. The cell suspensions were transferred into Eppendorf tubes and immediately centrifuged (350 *g*, 15 minutes, 5 °C). Finally, the supernatant was aspirated and the cell pellets were suspended into 300 μ L of PBS and kept on ice to maintain cell integrity. FACS was performed on a BD Accuri C6 (BD Biosciences). The data were processed by FlowJo software.

4.8.3 confocal microscopy

First, a Hoechst stock solution of 1 mg/mL was prepared in dimethyl sulfoxide (DMSO). Alexa Fluor 647 Phalloidin was dissolved in 1.5 mL of methanol to obtain a stock concentration of 6.6 μM . Of these stock solutions 6 and 35 μL were added to 1.4 mL of PBS supplemented with 1 % bovine serum albumin (BSA), respectively. The commercial LysoTracker Deep Red 1 mM stock solution was diluted in culture medium to a working concentration of 60 nM. SKOV-3 cells were plated out on Willco-Dish glass bottom dishes (50 000 cells, suspended in 200 μL of culture medium) and incubated overnight. Next, 5 μL of 10 mg/mL R18-labeled poly(HEA)_x-*b*-poly(HEA_m-*c**o*-DMDMA_n)_y (section 4.8.1) was added, followed by 24 hours of incubation. R18 in pure PBS, described in section 4.8.1, was used as blank.

Simultaneous Hoechst and Alexa Fluor 647 Phalloidin staining was carried out on fixed cells. In summary, culture medium was aspirated and cells were washed with PBS. Next, 200 μL of 4 % paraformaldehyde was added and allowed to fixate for 15 minutes. After aspiration and washing, 200 μL of Hoechst-Alexa Fluor 647 Phalloidin working solution was added and incubated for 40 minutes at room temperature. Finally, the samples were washed with PBS.

Further, staining with LysoTracker Deep Red was performed on live cells. Briefly, culture medium was aspirated and cells were washed twice with PBS. Next, 200 μL of LysoTracker Deep Red working solution was added and allowed to incubate for 1.5 hours before performing confocal microscopy. Confocal microscopy was carried out on a Leica DMI6000 B inverted microscope equipped with an oil immersion objective (Zeiss, 63x, NA 1.40) and attached to an Andor DSD2 confocal scanner. Images were processed with Imaris software.

4.9 drug loading

Paclitaxel (PTX) loaded poly(HEA)_x-*b*-poly(HEA_m-*c**o*-DMDMA_n)_y nanoparticles were formulated based on the protocol described in section 4.8.1. A 5 mg/mL solution of PTX in ethanol was prepared and sealed to prevent solvent evaporation. Next, 1 mL of poly(HEA)_x-*b*-poly(HEA_m-*c**o*-DMDMA_n)_y dispersions (10 mg/mL) were prepared in PBS as described in section 4.4. To these polymer dispersions 100 μL of PTX solution was added under vigorous stirring. The polymeric nanoparticles were allowed to stabilize overnight at room temperature with the lid kept open to enable evaporation of the ethanol. Finally, precipitated PTX was removed by membrane filtration (0.450 μm).

To determine the concentration of loaded paclitaxel by LC-MS the following sample preparation was performed. Briefly, 50 μL of PTX loaded nanoparticle dispersion was diluted into 950 μL of methanol. Of this solution 500 μL was 2-fold diluted in 500 μL methanol. Finally, 100 μL of the latter dilution was added to 100 μL of MilliQ water. Of the sample 2 μL was injected into an Agilent 1200 series HPLC system equipped with a Phenomenex Luna C18 (2) (100 A, 50 x 2.00 mm, 3 μm) preceded by a Grace Alltima C18 (7.5 x 2.1 mm, 5 μm) guard column. The column temperature was 40 $^{\circ}\text{C}$ and the sample compartment was maintained at room temperature. A binary solvent system was used in gradient mode with an initial flow rate of 0.2 ml/min. To allow shorter runtimes, this flow rate was increased to 0.3 ml/min after 5.6 minutes, maintained for 6 minutes and then switched back to the initial flow rate to be maintained up to the end of the run (12.5 min). The solvents used were as follows: solvent A (90/10 % v/v $\text{H}_2\text{O}/\text{MeOH}$) and solvent B (100 % v/v MeOH). The runs started with a 36/64 volume ratio of solvent A and B which switched to 10/90 after 1.5 minutes. The latter ratio was maintained for 2.6 minutes and subsequently switched back to the initial ratio to be maintained up to the end of the run. The drug was detected by mass spectrometry using an API 3000 (AB Sciex) triple quadrupole mass spectrometer operated in the multiple reaction monitoring (MRM) mode. From the determined PTX concentration, encapsulation efficiency (EE) and loading capacity (LC) can be calculated. These parameters are defined by the formulas below:

$$\text{EE} = \frac{\text{conc PTX (LC-MS)}}{\text{conc PTX (added)}} \times 100 \%$$

$$\text{LC} = \frac{\text{concentration PTX (LC-MS)}}{\text{conc PTX (LC-MS)} + \text{conc polymer (added)}} \times 100 \%$$

4.10 *in vitro* cytotoxicity

The MTT assay was inspired on previously described methods in literature.^{[69],[70]} Dispersions of poly(HEA)_x-*b*-poly(HEA_m-*co*-DMDMA_n)_y (10 mg/mL) were prepared in cold PBS as described in **section 4.4**. Of these dispersions, dilution series were made (concentrations ranging from 5 x 10⁻³ to 5 mg/mL). The PTX loaded nanoparticles, prepared as described in **section 4.9**, were diluted (concentrations ranging from 5 x 10⁻⁵ to 50 $\mu\text{g}/\text{mL}$) along with two control nanoparticle formulations: Abraxane (Celgene) and Genexol-PM (Samyang Biopharmaceuticals). The MTT stock solution was prepared by dissolving 100 mg MTT in 20 mL of PBS and subsequent membrane filtration (0.220 μm). Before use, the MTT stock solution was 5-fold diluted with culture medium.

Briefly, SKOV-3 cells were seeded into 96-well titer plates (10 000 cells per well, suspended in 200 μ L of culture medium) and incubated overnight. Next, 50 μ L of sample, DMSO (positive control = 0 % viability) or PBS (negative control = 100 % viability) was added to the cells, followed by 72 hours of incubation. Subsequently, the medium was aspirated and the cells were washed with 250 μ L of PBS. After aspiration, 100 μ L of MTT working solution was added and the cells were incubated for 2.5 hours. Finally, the MTT working solution was aspirated and the formed purple formazan crystals were dissolved in 50 μ L of DMSO. Absorbance was determined at 590 nm using an EnVision Multilabel plate reader. The absorbance of the positive control was used as blank and therefore subtracted from all values. Cell viability (%) was defined as follows:

$$\text{Cell Viability} = \frac{\text{Abs}(\text{sample}) - \text{Abs}(+ \text{ control})}{\text{Abs}(- \text{ control}) - \text{Abs}(+ \text{ control})} \times 100 \%$$

5 references

- [1] B. C. Baguley, D. J. Kerr, *Anticancer Drug Development*, 1 ed., Academic Press, San Diego, **2001**.
- [2] R. Panchagnula, *Int. J. Pharm.* **1998**, *172*, 1-15.
- [3] S. C. Lee, K. M. Huh, J. Lee, Y. W. Cho, R. E. Galinsky, K. Park, *Biomacromolecules* **2007**, *8*, 202-208.
- [4] O. Soga, C. F. van Nostrum, M. Fens, C. J. F. Rijcken, R. M. Schiffelers, G. Storm, W. E. Hennink, *J. Controlled Release* **2005**, *103*, 341-353.
- [5] H. Lee, K. Lee, T. G. Park, *Bioconjugate Chem.* **2008**, *19*, 1319-1325.
- [6] H. Gelderblom, J. Verweij, K. Nooter, A. Sparreboom, *Eur. J. Cancer* **2001**, *37*, 1590-1598.
- [7] I. Rivkin, K. Cohen, J. Koffler, D. Melikhov, D. Peer, R. Margalit, *Biomaterials* **2010**, *31*, 7106-7114.
- [8] H. B. Chen, C. Khemtong, X. L. Yang, X. L. Chang, J. M. Gao, *Drug Discovery Today* **2011**, *16*, 354-360.
- [9] A. P. R. Johnston, G. K. Such, S. L. Ng, F. Caruso, *Curr. Opin. Colloid Interface Sci.* **2011**, *16*, 171-181.
- [10] V. J. Venditto, F. C. Szoka, *Adv. Drug Delivery Rev.* **2013**, *65*, 80-88.
- [11] M. E. Davis, Z. Chen, D. M. Shin, *Nat. Rev. Drug Discovery* **2008**, *7*, 771-782.
- [12] D. Peer, J. M. Karp, S. Hong, O. C. Farokhzad, R. Margalit, R. Langer, *Nat. Nanotechnol.* **2007**, *2*, 751-760.
- [13] R. Duncan, *Nat. Rev. Cancer* **2006**, *6*, 688-701.
- [14] H. Maeda, J. Wu, T. Sawa, Y. Matsumura, K. Hori, *J. Controlled Release* **2000**, *65*, 271-284.
- [15] A. Z. Wang, R. Langer, O. C. Farokhzad, *Annu. Rev. Med.* **2012**, *63*, 185-198.
- [16] E. Miele, G. P. Spinelli, F. Tomao, S. Tomao, *Int. J. Nanomed.* **2009**, *4*, 99-105.
- [17] J. K. C. Ma, P. M. W. Drake, P. Christou, *Nat. Rev. Genet.* **2003**, *4*, 794-805.
- [18] N. Kamaly, Z. Y. Xiao, P. M. Valencia, A. F. Radovic-Moreno, O. C. Farokhzad, *Chem. Soc. Rev.* **2012**, *41*, 2971-3010.
- [19] K. K. Upadhyay, J. F. Le Meins, A. Misra, P. Voisin, V. Bouchaud, E. Ibarboure, C. Schatz, S. Lecommandoux, *Biomacromolecules* **2009**, *10*, 2802-2808.
- [20] E. S. Lee, K. Na, Y. H. Bae, *J. Controlled Release* **2003**, *91*, 103-113.
- [21] X. Y. Zhao, Z. Poon, A. C. Engler, D. K. Bonner, P. T. Hammond, *Biomacromolecules* **2012**, *13*, 1315-1322.
- [22] Y. Shi, E. T. A. van den Dungen, B. Klumperman, C. F. van Nostrum, W. E. Hennink, *ACS Macro Lett.* **2013**, *2*, 403-408.
- [23] A. E. Smith, X. W. Xu, C. L. McCormick, *Prog. Polym. Sci.* **2010**, *35*, 45-93.
- [24] X. Huang, D. Appelhans, P. Formanek, F. Simon, B. Voit, *ACS Nano* **2012**, *6*, 9718-9726.
- [25] T. Smart, H. Lomas, M. Massignani, M. V. Flores-Merino, L. R. Perez, G. Battaglia, *Nano Today* **2008**, *3*, 38-46.
- [26] S. Venkataraman, J. L. Hedrick, Z. Y. Ong, C. Yang, P. L. R. Ee, P. T. Hammond, Y. Y. Yang, *Adv. Drug Delivery Rev.* **2011**, *63*, 1228-1246.
- [27] A. Schroeder, D. A. Heller, M. M. Winslow, J. E. Dahlman, G. W. Pratt, R. Langer, T. Jacks, D. G. Anderson, *Nat. Rev. Cancer* **2012**, *12*, 39-50.
- [28] Y. Bae, W. D. Jang, N. Nishiyama, S. Fukushima, K. Kataoka, *Mol. Biosyst.* **2005**, *1*, 242-250.
- [29] M. Yokoyama, *Expert Opin. Drug Delivery* **2010**, *7*, 145-158.
- [30] S. Kim, Y. Z. Shi, J. Y. Kim, K. Park, J. X. Cheng, *Expert Opin. Drug Delivery* **2010**, *7*, 49-62.
- [31] J. Gong, M. W. Chen, Y. Zheng, S. P. Wang, Y. T. Wang, *J. Controlled Release* **2012**, *159*, 312-323.
- [32] C. Deng, Y. J. Jiang, R. Cheng, F. H. Meng, Z. Y. Zhong, *Nano Today* **2012**, *7*, 467-480.
- [33] K. Bourzac, *Nature* **2012**, *491*, S58-S60.
- [34] E. Fleige, M. A. Quadir, R. Haag, *Adv. Drug Delivery Rev.* **2012**, *64*, 866-884.
- [35] C. Pietsch, U. Mansfeld, C. Guerrero-Sanchez, S. Hoepfener, A. Vollrath, M. Wagner, R. Hoogenboom, S. Saubern, S. H. Thang, C. R. Becer, J. Chiefari, U. S. Schubert, *Macromolecules* **2012**, *45*, 9292-9302.
- [36] M. A. Quadir, S. W. Morton, Z. J. Deng, K. E. Shopsowitz, R. P. Murphy, T. H. Epps, P. T. Hammond, *Mol. Pharm.* **2014**, *11*, 2420-2430.
- [37] L. M. Randolph, M. P. Chien, N. C. Gianneschi, *Chem. Sci.* **2012**, *3*, 1363-1380.
- [38] P. A. FitzGerald, S. Gupta, K. Wood, S. Perrier, G. G. Warr, *Langmuir* **2014**, *30*, 7986-7992.
- [39] Z. L. Yao, K. C. Tam, *Polymer* **2012**, *53*, 3446-3453.
- [40] R. Hoogenboom, *Angew. Chem., Int. Ed.* **2009**, *48*, 7978-7994.

- [41] G. Vancoillie, D. Frank, R. Hoogenboom, *Prog. Polym. Sci.* **2014**, *39*, 1074-1095.
- [42] J. Z. Du, Y. Q. Tang, A. L. Lewis, S. P. Armes, *J. Am. Chem. Soc.* **2005**, *127*, 17982-17983.
- [43] J. Heller, J. Barr, S. Y. Ng, H. R. Shen, K. Schwach-Abdellaoui, S. Emmahl, A. Rothen-Weinhold, R. Gurny, *Eur. J. Pharm. Biopharm.* **2000**, *50*, 121-128.
- [44] R. A. Shenoi, J. K. Narayanannair, J. L. Hamilton, B. F. L. Lai, S. Horte, R. K. Kainthan, J. P. Varghese, K. G. Rajeev, M. Manoharan, J. N. Kizhakkedathu, *J. Am. Chem. Soc.* **2012**, *134*, 14945-14957.
- [45] X. Huang, S. I. Sevimli, V. Bulmus, *Eur. Polym. J.* **2013**, *49*, 2895-2905.
- [46] K. Miyata, R. J. Christie, K. Kataoka, *React. Funct. Polym.* **2011**, *71*, 227-234.
- [47] W. B. Liechty, N. A. Peppas, *Eur. J. Pharm. Biopharm.* **2012**, *80*, 241-246.
- [48] V. P. Torchilin, *Adv. Drug Delivery Rev.* **2012**, *64*, 302-315.
- [49] L. Zhang, J. Bernard, T. P. Davis, C. Barner-Kowollik, M. H. Stenzel, *Macromol. Rapid Commun.* **2008**, *29*, 123-129.
- [50] I. Lee, M. Park, Y. Kim, O. Hwang, G. Khang, D. Lee, *Int. J. Pharm.* **2013**, *448*, 259-266.
- [51] M. J. Heffernan, N. Murthy, *Bioconjugate Chem.* **2005**, *16*, 1340-1342.
- [52] X. W. Xu, J. D. Flores, C. L. McCormick, *Macromolecules* **2011**, *44*, 1327-1334.
- [53] M. H. Stenzel, *Chem. Commun. (Cambridge, U. K.)* **2008**, 3486-3503.
- [54] H. Mori, T. Endo, *Macromol. Rapid Commun.* **2012**, *33*, 1090-1107.
- [55] W. A. Braunecker, K. Matyjaszewski, *Prog. Polym. Sci.* **2007**, *32*, 93-146.
- [56] G. Moad, E. Rizzardo, S. H. Thang, *Aust. J. Chem.* **2012**, *65*, 985-1076.
- [57] I. Kurtulus, G. Yilmaz, M. Ucuncu, M. Emrullahoglu, C. R. Becer, V. Bulmus, *Polym. Chem.* **2014**, *5*, 1593-1604.
- [58] R. W. Guo, X. X. Wang, C. G. Guo, A. J. Dong, J. H. Zhang, *Macromol. Chem. Phys.* **2012**, *213*, 1851-1862.
- [59] C. W. Scales, A. J. Convertine, C. L. McCormick, *Biomacromolecules* **2006**, *7*, 1389-1392.
- [60] N. Vanparijs, S. Maji, B. Louage, L. Voorhaar, D. Laplace, Q. Zhang, Y. Shi, W. E. Hennink, R. Hoogenboom, B. G. De Geest, *Polym. Chem.* **2015**, DOI: 10.1039/C4PY01224K
- [61] Q. L. Zhang, N. Vanparijs, B. Louage, B. G. De Geest, R. Hoogenboom, *Polym. Chem.* **2014**, *5*, 1140-1144.
- [62] Q. Zhang, B. Louage, N. Vanparijs, B. G. De Geest, R. Hoogenboom, *Submitted*.
- [63] D. J. Keddie, *Chem. Soc. Rev.* **2014**, *43*, 496-505.
- [64] C. J. Ferguson, R. J. Hughes, D. Nguyen, B. T. T. Pham, R. G. Gilbert, A. K. Serelis, C. H. Such, B. S. Hawkett, *Macromolecules* **2005**, *38*, 2191-2204.
- [65] D. W. Zhang, H. Zhang, J. Nie, J. Yang, *Polym. Int.* **2010**, *59*, 967-974.
- [66] L. Voorhaar, S. Wallyn, F. E. Du Prez, R. Hoogenboom, *Polym. Chem.* **2014**, *5*, 4268-4276.
- [67] Y. Shi, M. J. van Steenberg, E. A. Teunissen, L. Novo, S. Gradmann, M. Baldus, C. F. van Nostrum, W. E. Hennink, *Biomacromolecules* **2013**, *14*, 1826-1837.
- [68] K. Kalyanasundaram, J. K. Thomas, *J. Am. Chem. Soc.* **1977**, *99*, 2039-2044.
- [69] T. Mosmann, *J. Immunol. Methods* **1983**, *65*, 55-63.
- [70] M. Bauer, C. Lautenschlaeger, K. Kempe, L. Tauhardt, U. S. Schubert, D. Fischer, *Macromol. Biosci.* **2012**, *12*, 986-998.
- [71] A. M. Van Herk, **1998**.
- [72] R. Motokawa, K. Morishita, S. Koizumi, T. Nakahira, M. Annaka, *Macromolecules* **2005**, *38*, 5748-5760.
- [73] J. F. Lutz, K. Weichenhan, O. Akdemir, A. Hoth, *Macromolecules* **2007**, *40*, 2503-2508.
- [74] L. T. T. Trinh, H. M. L. Lambermont-Thijs, U. S. Schubert, R. Hoogenboom, A. L. Kjoniksen, *Macromolecules* **2012**, *45*, 4337-4345.
- [75] G. Battaglia, A. J. Ryan, *J. Am. Chem. Soc.* **2005**, *127*, 8757-8764.
- [76] I. Canton, G. Battaglia, *Chem. Soc. Rev.* **2012**, *41*, 2718-2739.
- [77] B. S. Lele, J. C. Leroux, *Macromolecules* **2002**, *35*, 6714-6723.
- [78] S. Miotti, M. Bagnoli, F. Ottone, A. Tomassetti, M. I. Colnaghi, S. Canevari, *J. Cell. Biochem.* **1997**, *65*, 479-491.
- [79] G. Journo-Gershfeld, D. Kapp, Y. Shamay, J. Kopecek, A. David, *Pharm. Res.* **2012**, *29*, 1121-1133.
- [80] R. C. Bast, B. Hennessy, G. B. Mills, *Nat. Rev. Cancer* **2009**, *9*, 415-428.
- [81] H. Ponta, L. Sherman, P. A. Herrlich, *Nat. Rev. Mol. Cell Biol.* **2003**, *4*, 33-45.

6 supporting info

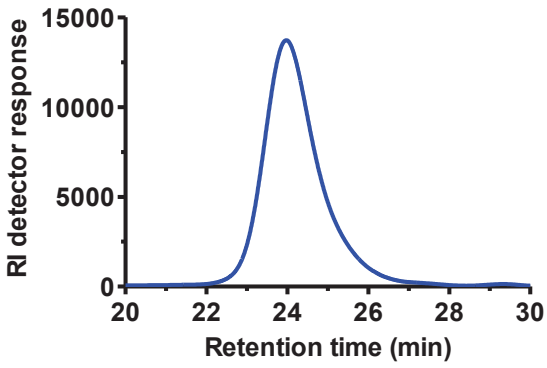


Figure S1. SEC-trace of poly(HEA)_x macroCTA.

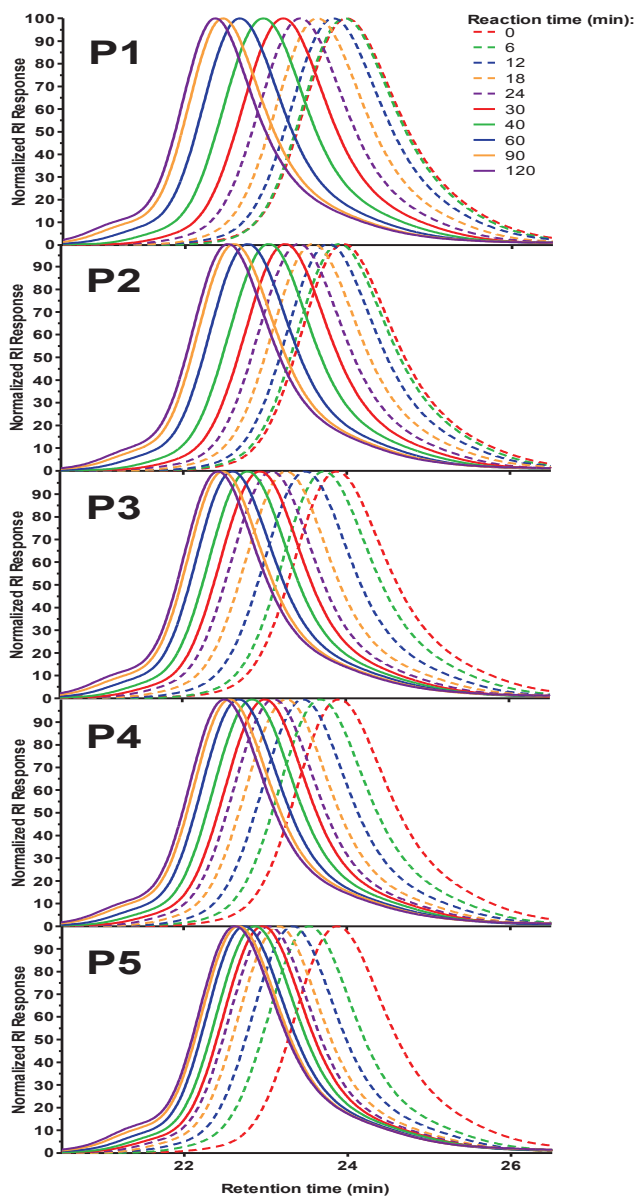


Figure S2. Kinetic SEC-traces for the synthesis of poly(HEA)_x-*b*-poly(HEA_m-*co*-DMDMA)_y.

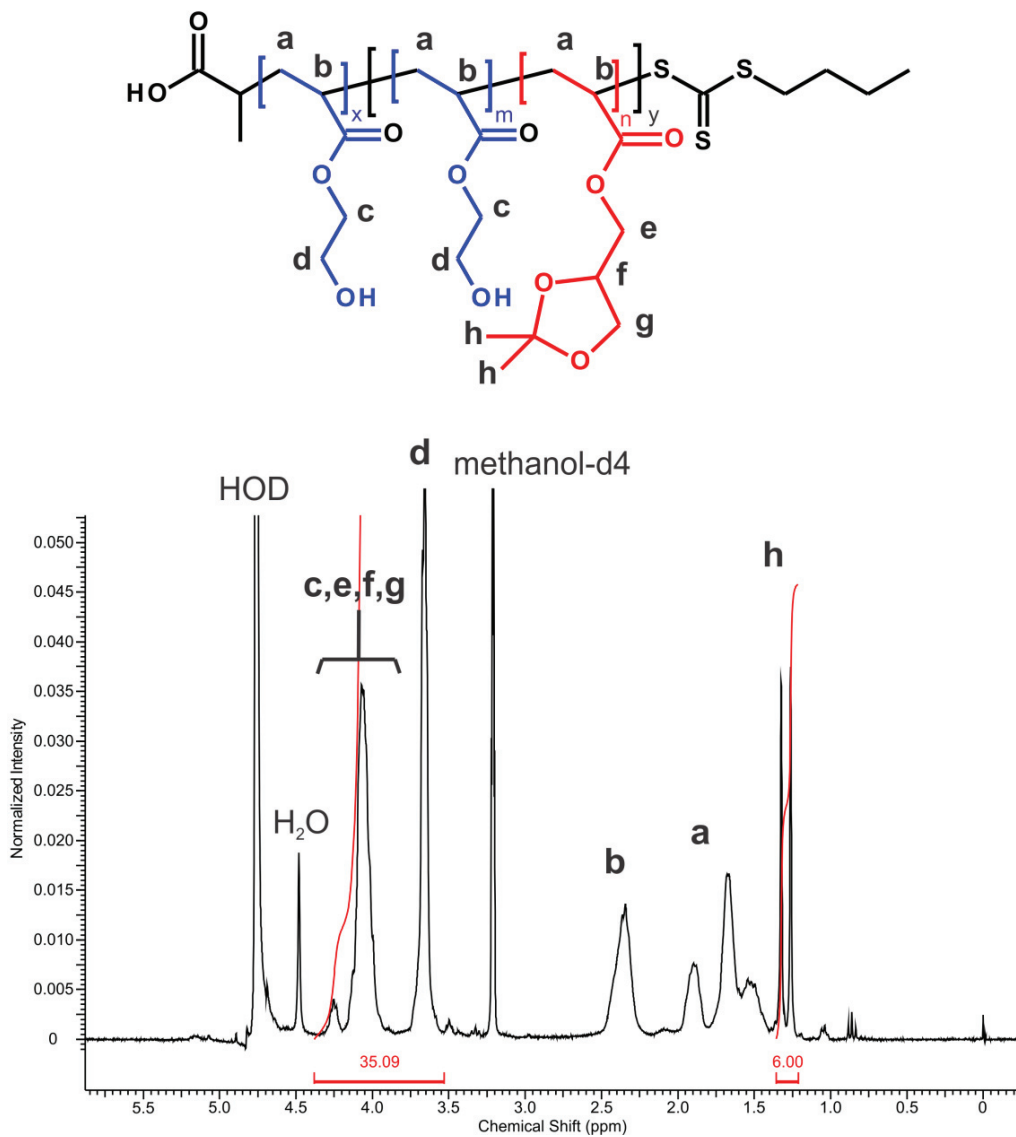


Figure S3. ¹H-NMR spectrum of P1 in methanol-d₄.

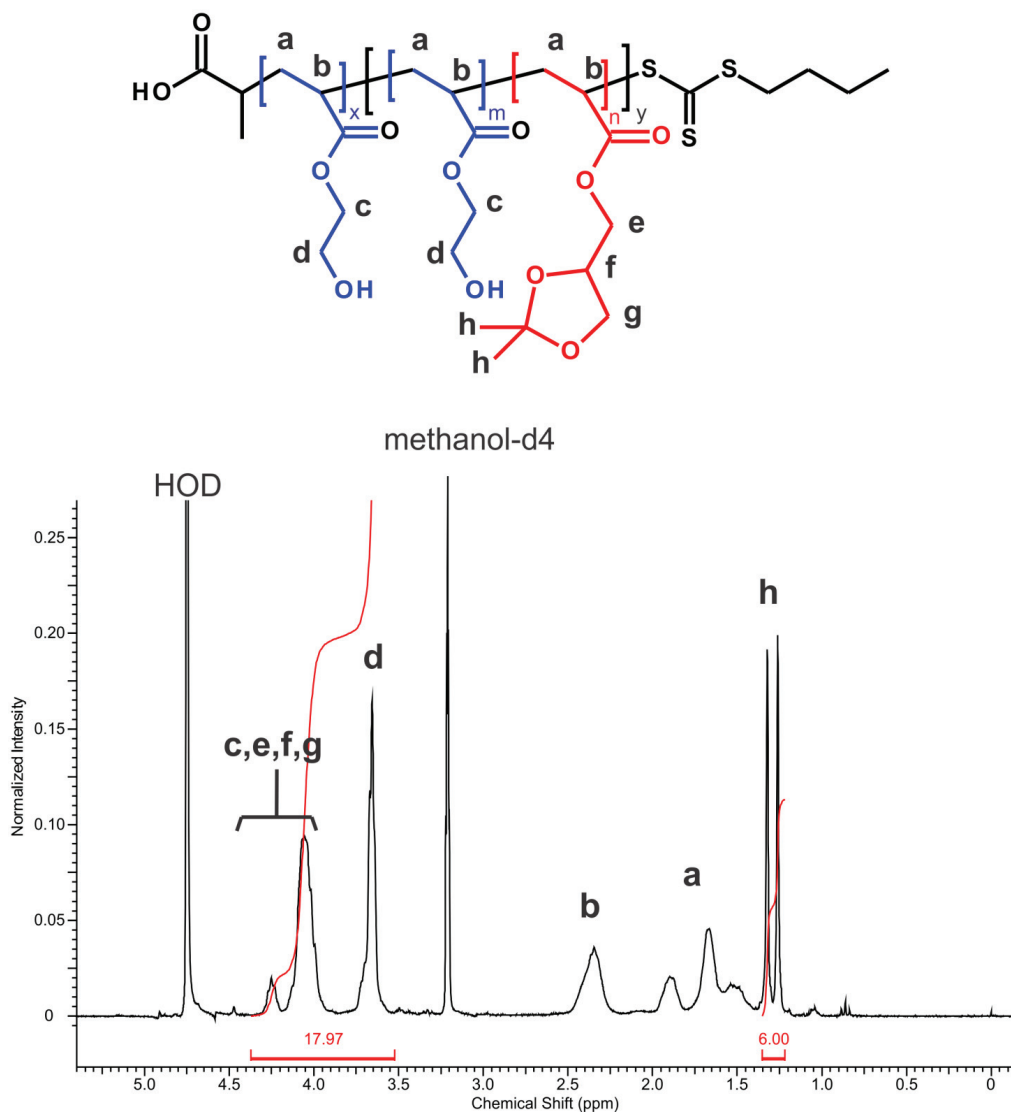


Figure S4. $^1\text{H-NMR}$ spectrum of P2 in methanol-d_4 .

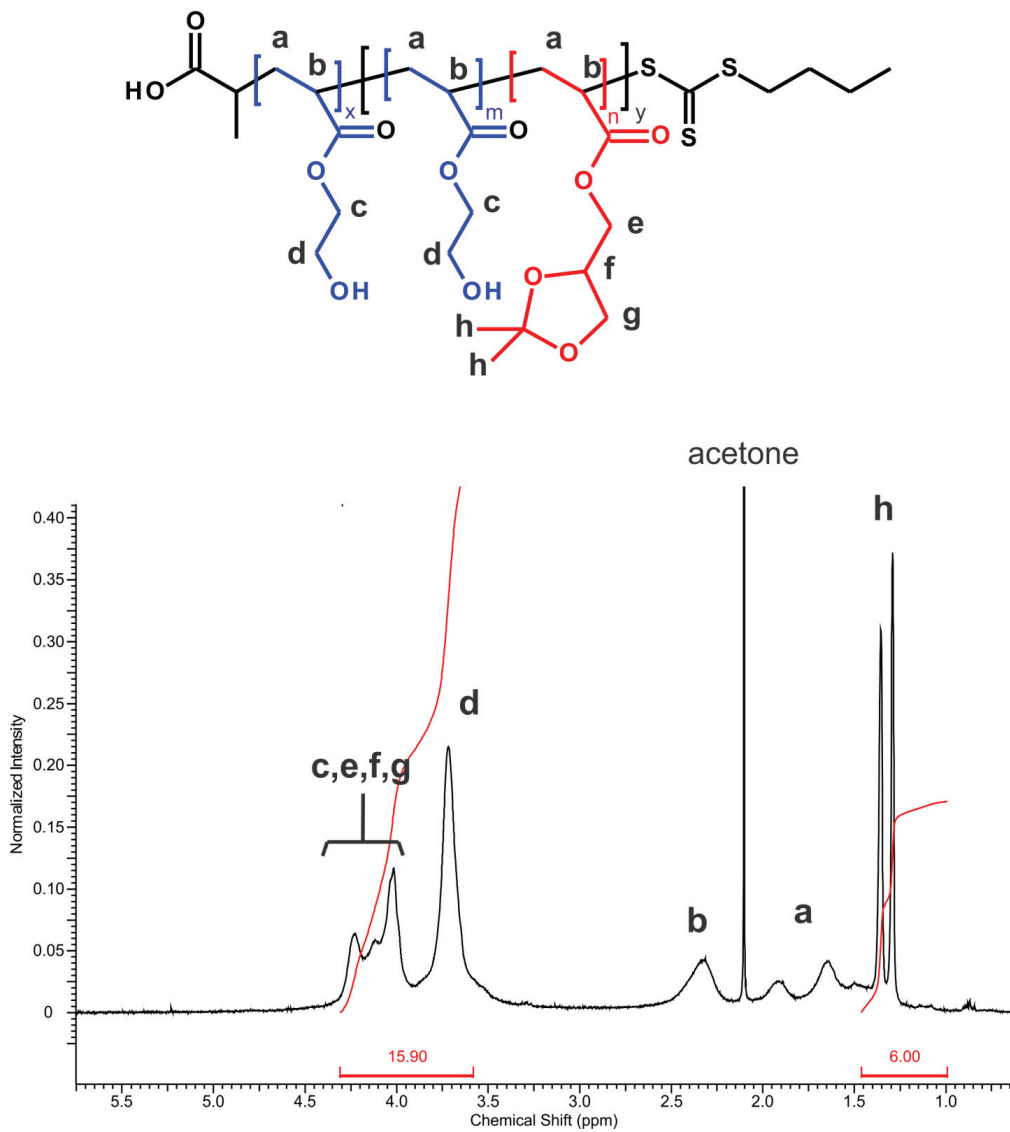


Figure S5. $^1\text{H-NMR}$ spectrum of P3 in chloroform-d.

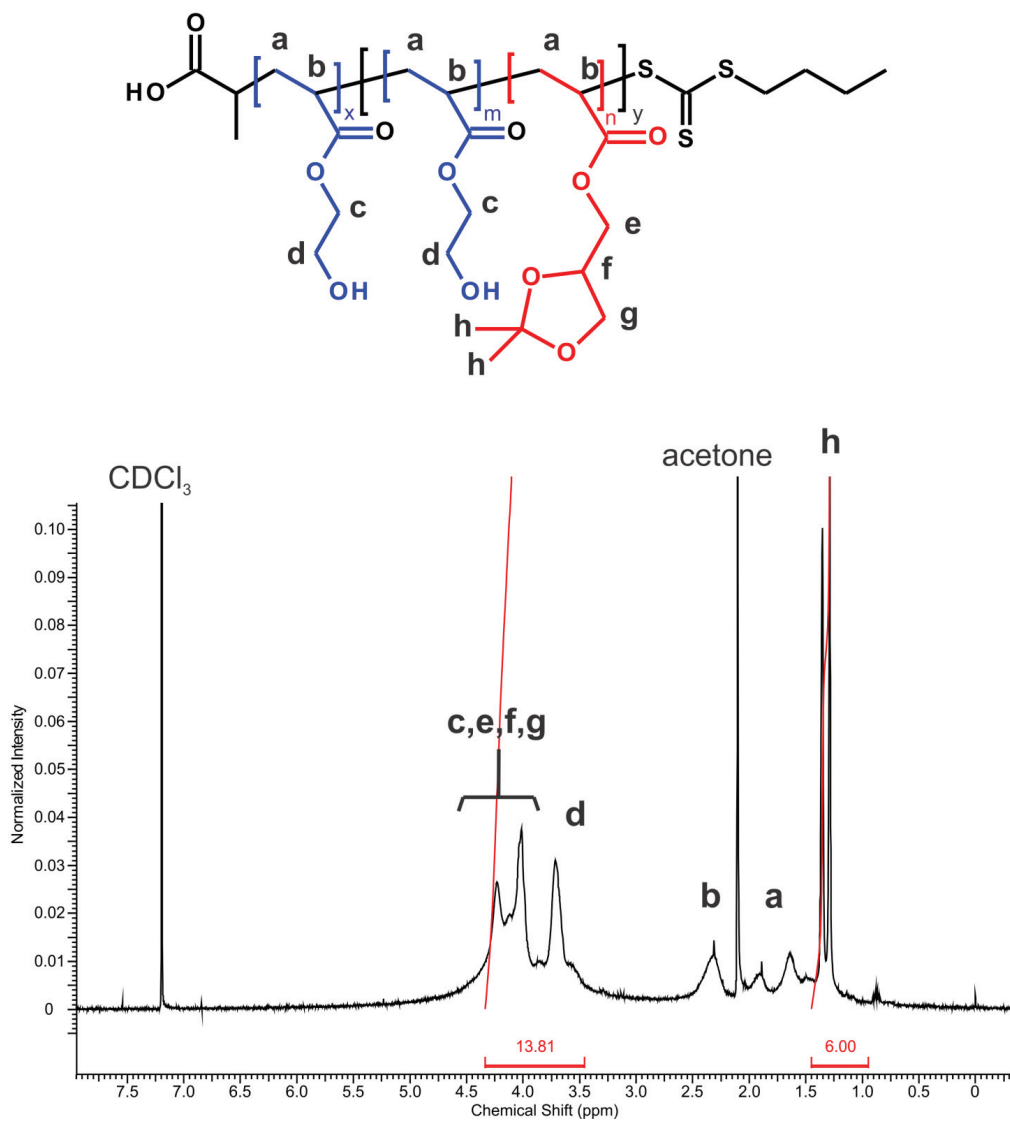


Figure S6. ¹H-NMR spectrum of P4 in chloroform-d.

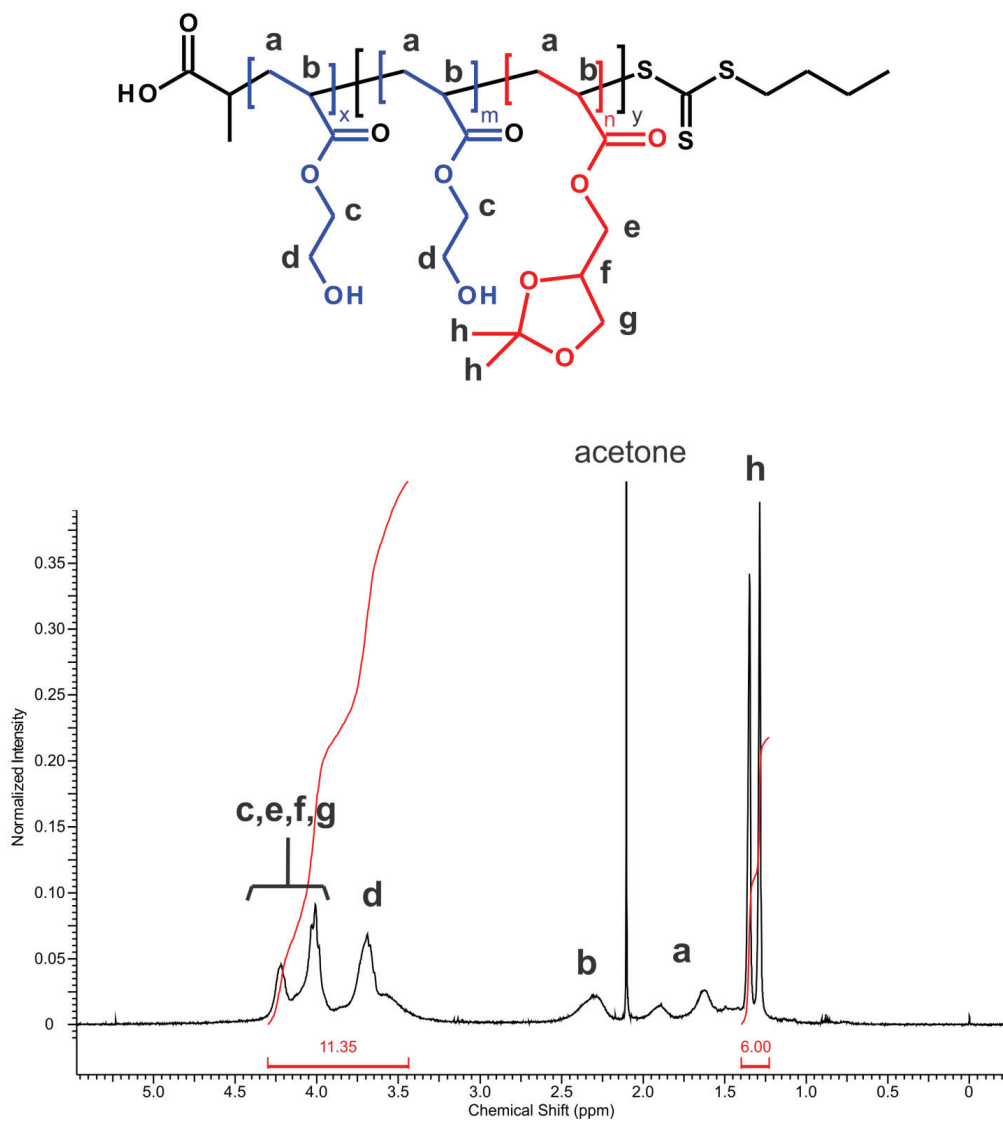


Figure S7. $^1\text{H-NMR}$ spectrum of P5 in chloroform- d .

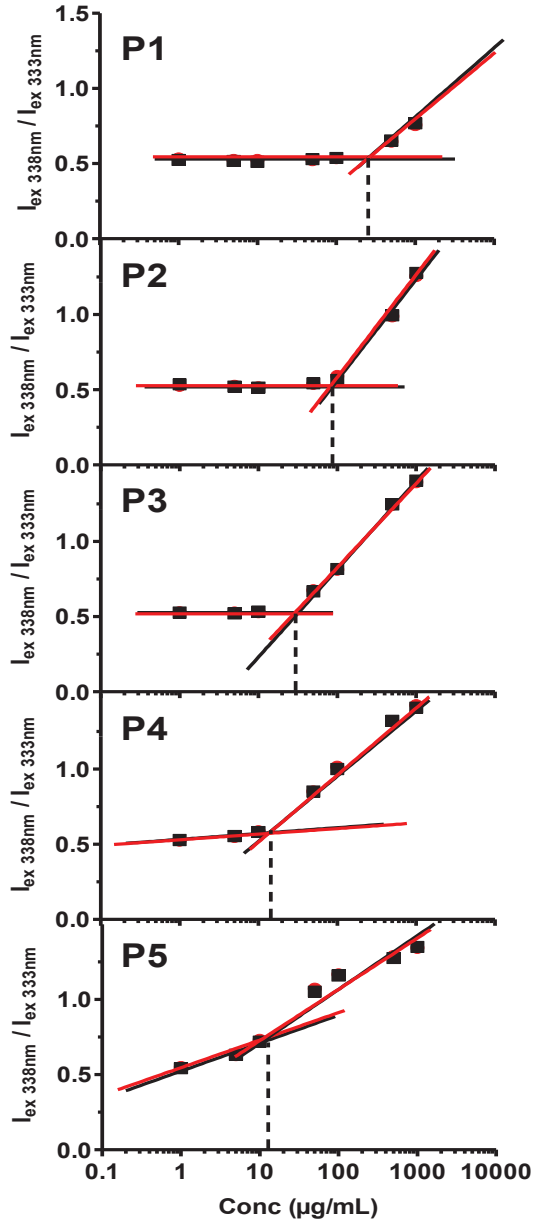


Figure S8. CAC fitting parameters ($n = 2$) of poly(HEA)_x-*b*-poly(HEA_m-*co*-DMDMA_n)_y.

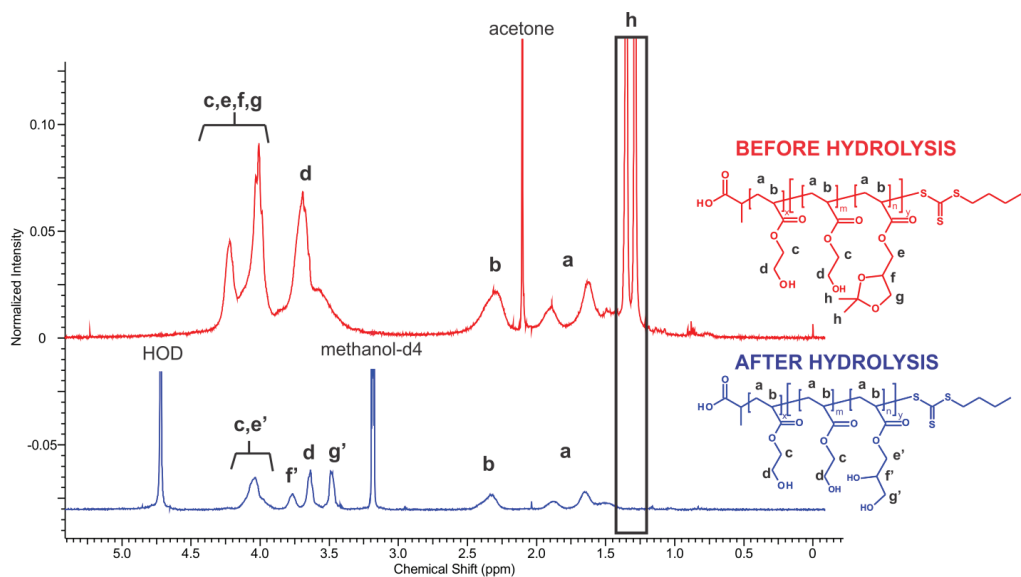


Figure S9. $^1\text{H-NMR}$ spectrum of PS (45 mol% DMDMA) before (red, solvent: chloroform- d) and after (blue, solvent: methanol- d_4) hydrolysis.

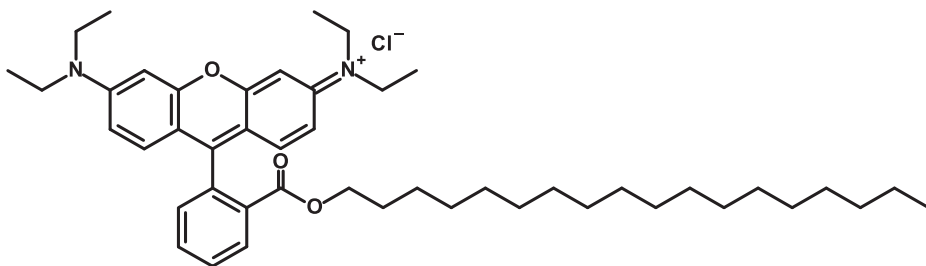


Figure S10. Molecular structure of octadecyl rhodamine B chloride (R18).

PART III

DESIGN OF ADVANCED

TAXANE-POLYMER

CONJUGATES

chapter 5

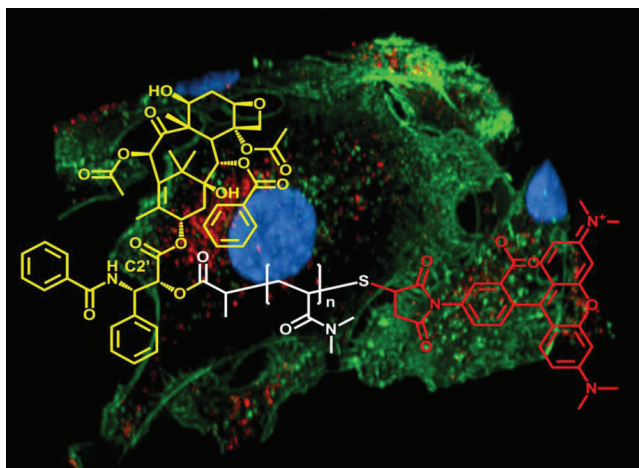
well-defined polymer-paclitaxel prodrugs by a grafting-from-drug approach

Benoit Louage,^a Lutz Nuhn,^a Martijn D. P. Risseeuw,^b Nane Vanparijs,^a Ruben De Coen,^a Izet Karalic,^b
Serge Van Calenbergh,^b Bruno G. De Geest^a

^a Laboratory of Pharmaceutical Technology, Department of Pharmaceutics,
Ghent University, Ottergemsesteenweg 460, 9000 Ghent, Belgium

^b Laboratory for Medicinal Chemistry, Department of Pharmaceutics,
Ghent University, Ottergemsesteenweg 460, 9000 Ghent, Belgium

Angewandte Chemie International Edition 2016, 55 (39), 11791-6



abstract

We report on the polymeric prodrug design of the anti-cancer agent paclitaxel via a grafting-from-drug approach. A chain transfer agent for Reversible Addition-Fragmentation chain Transfer (RAFT) polymerization was efficiently and regioselectively linked to the C2' position of paclitaxel which is crucial for its bioactivity. Subsequent RAFT polymerization of a hydrophilic monomer yielded well-defined paclitaxel-polymer conjugates with high drug loading, water-solubility and stability. The versatility of our approach was further demonstrated by ω -end post-functionalization with a fluorescent tracer. *In vitro* experiments showed that these conjugates are readily taken up into endosomes from where native PTX can efficiently be cleaved off and reach its subcellular target, as observed by the cytotoxicity profile matching those of commercial PTX formulations based on mere physical encapsulation.

1 introduction

The high incidence of side-effects caused by conventional chemotherapeutics urges the development of novel, more efficient, formulations of this class of drug molecules. Taxanes rank amongst the most potent and widely available drugs for anti-cancer treatment. However, taxanes (i.e. paclitaxel (PTX) and docetaxel (DTX)) have very limited water-solubility and their respective first clinically approved formulations Taxol and Taxotere, contain surfactants (i.e. Cremophor EL and polysorbate 80, respectively) which by itself are prone to cause severe side effects. Extensive research endeavors have been devoted to taxane formulation into alternative, non-toxic surfactant-based nanoparticulate formulations based on albumin (e.g. Abraxane) or amphiphilic block copolymers (e.g. Genexol-PM).^[1-4] The latter two commercial PTX formulations have proven to reduce surfactant-related side-effects and allow higher PTX dosing.^[5,6] Though considered as nanoformulations, both do not show significant differences in pharmacokinetics as compared to free PTX.^[7] Literature suggests that this is due to fast systemic release of taxanes from nanoparticles by passive diffusion and subsequent binding to plasma proteins such as endogenous human serum albumin (HSA), thereby annihilating controlled drug release.^[8] Chemical conjugation of taxanes might offer a promising solution to limit burst release effects. Not only does this allow prevention of abrupt systemic toxicity, this strategy can also confer longer blood circulation and tumor accumulation by the EPR effect.

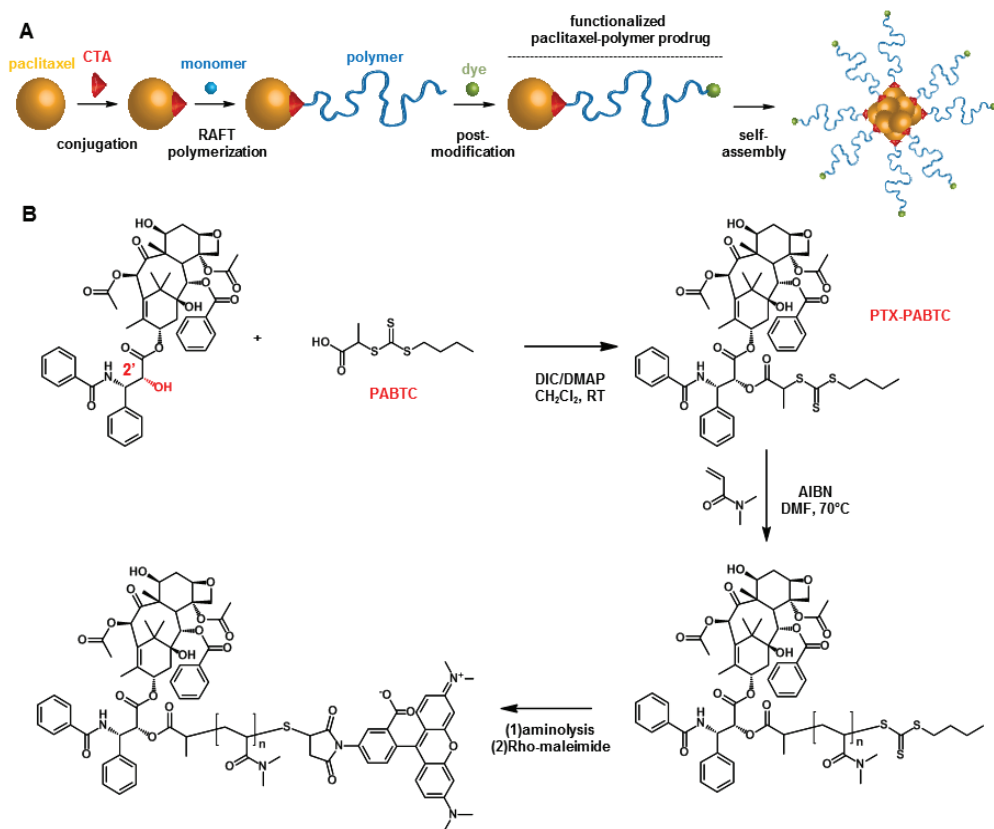
In this regard, drug-polymer conjugates have witnessed intensive development since they were introduced by Ringsdorf in the 1970s.^[9] A popular ligation strategy involves linking a hydrophilic polymer to taxanes through esterification of the hydroxyl moieties of the drug. In particular for PTX, drug-polymer conjugates have been developed based on post-polymerization modification with PTX of pre-formed polymers at their backbone or chain end.^[10] Such grafting-onto approach however suffers from similar limitations as witnessed in the polymer-protein conjugation field,^[11,12] including steric hindrance to achieve high conjugation efficiency, difficulties to control and assess site-specificity and cumbersome purification challenges to remove non-reacted polymer and drug. With respect to the use of drug-linked monomers, issues can arise concerning very hydrophobic pocket formation at high drug loading and hence very slow drug release kinetics due to limited access of water. Furthermore, as drug conjugation is typically done via ester, hydrazone or ketal formation, the resulting polymeric degradation products are polyanionic, polycationic or contain polyhydrazine/polyhydrazides or polyaldehydes/polyketones. These polymeric species hold toxicity risks, including long term accumulation in the body.

Therefore, alternative synthetic techniques are required for designing well-defined polymeric taxane prodrugs with reduced heterogeneity, combining high drug loading with high water-solubility and the possibility to introduce additional functionalities. An emerging strategy to address these issues is by applying grafting-from-drug polymerization, an approach which also gained interest in the polymer-protein conjugation field.^[13-18] With the advent of controlled polymerization, this strategy yields access to well-defined drug-polymer conjugates with good control over polymer length, bearing one drug per polymer chain and importantly, allows for simple purification, i.e. removal of residual monomer. Ring-opening polymerization of lactide from PTX towards poly(lactide) has been reported,^[19] to yield well-defined, but hydrophobic, polymeric prodrugs which require additional surfactants to obtain a stable formulation in aqueous medium. The Nicolas group has reported on the preparation of hydrophobic nanoparticles by RAFT- and NMP-mediated polymerization of squalene-methacrylate from another drug molecule (i.e. gemcitabine) which was covalently modified with a RAFT chain transfer agent or NMP initiator.^[20]

2 results and discussion

Here we report on the design of regioselective amphiphilic PTX-polymer conjugates prepared via RAFT polymerization using a PTX-ligated chain transfer agent (CTA) in which PTX and polymer chain serve as hydrophobic and hydrophilic segment, respectively. To highlight the versatility of this approach we also demonstrate the possibility for post-polymerization modification of the opposite polymer chain end. This is exemplified for the attachment of a fluorescent tracer molecule, but also small molecule cancer cell targeting ligands could be used. Our synthesis strategy is depicted in **Scheme 1** and comprises in a first step direct ligation of a RAFT CTA (i.e. 2-(butylthiocarbonothioylthio)propanoic acid (PABTC)) to the C2' hydroxyl group of PTX which possesses the highest reactivity for esterification.^[21] After purification via flash chromatography, PTX RAFT CTA (PTX-PABTC) was obtained in high yield (93 %) and high purity as shown by detailed NMR spectroscopy and mass spectrometry (ESI-MS) (**Figure 1** and **Figures S10-S15** in Supporting Information) showing proton signals from PTX and PATBC being in excellent agreement. Regioselective modification at the C2' position of PTX is clearly proven by the disappearance of C2' OH proton at 3.85 ppm (d, $J = 5.5$ Hz, 1H) in addition to a shift of the adjacent C2' proton from 4.77 ppm (dd, $J = 5.5, 2.8$ Hz, 1H) to 5.45 ppm (dd, $J = 12.9, 2.6$ Hz, 1H). As the C2' hydroxyl is crucial for the bioactivity of PTX,^[22] an inactive polymeric prodrug is obtained. Subsequently, PTX-PABTC was used for RAFT polymerization of *N,N*-dimethylacrylamide (DMA). PolyDMA is a hydrophilic and biocompatible polymer,^[23] but also

other vinyl monomers can be used as long as they are compatible with an organic solvent in which a PTX-functionalized RAFT CTA can be dissolved. A moderate degree of polymerization (DP) of 30 DMA repeating units was targeted to obtain a conjugate with both high water-solubility and PTX loading. In addition, a PTX-polyDMA conjugate with a DP of 15 was prepared with PTX-PABTC and a non-PTX containing polymer with a DP of 30 with PABTC. Triple precipitation from ether in which both CTAs as well as free PTX are soluble but polyDMA and PTX-polyDMA are not, allowed isolation of pure PTX-polymer conjugate. Size exclusion chromatography (SEC; **Figure 2A**) revealed narrowly distributed polymers with no significant low or high molecular weight shoulders. ¹H-NMR analysis (**Figure 1A** and **Figure S17-S20** in Supporting Information) proved high chain end fidelity from the excellent agreement between proton signals from PTX and PATBC. Absence of free PTX and PTX-PABTC was further confirmed by DOSY NMR (**Figure 1B**) which showed polyDMA and PTX signals exhibiting similar diffusional behavior in the spectra of both PTX-polyDMA₁₅ and PTX-polyDMA₃₀. **Table 1** summarizes the properties of the respective polymers after purification.



Scheme 1. (A) Conceptual illustration of the functionalized PTX-polymer prodrug design and (concentration-dependent) aqueous self-assembly into nanoparticles. (B) Corresponding reaction scheme based on esterification of PTX with a RAFT CTA, followed by polymerization of *N,N*-dimethylacrylamide and post-polymerization modification of the trithiocarbonate endgroup with a maleimide-functional fluorescent dye.

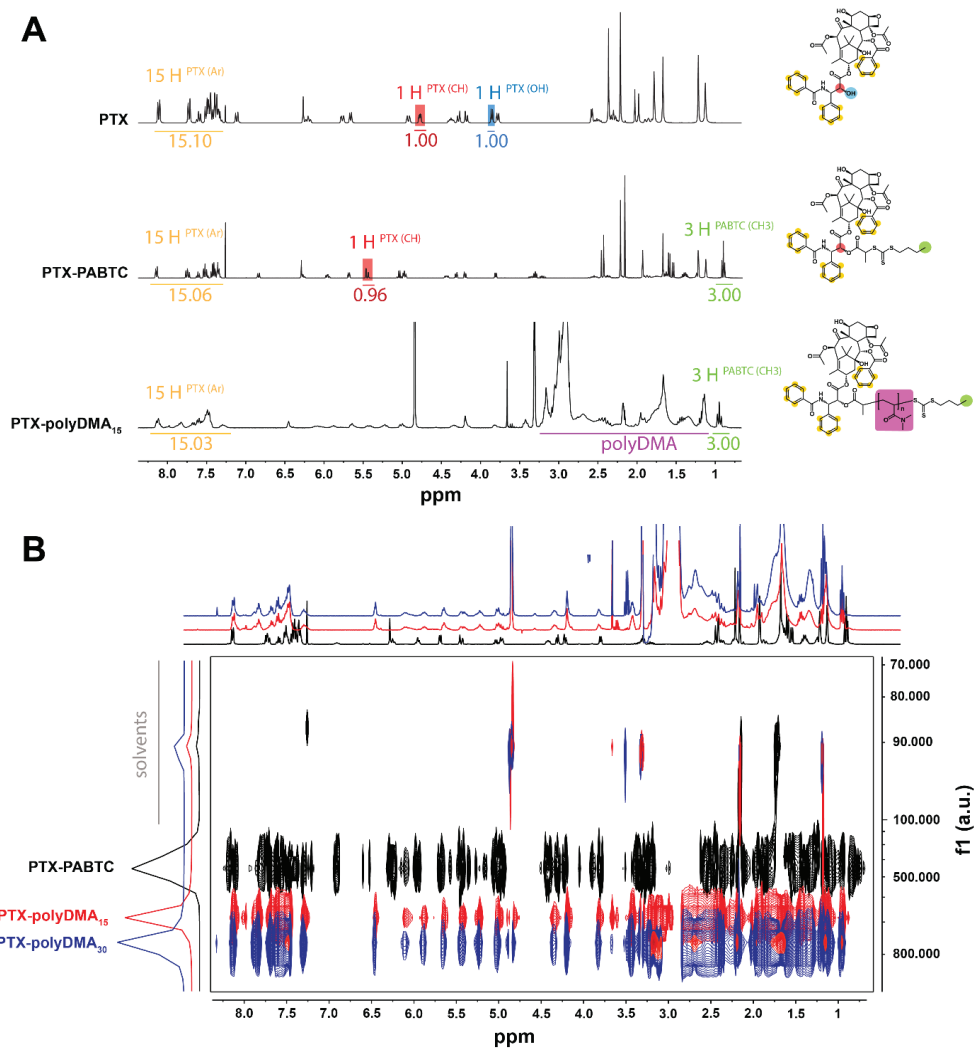


Figure 1. $^1\text{H-NMR}$ (A) and DOSY NMR (B) spectra of PTX, PTX-PABTC and PTX-polyDMA_{15/30}.

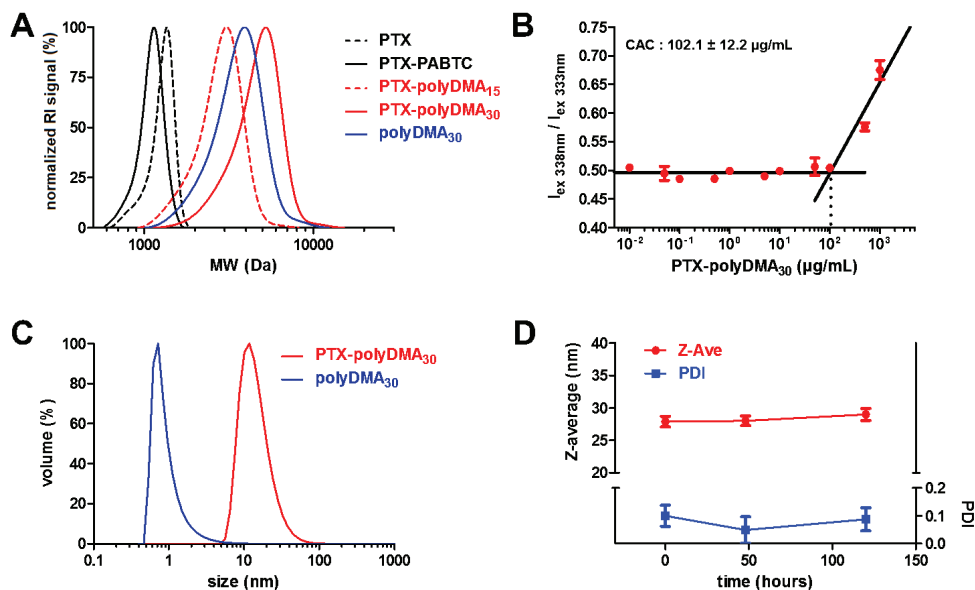


Figure 2. (A) SEC elugrams of PTX, PTX-PABTC, PTX-polyDMA_{15/30} and polyDMA₃₀. (B) CAC of PTX-polyDMA₃₀ in PBS measured by pyrene assay ($n = 2$). (C) Size distribution of PTX-polyDMA₃₀ and polyDMA₃₀ (30 mg/mL in PBS) measured by DLS ($n = 4$). (D) Colloidal stability of PTX-polyDMA₃₀ measured by DLS (30 mg/mL in PBS, 37 °C) ($n = 4$).

In a next series of experiments, we investigated the behavior of the PTX-polymer conjugates in aqueous medium. PTX-polyDMA₃₀ afforded a transparent formulation, both in H₂O and PBS at concentrations up to at least 30 mg/mL. At a drug loading of around 21 %, PTX-solubility in aqueous medium is increased by more than 2×10^4 -fold.^[24] By contrast, the PTX-polymer conjugate with a DP of 15 (i.e. PTX-polyDMA₁₅) could not be solubilized nor properly dispersed in aqueous medium (i.e. PBS), even after extensive sonication or decrease in concentration. This highlights the importance of the hydrophilic polymer chain length on the resulting solution behavior, but also opens avenues to prepare solid hydrophobic nanoparticles using this approach, e.g. via solvent displacement in surfactant solution. We subsequently characterized the supramolecular behavior of the PTX-polyDMA₃₀ in aqueous medium. At a concentration of 30 mg/mL in PBS, dynamic light scattering (DLS; **Figure 2C**) indicated the presence of self-assembled nanostructures, with a Z-average hydrodynamic diameter of $27.9 \text{ nm} \pm 0.8$ and a narrow dispersity (PDI) of 0.100 ± 0.038 (**Figure 2D**). Note that the control polymer polyDMA₃₀ formed soluble unimers in PBS at equal concentration (i.e. 30 mg/mL). Importantly, over a time course of at least 5 days, neither a change in size and PDI nor crystallization of released PTX was observed in PBS. These findings highlight the potential of this strategy

to obtain stable aqueous PTX formulations and avoid burst drug release. The critical aggregation concentration (CAC) of PTX-polyDMA₃₀ was determined by fluorescence spectrophotometry (**Figure 2B**; pyrene assay) to be 102 µg/mL ± 12. This is relatively high, compared to typical amphiphilic block copolymers and can be explained by the relative small hydrophobic proportion of the PTX-polyDMA₃₀ conjugate. The CAC implies that under physiological conditions, the polymer will likely be present as soluble unimer and is also likely to bind serum proteins. However, in case a stable nanoparticulate formulation is desired, the versatility of RAFT polymerization also offers the possibility to introduce reactive co-monomers which could be used for crosslinking, or to use degradable monomers with transient solubility.^[19]

Table 1. Compositional data of the synthesized polymers.

polymer	[DMA] ₀ / [CTA]	conversion DMA (%) ^a	<i>DP</i> ^{conv,b}	<i>DP</i> ^{endgroup,c}	<i>M</i> _n (Da) ^d	<i>g</i> ^d	PTX loading capacity (%) ^e
PTX-polyDMA ₁₅	15	90	14	16	2648	1.09	35
PTX-polyDMA ₃₀	30	99	30	31	4356	1.07	21
polyDMA ₃₀	30	91	27	29	3477	1.09	-

^a Determined by ¹H-NMR spectroscopy. ^b Determined by ¹H-NMR spectroscopy based on monomer conversion. ^c Determined by ¹H-NMR spectroscopy based on endgroup analysis. ^d Analyzed by SEC in DMAc, calibrated with PMMA standards. ^e Calculated based on conversion by ¹H-NMR spectroscopy: $MW_{PTX}/MW_{PTX-polyDMA} \times 100\%$.

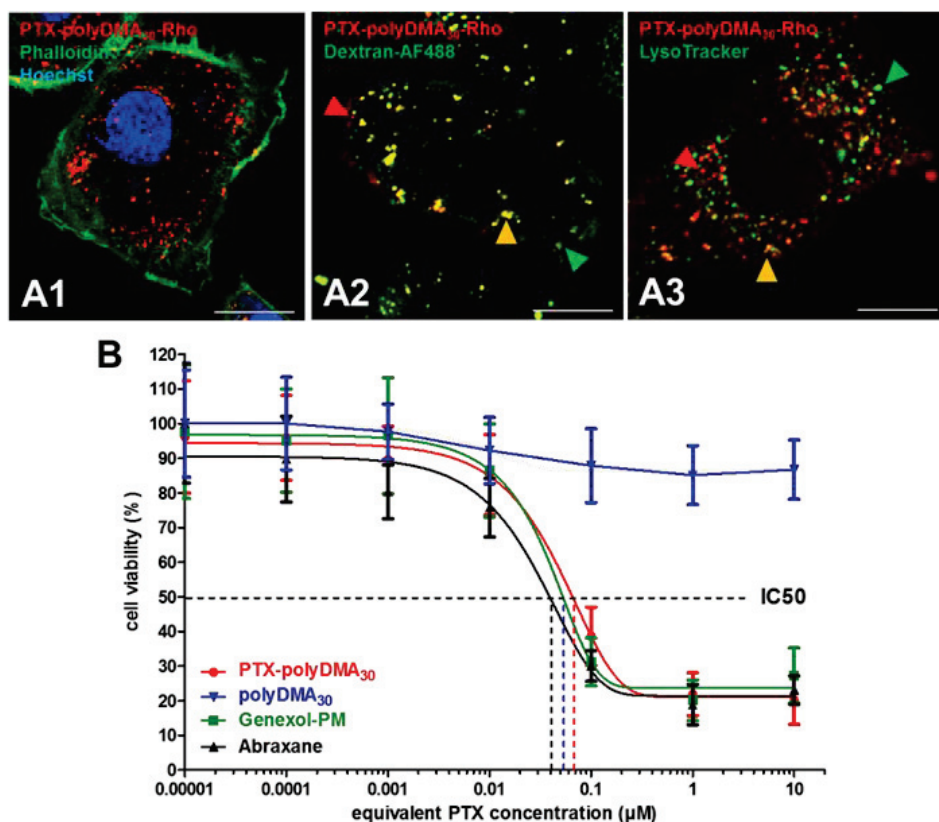


Figure 3. (A) Confocal microscopy images of SKOV-3 human ovarian cancer cells pulsed with PTX-polyDMA₃₀-Rho conjugate. Counterstaining was performed with Hoechst and Phalloidin to stain cell nuclei and plasma membrane, respectively (A1). The conjugate was co-incubated with Dextran-AF488 to stain (early) endosomes (A2). Lysosomal vesicles were stained with LysoTracker (A3). For guidance, in panels A2 and A3, a co-localization event is marked with a yellow arrow and two non-co-localization events are marked with a red, respectively green arrow. Scale bars (white, bottom right in each panel) correspond to a length of 15 μm . (B) *In vitro* cytotoxicity of PTX-polyDMA₃₀ versus commercial PTX nanoformulations Abraxane and Genexol-PM. Non-PTX-conjugated polyDMA₃₀ was used as a control ($n = 6$).

As mentioned earlier, one of the major advantages of RAFT over other polymerization techniques is the direct access towards α,ω -telechelic polymers.^[25] PTX-polyDMA₃₀ has PTX at the α -end, thereby offering an opportunity for post-polymerization modification of the ω -endgroup.^[26] We demonstrate this by attachment of a fluorescent dye tetramethyl rhodamine maleimide. First, the trithiocarbonate moiety at the ω -end was converted into a thiol by aminolysis (confirmed by UV-VIS spectroscopy **Figure S21** in Supporting Information) and subsequently reacted with tetramethyl rhodamine (Rho) maleimide to form a stable thioether bond between polymer and dye. A similar strategy however could also be used to introduce radiotracers or targeting ligands.

After dialysis, absence of free dye was observed by reversed phase TLC (**Figure S22** in Supporting Information). DLS further proved that conjugation of the rhodamine dye, thereby obtaining PTX-polyDMA₃₀-Rho, did not significantly alter the supramolecular behavior of the conjugate (**Figure S23** in Supporting Information).

Subsequently, we evaluated the *in vitro* behavior of the PTX-polyDMA₃₀-Rho conjugate on SKOV-3 human ovarian cancer cells. After 2 h of incubation, intracellular localization of the PTX-polyDMA₃₀-Rho was investigated by confocal microscopy. As shown in **Figure 3A1**, a punctuated fluorescence pattern is observed inside the cells which proves the polymeric prodrug is efficiently internalized. To shed light on the uptake mechanism, PTX-polyDMA₃₀-Rho was co-incubated with Alexa Fluor 488 (AF488) labeled dextran (**Figure 3A2**) or counterstained with LysoTracker (**Figure 3A3**). Dextran conjugates are known to be taken up by pinocytosis,^[27] thereby staining endosomes, whereas LysoTracker is known to stain lysosomal vesicles. The strong co-localization of PTX-polyDMA₃₀-Rho with Dextran-AF488 and partial co-localization with LysoTracker, indicates active endocytosis into intracellular acidic vesicles. When the experiment was repeated at 4 °C where energy-dependent endocytosis is blocked, no uptake of the conjugate was observed (data not shown). These findings show that, in contrast to PTX which is a membrane-permeable molecule,^[28] the polymeric prodrug is actively taken up by endocytosis (i.e. pinocytosis) but not yet abundantly present in lysosomal vesicles within 2 h. As PTX is known to exit cancer cells through P-glycoprotein efflux, altering the route through which PTX enters the cell might prolong its intracellular residence and might hold potential to overcome multidrug resistance.^[29]

Next, the effect of PTX-polyDMA₃₀ on the *in vitro* viability of SKOV-3 cells was investigated. Cells were incubated for 72 h with PTX-polyDMA₃₀, polyDMA₃₀ control polymer and 2 commercial PTX nanoformulations Abraxane and Genexol-PM. Cell viability was assessed by MTT assay. As shown in **Figure 3B**, no cytotoxicity was observed for control polyDMA₃₀, suggesting that polyDMA is cytocompatible within the experimental window. Interestingly, PTX-polyDMA₃₀ exhibits an IC₅₀ of 79 nM ± 7, comparable to both Abraxane and Genexol-PM (IC₅₀ of 56 nM ± 11 and 65 nM ± 13, respectively). These findings demonstrate that despite covalent polymer ligation to a position on PTX crucial for its bioactivity (i.e. the C2' OH), a similar *in vitro* cytotoxicity effect is exerted as for formulations which rely on mere physical encapsulation. In other words, upon storage in endosomal/lysosomal vesicles, where esterases like cathepsin B^[30] are present, native PTX is released from an inactive polymeric prodrug and can subsequently still reach its subcellular target and exert its cytotoxic activity.

3 conclusions

Summarizing, we demonstrated the synthesis of well-defined polymeric prodrugs of the anti-cancer drug PTX via a grafting-from-drug RAFT approach. PolyDMA grown from a regioselectively modified PTX-ester CTA affords a dramatic increase in drug aqueous solubility upon formation of stable nanoparticles or unimers depending on the concentration. We further demonstrated the introduction a fluorophore at the ω -end of the polymer chain via post-polymerization modification which allowed for tracking the intracellular fate of the prodrug. Importantly, the PTX-polymer conjugate showed no loss in activity *in vitro*.

We believe the attractiveness of our approach lies in its versatility as it allows for the synthesis of a library of polymer-PTX conjugates starting from a single well-characterized PTX-CTA. Such library could encompass different polymer chain lengths, monomers and side chain or end group functionalities, and could offer a valuable tool to investigate structure-property relationships to alter the pharmacokinetic profile of PTX towards optimal tumour targeting. Furthermore, as the PTX-polymer conjugate is an inactive prodrug, our strategy also holds promise to enhance the maximum tolerable dose (MTD) and thus further improve the therapeutic effect by increasing the administered dose. These investigations, along with exploring active targeting strategies, the use of transiently soluble monomers and assessing the potential to overcome multidrug resistance are currently ongoing.

4 experimental

4.1 materials

All chemicals were purchased from Sigma Aldrich unless mentioned otherwise. The RAFT CTA 2-(butylthiocarbonothioylthio)propanoic acid (PABTC) was synthesized according to literature.^[31] TLC plates were purchased from Macherey Nagel. Dulbecco's phosphate buffered saline (PBS), Dulbecco's modified Eagle medium (DMEM), fetal bovine serum (FBS), L-glutamine, sodium pyruvate, penicillin, streptomycin, Hoechst, Alexa Fluor 488 Phalloidin, Dextran Alexa Fluor 488 (10 000 Da) and LysoTracker Green were obtained from Thermo Fisher Scientific. SKOV-3 cells were supplied by ATCC. Tetramethyl rhodamine (Rho) maleimide was purchased from Anaspec.

4.2 analysis

NMR spectra were recorded on a Bruker 300 and 400 MHz FT-NMR spectrometer. Chemical shifts (δ) are given in ppm relative to TMS. Samples were prepared in given deuterated solvents and their signals referenced to residual non-deuterated signals of the solvent.

Electron spray ionization-mass spectroscopy (ESI-MS) measurements were performed on a Waters (Milford, Mass, USA) LCT Premier XE TOF equipped with an electrospray ionization interface. Samples were infused in an acetonitrile:formic acid (1000:1) mixture at 0.1 mL/min.

Size exclusion chromatography (SEC) was carried out on an Agilent 1260 system, equipped with a 1260 ISO-pump, a 1260 diode array detector (DAD) and a 1260 refractive index detector (RID). Measurements were performed in *N,N*-dimethylacetamide (DMAc) containing 50 mM LiCl at 50 °C, using a flow rate of 0.593 mL/min. A guard column and two PL gel 5 μ m mixed-D columns were used in series, calibrated with poly(methyl methacrylate) (PMMA) standards obtained from PSS (Mainz, Germany).

Dynamic light scattering (DLS). DLS measurements were carried out on a Zetasizer Nano S (Malvern) with a HeNe laser ($\lambda = 633$ nm) at a scattering angle of 173°.

Fluorescence excitation spectra were collected at room temperature on a Cary Eclipse fluorescence spectrophotometer (Agilent Technologies) equipped with a Varian Cary Temperature Controller.

4.3 synthesis PTX RAFT CTA

In a 10 mL round-bottom flask, PABTC (0.386 mmol, 0.092 g), 4-(dimethylamino)pyridine (DMAP) (0.039 mmol, 0.005 g) and PTX (0.351 mmol, 0.300 g) were dissolved in 3.865 mL anhydrous dichloromethane (DCM). Next, *N,N'*-diisopropylcarbodiimide (DIC) (0.386 mmol, 0.049 g) was added dropwise and reaction was stirred for 1 hour at room temperature and monitored by TLC. Subsequently, mixture was filtered and concentrated *in vacuo*. The crude product was purified by silica gel chromatography (eluent 6:4 hexane:ethyl acetate v/v). After concentration and subsequent drying under high vacuum, the obtained yellow solid (0.326 mmol, 0.350 g, 93 %) was analyzed by NMR spectroscopy and ESI-MS.

4.4 RAFT polymerization

PTX-PABTC (0.186 mmol, 0.200 g), 2,2'-azobis(2-methylpropionitrile) (AIBN) (0.037 mmol, 0.006 g) and *N,N*-dimethylacrylamide (DMA) (5.592 mmol, 0.554 g or 2.796 mmol, 0.277 g; for targeted degree of polymerization (DP) of 30 and 15, respectively) were dissolved in a Schlenk tube in *N,N*-dimethylformamide (DMF) to obtain a monomer concentration of 2 M and a CTA:initiator molar ratio of 5:1. The solutions were subjected to 5 freeze-pump-thaw cycles before polymerization was initiated at 70 °C for 3 h under vacuum. Monomer conversion was determined by ¹H-NMR spectroscopy. Polymers were collected by triple precipitation from cold (4 °C) diethyl ether and the obtained light yellow solids were subsequently dried under high vacuum (PTX-polyDMA₃₀ (0.158 mmol, 0.635 g, 85 %) and PTX-polyDMA₁₅ (0.117 mmol, 0.282 g, 63 %)).

A similar protocol was used for the synthesis of polyDMA₃₀ control polymer by dissolving PABTC (0.210 mmol, 0.050 g), DMA (6.303 mmol, 0.625 g) and AIBN (0.042 mmol, 0.007 g) in 2.364 mL dry DMF and subsequent RAFT polymerization and purification described above (0.166 mmol, 0.488 g, 79 %).

4.5 critical aggregation concentration (CAC)

CAC of PTX-polyDMA₃₀ was determined by fluorescence spectroscopy using pyrene as a fluorescent probe based on a described protocol.^[4] First, a dilution series of polymeric prodrug was prepared in PBS with concentrations ranging from 10⁻² to 10³ µg/mL. Secondly, a 3.6 mg/mL (1.8 x 10⁻² M) stock solution of pyrene in acetone was prepared and kept on ice to prevent evaporation of the acetone. Next, 10 µL of this solution was diluted to 1 mL acetone and kept on ice. To 6 mL of each conjugate dilution, 20 µL of the latter pyrene solution was added under stirring leading to a pyrene concentration of 6.0 x 10⁻⁷ M. The CAC was quantified by fluorescence spectrophotometry at room temperature based on the change in excitation intensity ratio at 338 and 333 nm with varying concentration.

4.6 rhodamine post-functionalization

PTX-polyDMA₃₀ was fluorescently labeled by post-functionalization of the ω-end group. First, trithiocarbonate ω-end group was removed by aminolysis. In a Schlenk tube, PTX-polyDMA₃₀ (0.007 mmol, 0.030 g) was dissolved in 1 mL dry DMF. To this yellow colored solution, 1-propylamine (0.297 mmol, 0.018 g) was added dropwise and reaction was stirred at room temperature for 30 minutes until the solution turned colorless. PTX-

polyDMA₃₀^{SH} (SH refers to the free thiol which was unmasked at the polymer chain end upon aminolysis of the trithiocarbonate) was collected by triple precipitation from cold (4 °C) diethyl ether and obtained white solid was subsequently dried under high vacuum. UV-VIS spectroscopy was performed to confirm removal of trithiocarbonate ω-end group.

In a next step, the obtained PTX-polyDMA₃₀^{SH} was dissolved in 3 mL 50 mM phosphate buffer containing 10 mM TCEP (tris(2-carboxyethyl)phosphine). To another Schlenk tube, tetramethyl rhodamine (Rho) maleimide (0.009 mmol, 0.005 g) was dissolved in 1 mL dimethyl sulfoxide (DMSO). Both Schlenk tubes were subjected to 3 freeze-pump-thaw cycles. Next, the rhodamine solution was added dropwise to polymer. After overnight stirring at room temperature, reaction was quenched for 5 h with *N*-hydroxyethyl acrylamide (0.370 mmol, 0.043 g) and dialyzed against 1 : 1 methanol : distilled water for 1 day and finally against distilled water for 4 days (MWCO 1 kDa). The sample was subsequently freeze-dried and analyzed by SEC in DMAc, reversed-phase (RP)-TLC and DLS (0.003 mmol, 0.015 g, 45 %).

4.7 cell culture

SKOV-3 human ovarian cancer cells were cultured in DMEM, supplemented with 10 % FBS, 2 mM L-glutamine, 1 mM sodium pyruvate and antibiotics (50 units/mL penicillin and 50 µg/mL streptomycin). Cells were incubated at 37 °C in a controlled, sterile environment of 95 % relative humidity and 5 % CO₂.

4.8 confocal microscopy

Hoechst stock solution of 1 mg/mL was prepared in DMSO. Alexa Fluor 488 Phalloidin stock solution of 6.6 µM was prepared in methanol. Of both stock solutions 6 and 35 µL were added to 1.4 mL of PBS supplemented with 1 % bovine serum albumin (BSA), respectively. LysoTracker Green 1 mM stock solution in DMSO was diluted in culture medium to obtain a working concentration of 60 nM. SKOV-3 cells were plated out on Willco-Dish glass bottom dishes (5 000 cells, suspended in 200 µL of culture medium) and incubated overnight at 37 °C. Next, 20 µL of a 5 mg/mL PTX-polyDMA₃₀-Rho solution in PBS was added to obtain a well concentration of 455 µg/mL. The labeled PTX-polymer conjugate was subsequently incubated for 2 h either at 4 °C or 37 °C.

Hoechst-Phalloidin co-staining was carried out on fixed cells. In summary, culture medium was aspirated and cells were washed three times with PBS. Next, 200 µL of 4 % paraformaldehyde was added and allowed to

fixate for 15 minutes. After aspiration and washing, 200 μ L of Hoechst-Phalloidin working solution was added and incubated for 30 minutes at 37 °C. Samples were washed with PBS prior to imaging.

LysoTracker staining was performed on live cells. Briefly, culture medium was aspirated and cells were washed with PBS. Next, 200 μ L of LysoTracker working solution was added and allowed to incubate 1 h at 37 °C before performing confocal microscopy.

In an additional experiment, 5 000 SKOV-3 cells were incubated for 2 h in culture medium supplemented with 455 μ g/mL PTX-polyDMA₃₀-RHO and 2 mg/mL Dextran Alexa Fluor 488. After incubation, cells were washed with PBS and fixed with 4 % paraformaldehyde as described earlier. Confocal microscopy was carried out on a Leica DM16000 B inverted microscope equipped with an oil immersion objective (Leica, 63 \times , NA 1.40) and attached to an Andor DSD2 confocal scanner. Images were processed with the ImageJ software package.

4.9 *in vitro* cytotoxicity

In vitro cytotoxicity was assessed by MTT assay. Dilution series of polyDMA₃₀ control polymer and PTX-polyDMA₃₀ conjugate were prepared in PBS with concentrations ranging from 5 \times 10⁻⁵ to 50 μ M. Two control nanoparticle PTX formulations Abraxane (Celgene) and Genexol-PM (Samyang Biopharmaceuticals) were diluted in PBS to obtain PTX concentrations ranging from 5 \times 10⁻⁵ to 50 μ M. MTT stock solution was prepared by dissolving 100 mg MTT in 20 mL PBS and subsequent membrane filtration (0.220 μ m). Before use, the MTT stock solution was 5-fold diluted in culture medium.

Briefly, SKOV-3 cells were seeded into 96-well plates (10 000 cells per well, suspended in 200 μ L of culture medium) and incubated overnight. Next, 50 μ L of sample, DMSO (positive control = 0 % viability) or PBS (negative control = 100 % viability) was added, followed by 72 h of incubation. Subsequently, medium was aspirated and cells were washed with 250 μ L of PBS. After aspiration, 100 μ L of MTT working solution was added and cells were incubated for 2 h. Finally, MTT working solution was aspirated and the formed purple formazan crystals were dissolved in 50 μ L of DMSO. Absorbance was determined at 590 nm using an EnVision Multilabel plate reader. The absorbance of the positive control was used as blank and therefore subtracted from all values.

5 references

- [1] A. Z. Wang, R. Langer, O. C. Farokhzad, in *Annu. Rev. Med.* (Eds.: C.T. Caskey, C.P. Austin, J.A. Hoxie), **2012**, pp. 185–198.
- [2] M. Elsabahy, K. L. Wooley, *Chem. Soc. Rev.* **2012**, *41*, 2545–61.
- [3] S. Kasmi, B. Louage, L. Nuhn, A. Van Driessche, J. Van Deun, I. Kalalic, M. Risseeuw, S. Van Calenbergh, R. Hoogenboom, R. De Rycke, et al., *Biomacromolecules* **2016**, *17*, 119–127.
- [4] B. Louage, Q. Zhang, N. Vanparijs, L. Voorhaar, S. Vande Castelee, Y. Shi, W. E. Hennink, J. Van Bocxlaer, R. Hoogenboom, B. G. De Geest, *Biomacromolecules* **2015**, *16*, 336–50.
- [5] N. Desai, *Clin. Cancer Res.* **2006**, *12*, 1317–1324.
- [6] T.-Y. Kim, *Clin. Cancer Res.* **2004**, *10*, 3708–3716.
- [7] Y. Shi, R. van der Meel, B. Theek, E. O. Blenke, E. H. E. Pieters, M. Fens, J. Ehling, R. M. Schiffelers, G. Storm, C. F. van Nostrum, et al., *ACS Nano* **2015**, *9*, 3740–3752.
- [8] H. Chen, S. Kim, L. Li, S. Wang, K. Park, J.-X. Cheng, *Proc. Natl. Acad. Sci. U. S. A.* **2008**, *105*, 6596–601.
- [9] N. Larson, H. Ghandehari, *Chem. Mater.* **2012**, *24*, 840–853.
- [10] F. Greco, M. J. Vicent, *Adv. Drug Deliv. Rev.* **2009**, *61*, 1203–13.
- [11] E. M. Pegreli-O'Day, E.-W. Lin, H. D. Maynard, *J. Am. Chem. Soc.* **2014**, *136*, 14323–32.
- [12] N. Vanparijs, S. Maji, B. Louage, L. Voorhaar, D. Laplace, Q. Zhang, Y. Shi, W. E. Hennink, R. Hoogenboom, B. G. De Geest, *Polym. Chem.* **2015**, *6*, 5602–5614.
- [13] K. L. Heredia, D. Bontempo, T. Ly, J. T. Byers, S. Halstenberg, H. D. Maynard, *J. Am. Chem. Soc.* **2005**, *127*, 16955–60.
- [14] B. S. Sumerlin, *ACS Macro Lett.* **2012**, *1*, 141–145.
- [15] P. De, M. Li, S. R. Gondi, B. S. Sumerlin, *J. Am. Chem. Soc.* **2008**, *130*, 11288–9.
- [16] J. Xu, K. Jung, N. A. Corrigan, C. Boyer, *Chem. Sci.* **2014**, *5*, 3568.
- [17] Q. Zhang, M. Li, C. Zhu, G. Nurumbetov, Z. Li, P. Wilson, K. Kempe, D. M. Haddleton, *J. Am. Chem. Soc.* **2015**, *137*, 9344–53.
- [18] N. Vanparijs, R. De Coen, D. Laplace, B. Louage, S. Maji, L. Lybaert, R. Hoogenboom, B. G. De Geest, *Chem. Comm.* **2015**, *51*, 13972–13975.
- [19] R. Tong, J. Cheng, *Angew. Chem. Int. Ed. Engl.* **2008**, *47*, 4830–4834.
- [20] D. Trung Bui, A. Maksimenko, D. Desmaële, S. Harrison, C. Vauthier, P. Couvreur, J. Nicolas, *Biomacromolecules* **2013**, *14*, 2837–47.
- [21] H. M. Deutsch, J. A. Glinski, M. Hernandez, R. D. Haugwitz, V. L. Narayanan, M. Suffness, L. H. Zalkow, *J. Med. Chem.* **1989**, *32*, 788–792.
- [22] D. G. I. Kingston, *Chem. Comm.* **2001**, 867–880.
- [23] P. H. Kierstead, H. Okochi, V. J. Venditto, T. C. Chuong, S. Kivimae, J. M. J. Fréchet, F. C. Szoka, *J. Control. Release* **2015**, *213*, 1–9.
- [24] Y. Shi, M. J. van Steenbergen, E. A. Teunissen, L. Novo, S. Gradmann, M. Baldus, C. F. van Nostrum, W. E. Hennink, *Biomacromolecules* **2013**, *14*, 1826–1837.
- [25] C. Boyer, V. Bulmus, T. P. Davis, V. Ladmira!, J. Q. Liu, S. Perrier, *Chem. Rev.* **2009**, *109*, 5402–5436.
- [26] H. Willcock, R. K. O'Reilly, *Polym. Chem.* **2010**, *1*, 149–157.
- [27] E. L. Racoosin, *J. Cell Biol.* **1993**, *121*, 1011–1020.
- [28] C. Ryppa, H. Mann-Steinberg, M. L. Biniossok, R. Satchi-Fainaro, F. Kratz, *Int. J. Pharm.* **2009**, *368*, 89–97.
- [29] M. M. Gottesman, T. Fojo, S. E. Bates, *Nat. Rev. Cancer* **2002**, DOI 10.1038/nrc706.
- [30] A. Eldar-Boock, K. Miller, J. Sanchis, R. Lupu, M. J. Vicent, R. Satchi-Fainaro, *Biomaterials* **2011**, *32*, 3862–74.
- [31] C. J. Ferguson, R. J. Hughes, D. Nguyen, B. T. T. Pham, R. G. Gilbert, A. K. Serelis, C. H. Such, B. S. Hawkett, *Macromolecules* **2005**, *38*, 2191–2204.

6 supporting info

6.1 paclitaxel

PTX was purchased from LC Laboratories and its purity was confirmed by NMR spectroscopy and ESI-MS.

$^1\text{H-NMR}$ (300 MHz, CDCl_3): δ [ppm] = 8.11 (d, J = 7.1 Hz, 2H, *o*-20-ArH); 7.72 (d, J = 7.1 Hz, 2H, *o*-3'NH-ArH); 7.60 (t, J = 7.4 Hz, 1H, *p*-20-ArH); 7.53 – 7.30 (m, 10H, 3'-ArH and 20-ArH and 3'NH-ArH); 7.12 (d, J = 8.9 Hz, 1H, 3'-NH); 6.27 (s, 1H, 10-H); 6.20 (t, J = 8.6 Hz, 1H, 13-H); 5.76 (dd, J = 8.9, 2.8 Hz, 1H, 3'-H); 5.66 (d, J = 7.1 Hz, 1H, 2-H); 4.92 (dd, J = 9.7, 2.2 Hz, 1H, 5-H); 4.77 (dd, J = 5.5, 2.8 Hz, 1H, 2'-H); 4.38 (ddd, J = 11.0, 6.6, 4.4 Hz, 1H, 7-H); 4.24 (dd, J = 29.7, 8.4 Hz, 2H, 20-HH); 3.85 (d, J = 5.5 Hz, 1H, 2'-OH); 3.78 (d, J = 7.0 Hz, 1H, 3'-H); 2.58 (d, J = 4.3 Hz, 1H, 7'-OH); 2.55 – 2.42 (m, 1H, 6-HH); 2.36 (s, 3H, 40-Ac-H); 2.34 – 2.22 (m, 2H, 14-H₂); 2.21 (s, 3H, 100-Ac-H); 2.03 (s, 1H, 1-OH); 1.85 (ddd, J = 14.0, 11.0, 2.4 Hz, 1H, 6-HH); 1.78 (d, J = 1.4 Hz, 3H, 18-H₃); 1.67 (s, 3H, 19-H₃); 1.22 (s, 3H, 16-H₃); 1.13 (s, 3H, 17-H₃).

$^{13}\text{C-NMR}$ (75 MHz, CDCl_3): δ [ppm] = 209.73 (9-CO); 172.81 (1'-CO); 171.35 (10-O-CO); 170.49 (4-O-CO); 167.33 (3'-NH-CO); 167.02 (2-O-CO); 142.03 (12-C); 133.81 (12-C); 138.10, 133.73, 133.25, 132.06, 130.29, 129.29, 129.09, 128.82, 128.78, 128.42, 127.18 and 127.14 (20-ArH, 3'-NH-ArH and 3'-ArH); 84.50 (5-C); 81.22 (4-C); 79.03 (1-C); 76.60 (20-C); 75.69 (10-C); 75.06 (2-C); 73.32 (2'-C); 72.35 (13-C); 72.22 (7-C); 58.65 (8-C); 55.23 (3'-C); 45.78 (3-C); 43.27 (15-C); 35.80 (14-C); 35.76 (6-C); 26.93 (16-C); 22.71 (40-Ac-C); 21.93 (17-C); 20.97 (100-Ac-C); 14.92 (18-C); 9.70 (19-C).

ESI-MS (acetonitrile): calcd for $\text{C}_{47}\text{H}_{51}\text{NO}_{14}$ 853.33, found 854.34 [M+H]⁺

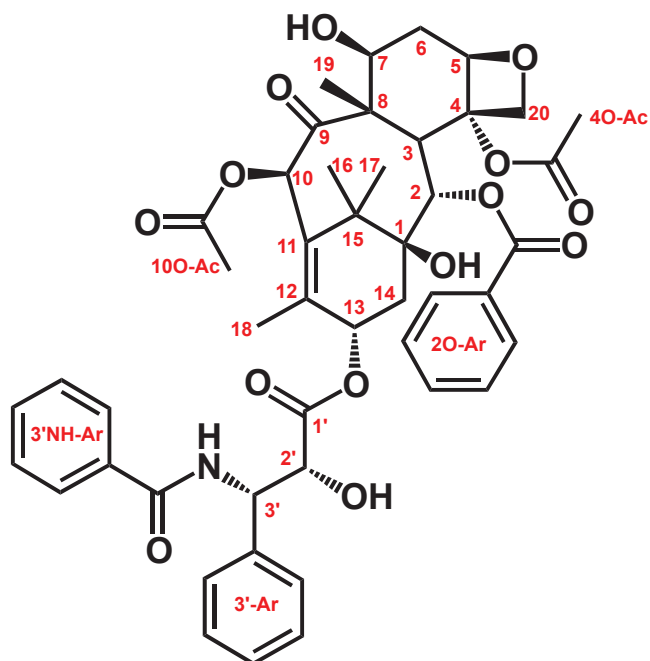


Figure S1. Structure and annotation of PTX.

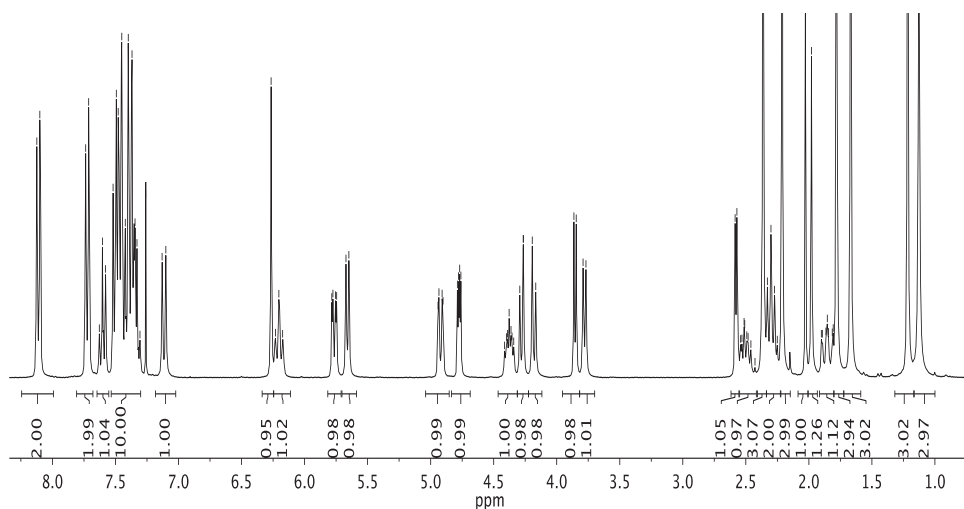


Figure S2. $^1\text{H-NMR}$ (300 MHz, CDCl_3) spectrum of PTX.

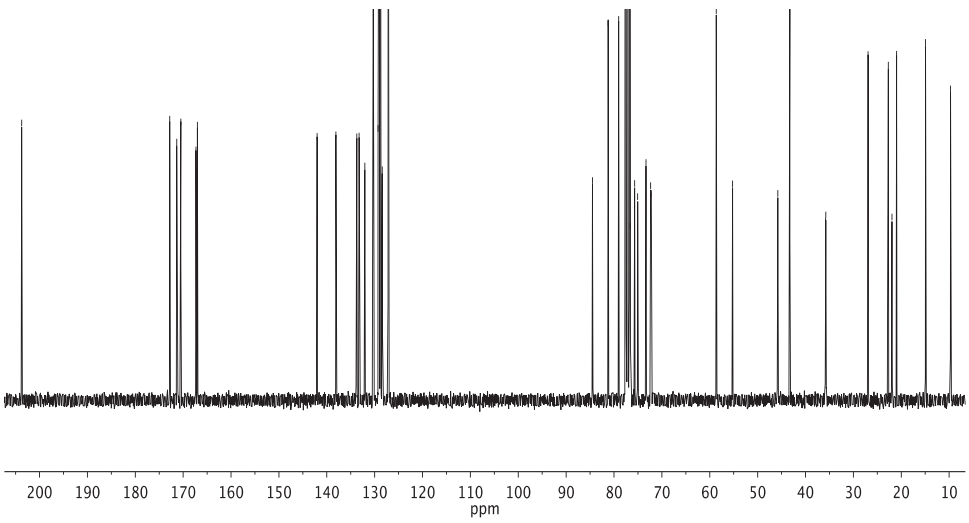


Figure S3. ^{13}C -NMR (75 MHz, CDCl_3) spectrum of PTX.

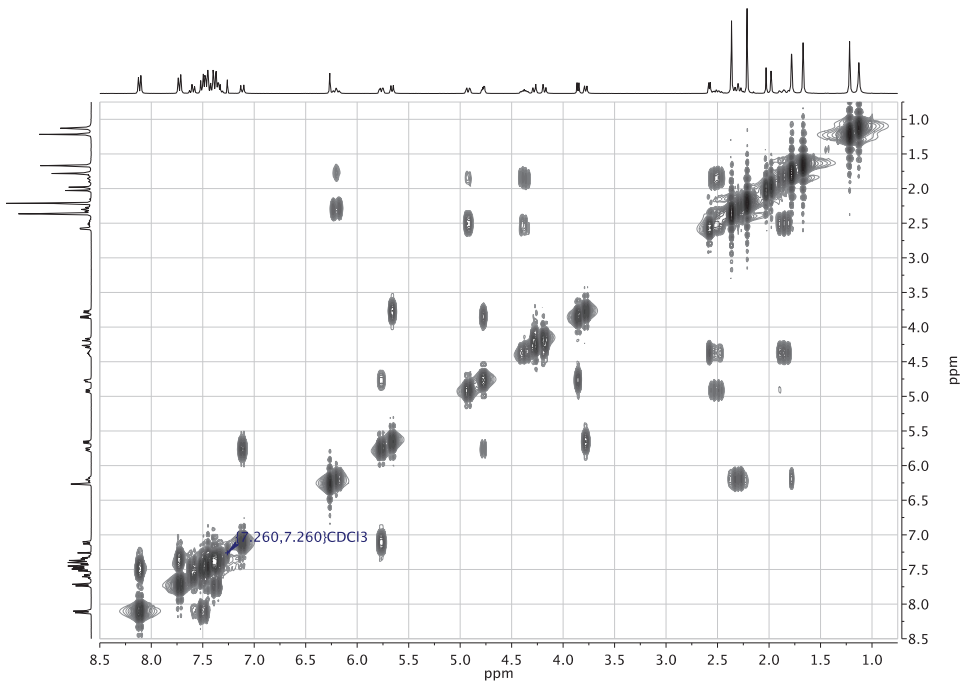


Figure S4. ^1H , ^1H -COSY spectrum of PTX.

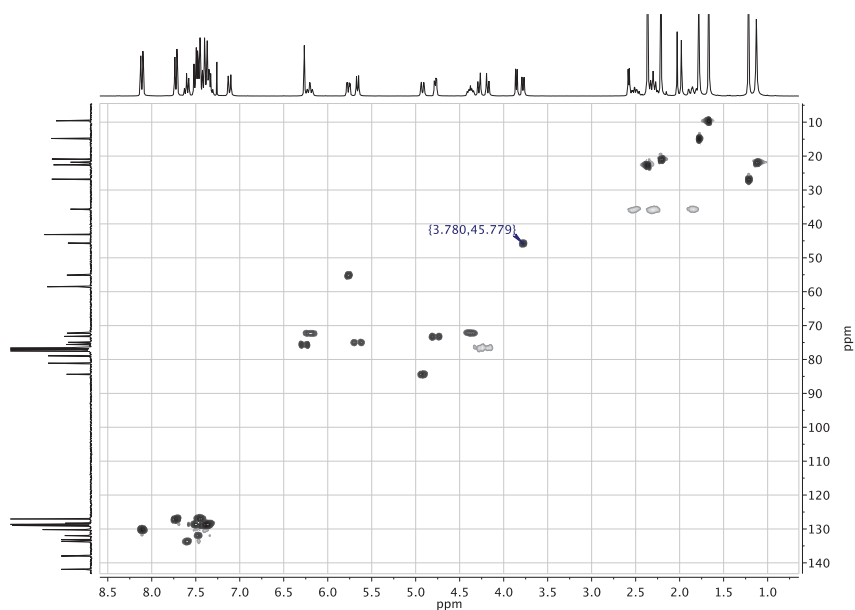


Figure S5. ^1H , ^{13}C -HSQC spectrum of PTX.

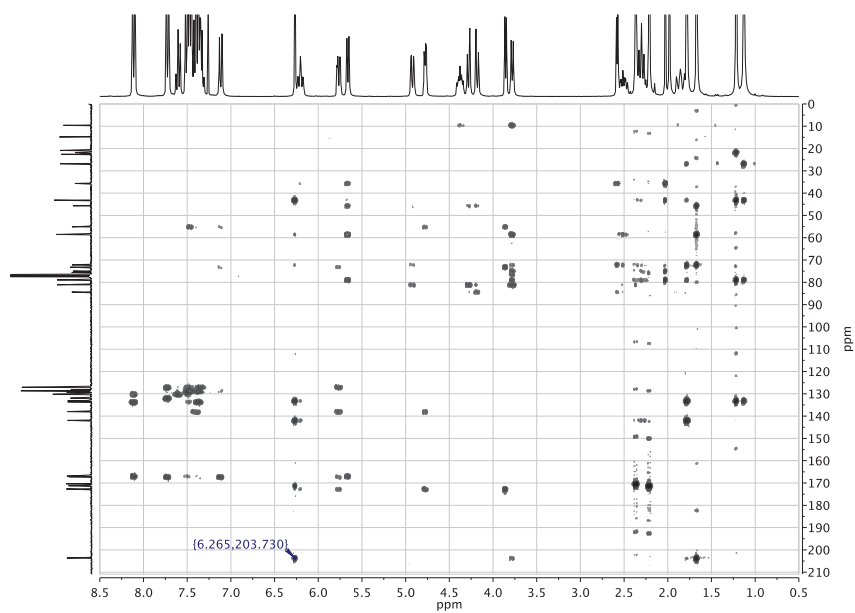


Figure S6. ^1H , ^{13}C -HMBC spectrum of PTX.

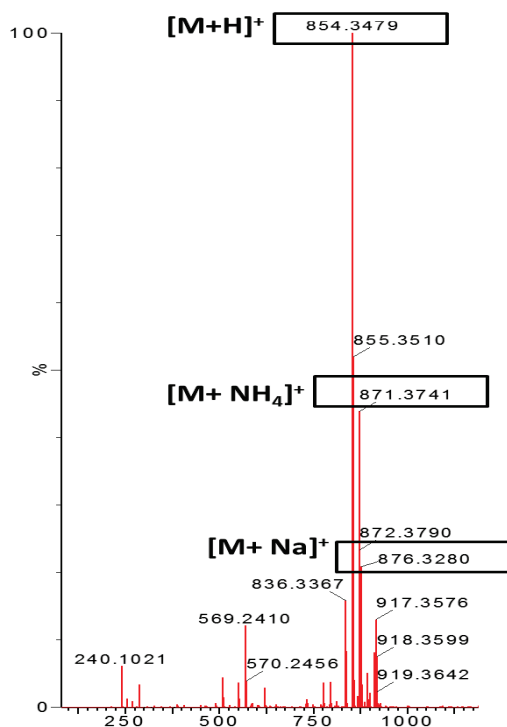


Figure S7. ESI-MS (acetonitrile) spectrum of PTX.

6.2 PTX RAFT CTA

$^1\text{H-NMR}$ (400 MHz, CDCl_3): δ [ppm] = 8.14 (dt, J = 8.6, 1.5 Hz, 2H, *o*-20-ArH); 7.81 – 7.70 (m, 2H, *o*-3'NH-ArH); 7.61 (tt, J = 7.4, 1.5 Hz, 1H, *p*-20-ArH); 7.53 – 7.30 (m, 10H, 3'-ArH and 20-ArH and 3'NH-ArH); 6.84 (d, J = 9.2 Hz, 1H, 3'-NH); 6.29 (s, 1H, 10'-H); 6.28 (t, J = 9.2 Hz, 1H, 13'-H); 5.96 (ddd, J = 9.2, 9.2, 2.7 Hz, 1H, 3'-H); 5.69 (d, J = 7.1 Hz, 1H, 2'-H); 5.45 (dd, J = 12.9, 2.6 Hz, 1H, 2'-H); 5.11 – 4.87 (m, 2H, 5'-H and -CH (PABTC)); 4.44 (ddd, J = 11.0, 6.7, 4.4 Hz, 1H, 7'-H); 4.26 (dd, J = 45.7, 8.3 Hz, 2H, 20'-HH); 3.81 (d, J = 7.0 Hz, 1H, 3'-H); 3.45 – 3.15 (m, 2H, -S-CH₂ (PABTC)); 2.61 – 2.51 (m, 1H, 6'-H); 2.47 (s, 1H, 7'-O-H); 2.44 (s, 3H, 40-Ac-H); 2.43 – 2.34 (m, 1H, 14-H-H); 2.22 (s, 3H, 100-Ac-H); 2.22 – 2.17 (m, 1H, 6-H-H); 2.17 (s, 1H, 1-O-H); 1.94 (d, J = 1.4 Hz, 3H, 18-H₃); 1.93 – 1.82 (m, 1H, 14'-H-H); 1.68 (s, 3H, 19-H₃); 1.66 – 1.61 (m, 2H, -S-CH₂-CH₂ (PABTC)); 1.58 (dd, J = 20.2, 7.5 Hz, 3H, -CH-CH₃ (PABTC)); 1.40 (dh, J = 7.6, 3.2 Hz, 2H, -S-CH₂-CH₂-CH₂ (PABTC)); 1.23 (s, 3H, 16-H₃); 1.13 (s, 3H, 17-H₃); 0.91 (t, J = 7.3, 3H, -S-CH₂-CH₂-CH₂-CH₃ (PABTC)).

^{13}C -NMR (100 MHz, CDCl_3): δ [ppm] = [>220.0 (S-C-S)]; 209.96 (9-CO); 171.38 (10-O-CO); 170.54 (d, -CO- (PABTC)); 169.89 (4-O-CO); 167.55 (d, 1'-CO); 167.18 (2-O-CO); 167.12 (d, 3'-NH-CO); 142.87 (12-C); 133.82 (12-C); 136.95(d), 133.71, 132.95(d), 132.15(d), 130.37, 129.31, 129.19, 128.89, 128.86, 128.60, 127.30 and 126.72(d) (20-ArH, 3'-NH-ArH and 3'-ArH); 84.59 (5-C); 81.21 (4-C); 79.29 (1-C); 76.59 (20-C); 75.69 (10-C); 75.24 (2-C); 75.07 (d, 2'-C); 72.27 (7-C); 72.07 (d, 13-C); 58.66 (8-C); 52.85 (3'-C); 46.59 (d, -CH- (PABTC)); 45.69 (3-C); 43.33 (15-C); 37.38 (-S-CH₂- (PABTC)); 35.70 (14-C); 35.65 (6-C); 29.96 (d, -S-CH₂-CH₂- (PABTC)); 26.97 (16-C); 22.86 (40-Ac-C); 22.30 (17-C); 22.19 (S-CH₂-CH₂-CH₂- (PABTC)); 20.96 (100-Ac-C); 16.04 (d, -CH-CH₃ (PABTC)); 14.98 (18-C); 13.70 (d, -S-CH₂-CH₂-CH₂-CH₃ (PABTC)); 9.74 (19-C).

ESI-MS (acetonitrile): m/z = calcd for $\text{C}_{55}\text{H}_{63}\text{NO}_{15}\text{S}_5$ 1073.33, found 1074.34 [M+H]⁺

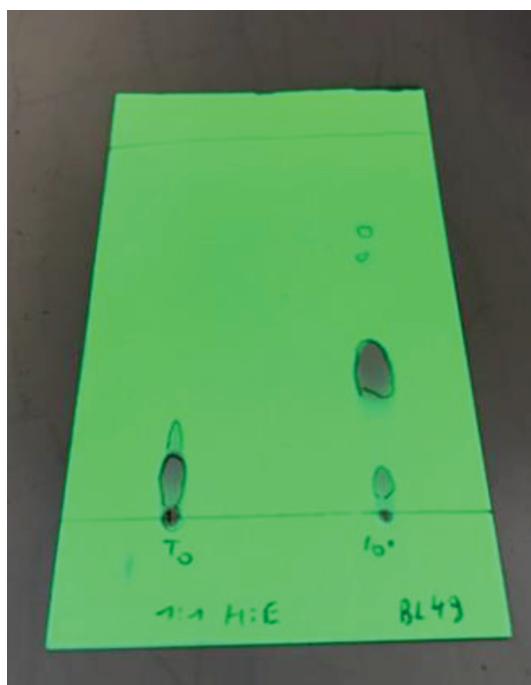


Figure S8. TLC before (left) and 10 minutes after adding DIC (right) to PABTC:PTX reaction mixture (eluent: 1:1 hexane:ethyl acetate v/v).

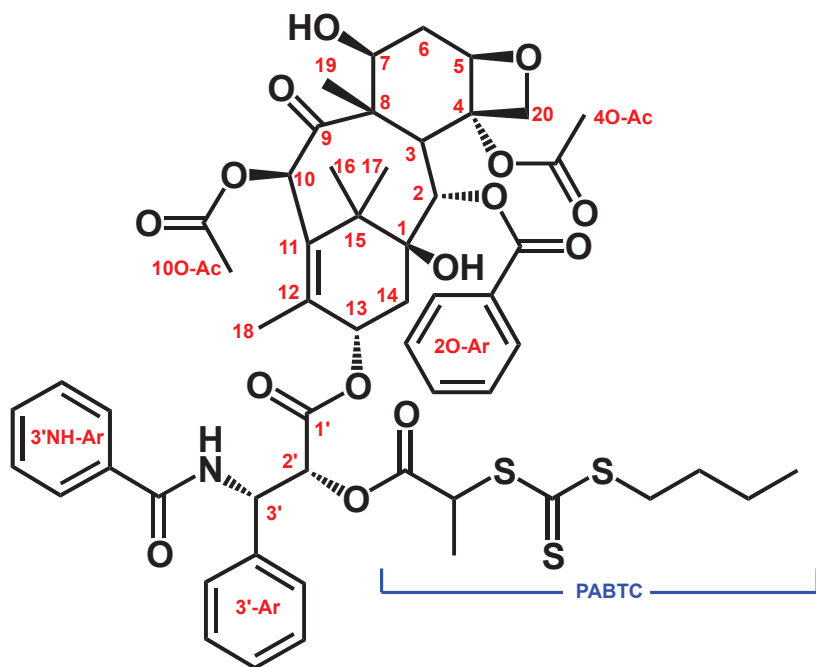


Figure S9. Structure and annotation of PTX-PABTC.

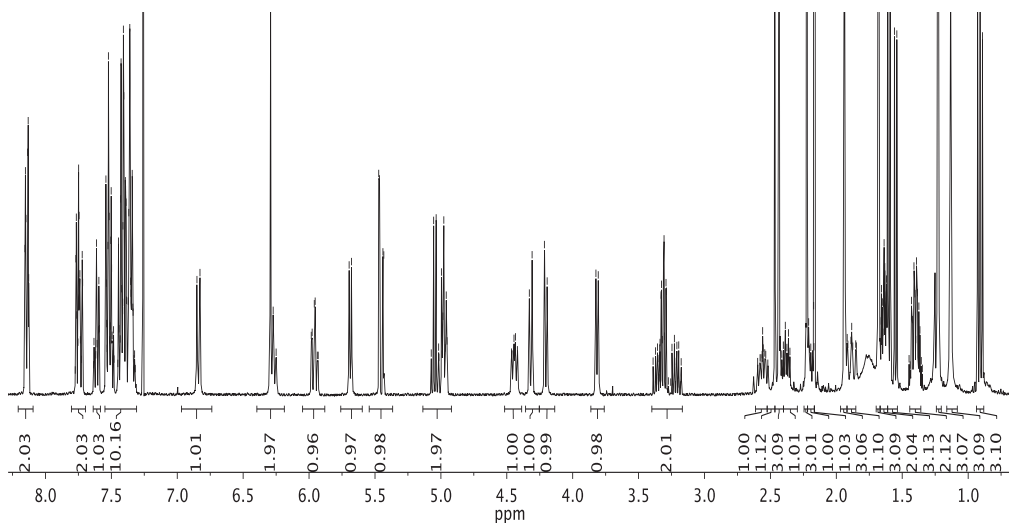


Figure S10. ¹H-NMR (400 MHz, CDCl₃) spectrum of PTX-PABTC.

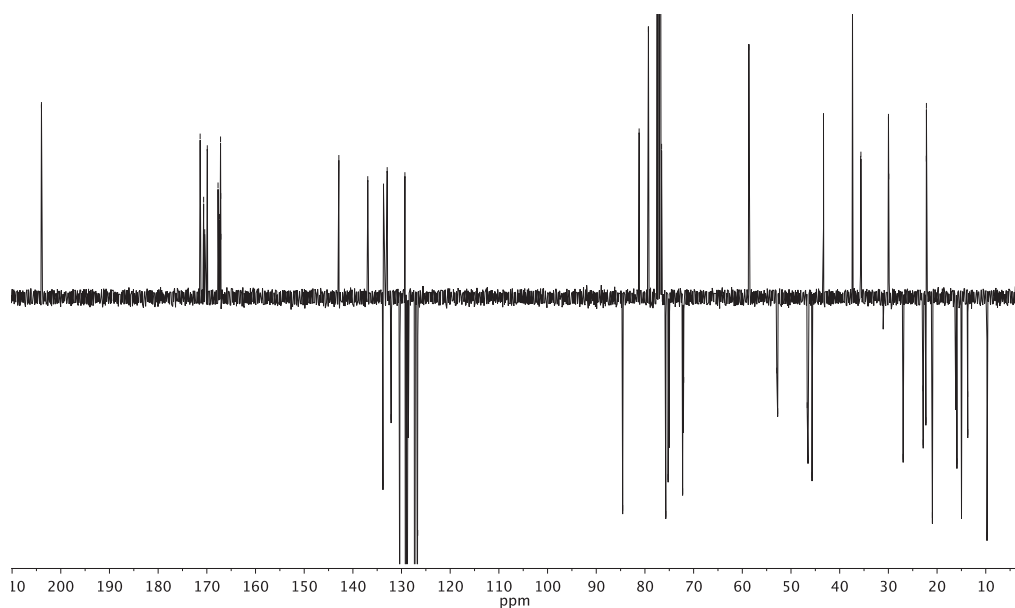


Figure S11. ^{13}C -APT-NMR (100 MHz, CDCl_3) spectrum of PTX-PABTC.

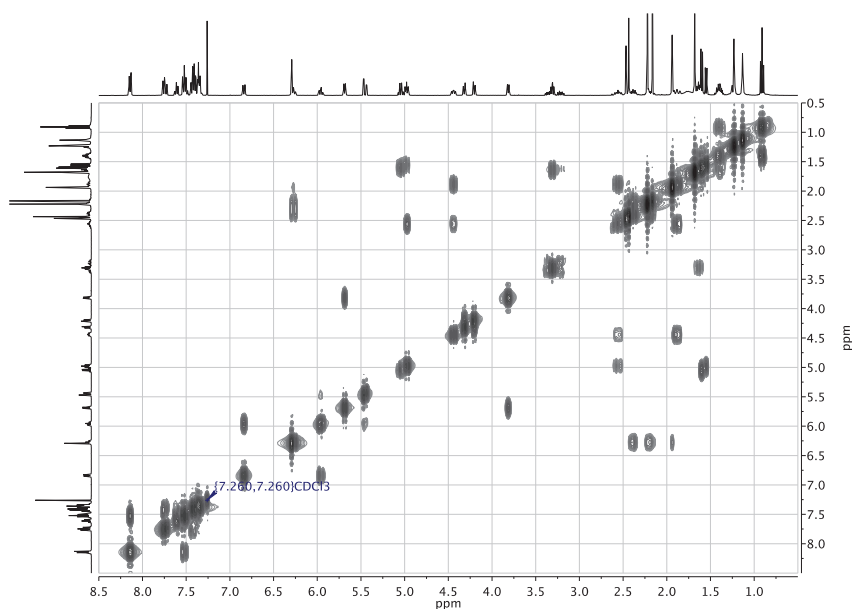


Figure S12. ^1H , ^1H -COSY spectrum of PTX-PABTC.

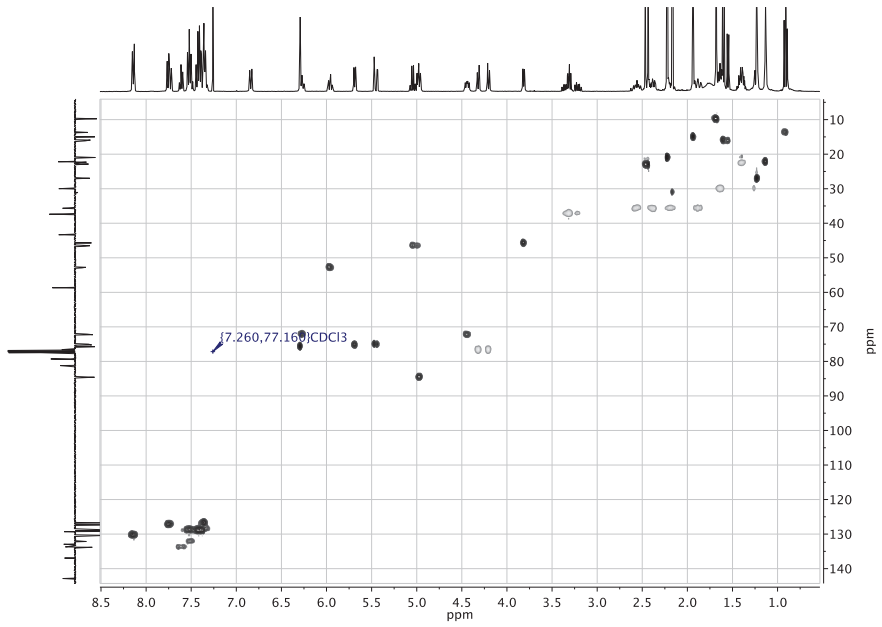


Figure S13. ^1H , ^{13}C -HSQC spectrum of PTX-PABTC.

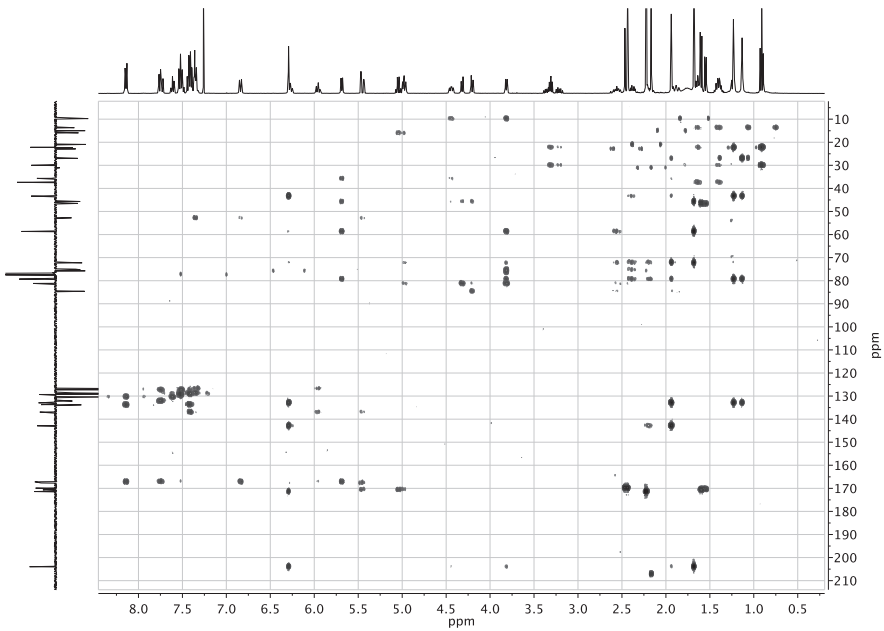


Figure S14. ^1H , ^{13}C -HMBC spectrum of PTX-PABTC.

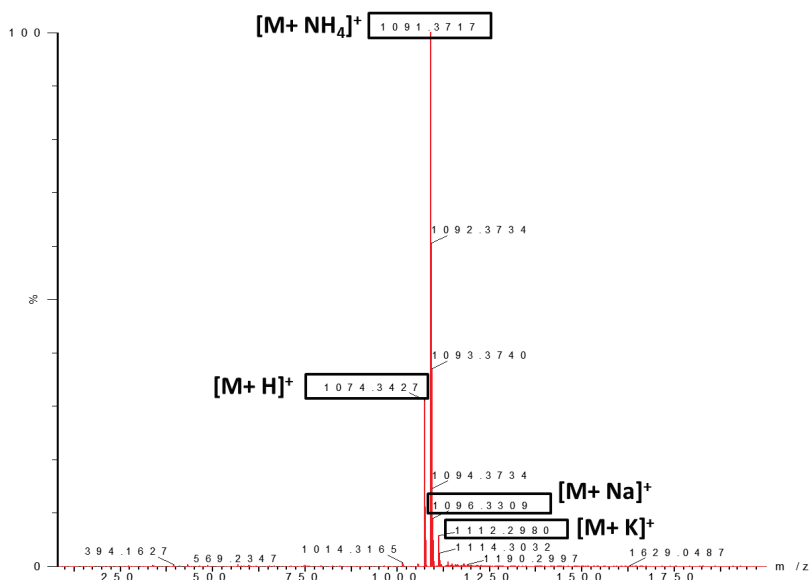


Figure S15. ESI-MS (acetonitrile) spectrum of PTX-PABTC.

6.3 PTX-polyDMA

SEC(DMAC, PMMA-St.): Mn = 2648, PDI = 1.09 (PTX-polyDMA₁₅) and Mn = 4356, PDI = 1.07 (PTX-polyDMA₃₀).

¹H-NMR (300 MHz, MeOH-*d*₄): δ [ppm] = 8.14 (d, *J* = 7.6 Hz, 2H, *o*-20-Ar*H*); 7.84 (d, *J* = 7.8 Hz, 2H, *o*-3'NH-Ar*H*); 7.75 – 7.21 (m, 11H, 3'-Ar*H* and 20-Ar*H* and 3'NH-Ar*H*); 6.45 (s, 1H, 10-*H*); 6.08 (t, *J* = 9.5 Hz, 1H, 13-*H*); 5.97 – 5.69 (m, 1H, 3'-*H*); 5.64 (m, 1H, 2-*H*); 5.42 (m, 1H, 2'-*H*); 5.31 – 5.15 (m, 1H, -C*H* (PABTC)); 5.08 – 4.93 (m, 1H, 5-*H*); 4.34 (dd, *J* = 10.5, 6.5, 1H, 7-*H*); 4.18 (m, 2H, 20-*HH*); 3.86 – 3.70 (m, 1H, 3-*H*); 3.42 (td, *J* = 7.7, 2.4 Hz, 2H, -S-CH₂- (PABTC)); 3.25 – 1.08 (m, 173H [9x16=144H for polyDMA (DP16) and 22H for PTX and 7H for PABTC] for targeted DP15 and 308H [9x31=279H for polyDMA (DP31) and 22H for PTX and 7H for PABTC] for targeted DP30); 0.95 (td, *J* = 7.3, 1.6 Hz, 3H, -S-CH₂-CH₂-CH₂-CH₃ (PABTC)).

Calculation of the degree of polymerization for PTX-polyDMA₁₅, respectively PTX-polyDMA₃₀, was performed by integration of 3.3 -1.0 ppm (9 monomer protons overlap with 33 protons of the PTX-PABTC):

$$\Rightarrow \text{polyDMA}_{30}: \text{DP} = (307.47 - 33) / 9 = \underline{30.50}$$

$$\Rightarrow \text{polyDMA}_{15}: \text{DP} = (173.03 - 33) / 9 = \underline{15.56}$$

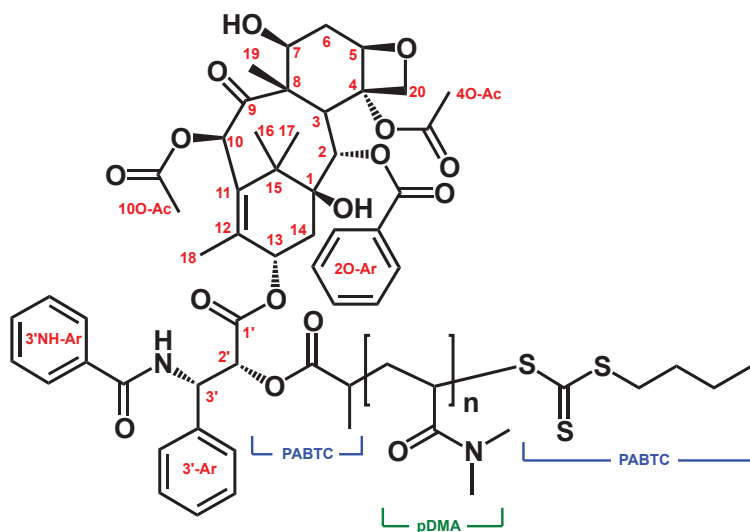


Figure S16. Structure and annotation of PTX-polyDMA.

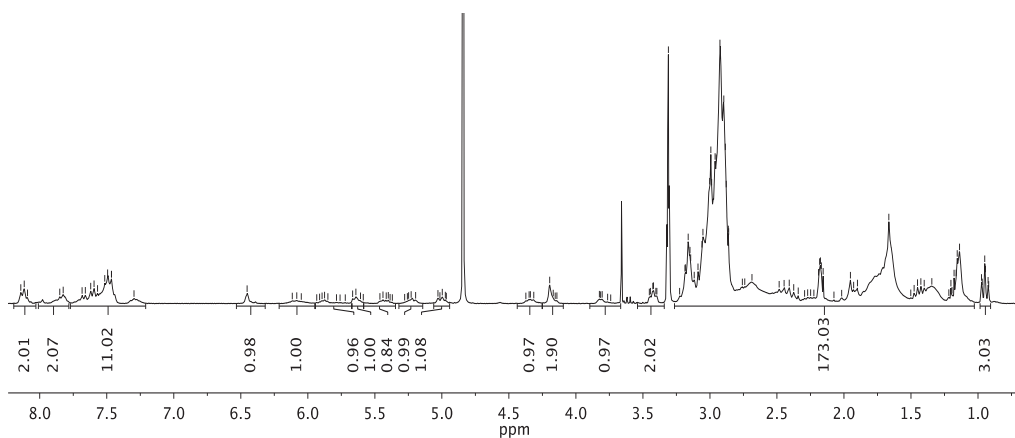


Figure S17. ¹H-NMR (300 MHz, MeOH-*d*₄) spectrum of PTX-polyDMA₁₅.

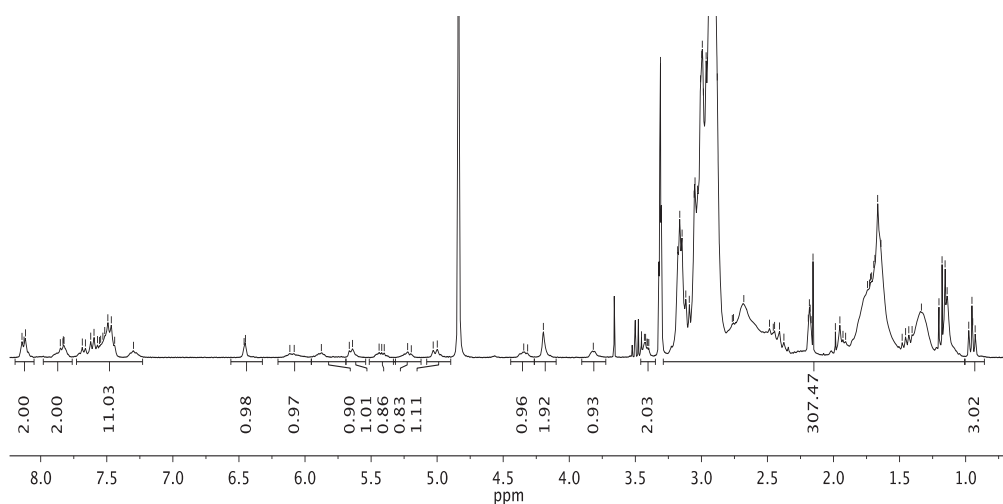


Figure S18. $^1\text{H-NMR}$ (300 MHz, $\text{MeOH-}d_4$) spectrum of PTX-polyDMA₃₀.

6.4 polyDMA

SEC(DMAC, PMMA-St.): $M_n = 3477$, PDI = 1.09

$^1\text{H-NMR}$ (300 MHz, $\text{MeOH-}d_4$): δ [ppm] = 5.30 – 5.14 (m, 1H, $-\text{C}=\text{H}$ (PABTC)); 3.47 – 3.34 (m, 2H, $-\text{S-CH}_2-$ (PABTC)); 3.22 – 1.23 (m, 268H [9x29=261H for polyDMA (DP29) and 7H for PABTC] for targeted DP30); 0.95 (td, $J = 7.3, 1.8$ Hz, 3H, $-\text{S-CH}_2-\text{CH}_2-\text{CH}_2-\text{CH}_3$ (PABTC)).

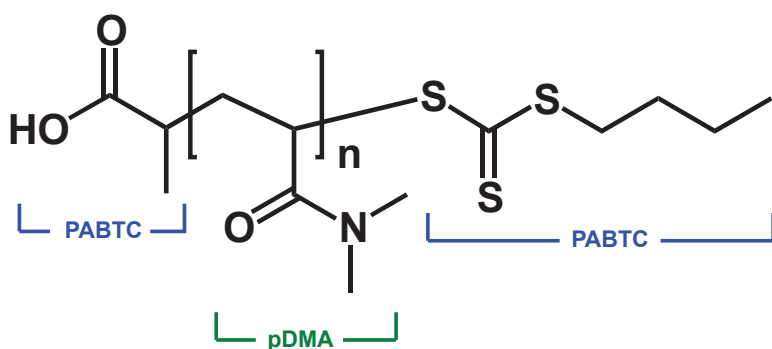


Figure S19. Structure of polyDMA.

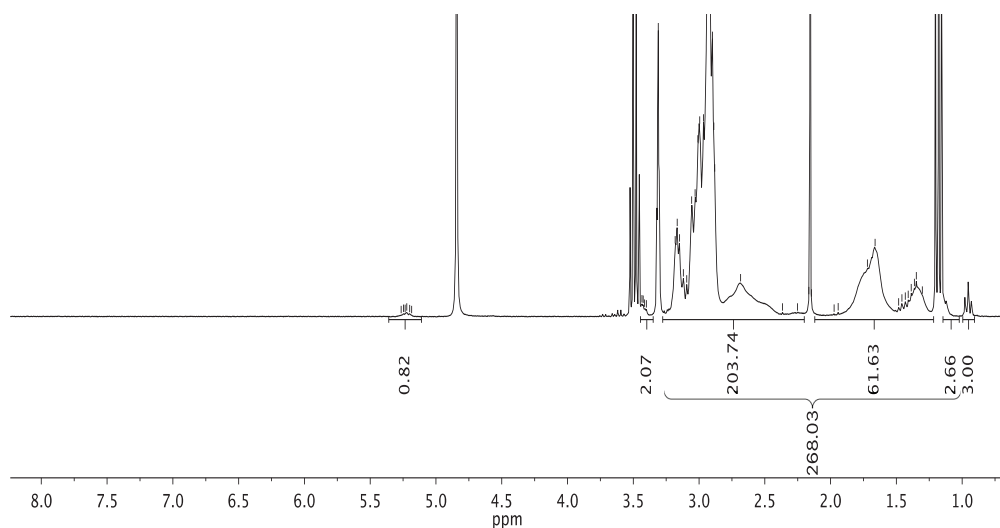


Figure S20. $^1\text{H-NMR}$ (300 MHz, MeOH-*d*₄) spectrum of polyDMA₅₀.

6.5 rhodamine post-functionalization

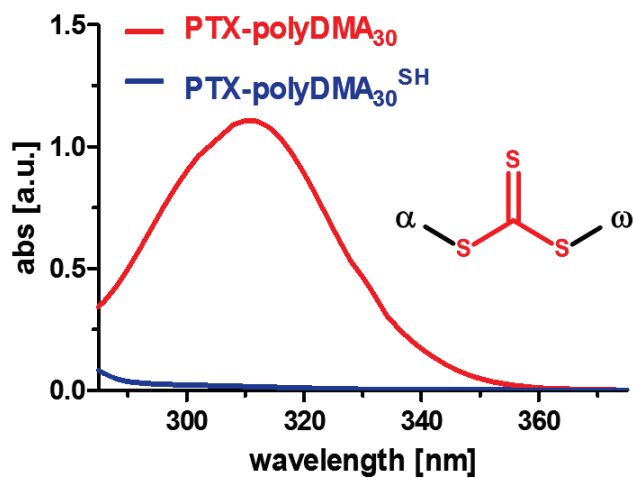


Figure S21. UV-VIS spectra confirming successful aminolysis of the trithiocarbonate RAFT end group.



Figure S22. Reversed phase TLC of free Rho dye (left) and PTX-polyDMA₃₀-Rho (right) (eluent: 1:1 H₂O:acetonitrile v/v, 1 % TFA).

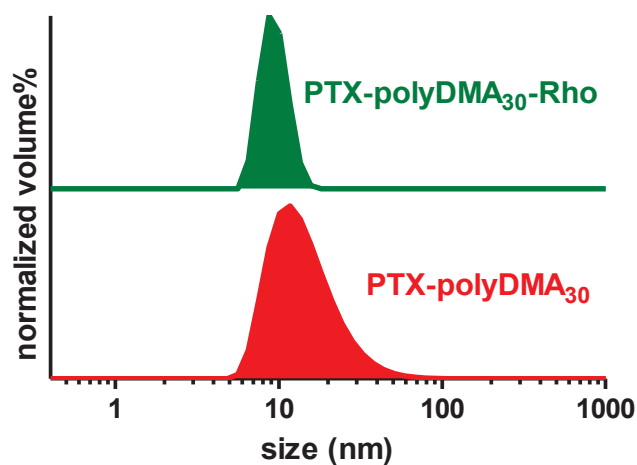


Figure S23. Size distribution measured by DLS of PTX-polyDMA₃₀ before and after labeling with rhodamine-maleimide.

chapter 6

micellar paclitaxel-initiated RAFT polymer conjugates with acid-sensitive behavior

Benoit Louage,^a Mies J. van Steenberg,^b Lutz Nuhn,^a Martijn D.P. Risseeuw,^c Izet Karalic,^c Johan Winne,^d
Serge Van Calenbergh,^c Wim E. Hennink,^b Bruno G De Geest^a

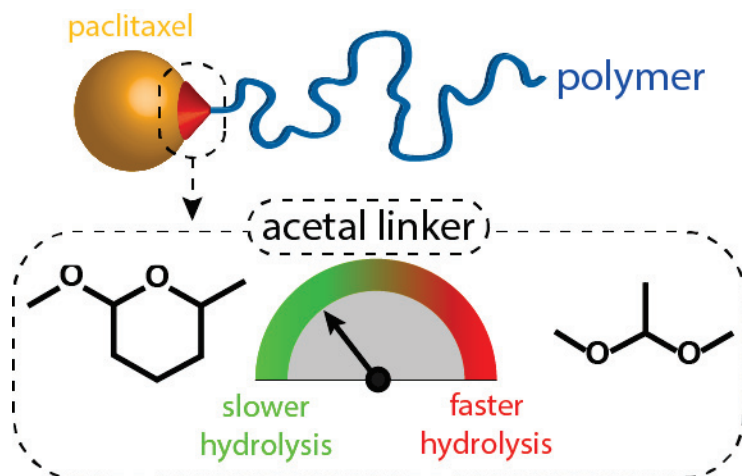
^a Laboratory of Pharmaceutical Technology, Department of Pharmaceutics,
Ghent University, Ottergemsesteenweg 460, 9000 Ghent, Belgium

^b Department of Pharmaceutics, Utrecht Institute for Pharmaceutical Sciences,
Utrecht University, Universiteitsweg 99, 3584CG Utrecht, The Netherlands

^c Laboratory for Medicinal Chemistry, Department of Pharmaceutics,
Ghent University, Ottergemsesteenweg 460, 9000 Ghent, Belgium

^d Department of Organic and Macromolecular Chemistry,
Ghent University, Krijgslaan 281 S4, 9000 Ghent, Belgium

ACS Macro Letters 2017, DOI: 10.1021/acsmacrolett.6b00977



abstract

Acid-sensitive PTX-polymer conjugates were designed by applying a grafting-from-drug RAFT approach. PTX was either linked through a cyclic or a linear, acid-sensitive acetal moiety. Relative to direct esterification of PTX, which occurred regioselectively at the C₂ OH-group, direct acetalization was observed at either the C₂ or the C₇ OH-group of PTX. This yielded 2 regio-isomers of acetal-based PTX-functionalized RAFT CTA. Subsequent polymerization with DMA resulted in amphiphilic highly-defined, acetal-based PTX-polymer conjugates with nearly identical features in terms of polymer definition and micellar self-assembly behavior, but with distinct PTX release kinetics and absence of burst release. This was further reflected by their *in vitro* biological performance, giving insights into the difference of release mechanism between ester- and cyclic and linear acetal-based PTX-polymer conjugates.

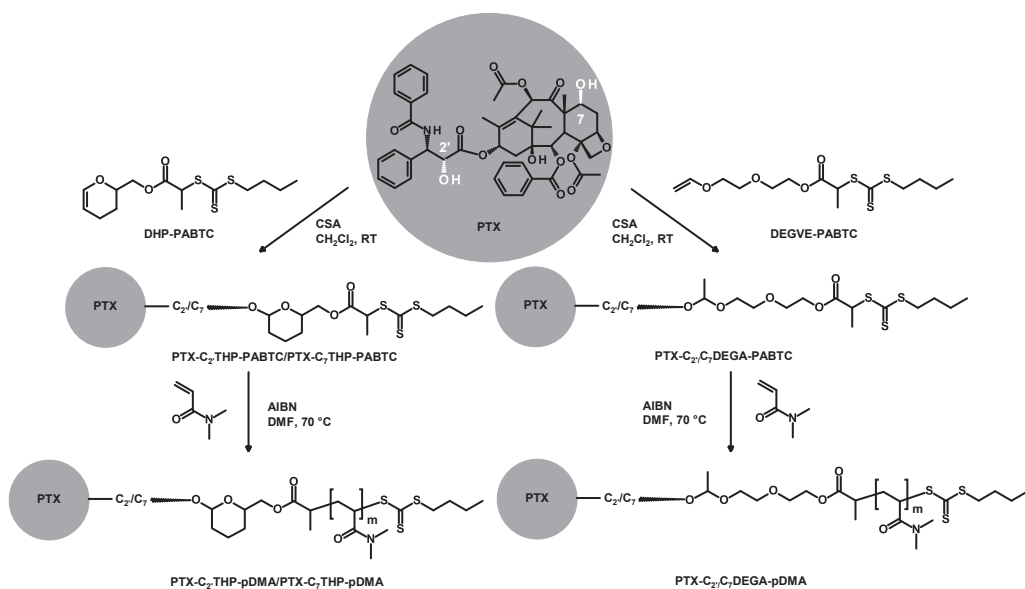
1 introduction

Taxanes (i.e. paclitaxel (PTX) and docetaxel (DTX)) are highly valuable anti-cancer drugs due to their broad-spectrum activity.^[1,2] However, the widespread use of these drugs in clinic remains elusive. During discovery and early development, it was found that both drugs exhibited very low water-solubility. In order to commercialize these drugs, formulation into a 1:1 ethanol:surfactant cosolvent mixture is required. Cremophor EL is used for the first commercial formulation of PTX (i.e. Taxol), whilst polysorbate 80 is exploited in the DTX formulation Taxotere. However, severe hypersensitivity reactions are attributed to these surfactants.^[3-7] This urged the development of formulations based on more benign excipients, leading to the FDA-approval of Abraxane (an albumin-stabilized PTX formulation) in 2005, and Genexol-PM (PTX, stabilized by poly(ethylene glycol)-*b*-poly(D,L-lactic acid); PEG-*b*-pDLLA) in South Korea 2 years later. The biocompatibility of both carriers significantly increased the therapeutic index, hence higher doses could be administered leading to a more effective chemotherapy.^[8]

However, as the aforementioned formulations are based on physical drug entrapment, intravenous administration still holds the risk of systemic release and distribution of drug and hence does not prevent the intrinsic side-effects of taxanes (i.e. neutropenia, neuropathy) from occurring. Besides physical drug entrapment by strong hydrophobic interaction, chemical conjugation is one of the most versatile strategies for more selective drug release.^[9,10] Typically, the drug is chemically conjugated to the (polymeric) carrier vehicle through a stimuli-responsive linker. The latter can then be cleaved either by a specific enzyme (e.g. by cathepsin B lysosomal enzymes)^[11] or by a subtle change in the chemical environment, as exploited by pH-sensitive (e.g. endosomal hydrolysis of acetals/ketals/hydrazone moieties) and redox-sensitive (e.g. cleavage of disulfides in response to hypoxic tumour microenvironment) carrier systems.^[12-14] Polymer-drug conjugates with the highest progress in clinical trials (e.g. Opaxio; PTX conjugated to 48 kDa poly(L-glutamic acid)) are typically prepared by post-functionalization of the polymer backbone with the drug.^[15] However, such strategy has inherent reproducibility challenges and requires tedious purification to remove excess unconjugated drug which could cause burst release upon intravenous administration.

A recently uprising trend in polymer-drug conjugate design is direct polymerization from a drug molecule.^[16,17] This technique is termed the 'grafting-from-drug' or 'drug-initiated' approach.^[18] The promise of this method has also been demonstrated for taxane-polymer conjugates. For example, direct ring-opening polymerization (ROP) of lactic acid (LA) conjugated to PTX and DTX resulted in defined, hydrophobic PTX/DTX-PLA conjugates which could subsequently be formulated into nanoparticles.^[16,17] Recently, our group has developed a

grafting-from-drug reversible addition-fragmentation chain transfer (RAFT) polymerization approach for acquiring defined, amphiphilic PTX-polymer prodrug conjugates with high drug loading and aqueous compatibility.^[19] The latter was obtained by functionalizing a RAFT chain transfer agent (CTA) with PTX by direct esterification. This ester-bond was effectively cleaved *in vitro* as the IC₅₀ matched the ones of Abraxane and Genexol-PM. These results motivated us to further explore this technique to develop acid-sensitive, acetal-based PTX-polymer conjugates which could hold the potential to more selectively release drug in response to the acidic environment in tumor tissue or upon endocytosis and storage in intracellular vesicles. Literature reports that cyclic and linear acetal moieties can exert significantly different, acidic hydrolysis rates (i.e. up to several orders of magnitude), wherein linear acetals are known to degrade faster than their cyclic counterparts.^[20] Hence, two acetal moieties were considered, one based on a cyclic, tetrahydropyran-based acetal (in this paper abbreviated as THP) and the other based on a linear, di(ethylene glycol)-based acetal (in this paper abbreviated as DEGA).



Scheme 1. Reaction scheme for the acid-catalyzed acetalization of paclitaxel (PTX) with a dihydropyran (DHP) or a di(ethylene glycol) vinyl ether (DEGVE) derivative of PABTC, yielding a PTX RAFT CTA, functionalized through a cyclic or linear acetal bond (i.e. THP or DEGA), respectively. Note that acetalization occurs either at the C₂' or at the C₇ OH-group of PTX. Whilst the regio-isomers of the THP-based PTX RAFT CTA could be separated, the regio-isomeric mixture of the DEGA-based PTX RAFT CTA was used as such for polymerization of N,N-dimethylacrylamide (DMA). Key abbreviations: THP, tetrahydropyran-based cyclic acetal; DEGA, di(ethylene glycol)-based linear acetal; C₂/C₇, regio-isomeric mixture, modified either through the C₂' or the C₇ OH-group of PTX.

2 results and discussion

Scheme 1 depicts the strategy applied for the syntheses of cyclic and linear acetal-based PTX-polymer conjugates. First, a RAFT CTA (i.e. 2-(butylthiocarbonothioylthio)propanoic acid (PABTC)) was modified, either with a dihydropyran (DHP) or a di(ethylene glycol) vinyl ether (DEGVE) moiety, yielding DHP-PABTC and DEGVE-PABTC, respectively. Both structures were confirmed by nuclear magnetic resonance (NMR) spectroscopy and electron spray ionization-mass spectroscopy (ESI-MS) (**Figure S1 - S4**). DHP-PABTC and DEGVE-PABTC were subsequently used for direct, acid-catalyzed acetalization of PTX through a cyclic or linear acetal, respectively. In contrast to the regioselective esterification of PTX at the C₂ hydroxyl(OH)-group we observed previously,^[19] in the present study we found that acetalization occurred at two sites (i.e. either at the C₂ or at the C₇ OH-group).

This resulted in 2 regio-isomers of PTX-THP-functionalized CTA, which could be separated by silica gel chromatography. Detailed NMR analysis (**Figure S5 - S14**) indeed confirmed the absence of the C₂ OH-group (at 2.51 ppm in the ¹H-NMR spectrum) and the presence of the C₇ OH-group (at 2.46 ppm) for PTX-C₂THP-PABTC regio-isomer, whilst the opposite was observed for PTX-C₇THP-PABTC regio-isomer. As expected, both isomers produced the identical product ion on ESI-MS (**Figure S15**). Synthesis of PTX-DEGA-PABTC resulted in a reaction mixture from which one fraction could be purified by silica gel chromatography. However, NMR characterization (**Figure S16 - S20**) confirmed the presence of the two regio-isomeric species, as in the ¹³C-NMR spectrum, the anomeric carbon of the acetal moiety was observed at 99.72 ppm and 100.52 ppm for the PTX-C₂DEGA-PABTC and PTX-C₇DEGA-PABTC isomer, respectively. Direct injection ESI-MS revealed ions related to the desired product (**Figure S21**). These ions were also detected by liquid chromatography diode array detection mass spectrometry (LC-DAD/MS), showing two fractions eluting closely after one another (**Figure S22**), further confirming that the obtained PTX-DEGA-PABTC is a regio-isomeric mixture. Both isomers could not be separated on a preparative scale, but LC analysis (**Figure S22**) yielded a 82/18 ratio of the respective isomers.

Both isomers of PTX-THP-PABTC and the regio-isomeric mixture of PTX-DEGA-PABTC were used for RAFT polymerization of *N,N*-dimethylacrylamide (DMA). pDMA is a hydrophilic polymer exhibiting excellent *in vivo* biocompatibility and significantly lower antibody-mediated accelerated blood clearance (ABC) compared to the widespread polyethylene glycol (PEG) and polyoxazolines (POx).^[21] In analogy to our previous endeavors using ester-based PTX-polymer conjugates (abbreviated as PTX-pDMA), a degree of polymerization (DP) of 30 was aimed to balance between solubility and high drug loading. For both the cyclic (PTX-THP-pDMA) and the linear acetal-based conjugates (PTX-DEGA-pDMA), similar molecular weight (MW) and narrow dispersity were measured by size

exclusion chromatography (SEC, **Figure 1A**) in addition to a high α - and ω -end group fidelity measured by NMR (**Figure S23** and **S24**). These findings underline the value, even at high monomer conversion, of the grafting-from-drug RAFT approach for the synthesis of well-defined polymer-drug conjugates. The high similarity between our earlier reported ester-based and present acetal-based conjugates in terms of total MW, polymer chain length and PTX loading capacity (**Table 1**), is highly favorable and allows an adequate, head-to-head comparison of both generations *in vitro*. As pDMA has good aqueous solubility, its conjugation with PTX yields an amphiphilic polymer due to the hydrophobicity of the PTX terminal end and therefore likely self-assembles in water into micellar structures.

We investigated the self-assembly behavior of the acetal-based conjugates in aqueous medium (i.e. phosphate buffered saline (PBS)) and compared their behavior to our previously synthesized ester-based conjugates. All conjugates could easily be dissolved in PBS up to elevated concentrations (at least 30 mg/mL). Both PTX-THP-pDMA and PTX-DEGA-pDMA self-assembled into micellar nanoparticles with similar size as the ester-based conjugates, as observed by dynamic light scattering (DLS, **Figure 1B** and **Table 2**). No difference in particle size was observed between the PTX-C₂THP-pDMA and PTX-C₇THP-pDMA isomers. The critical aggregation concentration (CAC) of the acetal-based conjugates were similar and in good concordance with the first-generation conjugates (**Figure 1C** and **Table 2**). Finally, all conjugates showed high colloidal stability in PBS for several days at 37 °C (**Figure 1D**).

Table 1. Compositional data of the synthesized polymers.

polymer	[DMA]/ [CTA]	conversion DMA (%) ^a	DP ^{conv,b}	DP ^{endgroup,c}	M _n (Da) ^d	ϕ ^d	PTX loading capacity (%) ^e
PTX-pDMA ₃₀	30	99	30	31	4356	1.07	21
PTX-C ₂ THP-pDMA ₃₀	30	94	28	30	3975	1.08	21
PTX-C ₇ THP-pDMA ₃₀	30	95	28	30	4226	1.09	21
*PTX-C ₂ /C ₇ DEGA-pDMA ₃₀	30	97	29	32	4999	1.08	21

^a Determined by ¹H-NMR spectroscopy. ^b Determined by ¹H-NMR spectroscopy based on monomer conversion. ^c Determined by ¹H-NMR spectroscopy based on endgroup analysis. ^d Analyzed by SEC in DMAc, calibrated with PMMA standards. ^e Calculated based on conversion by ¹H-NMR spectroscopy: $MW_{PTX} / MW_{PTX-polymer} \times 100 \%$. * regio-isomeric mixture of PTX-polymer conjugate, modified either through the C₂ or the C₇ OH-group of PTX.

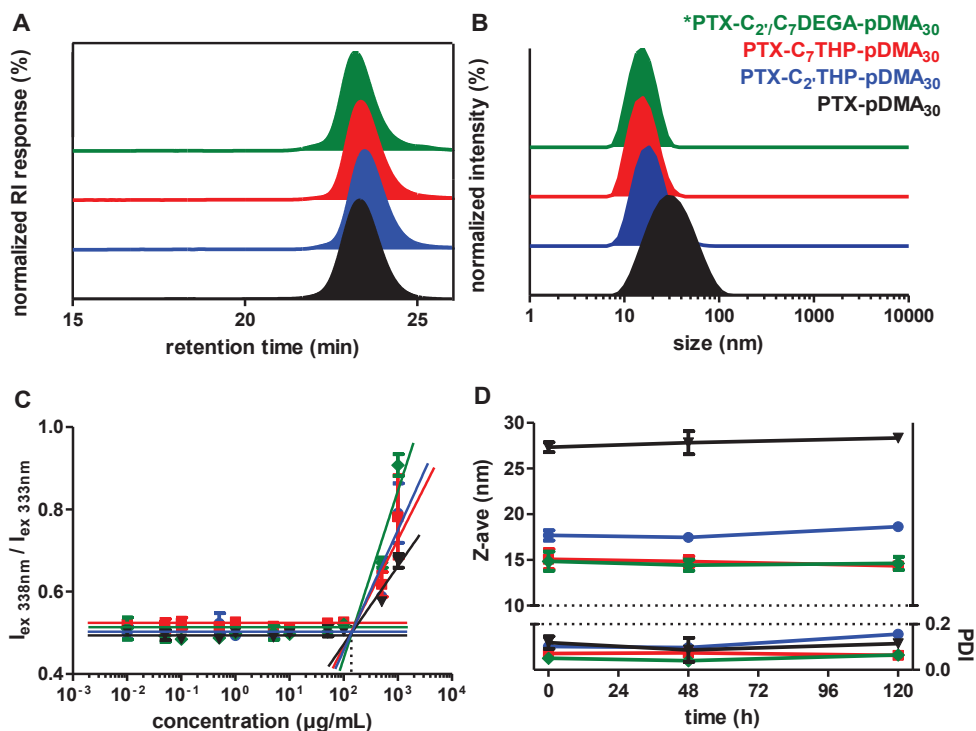


Figure 1. SEC elugrams (A), intensity size distribution (B), CAC (C) and colloidal stability (D) of PTX-polymer conjugates. B,D: $n = 3$, measured by DLS in PBS (30 mg/mL). C: $n = 2$; measured in PBS by pyrene assay. Data points and error bars in (C) and (D) represent mean value and standard deviation (SD), respectively. * regio-isomeric mixture of PTX-polymer conjugate, modified either through the C_2 or the C_7 OH-group of PTX.

Table 2. Supramolecular and cytotoxicity features of PTX-polymer conjugates.

polymer	Z-Ave (nm) ^a	PDI ^a	CAC ($\mu\text{g/mL}$) ^b	IC ₅₀ (μM) ^c
PTX-pDMA ₃₀	27.3 \pm 0.5	0.119 \pm 0.026	102 \pm 12	37 $\times 10^{-3}$
PTX- C_2 -THP-pDMA ₃₀	17.6 \pm 0.5	0.102 \pm 0.018	113 \pm 2	95
PTX- C_7 -THP-pDMA ₃₀	15.0 \pm 1.1	0.071 \pm 0.020	109 \pm 6	95
*PTX- C_2/C_7 -DEGA-pDMA ₃₀	14.8 \pm 1.0	0.051 \pm 0.001	100 \pm 1	51 $\times 10^{-1}$

^a Numeric values for Z-Average hydrodynamic diameter and PDI of PTX-polymer conjugates, measured in PBS (30 mg/mL) at 37 °C by DLS ($n = 3$). ^b CAC in PBS at 20 °C, measured by pyrene assay ($n = 2$). ^c Relative IC₅₀-values calculated by non-linear regression analysis of MTT data presented in Figure 3. IC₅₀-values of Abraxane and Genexol-PM were 45 $\times 10^{-3}$ and 46 $\times 10^{-3}$ μM , respectively. * regio-isomeric mixture of PTX-polymer conjugate, modified either through the C_2 or the C_7 OH-group of PTX.

Subsequently we investigated the hydrolysis behavior of the PTX-polymer conjugates at different pH-values (i.e. pH 7.4 to mimic the conditions in the circulation and extracellular fluids, pH 5 to mimic the acidic environment in intracellular vesicles and pH 4 to test an even more acidic environment) and in presence of serum (i.e. PBS supplemented with 10 % fetal bovine serum (FBS)). For this purpose, conjugates were incubated for fixed periods of time in the respective media, followed by ultra performance liquid chromatography (UPLC) analysis. Only limited (i.e. < 5 %) PTX release was observed at pH 7.4 in 96 hours for the ester-based conjugates, most probably through a base-catalyzed process, whilst the acetal-based conjugates remained fully stable within the timeframe of the experiment at this pH-value (**Figure 2A**). Additionally, the presence of serum did not substantially accelerate the PTX release rate for the ester- nor for the acetal-based conjugates, as for the latter the zero baseline also persisted in presence of FBS (**Figure 2B**). Next, the conjugates were incubated at endosomal pH (i.e. pH 5). Whilst release was observed for the linear acetal-based conjugate (i.e. 6 % in 96 hours), no release of PTX was observed for the cyclic acetal- and ester-based conjugates within similar time frame (**Figure 2C**). The latter confirms a higher stability of cyclic acetals compared to their linear counterparts and suggests that after swift endosomal uptake of the conjugates, which was reconfirmed by confocal microscopy for the cyclic acetal-based conjugates (**Figure S26**) as previously demonstrated for the ester-based conjugates,^[19] the ester-based conjugates most likely did not release PTX through an acid-catalyzed process, but predominantly through an enzymatic pathway instead. The acetal-based conjugates were also incubated at pH 4 to verify the influence of pH on acetal hydrolysis rate. Indeed, PTX-THP-pDMA showed higher, but still limited release at pH 4, whilst substantially higher PTX release was observed for the linear acetal-based conjugates (**Figure 2D**). This further suggests that the release of PTX from the acetal-based conjugates is primarily triggered chemically instead of enzymatically, more specifically by means of acid-catalyzed hydrolysis.

Finally, the biological performance of the acetal-based conjugates was evaluated *in vitro* on human ovarian SKOV-3 cells by MTT assay after 72 hours of co-incubation. Prior to these experiments we verified that none of the conjugates showed a tendency towards aggregate formation in presence of serum (**Figure S25**). As depicted in **Figure 3**, pDMA did not exert any intrinsic cytotoxic effect. Both the acetal-based conjugates induced a decrease in cell viability up to the same extent as the ester-based conjugates and two commercial PTX formulations based on physical entrapment, albeit significantly higher concentrations are required. These data are in accordance with the *in vitro* release studies, which demonstrated that the extent of PTX release is incomplete at pH 5 after 72 hours of incubation. Additionally, the higher release rate observed for PTX-DEGA-pDMA compared to PTX-THP-pDMA indeed results in a higher IC₅₀-value of the latter (**Table 2**). Finally, the MTT results further propose a difference in

release mechanism between ester- and acetal-based PTX-polymer conjugates (i.e. enzyme- and acid-catalyzed, respectively). Both mechanisms can be of interest in developing advanced polymer-drug conjugates with adequate, selective drug release and limited systemic burst release. For acquiring PTX-polymer conjugates with faster release kinetics at pH 5, highly pH-sensitive acetal-/ketal- moieties are to be considered. The acetal-/ketal-chemistry, developed by Fréchet and co-workers, could provide valuable insights for achieving the latter.^[22,23]

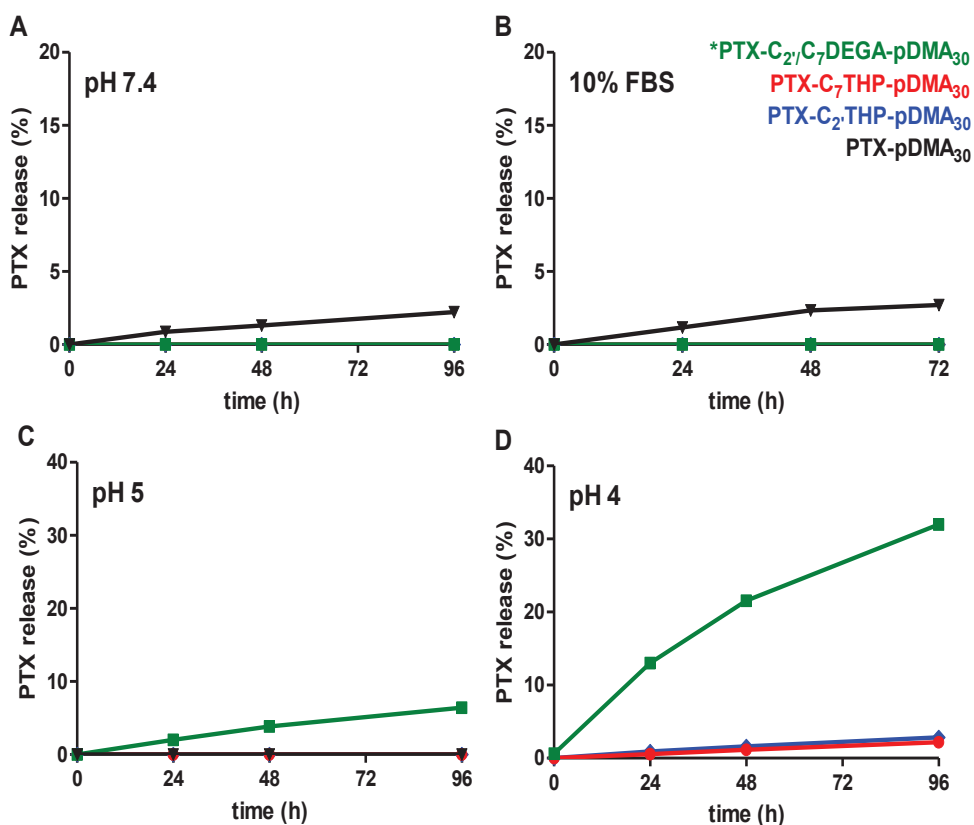


Figure 2. Drug release kinetics at 37 °C of PTX-polymer conjugates (10 mg/mL) in 100 mM citrate buffer (pH 4; A and pH 5; B), phosphate buffer (pH 7.4; C) and PBS supplemented with 10 % FBS (D), determined by UPLC (n = 2). Data points represent mean value. * regio-isomeric mixture of PTX-polymer conjugate, modified either through the C₂ or the C₇ OH-group of PTX.

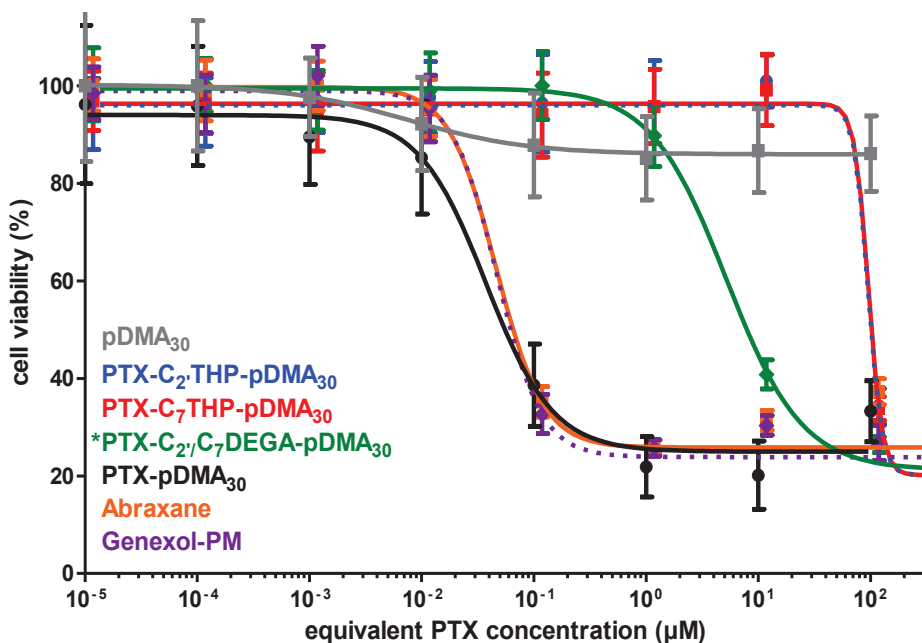


Figure 3. *In vitro* cytotoxicity of PTX-polymer conjugates versus commercial PTX nanoformulations Abraxane and Genexol-PM ($n = 6$), co-incubated with SKOV-3 cells for 72 hours. Data points and error bars represent mean value and SD, respectively. * regio-isomeric mixture of PTX-polymer conjugate, modified either through the C₂ or the C₇ OH-group of PTX

3 conclusions

In conclusion, the grafting-from-drug RAFT approach allowed the preparation of well-defined acetal-based PTX-polymer conjugates with nearly identical features in terms of polymer composition and amphiphilic properties, but with distinct PTX release properties. The findings of this paper clearly highlight the broad chemical versatility and robustness of the polymerization technique and show that, due to the high definition of the obtained polymers, RAFT should be considered as a key player in future rational design of advanced polymer-drug conjugates. Whereas the *in vivo* behavior of these systems remains to be elucidated, ester-based systems show the advantage of a potentially higher activity on a short term scale. However, the specific acid-triggered PTX release, exhibited by acetal-based systems in combination with their resilience to enzymatic cleavage might be beneficial as well.

4 experimental

4.1 materials

All chemicals were purchased from Sigma Aldrich and were used as received unless mentioned otherwise. The RAFT CTA 2-(butylthiocarbonothioylthio)propanoic acid (PABTC) was synthesized according to a literature procedure.^[24] TLC plates were purchased from Macherey Nagel. PTX was purchased from LC Laboratories. PTX-pDMA₅₀ (ester-based PTX-polymer prodrug conjugate) was synthesized as previously reported.^[19] Dulbecco's phosphate buffered saline (PBS), Dulbecco's modified Eagle medium (DMEM), fetal bovine serum (FBS), L-glutamine, sodium pyruvate, penicillin and streptomycin were obtained from Thermo Fisher Scientific. SKOV-3 cells were supplied by ATCC.

4.2 analysis

NMR spectra were recorded on a Bruker 300 MHz FT-NMR spectrometer. Chemical shifts (δ) are given in ppm relative to TMS. Samples were prepared in given deuterated solvents and their signals referenced to residual non-deuterated signals of the solvent.

Electron spray ionization-mass spectroscopy (ESI-MS) measurements were performed on a Waters (Milford, Mass, USA) LCT Premier XE time-of-flight (TOF) mass spectrometer equipped with an ESI interface. Samples were infused in an acetonitrile:formic acid (1000:1) mixture at 0.1 mL/min.

Liquid chromatography diode array detection mass spectrometry (LC-DAD/MS) was carried out on a Waters Alliance 2695 XE separation Module equipped with a Phenomenex Luna reversed-phase C₁₈ (2) column (100 Å, 100 x 2.00 mm, 3 μ m), coupled to a 996 diode array detector and a Waters LCT Premier XE TOF mass spectrometer. A gradient system of ammonium bicarbonate in H₂O (10 mM)/acetonitrile was used at a flow rate of 0.4 mL/min. The mobile phase was 50/50 (v/v) for 0 to 1 min. Next, acetonitrile fraction was increased from 50/50 (v/v) to 0/100 (v/v) from 1 to 10 min, maintained from 10 to 12 min and subsequently decreased back to 50/50 from 12 to 15 min.

Size exclusion chromatography (SEC) was carried out on an Agilent 1260 system, equipped with a 1260 ISO-pump, a 1260 diode array detector (DAD) and a 1260 refractive index detector (RID). Measurements were performed in *N,N*-dimethylacetamide (DMAc) containing 50 mM LiCl at 50 °C, using a flow rate of 0.593 mL/min. A guard column and two PL gel 5 μ m mixed-D columns were used in series, calibrated with poly(methyl methacrylate) (PMMA) standards obtained from PSS (Mainz, Germany).

Dynamic light scattering (DLS). DLS measurements were carried out on a Zetasizer Nano S (Malvern) with a HeNe laser ($\lambda = 633$ nm) at a scattering angle of 173° .

Fluorescence excitation spectra were collected at room temperature on a Cary Eclipse fluorescence spectrophotometer (Agilent Technologies) equipped with a Varian Cary Temperature Controller.

Ultra performance liquid chromatography (UPLC) analysis was performed using a Waters Acquity system. Eluent acetonitrile/water = 45/55 (v/v) with 0.1 % formic acid. An ACQUITY UPLC BEH C_{18} column was used and the detection wavelength was 227 nm. At a flow of 1 mL/min the retention time was 0.97 minutes. Total runtime 1.5 minutes. Two microliters of sample (i.e. supernatant) was injected and the PTX concentration in the different samples was calculated using a calibration curve of PTX standards prepared in acetonitrile in a concentration range of 2 - 250 $\mu\text{g/mL}$. The system was controlled, and calculations were done with the Empower3 software.

4.3 synthesis DHP-PABTC

In a 500 mL round-bottom unineck flask, PABTC (18.90 mmol, 4.500 g), 4-(dimethylamino)pyridine (DMAP) (1.89 mmol, 0.231 g) and (\pm) 3,4-dihydro-2H-pyran-2-methanol (DHP) (20.80 mmol, 2.374 g) were dissolved in 189 mL anhydrous dichloromethane (CH_2Cl_2) and cooled on ice. Next, *N,N'*-diisopropylcarbodiimide (DIC) (20.80 mmol, 2.625 g) was added dropwise and the mixture was stirred for 1 hour at room temperature and monitored by TLC. Subsequently, the reaction mixture was filtered and concentrated in vacuo. The crude product was purified by silica gel chromatography (eluent CH_2Cl_2). After concentration and subsequent drying under high vacuum, the obtained yellow oil (17.74 mmol, 5.926 g, 94 %) was analyzed by NMR-spectroscopy and ESI-MS.

4.4 synthesis DEGVE-PABTC

In a 500 mL round-bottom unineck flask, PABTC (18.90 mmol, 4.500 g), DMAP (1.89 mmol, 0.231 g) and di(ethylene glycol) vinyl ether (DEGVE) (20.80 mmol, 2.749 g) were dissolved in 189 mL anhydrous CH_2Cl_2 and cooled on ice. Next, DIC (20.80 mmol, 2.625 g) was added dropwise and the mixture was stirred for 1 hour at room temperature and monitored by TLC. Subsequently, the reaction mixture was filtered and concentrated in vacuo. The crude product was purified by silica gel chromatography (eluent CH_2Cl_2). After concentration and subsequent drying under high vacuum, the obtained yellow oil (15.78 mmol, 5.553 g, 83 %) was analyzed by NMR-spectroscopy and ESI-MS.

4.5 synthesis PTX-THP-PABTC

Following procedure was conducted for acquiring PABTC, functionalized with PTX through a tetrahydropyran-based cyclic acetal (THP). Paclitaxel (PTX) (2.93 mmol, 2.500 g) and camphor-10-sulfonic acid (CSA) (0.322 mmol, 0.075 g) were weighed into two separate 50 mL round-bottom twin neck flasks and dried overnight under high vacuum over phosphorus pentoxide (P_2O_5). PTX and CSA were dissolved in 21 mL and 7.5 mL of anhydrous CH_2Cl_2 , respectively. DHP-PABTC (3.220 mmol, 1.077 g) was added dropwise to the PTX solution. Finally, reaction was initiated by dropwise addition of the CSA solution. Reaction was carried out for 3 hours at room temperature and monitored by TLC. Next, reaction was quenched with 90 μ L of triethylamine (TEA) (0.644 mmol) and concentrated in vacuo. Two purified fractions were isolated from the crude product by silica gel chromatography (eluent 3:1 to 2:1 hexane:ethyl acetate v/v with 1 % TEA). After concentration and subsequent drying under high vacuum, the two obtained yellow solids (0.65 mmol, 0.771 g, 44 % PTX-C₂THP-PABTC (assuming a maximum yield of 0.5 PTX eq. for both regio-isomers); 0.56 mmol, 0.666 g, 38 % PTX-C₇THP-PABTC) were analyzed by NMR-spectroscopy and ESI-MS.

4.6 synthesis PTX-DEGA-PABTC

Following procedure was conducted for acquiring PABTC, functionalized with PTX through a di(ethylene glycol)-based linear acetal (DEGA). PTX (1.17 mmol, 1.000 g) and CSA (0.117 mmol, 0.027 g) were weighed into two separate 50 mL round-bottom twin neck flasks and dried overnight under high vacuum over P_2O_5 . PTX and CSA were dissolved in 8.6 mL and 2.7 mL of anhydrous CH_2Cl_2 , respectively. DEGVE-PABTC (1.287 mmol, 0.453 g) was added dropwise to the PTX solution. Finally, reaction was initiated by dropwise addition of the CSA solution. Reaction was carried out for 3 hours at room temperature and monitored by TLC. Next, reaction was quenched with 33 μ L of TEA (0.234 mmol) and concentrated in vacuo. The crude product was purified by silica gel chromatography (eluent 5:1 toluene:ethyl acetate v/v with 1 % TEA). After concentration and subsequent drying under high vacuum, the obtained yellow solid (0.42 mmol, 0.510 g, 36 %) was analyzed by NMR-spectroscopy, ESI-MS and LC-MS. NMR spectroscopy was done in $DMSO-d_6$ due to acetal instability in the slightly acidic $CDCl_3$.

4.7 RAFT polymerization

4.7.1 synthesis PTX-THP-pDMA₃₀

PTX-THP-PABTC (C₂ or C₇ purified regio-isomer) (0.295 mmol, 0.350 g), 2,2'-azobis(2-methylpropionitrile) (AIBN) (0.059 mmol, 0.010 g) and *N,N*-dimethylacrylamide (DMA) (8.843 mmol, 0.877 g; for targeted degree of polymerization (DP) of 30) were dissolved in a Schlenk tube in anhydrous *N,N*-dimethylformamide (DMF) to obtain a monomer concentration of 2 M and a CTA:initiator molar ratio of 5:1. The solutions were subjected to 5 freeze-pump-thaw cycles before polymerization was initiated at 70 °C for 3 hours under vacuum. Monomer conversion was determined by ¹H-NMR spectroscopy. Polymers were collected by triple precipitation from cold (4 °C) diethyl ether and the obtained light yellow solids were subsequently dried under high vacuum (PTX-C₂THP-pDMA₃₀ (0.259 mmol, 1.030 g, 88 %) and PTX-C₇THP-pDMA₃₀ (0.257 mmol, 1.031 g, 87 %)).

4.7.2 synthesis PTX-DEGA-pDMA₃₀

PTX-C₂/C₇DEGA-PABTC (regio-isomeric mixture, modified either through the C₂ or the C₇ OH-group of PTX) (0.166 mmol, 0.200 g), AIBN (0.033 mmol, 0.005 g) and DMA (4.975 mmol, 0.493 g; for targeted DP of 30) were dissolved in a Schlenk tube in anhydrous DMF to obtain a monomer concentration of 2 M and a CTA:initiator molar ratio of 5:1. The solutions was subjected to 5 freeze-pump-thaw cycles before polymerization was initiated at 70 °C for 3 hours under vacuum. Monomer conversion was determined by ¹H-NMR spectroscopy. Polymer was collected by triple precipitation from cold (4 °C) diethyl ether and the obtained light yellow solid was subsequently dried under high vacuum (0.134 mmol, 0.546 g, 80 %).

4.8 critical aggregation concentration (CAC)

The CAC of the polymeric PTX conjugates was determined by fluorescence spectroscopy using pyrene as a fluorescent probe. First, a dilution series of the polymeric prodrugs was prepared in duplicate in PBS with concentrations ranging from 10^{-2} to 10^3 $\mu\text{g/mL}$. Secondly, a 3.6 mg/mL (1.8×10^{-2} M) stock solution of pyrene in acetone was prepared and kept on ice to prevent evaporation of the acetone. Next, 10 μL of this solution was diluted to 1 mL acetone and kept on ice. To 2.5 mL of each conjugate dilution, 8.3 μL of the latter pyrene solution was added under stirring leading to a pyrene concentration of 6.0×10^{-7} M. The CAC was quantified by fluorescence spectrophotometry at room temperature based on the change in excitation intensity ratio at 338 and 333 nm with varying concentration.

4.9 PTX release kinetics in aqueous buffers and diluted serum

PTX-pDMA₃₀, PTX-C₂THP-pDMA₃₀, PTX-C₇THP-pDMA₃₀ and PTX-C₂₇C₇DEGA-pDMA₃₀ were formulated (10 mg/mL) in 100 mM citrate buffer (pH 4 and pH 5) and 100 mM phosphate buffer (pH 7.4), and incubated at 37 °C for 96 hours (pH 4) or 336 hours (pH 5 and pH 7.4). After 0, 24, 48, 96, 168, 240 and 336 hours of incubation, samples of 100 μL were taken. All samples were diluted into 900 μL of acetonitrile. The diluted samples were subsequently centrifuged (20 000 g, 10 minutes, 5 °C). Finally, the supernatants were analyzed by UPLC.

In a separate experiment, PTX-pDMA₃₀, PTX-C₂THP-pDMA₃₀, PTX-C₇THP-pDMA₃₀ and PTX-C₂₇C₇DEGA-pDMA₃₀ were formulated (10 mg/mL) in PBS, supplemented with 10 % FBS, and incubated at 37 °C. After 0, 5, 24 and 72 hours of incubation, samples of 100 μL were taken. Samples were diluted into 900 μL of acetonitrile and thoroughly vortexed for 1 minute. Next, the diluted samples were centrifuged (20 000 g, 10 minutes, 5 °C) and supernatants were analyzed by UPLC.

4.10 cell culture

SKOV-3 human ovarian cancer cells were cultured in DMEM, supplemented with 10 % FBS, 2 mM L-glutamine, 1 mM sodium pyruvate and antibiotics (50 units/mL penicillin and 50 µg/mL streptomycin). Cells were incubated at 37 °C in a controlled, sterile environment of 95 % relative humidity and 5 % CO₂.

4.11 *in vitro* cytotoxicity

In vitro cytotoxicity was assessed by MTT assay. Formulations of PTX-C₂THP-pDMA₃₀, PTX-C₇THP-pDMA₃₀ and PTX-C₂/C₇DEGA-pDMA₃₀ were diluted in PBS with concentrations ranging from 5.85 x 10⁻⁵ to 5.85 x 10² µM, along with two control nanoparticle PTX formulations Abraxane (Celgene) and Genexol-PM (Samyang Biopharmaceuticals). MTT stock solution was prepared by dissolving 100 mg MTT in 20 mL of PBS and subsequent membrane filtration (0.220 µm). Before use, the MTT stock solution was 5-fold diluted with culture medium.

Briefly, SKOV-3 cells were seeded into 96-well plates (10 000 cells per well, suspended in 200 µL of culture medium) and incubated overnight. Next, 50 µL of sample, DMSO (positive control = 0 % viability) or PBS (negative control = 100 % viability) was added to the cells, followed by 72 hours of incubation. Subsequently, the medium was aspirated and the cells were washed with 250 µL of PBS. After aspiration, 100 µL of MTT working solution was added and the cells were incubated for 2.5 hours. Finally, the MTT working solution was aspirated and the formed purple formazan crystals were dissolved in 50 µL of DMSO. Absorbance was determined at 590 nm using an EnVision Multilabel plate reader. The absorbance of the positive control was used as blank and therefore subtracted from all values.

5 references

- [1] J. Crown, M. O'Leary, *Lancet* **2000**, *355*, 1176–1178.
- [2] D. G. I. Kingston, D. J. Newman, *Curr. Opin. Drug Discov. Devel.* **2007**, *10*, 130–144.
- [3] A. Sparreboom, C. D. Scripture, V. Trieu, P. J. Williams, T. De, A. Yang, B. Beals, W. D. Figg, M. Hawkins, N. Desai, *Clin. Cancer Res.* **2005**, *11*, 4136–4143.
- [4] H. Gelderblom, J. Verweij, K. Nooter, A. Sparreboom, *Eur. J. Cancer* **2001**, *37*, 1590–1598.
- [5] L. B. Norris, Z. P. Qureshi, P. B. Bookstaver, D. W. Raisch, O. Sartor, H. Chen, F. Chen, C. L. Bennett, *Community Oncol.* **2010**, *7*, 425–428.
- [6] A. J. ten Tije, J. Verweij, W. J. Loos, A. Sparreboom, *Clin. Pharmacokinet.* **2003**, *42*, 665–685.
- [7] Z. Weiszhar, J. Czucz, C. Revesz, L. Rosivall, J. Szebeni, Z. Rozsnyay, *Eur. J. Pharm. Sci.* **2012**, *45*, 492–498.
- [8] Y. Min, J. M. Caster, M. J. Eblan, A. Z. Wang, *Chem. Rev.* **2015**, *115*, 11147–11190.
- [9] N. Larson, H. Ghandehari, *Chem. Mater.* **2012**, *24*, 840–853.
- [10] R. Duncan, *Nat. Rev. Cancer* **2006**, *6*, 688–701.
- [11] L. Liang, S.-W. Lin, W. Dai, J.-K. Lu, T.-Y. Yang, Y. Xiang, Y. Zhang, R.-T. Li, Q. Zhang, *J. Control. Release* **2012**, *160*, 618–629.
- [12] L. Nuhn, N. Vanparijs, A. De Beuckelaer, L. Lybaert, G. Verstraete, K. Deswarthe, S. Lienenklaus, N. M. Shukla, A. C. Salyer, B. N. Lambrecht, et al., *Proc. Natl. Acad. Sci.* **2016**, *113*, 8098–8103.
- [13] Q. Zhang, Z. Hou, B. Louage, D. Zhou, N. Vanparijs, B. G. De Geest, R. Hoogenboom, *Angew. Chem. Int. Ed. Engl.* **2015**, *127*, 11029–11033.
- [14] K. Ulbrich, K. Hola, V. Subr, A. Bakandritsos, J. Tucek, R. Zboril, *Chem. Rev.* **2016**, *116*, 5338–5431.
- [15] J. W. Singer, *J. Control. Release* **2005**, *109*, 120–126.
- [16] R. Tong, J. J. Cheng, *Angew. Chem. Int. Ed. Engl.* **2008**, *47*, 4830–4834.
- [17] R. Tong, J. Cheng, *J. Am. Chem. Soc.* **2009**, *131*, 4744–4754.
- [18] J. Nicolas, *Chem. Mater.* **2016**, *28*, 1591–1606.
- [19] B. Louage, L. Nuhn, M. D. Risseeuw, N. Vanparijs, R. De Coen, I. Karalic, S. Van Calenbergh, B. G. De Geest, *Angew. Chem. Int. Ed. Engl.* **2016**, *55*, 11791–11796.
- [20] P. Deslongchamps, Y. L. Dory, S. G. Li, *Tetrahedron* **2000**, *56*, 3533–3537.
- [21] P. H. Kierstead, H. Okochi, V. J. Venditto, T. C. Chuong, S. Kivimae, J. M. J. Frechet, F. C. Szoka, *J. Control. Release* **2015**, *213*, 1–9.
- [22] E. R. Gillies, A. P. Goodwin, J. M. J. Frechet, *Bioconjug. Chem.* **2004**, *15*, 1254–1263.
- [23] L. Cui, J. L. Cohen, C. K. Chu, P. R. Wich, P. H. Kierstead, J. M. J. Frechet, *J. Am. Chem. Soc.* **2012**, *134*, 15840–15848.
- [24] C. J. Ferguson, R. J. Hughes, D. Nguyen, B. T. T. Pham, R. G. Gilbert, A. K. Serelis, C. H. Such, B. S. Hawkett, *Macromolecules* **2005**, *38*, 2191–2204.

6 supporting info

6.1 DHP-PABTC

$^1\text{H-NMR}$ (300 MHz, CDCl_3): δ [ppm] = 6.35 (dd, $J = 10.5, 1.7$ Hz, 1H), 4.84 (qd, $J = 12.3, 1.3$ Hz, 1H), 4.69 (dddd, $J = 10.2, 4.7$ Hz, 2.7 Hz, 1.2 Hz, 0.7 Hz, 1H), 4.23 (dd, $J = 9, 1.5$ Hz, 2H), 4.03 (m, 1H), 3.35 (t, $J = 12$ Hz, 2H), 2.05 (m, 2H), 1.83 (m, 1H), 1.71 (m, 1H), 1.66 (m, 2H), 1.61 (d, $J = 12.3$ Hz, 3H), 1.42 (sextet, $J = 12.2$ Hz, 2H), 0.92 (t, $J = 12.2$ Hz, 3H).

ESI-MS (acetonitrile): $m/z = \text{calcd for } \text{C}_{14}\text{H}_{22}\text{O}_3\text{S}_3, 334.07, \text{found } 335.07 [\text{M}+\text{H}]^+$

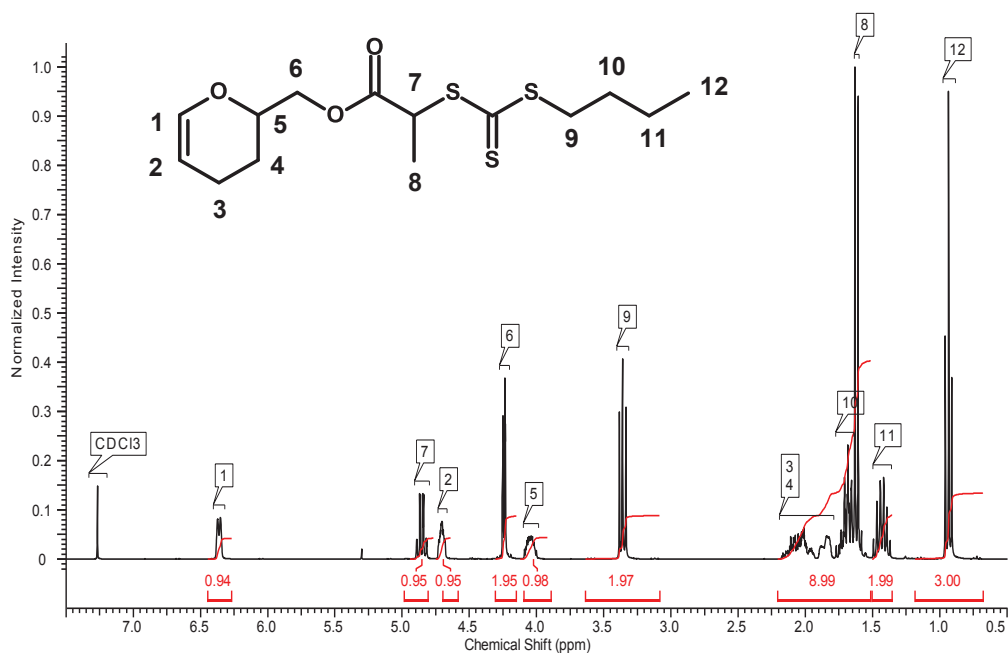


Figure S1. $^1\text{H-NMR}$ (300 MHz, CDCl_3) spectrum of DHP-PABTC.

6.2 DEGVE-PABTC

$^1\text{H-NMR}$ (300 MHz, CDCl_3): δ [ppm] = 6.49 (dd, $J = 14.3, 6.8$ Hz, 1H), 4.84 (q, $J = 7.4$ Hz, 1H), 4.30 (t, $J = 4.8$ Hz, 2H), 4.19 (dd, $J = 14.3, 2.2$ Hz, 1H), 4.02 (dd, $J = 6.8, 2.2$ Hz, 1H), 3.86 – 3.79 (m, 2H), 3.76 – 3.68 (m, 4H), 3.35 (t, $J = 7.4$ Hz, 2H), 1.73 – 1.63 (m, 2H), 1.60 (d, $J = 7.4$ Hz, 3H), 1.43 (h, $J = 7.3$ Hz, 2H), 0.93 (t, $J = 7.3$ Hz, 3H).

ESI-MS (acetonitrile): $m/z = \text{calcd for } \text{C}_{14}\text{H}_{24}\text{O}_4\text{S}_5, 352.08, \text{found } 353.09 [\text{M}+\text{H}]^+$

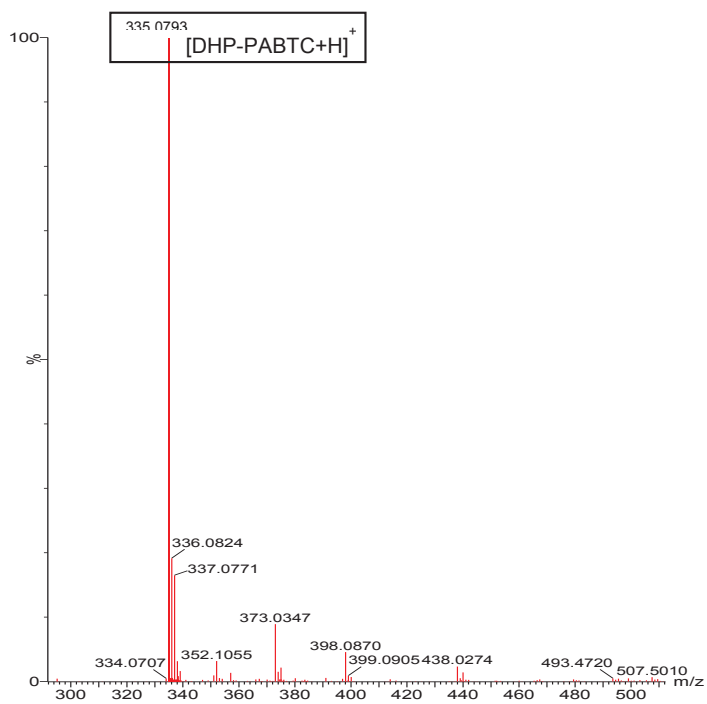


Figure S2. ESI-MS (acetonitrile) spectrum of DHP-PABTC.

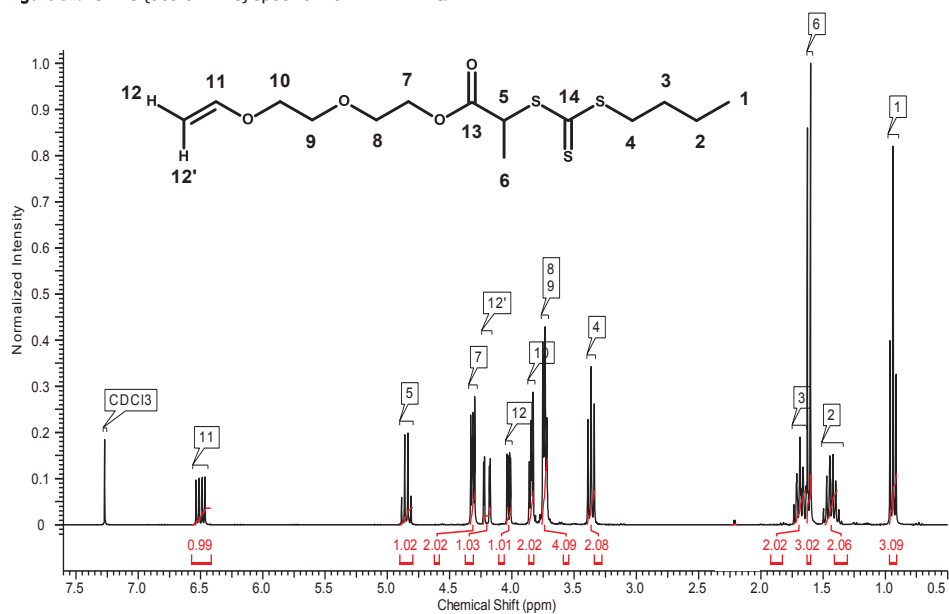


Figure S3. ¹H-NMR (300 MHz, CDCl₃) spectrum of DEGVE-PABTC.

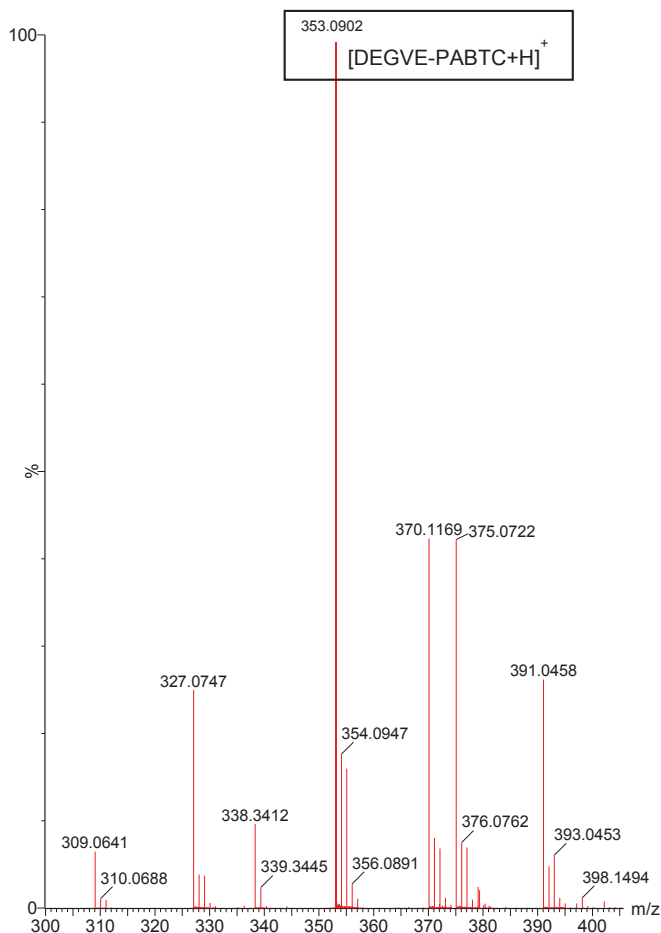


Figure S4. ESI-MS (acetonitrile) spectrum of DEGVE-PABTC.

6.3 PTX-THP-PABTC

PTX-C₂THP-PABTC:

¹H-NMR (300 MHz, CDCl₃): δ [ppm] = 8.14 (d, J = 6.9 Hz, 2H), 7.74 (d, J = 7.0 Hz, 1H), 7.60 (t, J = 7.3 Hz, 1H), 7.55 – 7.27 (m, 10H), 7.07 (dd, J = 9.0, 2.1 Hz, 1H), 6.30 (t, J = 9.1 Hz, 1H), 6.28 (s, 1H), 5.87 (dt, J = 8.8, 1.7 Hz, 1H), 5.68 (d, J = 7.1 Hz, 1H), 4.98 (d, J = 9.0 Hz, 1H), 4.91 (s, 1H), 4.90 – 4.82 (m, 1H), 4.76 (d, J = 2.9 Hz, 1H), 4.51 – 4.36 (m, 2H), 4.26 (dd, J = 36.4, 8.7 Hz, 2H), 3.90 – 3.76 (m, 2H), 3.67 (ddd, J = 11.7, 8.4, 4.1 Hz, 1H), 3.42 – 3.31 (m, 2H), 2.59 (d, J = 1.5 Hz, 3H), 2.59 – 2.53 (m, 1H), 2.57 – 2.46 (m, 1H), 2.46 (d, J = 4.1 Hz, 1H), 2.38 (dd, J = 15.3, 9.5 Hz, 1H), 2.23 (s, 3H), 2.17 (s, 1H),

2.15 – 2.06 (m, 1H), 1.97 – 1.90 (m, 1H), 1.89 (d, J = 1.4 Hz, 3H), 1.90 – 1.78 (m, 1H), 1.74 – 1.70 (m, 1H), 1.72 – 1.65 (m, 3H), 1.68 – 1.64 (m, 2H), 1.62 (dd, J = 7.4, 1.8 Hz, 3H), 1.62 – 1.50 (m, 3H), 1.50 – 1.35 (m, 2H), 1.24 (s, 3H), 1.23 – 1.21 (m, 1H), 1.13 (s, 3H), 0.93 (td, J = 7.3, 1.9 Hz, 3H).

¹³C-NMR (75 MHz, CDCl₃): δ [ppm] = 219.27, 203.87, 171.38, 171.37, 171.07, 171.00, 170.36, 170.35, 170.23, 167.24, 167.12, 142.45, 142.42, 138.34, 134.06, 133.82, 133.14, 133.11, 132.02, 130.38, 129.24, 128.92, 128.89, 128.84, 128.17, 127.23, 126.63, **96.12, 96.01**, 84.63, 81.17, 79.44, 79.42, 76.61, 75.90, 75.83, 75.68, 75.24, 72.27, 71.63, 67.79, 67.71, 66.98, 66.93, 58.67, 58.66, 54.63, 48.10, 47.90, 45.62, 43.38, 37.16, 37.15, 35.88, 35.70, 30.08, 30.05, 29.82, 29.10, 26.97, 23.12, 23.08, 22.45, 22.20, 20.98, 17.35, 17.19, 15.20, 15.16, 13.73 and 13.72, 9.77.

ESI-MS (acetonitrile): m/z = calcd for C₆₁H₇₃NO₁₇S₅ 1187.40, found 1188.41 [M+H]⁺

PTX-C₇THP-PABTC:

¹H-NMR (300 MHz, CDCl₃): δ [ppm] = 8.13 (d, J = 7.1 Hz, 2H), 7.75 (d, J = 8.2 Hz, 2H), 7.61 (t, J = 7.3 Hz, 1H), 7.52 – 7.34 (m, 10H), 7.02 (dd, J = 8.7, 4.2 Hz, 1H), 6.33 – 6.21 (m, 2H), 5.74 (dd, J = 8.8, 2.6 Hz, 1H), 5.68 (d, J = 7.1 Hz, 1H), 4.97 (d, J = 8.6 Hz, 1H), 4.81 (qd, J = 7.3, 2.3 Hz, 1H), 4.61 (dd, J = 3.2, 2.3 Hz, 1H), 4.52 (s, 1H), 4.50 – 4.37 (m, 1H), 4.26 (dd, J = 33.8, 8.5 Hz, 2H), 4.17 – 4.11 (m, 1H), 4.11 – 3.92 (m, 2H), 3.80 (d, J = 7.0 Hz, 1H), 3.33 (td, J = 7.4, 1.5 Hz, 2H), 2.61 – 2.54 (m, 1H), 2.51 (d, J = 4.1 Hz, 1H), 2.48 (d, J = 1.5 Hz, 3H), 2.39 – 2.29 (m, 1H), 2.24 (s, 3H), 2.23 (s, 1H), 2.13 (dd, J = 15.3, 8.8 Hz, 1H), 1.96 – 1.89 (m, 1H), 1.89 – 1.87 (m, 3H), 1.88 – 1.78 (m, 1H), 1.80 – 1.71 (m, 1H), 1.71 – 1.65 (m, 3H), 1.66 – 1.62 (m, 2H), 1.63 – 1.58 (m, 3H), 1.56 (dd, J = 7.4, 1.6 Hz, 3H), 1.48 – 1.35 (m, 2H), 1.26 (s, 3H), 1.25 – 1.18 (m, 1H), 1.14 (s, 3H), 0.92 (td, J = 7.4, 0.8 Hz, 3H).

¹³C-NMR (75 MHz, CDCl₃): δ [ppm] = 219.27, 203.95, 171.47, 171.43, 171.26, 171.08, 170.31, 170.11, 170.28, 167.20, 167.03, 142.71, 142.70, 138.10, 134.16, 133.82, 132.95, 132.98, 131.99, 130.35, 129.33, 129.09, 128.88, 128.86, 128.37, 127.20, 126.73, **100.40, 100.26**, 84.62, 81.20, 79.40, 77.36, 76.60, 75.70, 75.25, 72.27, 71.32, 68.17, 68.01, 67.78, 67.69, 58.64, 55.11, 47.99, 47.91, 45.63, 43.38, 37.08, 37.06, 35.93, 35.64, 30.06, 29.84, 29.80, 29.50, 26.97, 23.01, 22.40, 22.18, 21.04, 17.48, 17.01, 16.91, 14.94, 13.73, 9.77.

ESI-MS (acetonitrile): m/z = calcd for C₆₁H₇₃NO₁₇S₅ 1187.40, found 1188.42 [M+H]⁺

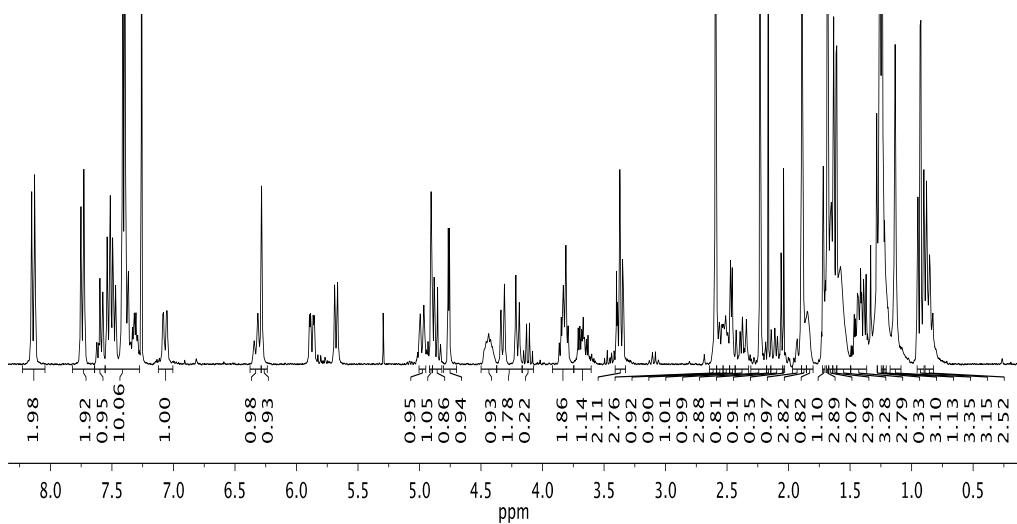


Figure S5. $^1\text{H-NMR}$ (300 MHz, CDCl_3) spectrum of PTX-C₂THP-PABTC.

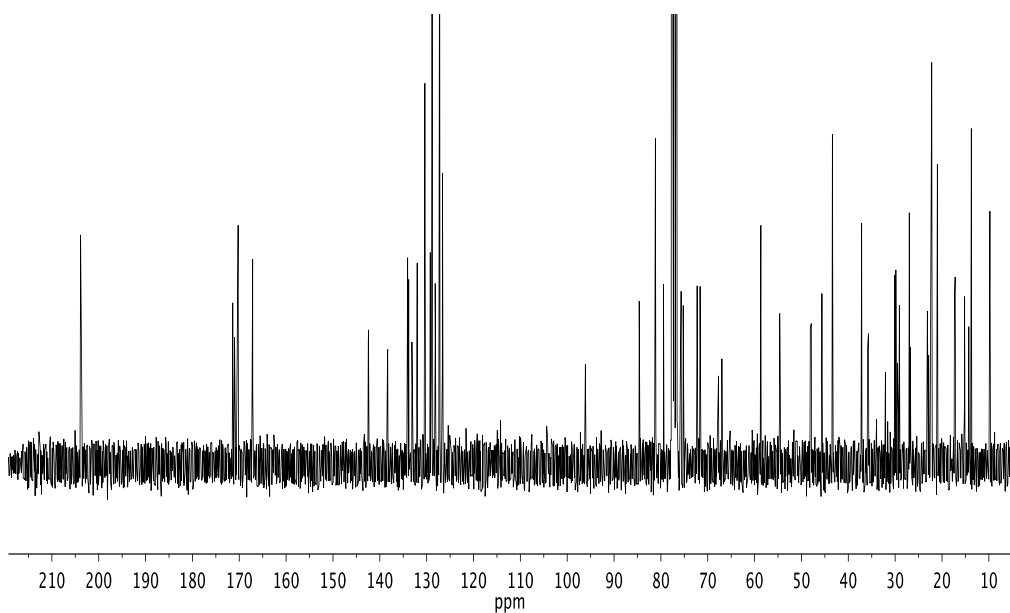


Figure S6. $^{13}\text{C-NMR}$ (75 MHz, CDCl_3) spectrum of PTX-C₂THP-PABTC.

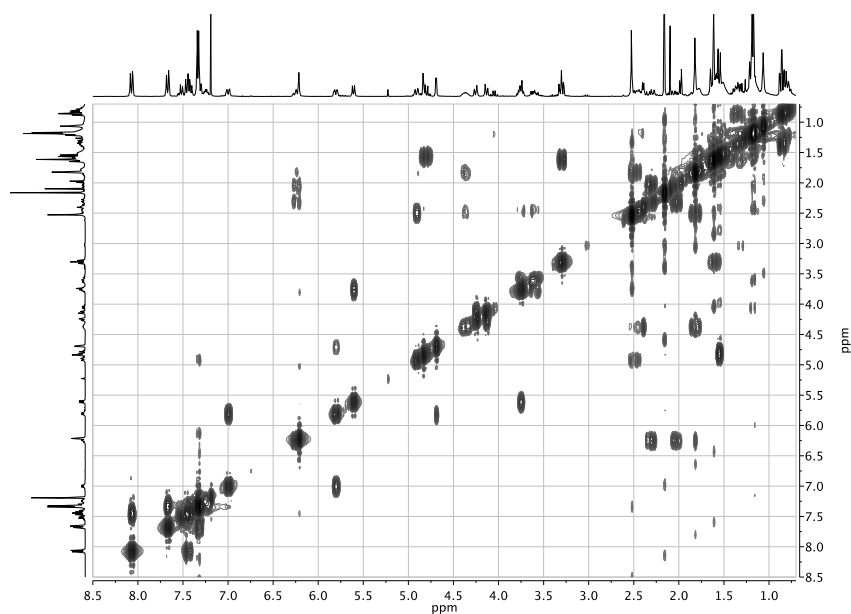


Figure S7. $^1\text{H},^1\text{H}$ -COSY spectrum of PTX-C₂-THP-PABTC.

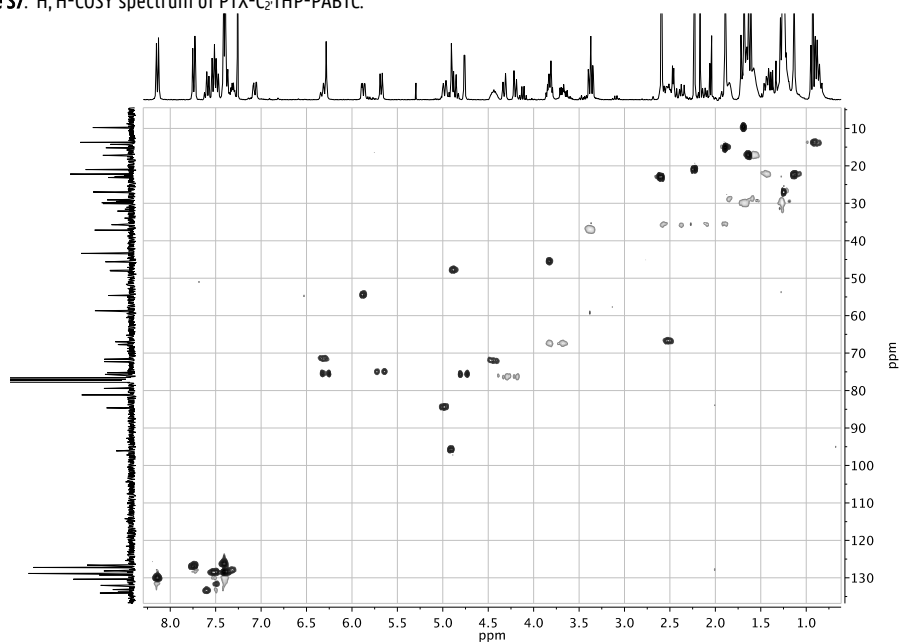


Figure S8. $^1\text{H},^{13}\text{C}$ -HSQC spectrum of PTX-C₂-THP-PABTC.

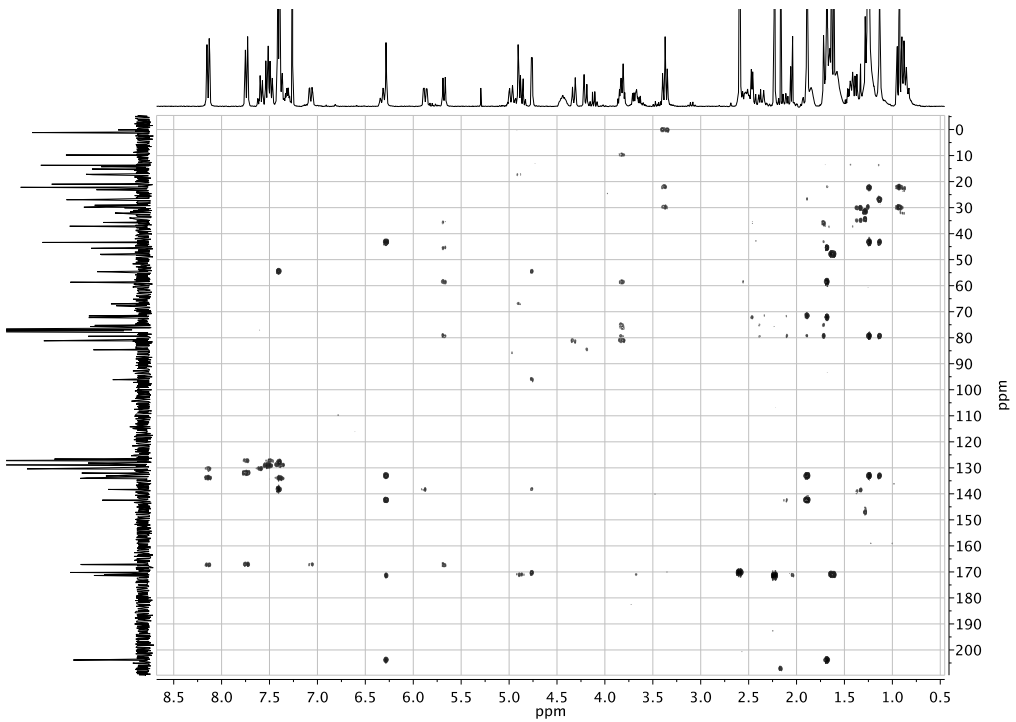


Figure S9. $^1\text{H},^{13}\text{C}$ -HMBC spectrum of PTX- C_2 -THP-PABTC.

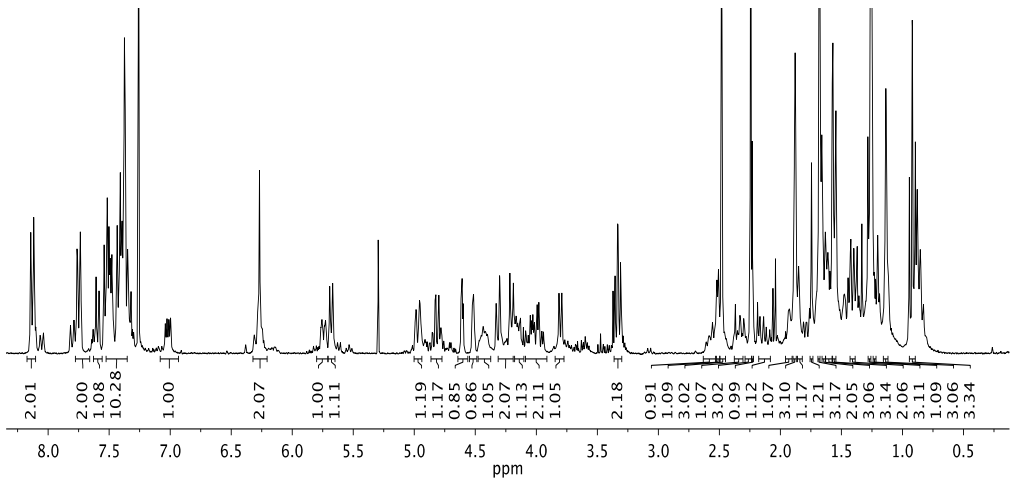


Figure S10. ^1H -NMR (300 MHz, CDCl_3) spectrum of PTX- C_7 -THP-PABTC.

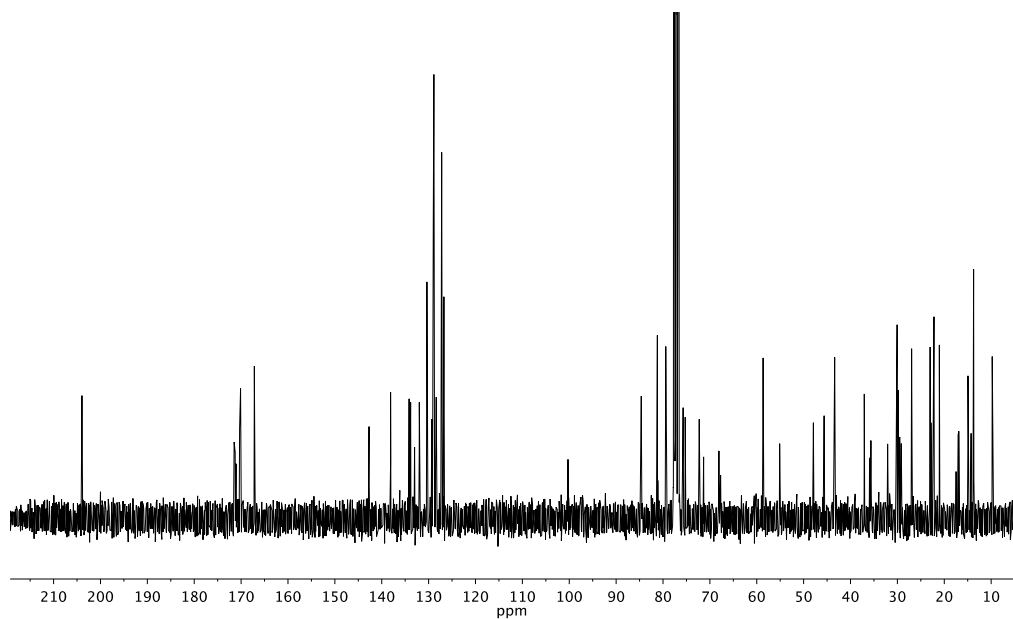


Figure S11. ^{13}C -NMR (75 MHz, CDCl₃) spectrum of PTX-C₇-THP-PABTC.

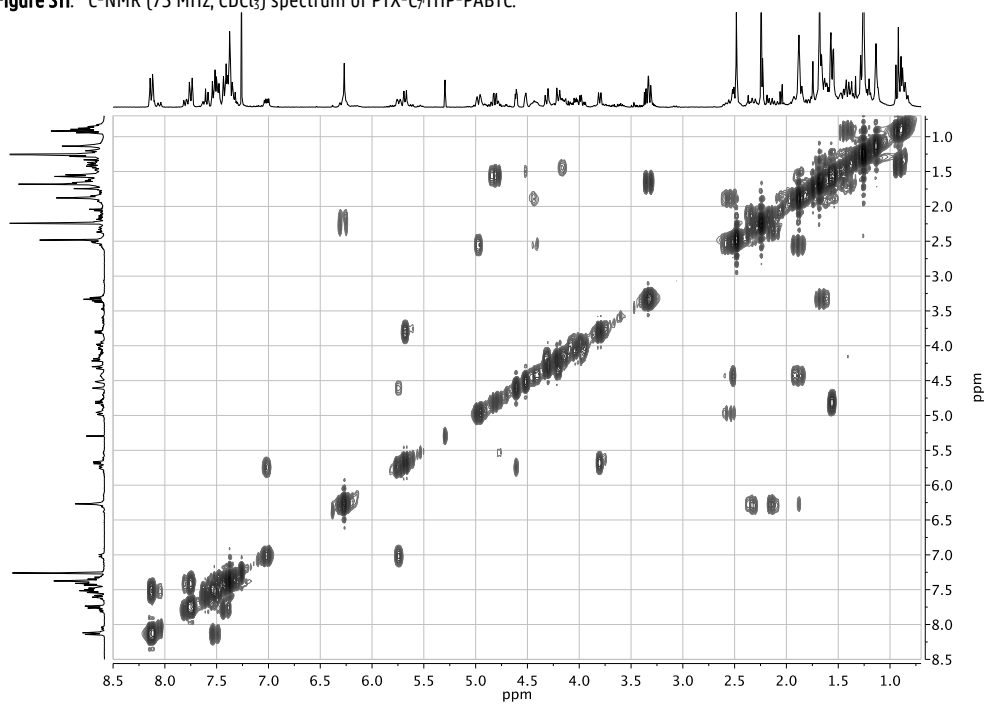


Figure S12. ^1H - ^1H -COSY spectrum of PTX-C₇-THP-PABTC.

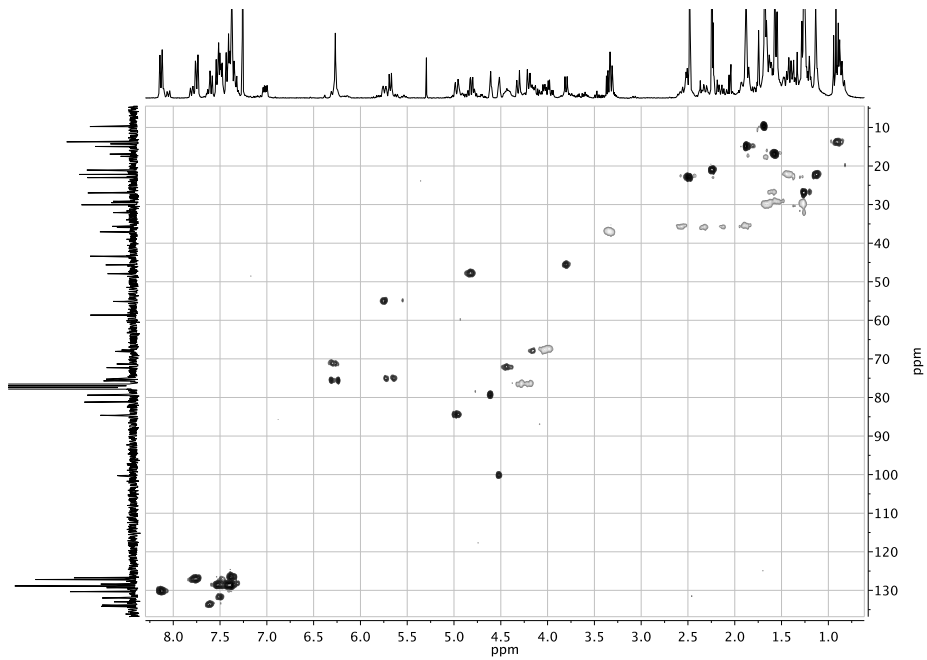


Figure S13. ^1H , ^{13}C -HSQC spectrum of PTX-C₇-THP-PABTC.

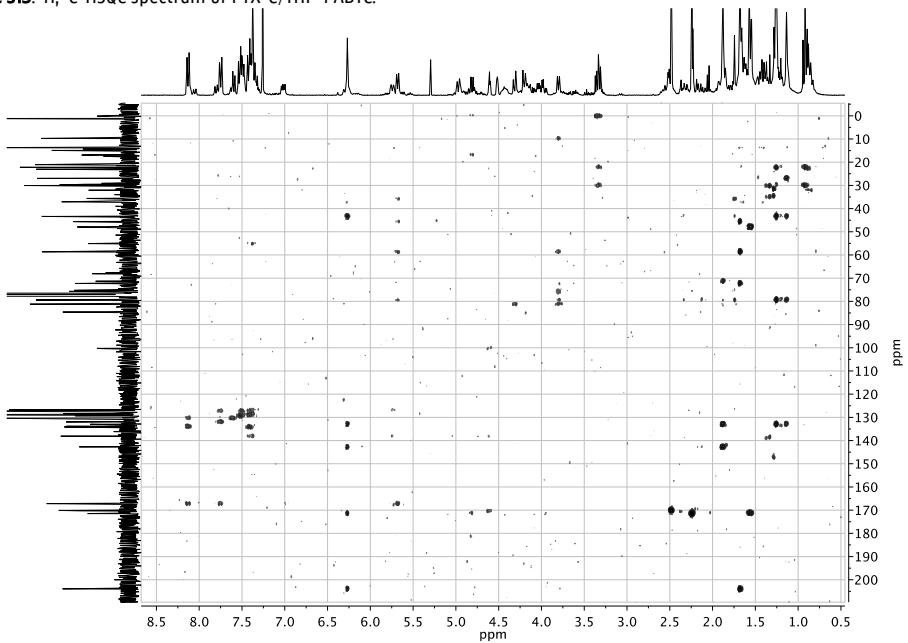


Figure S14. ^1H , ^{13}C -HMBC spectrum of PTX-C₇-THP-PABTC.

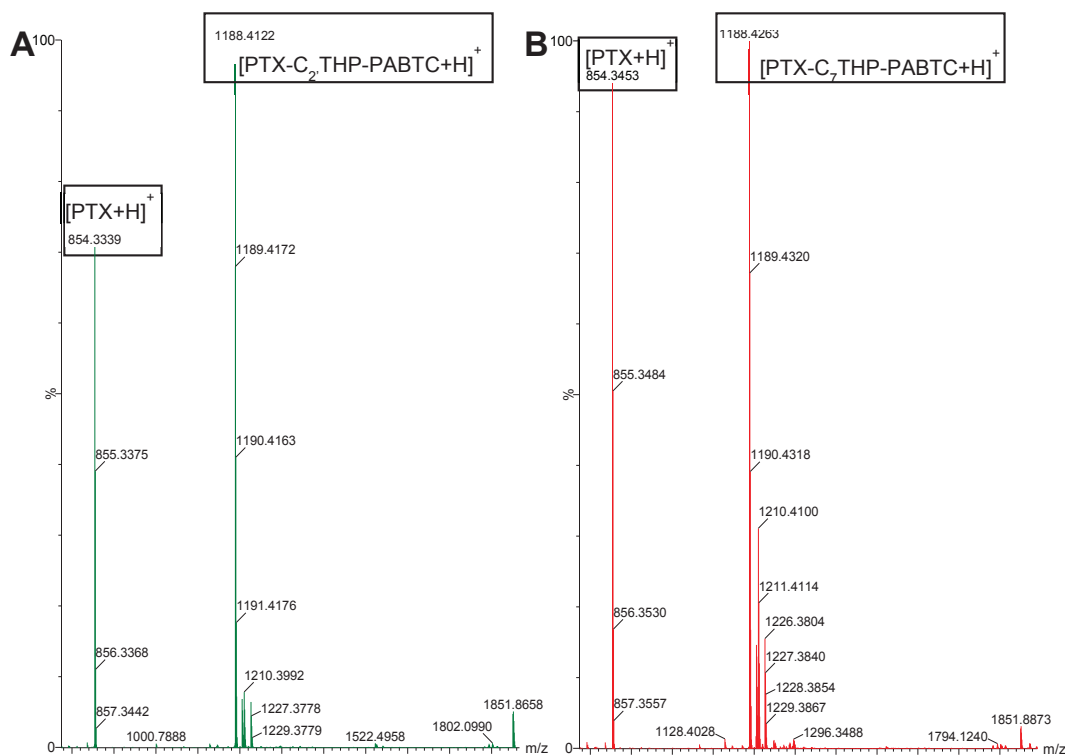


Figure S15. ESI-MS (acetonitrile) spectrum of PTX-C₂-THP-PABTC (A) and PTX-C₇-THP-PABTC (B).

6.4 PTX-DEGA-PABTC

¹H-NMR (300 MHz, DMSO-d₆): the spectrum shows resonances splits into bands of up to four separate peaks, as expected for the four possible isomers, which were for the sake of simplicity evaluated together referring to the similar proton: δ [ppm] = 8.91 (q, J = 8.4, 6.7 Hz, 1H), 7.98 (d, J = 7.1 Hz, 2H), 7.91 – 7.79 (m, 2H), 7.73 (t, J = 7.3 Hz, 1H), 7.67 – 7.12 (m, 10H), 6.30 (s, 1H), 5.97 – 5.75 (m, 1H), 5.50 (t, J = 9.0 Hz, 1H), 5.42 (d, J = 7.3 Hz, 1H), 4.92 (d, J = 7.1 Hz, 1H), 4.89 – 4.82 (m, 1H), 4.80 – 4.68 (m, 1H), 4.65 (s, 1H), 4.64 – 4.51 (m, 1H), 4.22 – 4.14 (m, 2H), 4.11 (dd, J = 7.0, 4.0 Hz, 1H), 4.06 – 3.94 (m, 2H), 3.69 – 3.60 (m, 2H), 3.59 – 3.52 (m, 2H), 3.51 – 3.40 (m, 3H), 3.37 (t, J = 7.3 Hz, 2H), 2.43 – 2.31 (m, 1H), 2.30 (s, 3H), 2.10 (s, 3H), 1.97 – 1.82 (m, 1H), 1.82 – 1.72 (m, 3H), 1.73 – 1.61 (m, 1H), 1.64 – 1.55 (m, 3H), 1.51 (s, 3H), 1.49 (d, J = 1.8 Hz, 3H), 1.35 (h, J = 7.4 Hz, 2H), 1.27 – 1.16 (m, 3H), 1.03 (s, 3H), 1.00 (s, 3H), 0.87 (t, J = 7.3 Hz, 3H).

^{13}C -APT-NMR (75 MHz, DMSO-d_6): δ [ppm] = 219.17, 202.36, 170.98, 170.81, 170.16, 169.90, 169.85, 168.72, 166.26, 165.17, 139.13 and 137.93, 134.44 and 133.31, 133.46, 131.34, 129.55, 128.88, 128.66, 128.40, 128.34, 128.28, 128.19, 127.98, 127.93, 127.38, **100.52** (PTX- C_7 DEGA-PABTC) or **99.72** (PTX- C_2 DEGA-PABTC), 83.66, 80.32, 76.69, 75.87, 75.39, 74.71, 74.47, 70.48, 70.08, 69.62, 68.07, 65.21, 64.70, 57.45, 55.11, 47.66, 46.07, 42.93, 36.56, 36.27, 34.65, 29.53, 26.24, 22.76, 21.38, 21.23, 20.65, 19.66, 16.42, 14.18, 13.39, 9.74.

ESI-MS (acetonitrile): m/z = calcd for $\text{C}_{61}\text{H}_{75}\text{NO}_{18}\text{S}_3$ 1205.41, found 1206.43 $[\text{M}+\text{H}]^+$

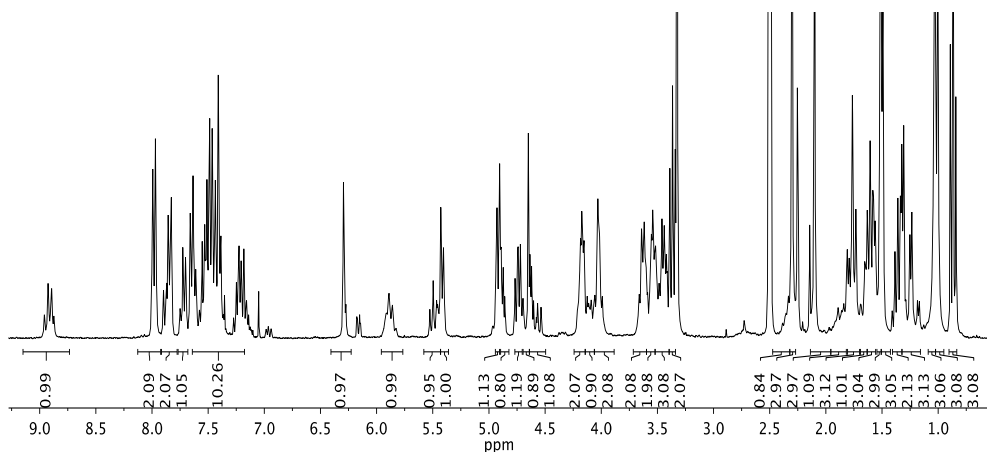


Figure S16. ^1H -NMR (300 MHz, DMSO-d_6) spectrum of PTX- C_{27}C_7 DEGA-PABTC.

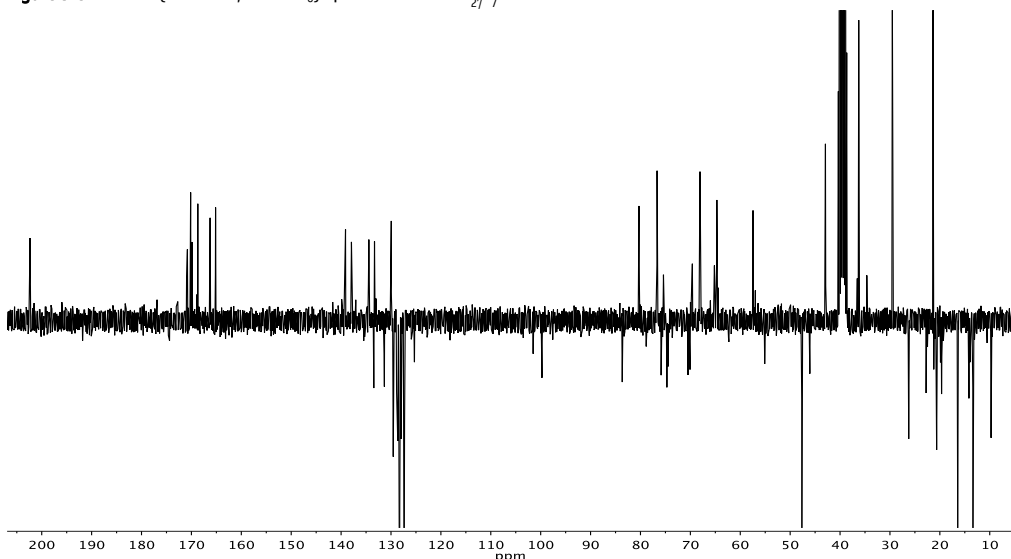


Figure S17. ^{13}C -APT-NMR (75 MHz, DMSO-d_6) spectrum of PTX- C_{27}C_7 DEGA-PABTC.

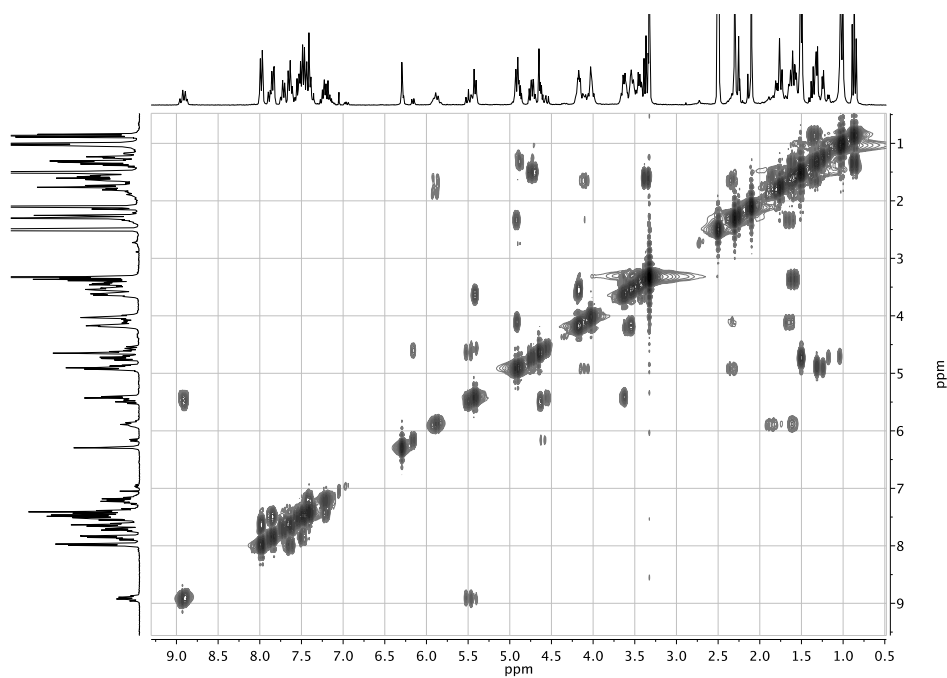


Figure S18. $^1\text{H},^1\text{H}$ -COSY spectrum of PTX- C_{27} DEGA-PABTC.

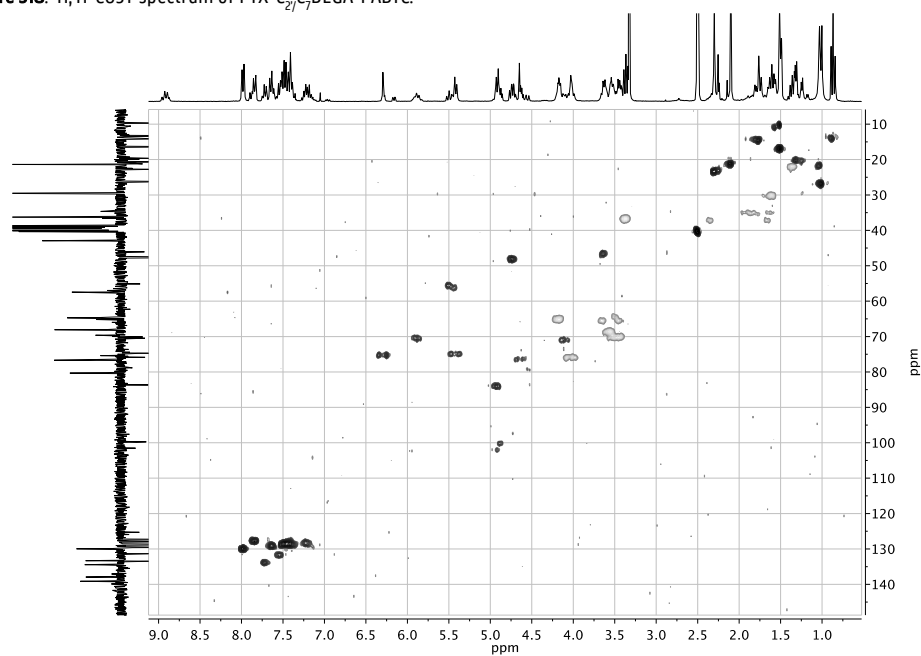


Figure S19. $^1\text{H},^{13}\text{C}$ -HSQC spectrum of PTX- C_{27} DEGA-PABTC.

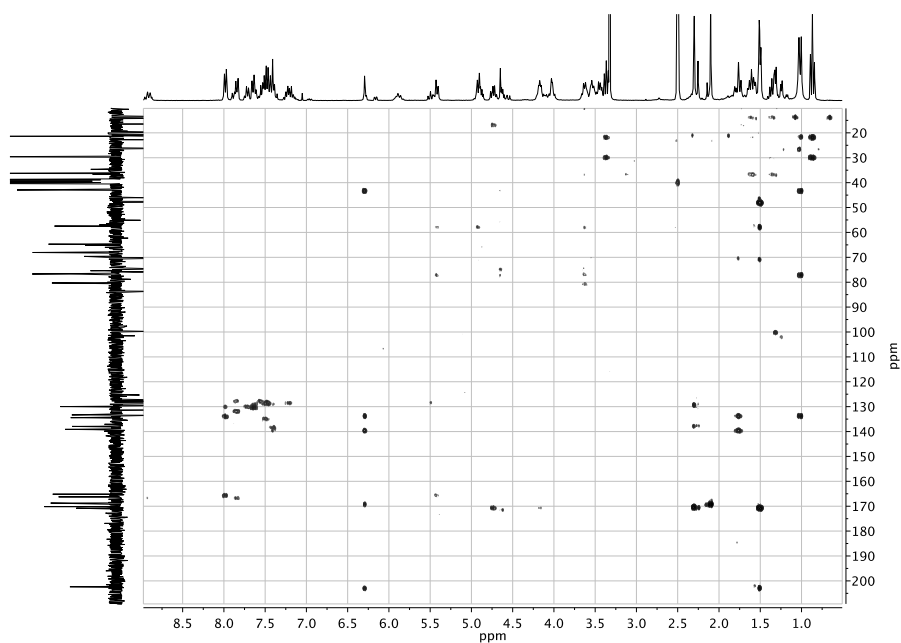


Figure S20. ^1H , ^{13}C -HMBC spectrum of PTX- C_{27}C_7 DEGA-PABTC.

6.5 PTX-THP-pDMA₃₀

SEC(DMAC, PMMA-St.): Mn = 3975, PDI = 1.08 (PTX- C_2 THP-pDMA₃₀) and Mn = 4226, PDI = 1.09 (PTX- C_7 THP-pDMA₃₀).

6.6 PTX-DEGA-pDMA₃₀

SEC(DMAC, PMMA-St.): Mn = 4999, PDI = 1.08 (PTX- C_{27}C_7 DEGA-pDMA₃₀).

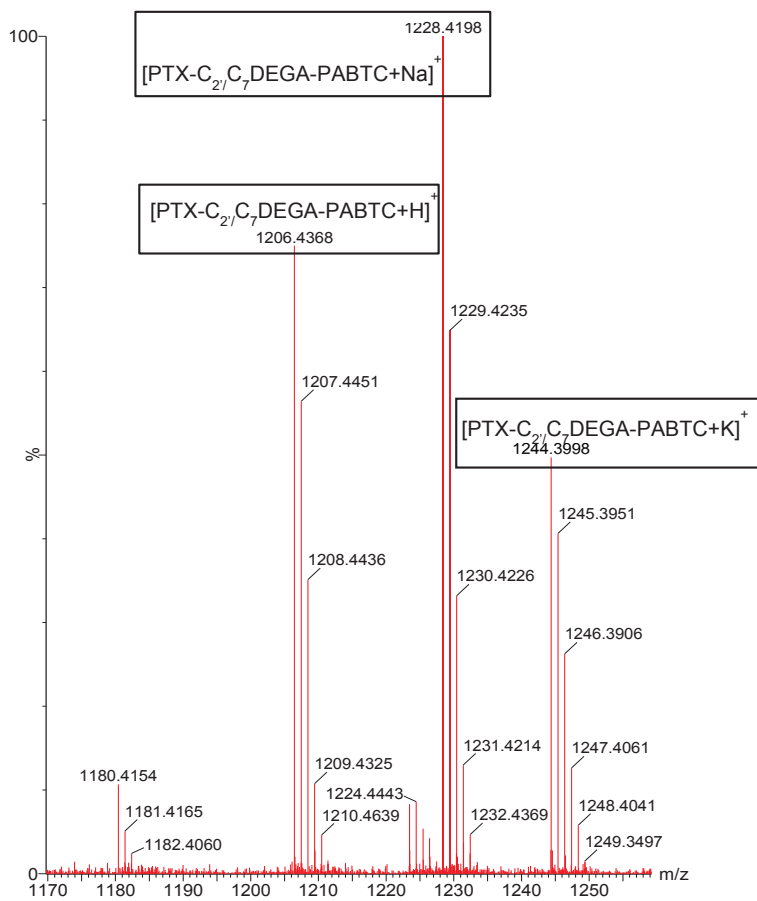


Figure S21. ESI-MS (acetonitrile) spectrum of PTX-C₂₁C₇DEGA-PABTC.

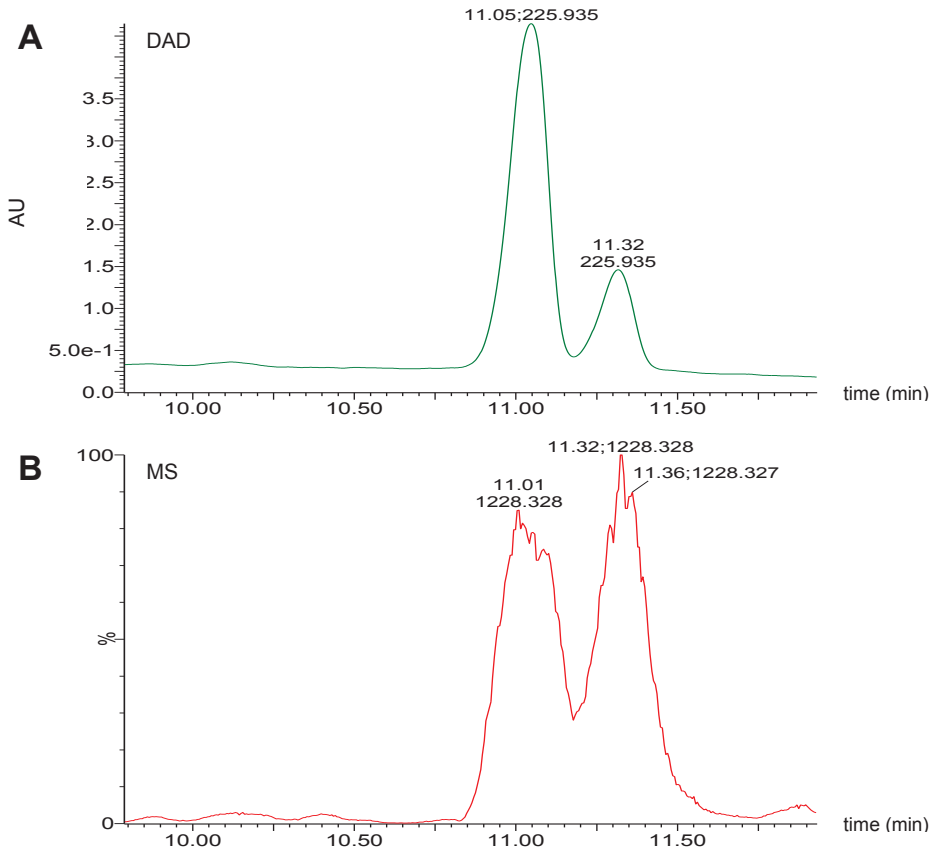
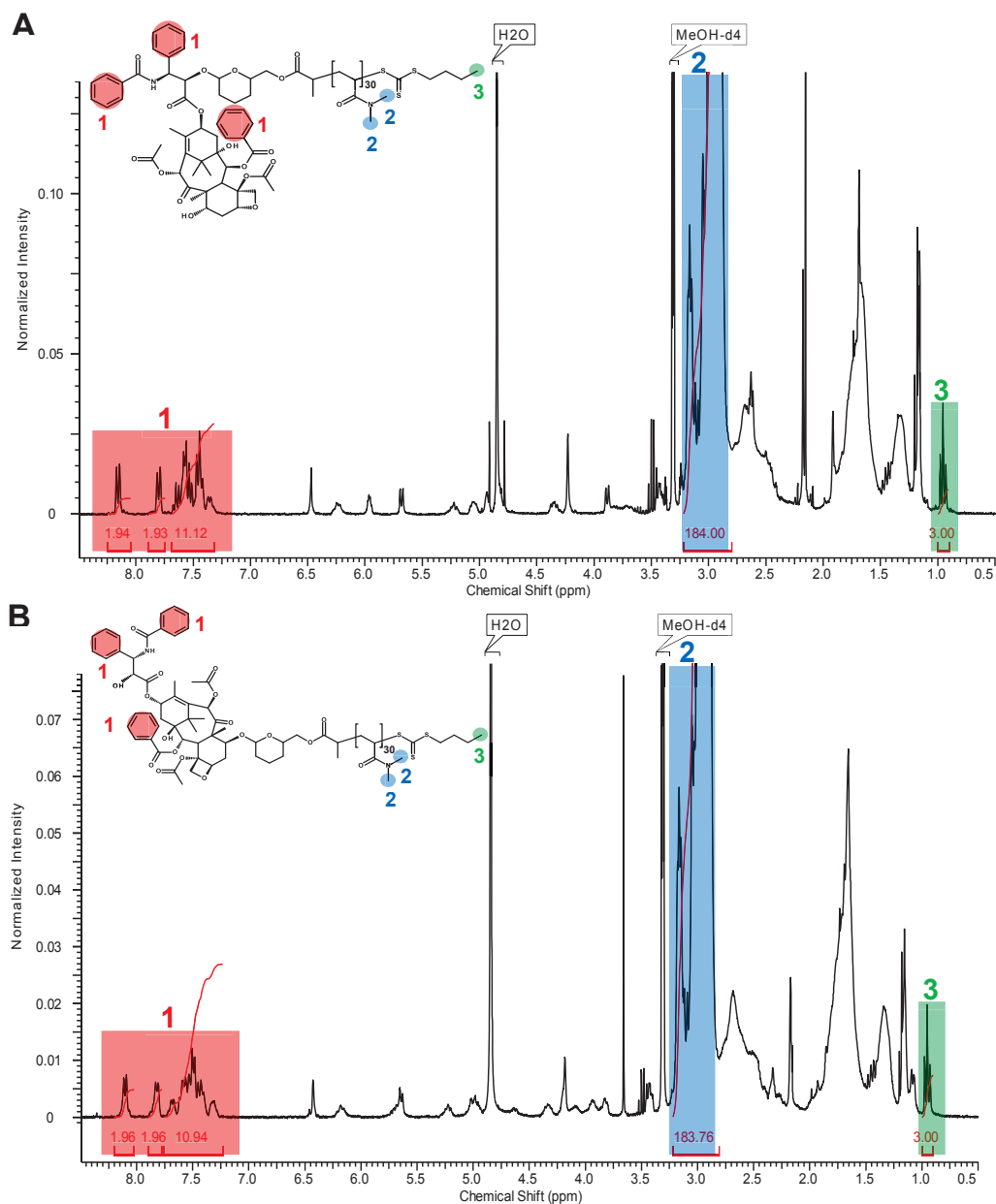


Figure S22. LC-DAD/MS of PTX-C₂₁C₇DEGA-PABTC: UV-chromatogram (A; retention times with corresponding λ_{max} are shown) and total ion chromatogram (TIC) (B; retention times with corresponding molecular ion are shown).



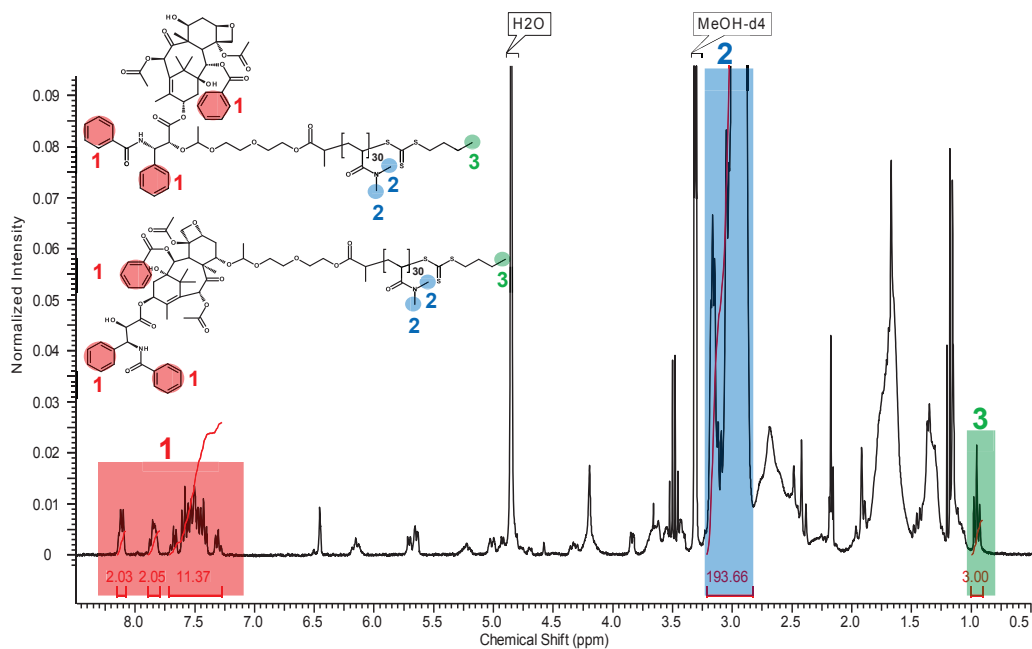


Figure S24. $^1\text{H-NMR}$ (300 MHz, MeOH-d_4) spectrum of $\text{PTX-C}_{27}/\text{C}_7\text{DEGA-pDMA}_{30}$.

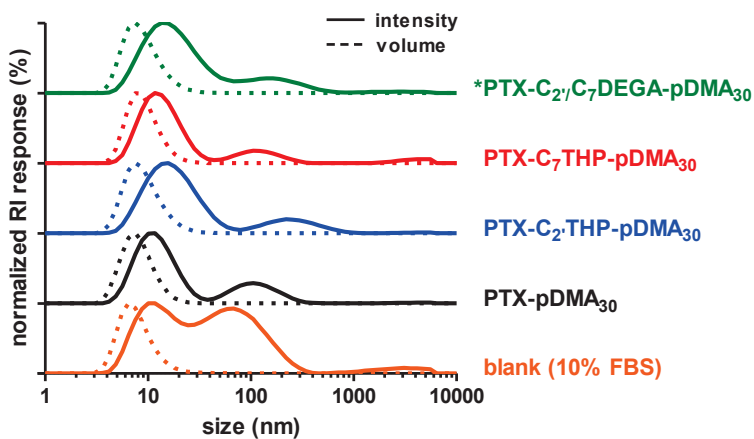


Figure S25. Size distribution measured by dynamic light scattering (DLS) of conjugates mixed with 10% of serum. *regio-isomeric mixture of PTX-polymer conjugate, modified either through the C_2 or the C_7 OH-group of PTX.

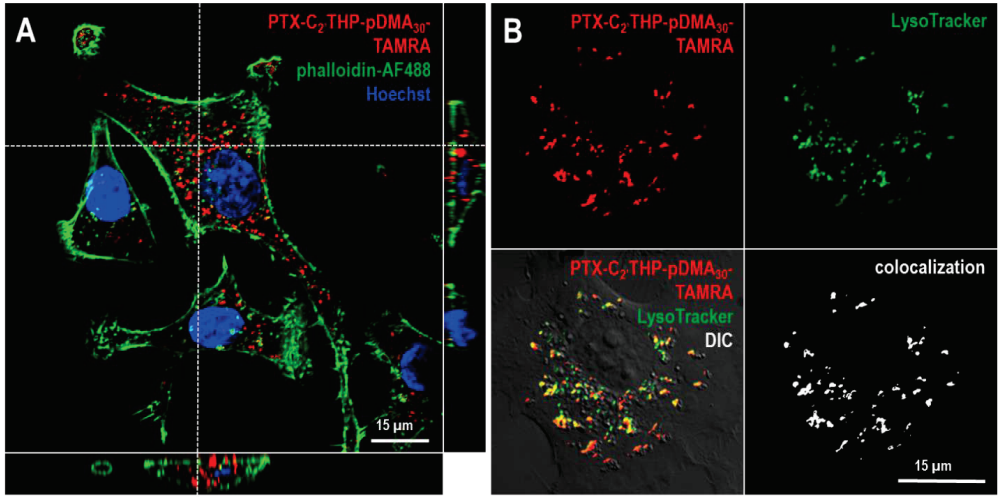


Figure S26. Confocal microscopy images of SKOV-3 human ovarian cancer cells pulsed with rhodamine-labelled PTX-C₂,THP-pDMA conjugates. In the left large panel, cells were counterstained with Hoechst (nuclei - blue) and phalloidin (green - actin/membrane). The right panels display counterstaining with LysoTracker and highlight the localization of the conjugates in intracellular acidic vesicles.

chapter 7

active targeted docetaxel-polymer prodrug conjugates

Benoit Louage,^a Lutz Nuhn,^a Fabian Hulpia,^b Kim Deswarte,^c Bart N. Lambrecht,^c Serge Van Calenbergh,^b
Bruno G De Geest^a

^a Laboratory of Pharmaceutical Technology, Department of Pharmaceutics,
Ghent University, Ottergemsesteenweg 460, 9000 Ghent, Belgium

^b Laboratory for Medicinal Chemistry, Department of Pharmaceutics,
Ghent University, Ottergemsesteenweg 460, 9000 Ghent, Belgium

^c VIB Inflammation Research Center, Technologiepark 927, 9052 Ghent, Belgium

manuscript in preparation

abstract

Based on the developed grafting-from-drug approach, this chapter describes the synthesis of active targeted docetaxel-polymer prodrug conjugates, through a combination of grafting-from-drug RAFT polymerization and post-modification with a small molecule targeting ligand for prostate specific membrane antigen (PSMA). Docetaxel (DTX) was ligated to a RAFT CTA by regioselective esterification at the C₂ OH-group of DTX. Subsequent RAFT polymerization with DMA yielded well-defined, amphiphilic, micellar DTX-polymer prodrug conjugates with similar high drug loading, aqueous compatibility, colloidal stability and small particle size as compared to the previously reported first- and second-generation PTX-polymer conjugates. Fluorescently labeled analogues were prepared by incorporating a minimal fraction of rhodamine-labeled monomer during the polymerization step. Additionally, a maleimide-modified derivative of the PSMA targeting ligand S,S-2-(3-(5-amino-1-carboxypentyl)-ureido)-pentanedioic acid (ACUPA) was synthesized and used for ligation to the other polymer chain end after aminolysis of the thiocarbonate moiety. Finally, FACS analysis provides a first indication of receptor-specific interaction between the polymer conjugates and PSMA-positive LNCaP cells as compared to non-ACUPA functionalized control polymer conjugates.

1 introduction

Despite their broad-spectrum activity as anti-cancer drugs, widespread use of taxanes (i.e. paclitaxel (PTX) and docetaxel (DTX)) in chemotherapy remains problematic due to toxic side-effects.^[1,2] The latter can be evoked intrinsically by the drugs and/or by allergenic excipients (e.g. Cremophor EL in Taxol (PTX) and polysorbate 80 in Taxotere (DTX)).^[3-7] Second-generation taxane formulations (i.e. Abraxane and Genexol-PM (PTX)) based on biocompatible surfactants significantly reduced toxicity (i.e. hypersensitivity reactions), increased the therapeutic index and thus the efficacy of taxanes.^[8-13] However, intrinsic side-effects (e.g. nausea, neuropathy, neutropenia) remain present due to systemic drug distribution throughout the body. Hence, selective accumulation (i.e. at the (metastatic) tumor site) is imperative in the development of the next generation taxane formulations.

Nanomedicine pushed the boundaries in targeted drug delivery since the discovery of the enhanced permeability and retention effect (EPR)^[14,15]. The latter involves 'leaky', highly fenestrated neoplastic endothelia through which nanomedicines can swiftly pass into the tumor microenvironment where they can reside due to an impaired drainage by neighboring lymphatic vessels. The latter phenomenon is termed 'passive' targeting as it is merely based on physical phenomena. Unfortunately, due to the vast heterogeneity of cancer disease, EPR cannot always be relied upon.^[16,17] Metastatic tumor tissue is often poorly vascularized and the intrinsic slower tumor growth in humans as compared to preclinical models often implies the formation of regular, dense vascular endothelium.^[18,19] More efficient and selective treatment would thus require additional, active targeting strategies.

Active targeting involves the interaction between a ligand and a receptor/antigen on the surface of the targeted cell prior to receptor-mediated endocytosis.^[20] This allows for more selective delivery of drugs to tissues, overexpressing the target receptor/antigen. Additionally, active uptake also suppresses multiple drug resistance (MDR) mechanisms such as P-glycoprotein (P-gp) efflux.^[21] Due to their superior selectivity and affinity towards any type of antigen, the benchmark in this field was set by monoclonal antibody-drug conjugates (ADCs).^[22-24] However, ADC-based chemotherapy is not without limitations. First, monoclonal antibodies (mAbs) cannot always thoroughly penetrate into the tumor tissue due to their high molecular weight (MW) and size.^[25] Secondly, ADCs can prematurely bind to detached, soluble receptor/antigen in tumor tissue fluid, thereby losing their targeting capabilities.^[26] Finally, the extremely high ADC manufacturing cost (i.e. mAb production, drug conjugation and purification) questions whether the use of ADCs is feasible on a global scale and hence whether or not economically more favorable platforms for active targeting should be explored more thoroughly.^[27]

An emerging field in targeted drug delivery comprises small molecule-drug conjugates (SMDCs).^[25,28] The basic design of the latter is similar to ADCs, with the great distinction that the mAb is substituted by a small-molecule ligand with high affinity ligand towards the target receptor. Not only is this a great tool for reducing costs as the latter does not require a biotechnological production process, the smaller MW and size of SMDCs could also allow for a more thorough tumor penetration and reduce off-site toxicity due to swift renal clearance of dose which has not reached the site of interest. Several SMDCs are currently evaluated in phase I/II trials as chemotherapeutic or imaging agent, showing promising clinical outlook.^[28] For the majority of these systems, the drug or imaging agent is attached to the small-molecule targeting ligand by a low MW, hydrophilic oligopeptide spacer^[29–32] and often requires multistep, solid phase peptide synthesis (SPPS) procedures.^[33,34]

This chapter investigates the chemical feasibility of our previously described grafting-from-drug approach to apply the same basic design principles of SMDCs and further simplify the synthesis of the spacer by substituting the oligopeptide with a low MW, hydrophilic polymer chain.^[35] As proof of concept, we aimed at developing a 'small molecule-polymer-drug conjugate' for prostate cancer. With DTX (i.e. Taxotere) regularly used for treatment of hormone-refractory prostate cancer,^[36] our goal was to design a DTX-polymer prodrug conjugate, functionalized with a targeting ligand for prostate specific membrane antigen (PSMA), a membrane receptor often overexpressed by prostate cancer cells and neovascular endothelium of solid tumors.^[37–39] Out of the several small-molecule ligands with high affinity for PSMA which have been developed,^[28,40] we selected the same ligand which was used for the BIND-014 technology (i.e. *S,S*-2-(3-(5-amino-1-carboxypentyl)-ureido)-pentanedioic acid (ACUPA)).^[41]

2 results and discussion

The developed synthesis strategy is depicted in **Scheme 1**. DTX (**Figure S1 – S3**) was regioselectively esterified at the C₂-hydroxyl (OH)-group with a reversible addition-fragmentation chain transfer (RAFT) chain transfer agent (CTA; 2-(butylthiocarbonothioylthio)propanoic acid (PABTC)), yielding DTX-PABTC. The structure of the latter was confirmed by nuclear magnetic resonance (NMR) spectroscopy (**Figure S4 – S8**) and electron spray ionization-mass spectroscopy (ESI-MS; **Figure S9**). This DTX-functionalized RAFT CTA was used for subsequent polymerization of *N,N*-dimethylacrylamide (DMA). A degree of polymerization (DP) of 15 and 30 was aimed to investigate the influence of hydrophilic polymer chain length on DTX-pDMA aqueous compatibility and to allow comparison with the previously reported PTX-pDMA conjugates. The difference in chain length was confirmed by DOSY NMR (**Figure 1A**) and size exclusion chromatography (SEC; **Figure 1D**). In analogy to the PTX-pDMA₁₅ conjugates

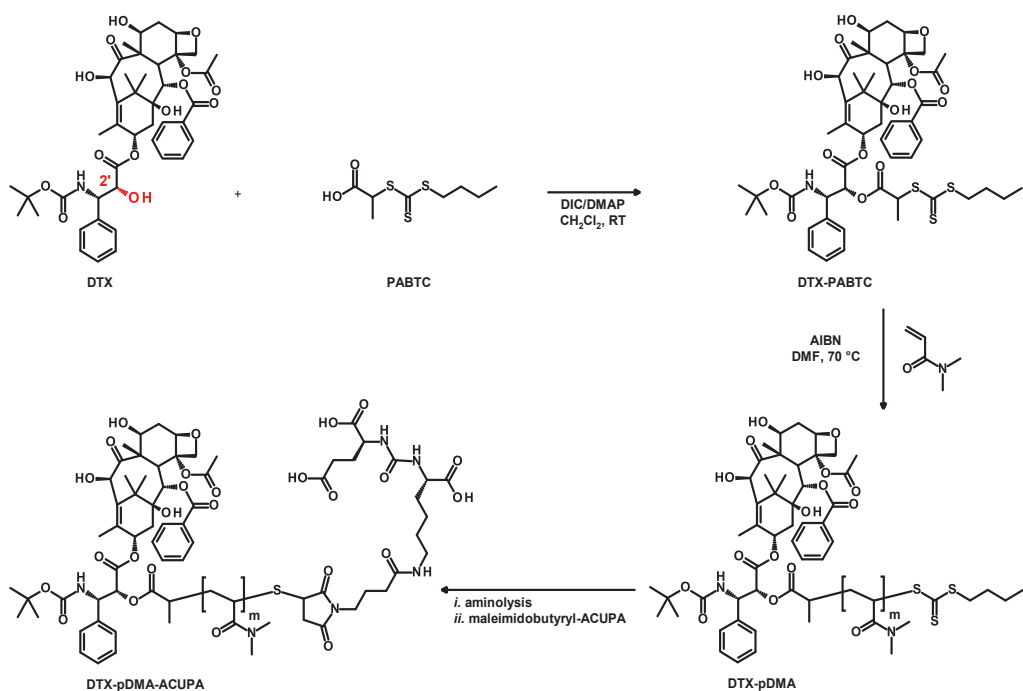
(Chapter 5), DTX-pDMA₁₅ was neither soluble nor dispersible in aqueous buffer. Both DTX-pDMA₁₅ (Figure S10 and S12A) and DTX-pDMA₃₀ (Figure S11 and S12B) were characterized by ¹H-NMR spectroscopy and showed high α,ω -endgroup fidelity. Narrow polymer dispersities were observed by SEC for both conjugates, even at high monomer conversions (Table 1). As revealed by dynamic light scattering (DLS), DTX-pDMA₃₀ self-assembled into micellar nanostructures with colloidal stability (Figure 1B), size (i.e. Z-average = 12.5 \pm 0.1 nm; n = 3) and dispersity (i.e. 0.064 \pm 0.004; n = 3) in concordance to the first- and second-generation PTX-pDMA₃₀ conjugates (Chapter 5 and Chapter 6). Fluorescently labeled DTX-pDMA₃₀ analogue conjugates (i.e. DTX-pDMA^{Rho}₃₀) were prepared by incorporating a small fraction of rhodamine-labeled monomer during the polymerization step. The latter had little influence on the polymer characteristics measured by NMR (Figure S13 and S14) and SEC (Table 1 and Figure S24). Likely due to the bulky nature of the rhodamine-labeled monomer, a modest increase in particle size was observed by DLS (i.e. Z-average = 23.6 \pm 0.1 nm; n = 3), while a narrow dispersity (i.e. 0.094 \pm 0.003; n = 3) was maintained (Figure 1C), indicating the rhodamine-labeled DTX-pDMA^{Rho}₃₀ conjugates are suitable for *in vitro* evaluation.

Table 1. Compositional data of the synthesized polymers.

polymer	[DMA] _f [CTA]	conversion DMA (%) ^a	DP ^{conv,b}	DP ^{endgroup,c}	M _n (Da) ^d	\mathcal{D} ^d	DTX loading capacity (%) ^e
DTX-pDMA ₁₅	15	88	13	17	2668	1.08	34
DTX-pDMA ₃₀	30	97	29	32	4491	1.09	20
DTX-pDMA ^{Rho} ₃₀	30	97	29	31	4365	1.09	20
DTX-pDMA ₃₀ -ACUPA	30 ^f	97 ^f	29 ^f	30	4876	1.12	19
DTX-pDMA ₃₀ -HA	30 ^f	97 ^f	29 ^f	31	5319	1.09	20
DTX-pDMA ^{Rho} ₃₀ -ACUPA	30 ^f	97 ^f	29 ^f	31	4997	1.13	19
DTX-pDMA ^{Rho} ₃₀ -HA	30 ^f	97 ^f	29 ^f	31	5222	1.09	20

^a Determined by ¹H-NMR spectroscopy. ^b Determined by ¹H-NMR spectroscopy based on monomer conversion. ^c Determined by ¹H-NMR spectroscopy based on endgroup analysis. ^d Analyzed by SEC in DMAc, calibrated with PMMA standards. ^e Calculated based on conversion by ¹H-NMR spectroscopy: $MW_{DTX}/MW_{DTX-conjugate} \times 100\%$. ^f Post-polymerization functionalized polymers with conversion/DP equal to corresponding unfunctionalized DTX-conjugates.

To allow for the preparation of active targeted DTX-pDMA₃₀ and DTX-pDMA^{Rho}₃₀, the PSMA-targeting ligand ACUPA was synthesized and modified with a maleimide moiety as depicted in **Scheme S1**. First, 4-maleimidebutyric acid was activated with pentafluorophenol (PFP) as confirmed by NMR spectroscopy (**Figure S15**). Next, carboxybenzyl- (Cbz) and tert-butyl ester-protected ACUPA was synthesized (**Figure S16** and **S17**). After Cbz-deprotection (**Figure S18**), the latter was used for subsequent reaction with maleimidobutyryl-PFP. Coupling was confirmed by NMR spectroscopy (**Figure S19**). Finally, tert-butyl ester-deprotection with trifluoroacetic acid (TFA) revealed maleimidobutyryl-ACUPA, as confirmed by NMR spectroscopy (**Figure S20 – S22**) and ESI-MS (**Figure S23**).



Scheme 1. Reaction scheme illustrating regioselective esterification of at the C₂ OH-group of DTX with a RAFT CTA (PABTC), followed by polymerization of *N,N*-dimethylacrylamide (DMA) and post-polymerization functionalization of the thiocarbonate endgroup with a maleimide-modified derivative of a PSMA targeting ligand (ACUPA).

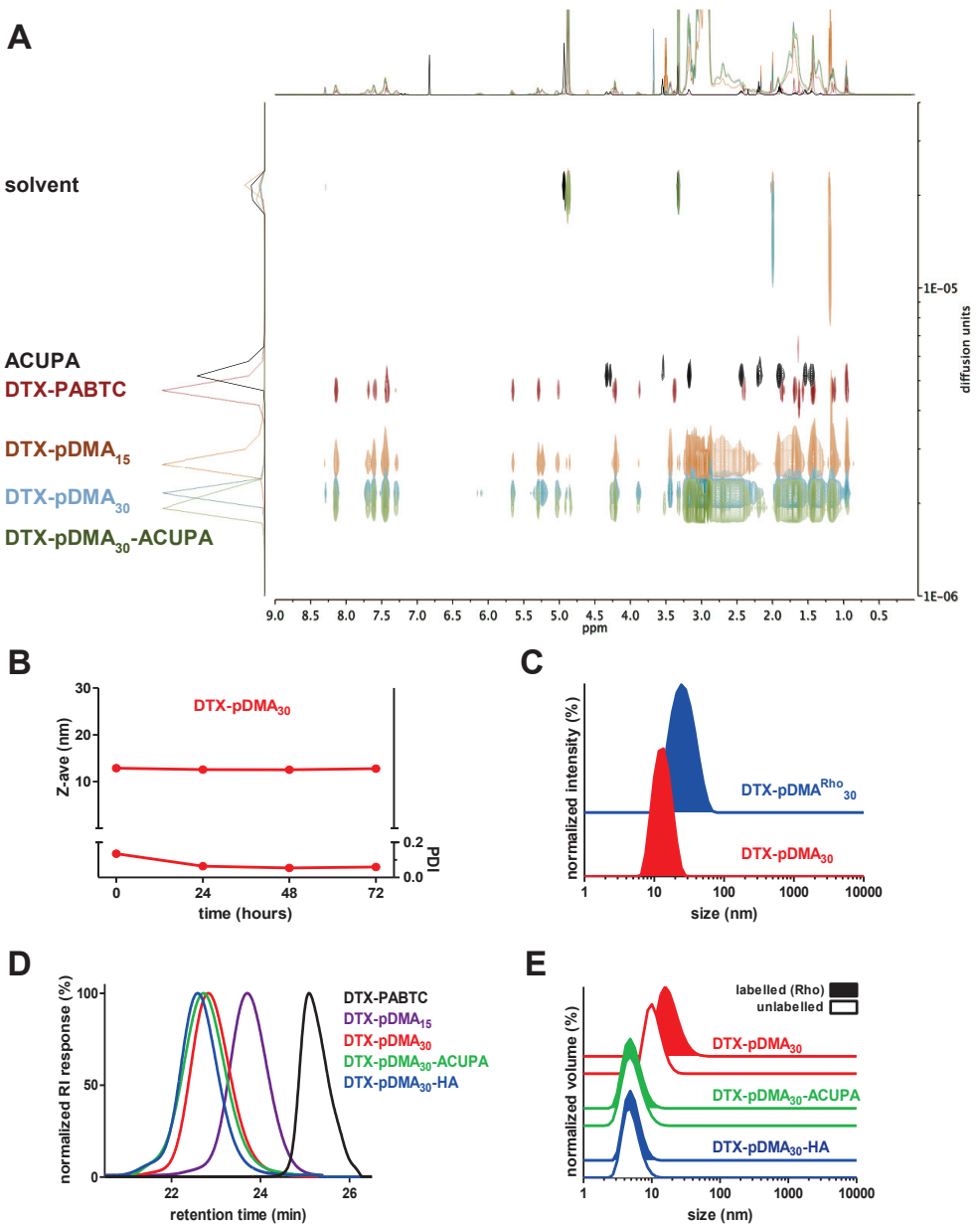


Figure 1. DOSY NMR spectra (A) and SEC elutograms (D) of DTX-pDMA conjugates. (B) Colloidal stability of DTX-pDMA₃₀ and size distribution (C,E) of DTX-pDMA conjugates (30 mg/mL in PBS) measured by DLS (n = 3).

In the final synthesis step, maleimidobutryl-ACUPA was used for post-polymerization functionalization of both DTX-pDMA₃₀ and DTX-pDMA^{Rho}₃₀ by sequential one-pot aminolysis/thiol–maleimide endgroup modification. For the preparation of non-targeted control conjugate, 6-maleimidohexanoic acid (MHA) was used instead. Removal of the RAFT trithiocarbonate endgroup (i.e. Z-group; **Figure S25**) and the structures of both PSMA-targeted DTX-pDMA₃₀-ACUPA (**Figure S26**) and non-targeted DTX-pDMA₃₀-HA (**Figure S27**) were confirmed by NMR spectroscopy. In addition, DOSY (**Figure 1A** and **Figure S28**) and SEC (**Figure 1D**) showed a subtle change in diffusional rate and increase in MW, respectively, whilst low polymer dispersity was maintained. Functionalization of DTX-pDMA^{Rho}₃₀ with maleimidobutryl-ACUPA or MHA SEC led to similar results as observed by SEC (**Figure S24**). Interestingly, DLS showed a significant and similar shift in particle size from supra to sub 10 nm range for both rhodamine-labeled and unlabeled DTX-pDMA₃₀-ACUPA and DTX-pDMA₃₀-HA, compared to their non-functionalized counterparts (**Figure 1E**). This can be attributed to the higher hydrophilic nature of the ω-endgroup due to the monocarboxylate (HA) and tricarboxylate (ACUPA) moieties compared to the butyl moiety before post-modification, inducing a switch from a self-assembled to a more water-soluble state of the DTX-polymer conjugates. Both DTX-pDMA^{Rho}₃₀-ACUPA and DTX-pDMA^{Rho}₃₀-HA contained equal rhodamine-labeling as confirmed by UV-VIS spectroscopy (**Figure S29**), and hence are suitable for accurate head-to-head comparison *in vitro*.

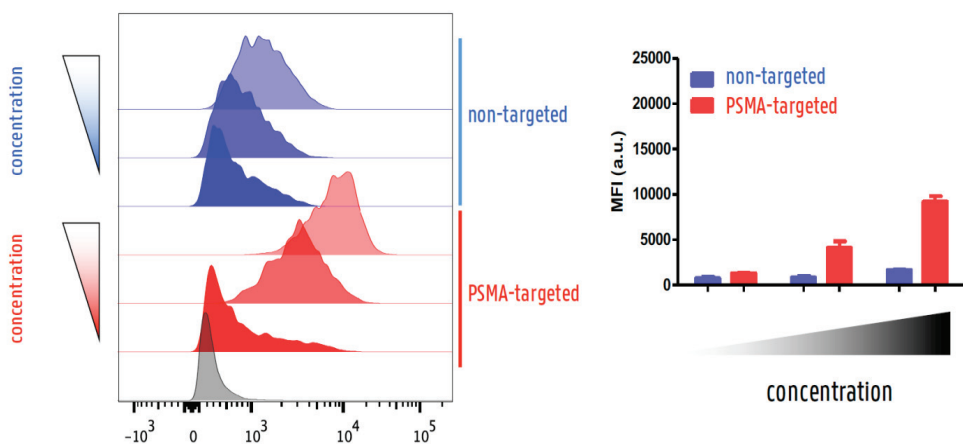


Figure 2. Histograms and mean fluorescence intensity values of LNCaP cells, co-incubated for 2 hours with 0.04, 0.2 and 1 mg/mL of targeted DTX-pDMA^{Rho}₃₀-ACUPA (red) or control DTX-pDMA^{Rho}₃₀-HA (blue), measured by FACS (n = 3).

Finally, *in vitro* cellular uptake was evaluated by flow cytometry (FACS) by co-incubation of DTX-pDMA₃₀^{Rho}-ACUPA or DTX-pDMA₃₀^{Rho}-HA with LNCaP cells. The latter is a human prostate cancer cell line, known for overexpressing the PSMA receptor at their surface. Both conjugates were incubated for 2 hours at 3 different concentrations prior to FACS analysis. As illustrated in **Figure 2**, significantly higher fluorescence values were observed at all concentrations tested for LNCaP cells co-incubated with DTX-pDMA₃₀^{Rho}-ACUPA. As the degree of rhodamine-labeling is equal for both conjugates (cfr. supra), these data suggest that DTX-pDMA₃₀^{Rho}-ACUPA has stronger interaction with LNCaP cells as compared to DTX-pDMA₃₀^{Rho}-HA, most likely evoked by the high affinity of ACUPA towards PSMA.

3 conclusions

As the previous chapters emphasized on first- and second-generation PTX-polymer conjugates, this chapter comprehensively demonstrates that a similar high degree of polymer definition and physicochemical features can be attained when the grafting-from-drug strategy is applied to DTX, further confirming the overall robustness and chemical versatility of the approach. Additionally, the combination with established maleimide coupling chemistry enabled synthesis of functionalized DTX-polymer conjugates for active PSMA-targeting. FACS evaluation of cellular uptake suggests a higher degree of interaction between targeted DTX-polymer conjugate and PSMA-positive LNCaP cells as compared to control conjugate. This not only encourages more elaborate *in vitro* evaluation, but also urges to extend beyond 'grafting-from-taxane' by exploring alternative APIs and maleimide-modified targeting ligands.

4 experimental

4.1 materials

All chemicals were purchased from Sigma Aldrich unless mentioned otherwise. The RAFT CTA 2-(butylthiocarbonothioylthio)propanoic acid (PABTC) was synthesized according to literature.^[42] TLC plates were purchased from Macherey Nagel. Docetaxel (DTX) was purchased from LC Laboratories. Acryloxyethyl thiocarbamoyl rhodamine B (ARho) and 4-maleimidobutyric acid were obtained from Polysciences Inc. and TCI, respectively. N-ε-Cbz-L-Lysine tert-butyl ester hydrochloride (H-Lys(Z)-O^tBu HCl) was purchased from Merck Millipore. L-Glutamic acid di-tert-butyl ester hydrochloride (H-Glu(O^tBu)-O^tBu HCl), 4',6'-diamidino-2-

phenylindole (DAPI) solution (1 mg/mL) in H₂O, Dulbecco's phosphate buffered saline (PBS), cell dissociation buffer (enzyme-free), Roswell Park Memorial Institute (RPMI) 1640 GlutaMAX medium, fetal bovine serum (FBS), L-glutamine, sodium pyruvate, penicillin and streptomycin were obtained from Thermo Fisher Scientific. LNCaP cells were supplied by ATCC.

4.2 analysis

NMR spectra were recorded on a Bruker 300 and 400 MHz FT-NMR spectrometer. Chemical shifts (δ) are given in ppm relative to TMS. Samples were prepared in given deuterated solvents and their signals referenced to residual non-deuterated signals of the solvent.

Electron spray ionization-mass spectroscopy (ESI-MS) measurements were performed on a Waters (Milford, Mass, USA) LCT Premier XE time-of-flight (TOF) mass spectrometer equipped with an ESI interface. Samples were infused in an acetonitrile:formic acid (1000:1) mixture at 0.1 mL/min.

Size exclusion chromatography (SEC) was carried out on an Agilent 1260 system, equipped with a 1260 ISO-pump, a 1260 diode array detector (DAD) and a 1260 refractive index detector (RID). Measurements were performed in *N,N*-dimethylacetamide (DMAc) containing 50 mM LiCl at 50 °C, using a flow rate of 0.593 mL/min. A guard column and two PL gel 5 μ m mixed-D columns were used in series, calibrated with poly(methyl methacrylate) (PMMA) standards obtained from PSS (Mainz, Germany).

Dynamic light scattering (DLS). DLS measurements were carried out on a Zetasizer Nano S (Malvern) with a HeNe laser (λ = 633 nm) at a scattering angle of 173°.

4.3 synthesis DTX-PABTC

In a 50 mL round-bottom unineck flask, PABTC (2.040 mmol, 0.486 g), 4-(dimethylamino)pyridine (DMAP) (0.204 mmol, 0.024 g) and docetaxel (DTX) (1.85 mmol, 1.500 g) were dissolved in 30 mL anhydrous dichloromethane (CH₂Cl₂). Next, *N,N*-diisopropylcarbodiimide (DIC) (2.04 mmol, 0.258 g) was added dropwise and the mixture was stirred for 3 hours at room temperature and monitored by TLC. Subsequently, the reaction mixture was filtered and concentrated *in vacuo*. The crude product was purified by silica gel chromatography (eluent 6:4 hexane:ethyl acetate v/v). After concentration and subsequent drying under high vacuum, the obtained yellow solid (0.90 mmol, 0.922 g, 49 %) was analyzed by NMR spectroscopy and ESI-MS.

4.4 synthesis DTX-pDMA

DTX-PABTC (0.146 mmol, 0.150 g), 2,2'-azobis(2-methylpropionitrile) (AIBN) (0.029 mmol, 0.004 g) and *N,N*-dimethylacrylamide (DMA) (4.377 mmol, 0.433 g or 2.188 mmol, 0.216 g; for targeted degree of polymerization (DP) of 30 and 15, respectively) were dissolved in a Schlenk tube in anhydrous *N,N*-dimethylformamide (DMF) to obtain a monomer concentration of 2 M and a CTA:initiator molar ratio of 5:1. The solutions were subjected to 5 freeze-pump-thaw cycles before polymerization was initiated at 70 °C for 3.5 hours under vacuum. Monomer conversion was determined by ¹H-NMR spectroscopy. Polymers were collected by triple precipitation from cold (4 °C) diethyl ether and the obtained light yellow solids were subsequently dried under high vacuum (DTX-pDMA₁₅ (0.068 mmol, 0.158 g, 47 %) and DTX-pDMA₃₀ (0.141 mmol, 0.553 g, 96 %)).

4.5 synthesis DTX-pDMA^{Rho}

DTX-PABTC (0.097 mmol, 0.100 g), AIBN (0.019 mmol, 0.003 g) and monomers (i.e. DMA (2.912 mmol, 0.288 g) and acryloxyethyl thiocarbamoyl rhodamine B (ARho) (0.005 mmol; 0.003 g); for targeted DP of 30) were dissolved in a Schlenk tube in anhydrous DMF to obtain a monomer concentration of 2 M and a CTA:initiator molar ratio of 5:1. The solution was subjected to 5 freeze-pump-thaw cycles before polymerization was initiated at 70 °C for 3.5 hours under vacuum. Monomer conversion was determined by ¹H-NMR spectroscopy. Polymer was collected by triple precipitation from cold (4 °C) diethyl ether and the obtained purple solid was subsequently dried under high vacuum (0.087 mmol, 0.343 g, 90 %).

4.6 synthesis PSMA targeting ligand

The trithiocarbonate endgroup of the polymers can be converted into a thiol. Hence, we aimed at designing a maleimide-derivative of the PSMA targeting ligand *S,S*-2-(3-(5-amino-1-carboxypentyl)-ureido)-pentanedioic acid (ACUPA) to allow post-polymerization functionalization (**Scheme S1**). The synthesis will be fully described in the following paragraphs.

4.6.1 synthesis maleimidobutyryl-PFP

In a 250 mL round-bottom unineck flask, 4-maleimidobutyric acid (5.459 mmol, 1.000 g), and pentafluorophenol (PFP) (6.005 mmol, 1.105 g) were dissolved in 60 mL anhydrous CH₂Cl₂ and put on ice. Next, DIC

(6.005 mmol, 0.757 g) was added dropwise and the mixture was stirred for 1.5 hours at room temperature and monitored by TLC. Subsequently, the reaction mixture was filtered and concentrated *in vacuo*. The crude product was purified by silica gel chromatography (eluent CH₂Cl₂). After concentration and subsequent drying under high vacuum, the obtained white solid (4.994 mmol, 1.743 g, 91 %) was analyzed by NMR spectroscopy.

4.6.2 synthesis tert-butyl ester ACUPA

Tert-butyl ester ACUPA as synthesized as previously described.^[43] L-Glutamic acid di-tert-butyl ester hydrochloride (H-Glu(O^tBu)-O^tBu HCl) (16.903 mmol, 5.000 g) and triethylamine (TEA) (55.442 mmol, 5.610 g) were dissolved in 150 mL anhydrous CH₂Cl₂ and the resulting solution was cooled to -78 °C. Triphosgene (5.747 mmol, 1.705 g) in 20 mL anhydrous CH₂Cl₂ was added dropwise via syringe to the reaction mixture. Upon complete addition, the reaction was allowed to warm to room temperature and stir for 30 minutes. N-ε-Cbz-L-Lysine tert-butyl ester hydrochloride (H-Lys(Z)-O^tBu HCl) (10.141 mmol, 3.781 g) was added, followed by TEA (10.141 mmol, 1.026 g). The reaction was allowed to stir at room temperature overnight. The reaction mixture was then washed with H₂O (2 x 150 mL), dried over Na₂SO₄ and concentrated *in vacuo*. The crude product was purified by silica gel chromatography (eluent 1.5:1 hexane:ethyl acetate v/v). After concentration and subsequent drying under high vacuum, the obtained colorless oil (9.236 mmol, 5.736 g, 91 %) was analyzed by NMR spectroscopy.

Next, in a 500 mL round-bottom unineck flask, the obtained product (9.236 mmol, 5.736 g) was dissolved in 100 mL dioxane and flushed with N₂. To the latter, dry 10% Pd/C (573 mg, 10 % by mass) was quickly added and the flask was again flushed with N₂. Reaction mixture was gently bubbled with H₂ for several hours, allowed to stir overnight under H₂-atmosphere and monitored by TLC until deemed complete. The mixture was first flushed with N₂, then filtered over a plug of celite and concentrated *in vacuo*. Subsequent drying under high vacuum yielded a viscous colorless oil (9.184 mmol, 4.473 g, 99 %). The latter was analyzed by NMR spectroscopy and the obtained tert-butyl ester ACUPA used in the next step without further purification.

4.6.3 synthesis maleimidobutyryl-ACUPA

In a 50 mL round-bottom unineck flask, maleimidobutyryl-PFP (2.578 mmol, 0.900 g), was dissolved in 12 mL anhydrous CH₂Cl₂. Next, tert-butyl ester ACUPA (Cbz-protected, 1.719 mmol, 0.837 g) and TEA (5.157 mmol, 0.521 g), dissolved in 8 mL anhydrous CH₂Cl₂, was added dropwise and the mixture was stirred for 2 hours at room temperature and monitored by TLC. Subsequently, the reaction mixture concentrated *in vacuo* and the crude was

purified by silica gel chromatography (eluent ethyl acetate). Concentration and subsequent drying under high vacuum yielded a white solid (1.467 mmol, 0.957 g, 85 %) and the tert-butyl ester maleimidobutyryl-ACUPA was analyzed by NMR spectroscopy and used as such in the final step (*vide infra*).

Finally, tert-butyl ester maleimidobutyryl-ACUPA (1.467 mmol, 0.957 g) was dissolved in 10 mL anhydrous CH_2Cl_2 . A total of 10 mL trifluoroacetic acid (TFA) was added dropwise and reaction was stirred for 2 hours at room temperature. Next, 10 mL toluene was added and the mixture was concentrated *in vacuo*. After subsequent drying under high vacuum, the obtained viscous colorless oil (1.453 mmol, 0.703 g, 99 %) was analyzed by NMR spectroscopy and ESI-MS.

4.7 post-polymerization functionalization

Post-polymerization modification was conducted using a reported protocol on sequential one-pot aminolysis/thiol-maleimide endgroup modification.^[44] DTX-pDMA₃₀ or DTX-pDMA^{Rho}₃₀ (0.020 mmol, 0.080 g) and trimethyl phosphite (TMP) (0.100 mmol, 0.012 g) were dissolved in a Schlenk tube in 0.645 mL acetonitrile. The solution was subjected to 3 freeze-pump-thaw cycles before propylamine (0.060 mmol, 0.003 g), dissolved in 0.2 mL acetonitrile (flushed with N_2) was added dropwise and allowed to react for 6 hours at room temperature. Next, maleimide ligand (maleimidobutyryl-ACUPA; 0.100 mmol, 0.048 g or 6-maleimidohexanoic acid (MHA) (0.100 mmol, 0.021 g); for obtaining DTX-pDMA conjugates post-functionalized with PSMA targeted ACUPA- and control HA-ligand, respectively) was dissolved in a Schlenk tube in 0.454 mL dimethyl sulfoxide (DMSO). The solution was subjected to 3 freeze-pump-thaw cycles before being added to the reaction mixture. After overnight reaction at room temperature, excess of TMP and propylamine were discarded by triple precipitation from cold (4 °C) diethyl ether. To remove excess of maleimide ligand, the obtained white (DTX-pDMA₃₀-ACUPA and DTX-pDMA₃₀-HA) and purple (DTX-pDMA^{Rho}₃₀-ACUPA and DTX-pDMA^{Rho}₃₀-HA) solids were dialyzed against 1:1 acetonitrile:H₂O v/v for 48 hours days, followed by dialysis against H₂O for 24 hours. The purified solutions were subsequently freeze-dried and yielded white (DTX-pDMA₃₀-ACUPA (0.013 mmol, 0.059 g, 69 %); DTX-pDMA₃₀-HA (0.015 mmol, 0.062 g, 77 %)) and purple (DTX-pDMA^{Rho}₃₀-ACUPA (0.014 mmol, 0.060 g, 70 %); DTX-pDMA^{Rho}₃₀-HA (0.015 mmol, 0.059 g, 77 %)) powders which were analyzed by SEC and NMR spectroscopy. For allowing adequate evaluation of *in vitro* uptake, UV-VIS spectroscopy was used to ascertain equal rhodamine labeling of DTX-pDMA^{Rho}₃₀-ACUPA and DTX-pDMA^{Rho}₃₀-HA.

4.8 *in vitro* cellular uptake

4.8.1 cell culture

LNCaP human cancer cells were cultured in RPMI 1640 GlutaMAX, supplemented with 10 % FBS, 2 mM L-glutamine, 1 mM sodium pyruvate and antibiotics (50 units/mL penicillin and 50 µg/mL streptomycin). Cells were incubated at 37 °C in a controlled, sterile environment of 95 % relative humidity and 5 % CO₂.

4.8.2 FACS

LNCaP cells were seeded into 24-well titer plates (150 000 cells per well, suspended in 1 mL of culture medium) and allowed to attach overnight. Next 1.3, 6.7 or 34.5 µL of 30 mg/mL DTX-pDMA^{Rho}₃₀-ACUPA or DTX-pDMA^{Rho}₃₀-HA in PBS was added to the cells, followed by 2 hours of incubation at 37 °C. After incubation, wells were aspirated, washed with 0.5 mL PBS and detached by 0.4 mL enzyme-free cell dissociation buffer. Cell suspensions were centrifuged (350 g, 7 min, 4 °C). Finally, supernatant was aspirated and the cell pellets were suspended into 200 µL of PBS and kept on ice to maintain cell integrity. Live/dead staining was performed by adding 0.5 µL of DAPI solution to each cell suspension before measurement. The experiment was conducted in triplicate. FACS was performed on a BD LSR Fortessa (BD Biosciences). Data were processed by FlowJo software.

5 references

- [1] D. G. I. Kingston, D. J. Newman, *Curr. Opin. Drug Discov. Devel.* **2007**, *10*, 130–144.
- [2] J. Crown, M. O'Leary, *Lancet* **2000**, *355*, 1176–1178.
- [3] L. B. Norris, Z. P. Qureshi, P. B. Bookstaver, D. W. Raisch, O. Sartor, H. Chen, F. Chen, C. L. Bennett, *Community Oncol.* **2010**, *7*, 425–428.
- [4] A. J. ten Tije, J. Verweij, W. J. Loos, A. Sparreboom, *Clin. Pharmacokinet.* **2003**, *42*, 665–685.
- [5] Z. Weiszhar, J. Czucz, C. Revesz, L. Rosivall, J. Szebeni, Z. Rozsnyay, *Eur. J. Pharm. Sci.* **2012**, *45*, 492–498.
- [6] H. Gelderblom, J. Verweij, K. Nooter, A. Sparreboom, *Eur. J. Cancer* **2001**, *37*, 1590–1598.
- [7] K. S. Lee, H. C. Chung, S. A. Im, Y. H. Park, C. S. Kim, S.-B. Kim, S. Y. Rha, M. Y. Lee, J. Ro, *Breast Cancer Res. Treat.* **2008**, *108*, 241–250.
- [8] T.-Y. Kim, *Clin. Cancer Res.* **2004**, *10*, 3708–3716.
- [9] N. V. Rajeshkumar, S. Yabuuchi, S. G. Pai, Z. Tong, S. Hou, S. Bateman, D. W. Pierce, C. Heise, D. D. Von Hoff, A. Maitra, et al., *Br. J. Cancer* **2016**, *115*, 442–453.
- [10] H. Shao, H. Tang, O. E. Salavaggione, C. Yu, B. Hylander, W. Tan, E. Repasky, A. A. Adjei, G. K. Dy, *J. Thorac. Oncol.* **2011**, *6*, 998–1005.
- [11] E. Miele, G. P. Spinelli, F. Tomao, S. Tomao, *Int. J. Nanomedicine* **2009**, *4*, 99–105.
- [12] N. K. Ibrahim, N. Desai, S. Legha, P. Soon-Shiong, R. L. Theriault, E. Rivera, B. Esmaeli, S. E. Ring, A. Bedikian, G. N. Hortobagyi, et al., *Clin. Cancer Res.* **2002**, *8*, 1038–1044.
- [13] A. Lluch, I. Alvarez, M. Munoz, M. A. Segui, I. Tusquets, L. Garcia-Estevez, *Crit. Rev. Oncol. Hematol.* **2014**, *89*, 62–72.
- [14] H. Maeda, J. Wu, T. Sawa, Y. Matsumura, K. Hori, *J. Control. Release* **2000**, *65*, 271–284.
- [15] V. Torchilin, *Adv. Drug Deliv. Rev.* **2011**, *63*, 131–135.
- [16] R. K. Jain, T. Stylianopoulos, *Nat. Rev. Clin. Oncol.* **2010**, *7*, 653–664.
- [17] J. I. Hare, T. Lammers, M. B. Ashford, S. Puri, G. Storm, S. T. Barry, *Adv. Drug Deliv. Rev.* **2016**, DOI 10.1016/j.addr.2016.04.025.
- [18] A. Schroeder, D. A. Heller, M. M. Winslow, J. E. Dahlman, G. W. Pratt, R. Langer, T. Jacks, D. G. Anderson, *Nat. Rev. Cancer* **2012**, *12*, 39–50.
- [19] A. Wicki, D. Witzigmann, V. Balasubramanian, J. Huwyler, *J. Control. Release* **2015**, *200*, 138–157.
- [20] I. Canton, G. Battaglia, *Chem. Soc. Rev.* **2012**, *41*, 2718–2739.
- [21] M. M. Gottesman, T. Fojo, S. E. Bates, *Nat. Rev. Cancer* **2002**, *2*, 48–58.
- [22] S. Panowski, S. Bhakta, H. Raab, P. Polakis, J. R. Junutula, in *MAbs*, Taylor & Francis, **2014**, pp. 34–45.
- [23] R. V. Chari, M. L. Miller, W. C. Widdison, *Angew. Chem. Int. Ed. Engl.* **2014**, *53*, 3796–3827.
- [24] P. Polakis, *Pharmacol. Rev.* **2016**, *68*, 3–19.
- [25] N. Krall, J. Scheuermann, D. Neri, *Angew. Chem. Int. Ed. Engl.* **2013**, *52*, 1384–1402.
- [26] G. Casi, D. Neri, *J. Med. Chem.* **2015**, *58*, 8751–8761.
- [27] C. Peters, S. Brown, *Biosci. Rep.* **2015**, *35*, 1–20.
- [28] M. Srinivasarao, C. V. Galliford, P. S. Low, *Nat. Rev. Drug Discov.* **2015**, *14*, 203–219.
- [29] C. P. Leamon, J. A. Reddy, P. J. Klein, I. R. Vlahov, R. Dorton, A. Bloomfield, M. Nelson, E. Westrick, N. Parker, K. Bruna, *J. Pharmacol. Exp. Ther.* **2011**, *336*, 336–343.
- [30] R. Kurzrock, N. Gabrail, C. Chandhasin, S. Moulder, C. Smith, A. Brenner, K. Sankhala, A. Mita, K. Elian, D. Bouchard, et al., *Mol. Cancer Ther.* **2012**, *11*, 308–316.
- [31] E. Kähkönen, I. Jambor, J. Kemppainen, K. Lehtiö, T. J. Grönroos, A. Kuisma, P. Luoto, H. J. Sipilä, T. Tolvanen, K. Alanen, *Clin. Cancer Res.* **2013**, *19*, 5434–5443.
- [32] A. J. Beer, M. Schwaiger, *J. Nucl. Med.* **2011**, *52*, 335–337.
- [33] S. A. Kularatne, K. Wang, H.-K. R. Santhapuram, P. S. Low, *Mol. Pharm.* **2009**, *6*, 780–789.
- [34] J. Roy, T. X. Nguyen, A. K. Kanduluru, C. Venkatesh, W. Lv, P. V. N. Reddy, P. S. Low, M. Cushman, *J. Med. Chem.* **2015**, *58*, 3094–3103.

- [35] B. Louage, L. Nuhn, M. D. Risseeuw, N. Vanparijs, R. De Coen, I. Karalic, S. Van Calenbergh, B. G. De Geest, *Angew. Chem. Int. Ed. Engl.* **2016**, *55*, 11791–11796.
- [36] P. A. Watson, V. K. Arora, C. L. Sawyers, *Nat. Rev. Cancer* **2015**, *15*, 701–711.
- [37] M. C. Haffner, J. Laimer, A. Chau, G. Schäfer, P. Obrist, A. Brunner, I. E. Kronberger, K. Laimer, B. Gurel, J.-B. Koller, *Mod. Pathol.* **2012**, *25*, 1079–1085.
- [38] D. Shen, F. Xie, W. B. Edwards, *PLoS One* **2013**, *8*, e68339.
- [39] V. Bagalkot, O. C. Farokhzad, R. Langer, S. Jon, *Angew. Chem. Int. Ed. Engl.* **2006**, *45*, 8149–8152.
- [40] S. M. Hillier, K. P. Maresca, F. J. Femia, J. C. Marquis, C. A. Foss, N. Nguyen, C. N. Zimmerman, J. A. Barrett, W. C. Eckelman, M. G. Pomper, *Cancer Res.* **2009**, *69*, 6932–6940.
- [41] J. Hrkach, D. Von Hoff, M. M. Ali, E. Andrianova, J. Auer, T. Campbell, D. De Witt, M. Figa, M. Figueiredo, A. Horhota, et al., *Sci. Transl. Med.* **2012**, *4*, 128–139.
- [42] C. J. Ferguson, R. J. Hughes, D. Nguyen, B. T. T. Pham, R. G. Gilbert, A. K. Serelis, C. H. Such, B. S. Hawkett, *Macromolecules* **2005**, *38*, 2191–2204.
- [43] R. P. Murelli, A. X. Zhang, J. Michel, W. L. Jorgensen, D. A. Spiegel, *J. Am. Chem. Soc.* **2009**, *131*, 17090–17092.
- [44] B. A. Abel, C. L. McCormick, *Macromolecules* **2016**, *49*, 6193–6202.

6 supporting info

6.1 docetaxel

DTX was purchased from LC Laboratories and its purity was confirmed by $^1\text{H-NMR}$ spectroscopy and compared to paclitaxel.

$^1\text{H-NMR}$ (400 MHz, CDCl_3): δ [ppm] = 8.10 (A, d, J = 7.3 Hz, 2H), 7.61 (B, tt, J = 6.9, 1.3 Hz, 1H), 7.49 (C, t, J = 7.6 Hz, 2H), 7.42 – 7.34 (D, m, 4H), 7.34 – 7.28 (E, m, 1H), 6.21 (F, t, J = 8.9 Hz, 1H), 5.67 (G, d, J = 7.1 Hz, 1H), 5.47 (H, d, J = 9.4 Hz, 1H), 5.29 – 5.22 (I, m, 1H), 5.21 (J, s, 1H), 4.94 (K, dd, J = 9.6, 2.2 Hz, 1H), 4.61 (L, s, 1H), 4.30 (M, d, J = 8.5 Hz, 1H), 4.23 (O, dd, J = 11.1, 6.6 Hz, 1H), 4.18 (N, dd, J = 8.4, 1.0 Hz, 1H), 3.90 (P, d, J = 6.9 Hz, 1H), 2.57 (Q, ddd, J = 14.4, 9.7, 6.6 Hz, 1H), 2.37 (R, s, 3H), 2.26 (S, d, J = 9.0 Hz, 2H), 1.90 – 1.79 (X, m, 4H), 1.74 (W, s, 3H), 1.34 (V, s, 9H), 1.23 (U, s, 3H), 1.12 (T, s, 3H).

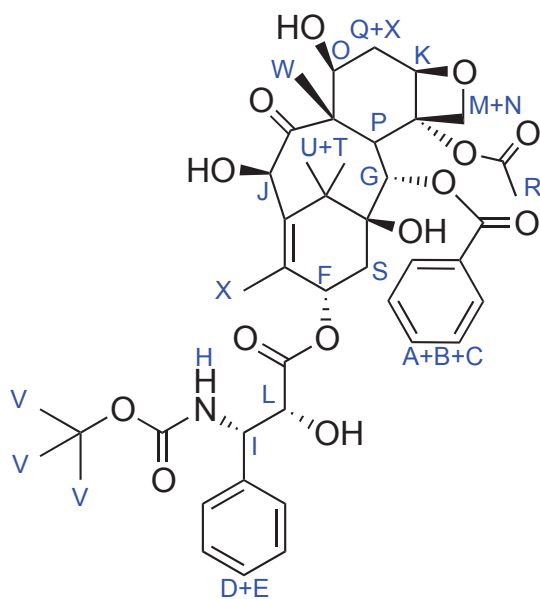


Figure S1. Structure (annotated) of docetaxel (DTX).

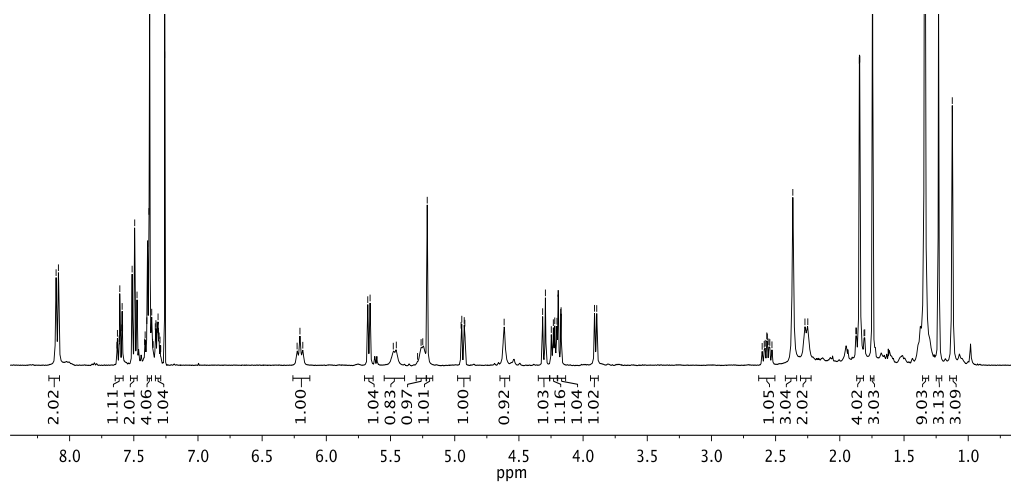


Figure S2. ¹H-NMR (400 MHz, CDCl₃) spectrum of DTX.

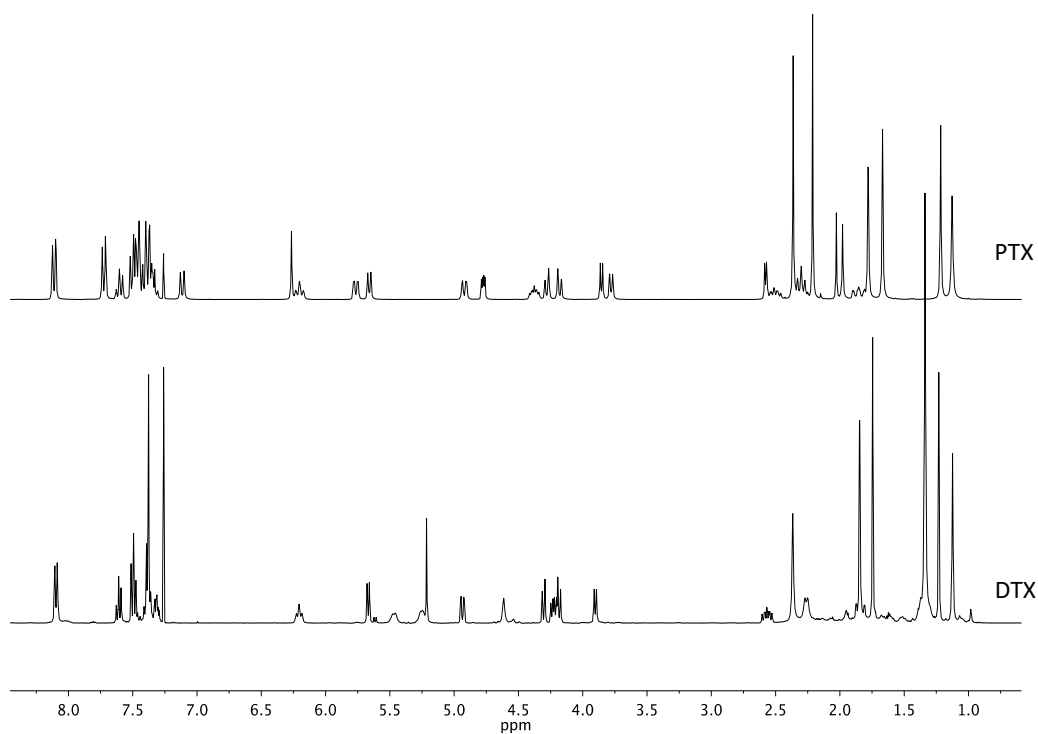


Figure S3. Overlay ¹H-NMR spectra of PTX and DTX.

6.2 DTX-PABTC

$^1\text{H-NMR}$ (400 MHz, CDCl_3): δ [ppm] = 8.12 (A, dt, J = 8.2, 1.1 Hz, 2H), 7.65 – 7.56 (B, m, 1H), 7.50 (C, td, J = 7.5, 1.2 Hz, 2H), 7.44 – 7.24 (D, m, 5H), 6.27 (E, t, J = 9.0 Hz, 1H), 5.68 (F, d, J = 7.1 Hz, 1H), 5.56 – 5.43 (G, m, 1H), 5.40 – 5.26 (H, m, 2H), 5.21 (I, s, 1H), 5.03 – 4.92 (J, m, 1H), 4.83 (K, dq, J = 11.8, 7.4 Hz, 1H), 4.32 (L, d, J = 8.5 Hz, 1H), 4.26 (N, ddd, J = 11.1, 6.5, 2.3 Hz, 1H), 4.19 (M, d, J = 8.5 Hz, 1H), 3.93 (O, d, J = 7.0 Hz, 1H), 3.41 – 3.25 (P, m, 2H), 2.65 – 2.52 (Q, m, 1H), 2.43 (R, s, 3H), 2.38 – 2.25 (S, m, 1H), 2.22 – 2.08 (T, m, 1H), 1.93 (U, s, 3H), 1.84 (V, ddd, J = 14.1, 11.2, 2.2 Hz, 1H), 1.75 (W, s, 3H), 1.71 – 1.63 (X, m, 2H), 1.61 (Y, s, 3H), 1.51 – 1.36 (Z, m, 2H), 1.34 (A1, s, 9H), 1.23 (B1, s, 3H), 1.12 (C1, s, 3H), 0.94 (D1, t, J = 7.3 Hz, 3H).

$^{13}\text{C-APT-NMR}$ (101 MHz, CDCl_3): δ [ppm] = $[>220.0$ (S-S)], 211.72 (A), 170.59 (F, d, J = 43.7 Hz), 169.83 (E), 167.58 (D, d, J = 35.2 Hz), 167.22 (C), 155.24 (B), 139.22 (G), 137.27 (H), 135.66 (N), 133.78 (I), 130.34 (J), 129.34 (K), 129.01 (L), 128.85 (M), 128.31 (M), 126.57 (O), 84.31 (Q), 81.09 (R), 80.57 (S), 79.07 (T), 76.70 (U), 75.37 (W, d, J = 7.3 Hz), 75.14 (X), 74.63 (V), 72.16 (Y), 72.04 (Z, d, J = 6.3 Hz), 57.68 (A1), 54.12 (B1), 47.19 (C1, d, J = 29.9 Hz), 46.54 (D1), 43.24 (E1), 37.24 (P1, d, J = 3.4 Hz), 37.06 (Q1), 35.69 (R1), 29.99 (F1, d, J = 3.0 Hz), 28.30 (G1), 26.47 (H1), 22.80 (J1), 22.22 (I1, d, J = 2.3 Hz), 21.06 (K1), 16.26 (L1, d, J = 28.4 Hz), 14.36 (M1), 13.73 (N1), 10.09 (O1).

ESI-MS (acetonitrile): m/z = calcd for $\text{C}_{51}\text{H}_{65}\text{NO}_{15}\text{S}_3$ 1027.35, found 1028.36 [M+H] $^+$

6.3 DTX-pDMA

SEC(DMAc, PMMA-St.): M_n = 2668, PDI = 1.08 (DTX-pDMA₁₅) and M_n = 4491, PDI = 1.09 (DTX-pDMA₃₀).

DTX-pDMA₁₅:

$^1\text{H-NMR}$ (300 MHz, MeOH-d_4): δ [ppm] = 8.11 (t, J = 6.4 Hz, 2H), 7.68 – 7.55 (m, 3H), 7.50 – 7.14 (m, 5H), 6.09 (br, 1H), 5.63 (br, 1H), 5.45 – 5.10 (m, 3H), 5.21 (br, 1H), 5.05 – 4.92 (m, 1H), 4.31 – 4.10 (m, 3H), 3.87 (br, 1H), 3.46 – 3.37 (m, 2H), 3.26 – 1.02 (m, 35H DTX-PABTC + 9H x 17(ΔP) = 188H), 0.95 (td, J = 7.4, 1.7 Hz, 3H).

DTX-pDMA₃₀:

$^1\text{H-NMR}$ (300 MHz, MeOH-d_4): δ [ppm] = 8.11 (t, J = 6.4 Hz, 2H), 7.68 – 7.55 (m, 3H), 7.50 – 7.14 (m, 5H), 6.09 (br, 1H), 5.63 (br, 1H), 5.45 – 5.10 (m, 3H), 5.21 (br, 1H), 5.05 – 4.92 (m, 1H), 4.31 – 4.10 (m, 3H), 3.87 (br, 1H), 3.46 – 3.37 (m, 2H), 3.26 – 1.02 (m, 35H DTX-PABTC + 9H x 32(ΔP) = 323H), 0.95 (td, J = 7.4, 1.7 Hz, 3H).

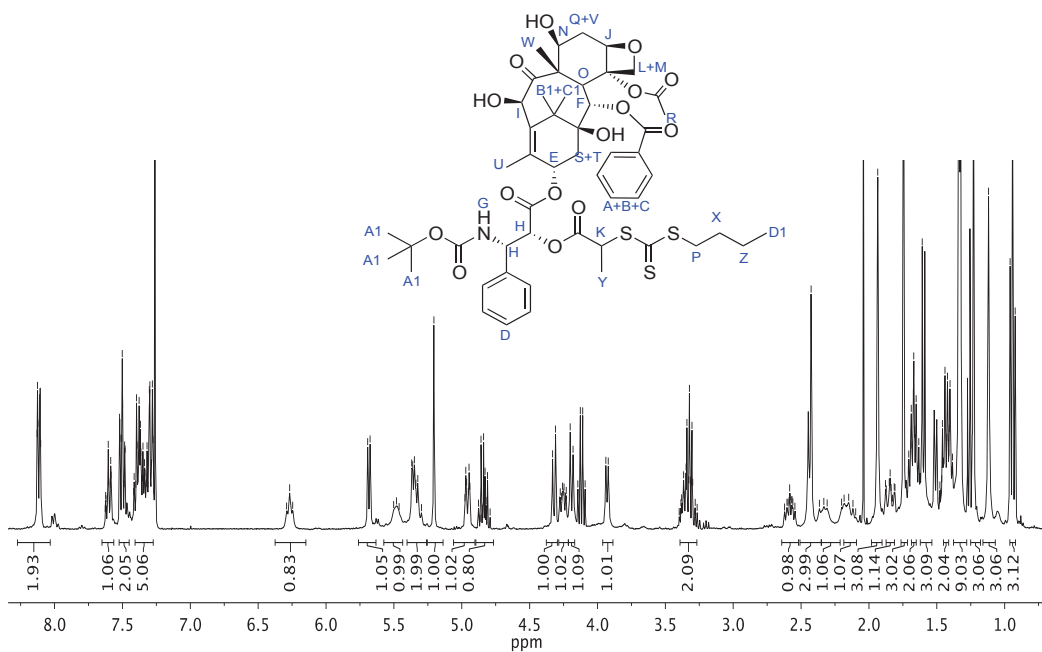


Figure S4. ¹H-NMR (400 MHz, CDCl₃) spectrum of DTX-PABTC (annotated).

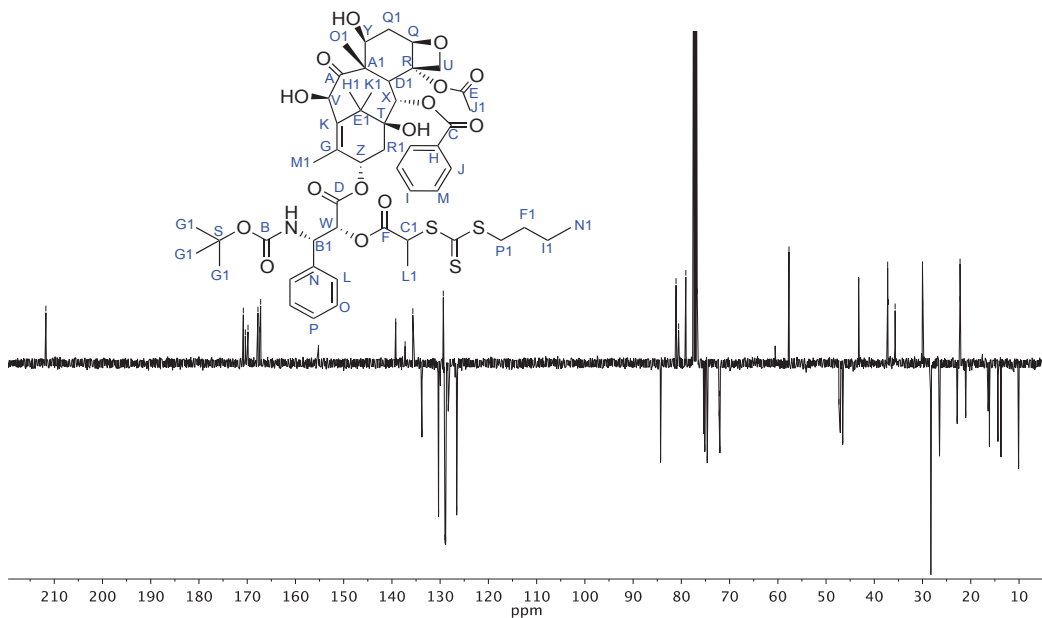


Figure S5. ¹³C-APT-NMR (101 MHz, CDCl₃) spectrum of DTX-PABTC (annotated).

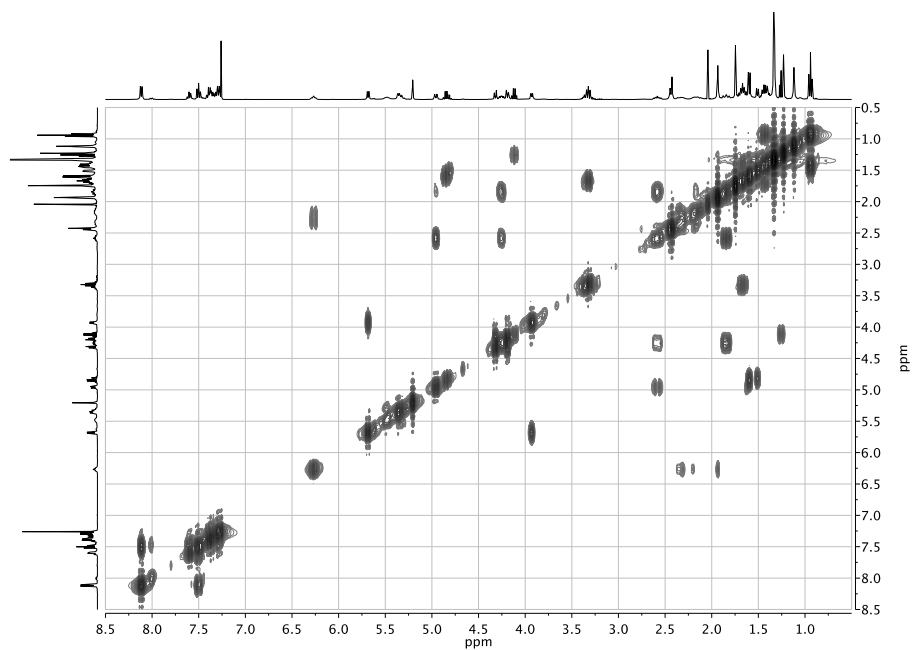


Figure S6. $^1\text{H},^1\text{H}$ -COSY spectrum of DTX-PABTC.

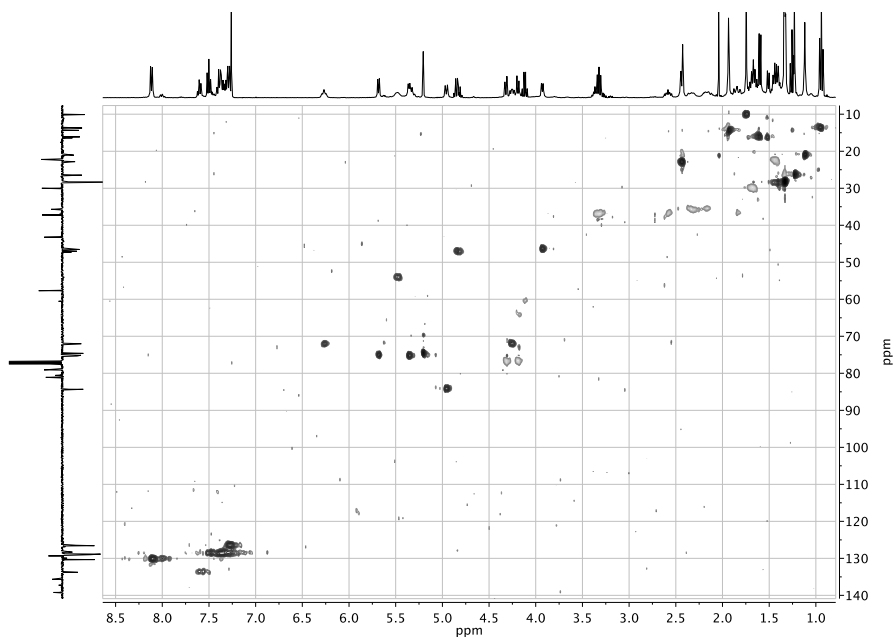


Figure S7. $^1\text{H},^{13}\text{C}$ -HSQC spectrum of DTX-PABTC.

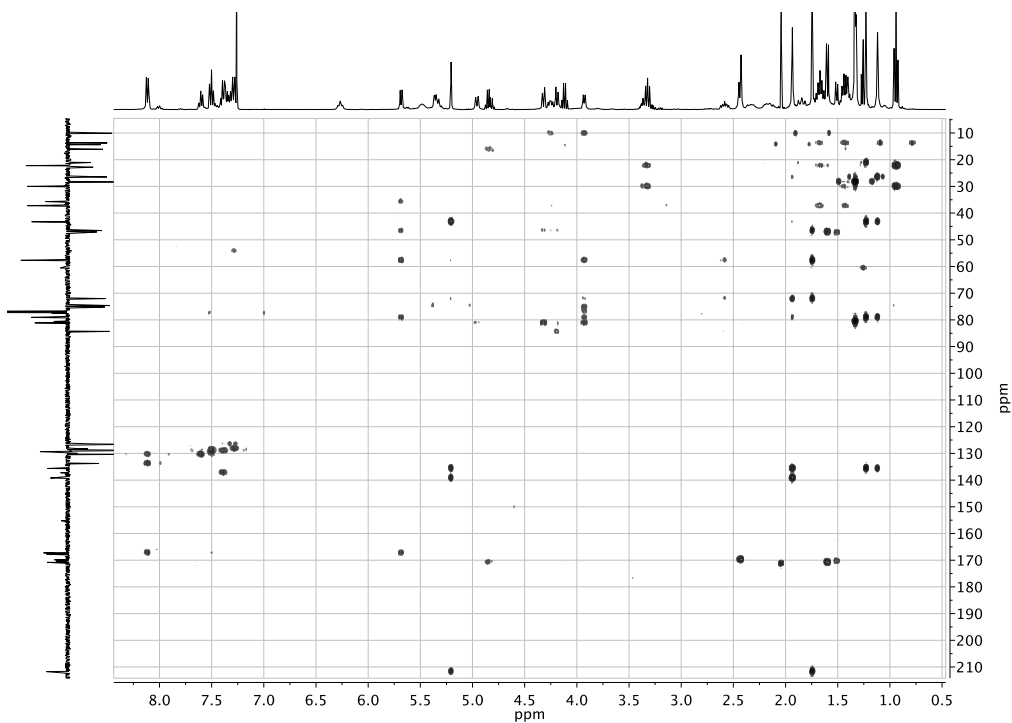


Figure S8. $^1\text{H},^{13}\text{C}$ -HMBC spectrum of DTX-PABTC.

6.4 DTX-pDMA^{Rho}

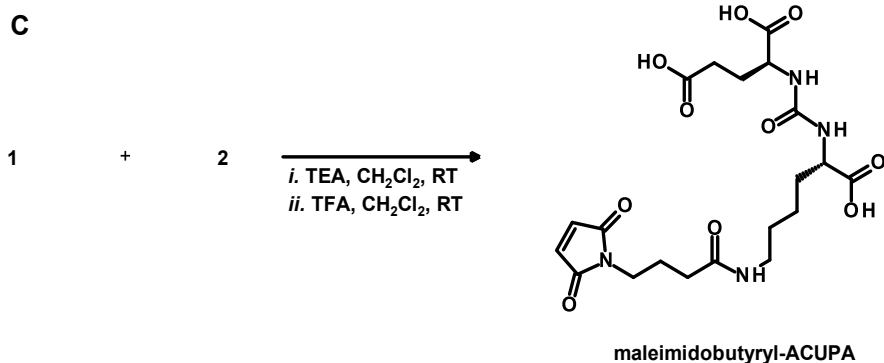
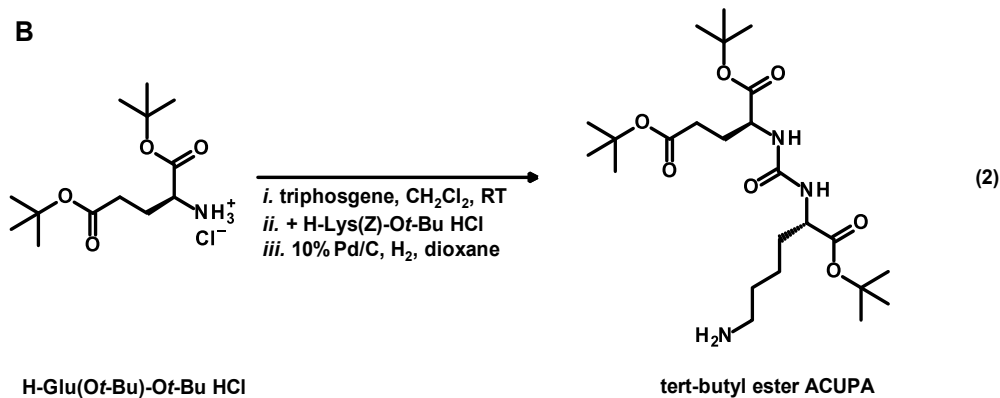
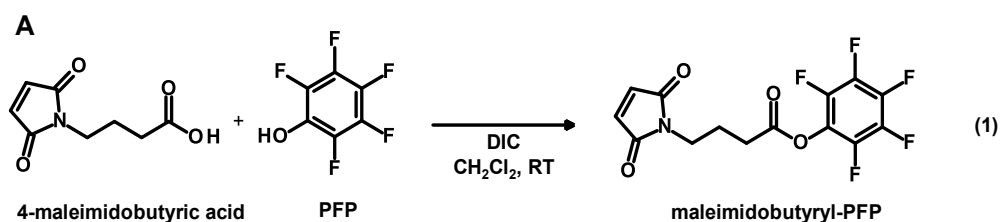
SEC(DMAc, PMMA-St.): $M_n = 4365$, PDI = 1.09 (DTX-pDMA^{Rho}₃₀).

^1H -NMR (300 MHz, MeOH- d_4): δ [ppm] = 8.11 (t, $J = 6.4\text{Hz}$, 2H), 7.68 – 7.55 (m, 3H), 7.50 – 7.14 (m, 5H), 6.09 (br, 1H), 5.63 (br, 1H), 5.45 – 5.10 (m, 3H), 5.21 (br, 1H), 5.05 – 4.92 (m, 1H), 4.31 – 4.10 (m, 3H), 3.87 (br, 1H), 3.46 – 3.37 (m, 2H), 3.26 – 1.02 (m, 35H DTX-PABTC + 9H x 31(\mathcal{D}) = 314H), 0.95 (td, $J = 7.4, 1.7\text{ Hz}$, 3H).

6.5 maleimidobutyryl-PFP

$^1\text{H-NMR}$ (300 MHz, CDCl_3): δ [ppm] = 6.73 (s, 2H), 3.66 (t, J = 6.7 Hz, 2H), 2.71 (t, J = 7.4 Hz, 2H), 2.07 (p, J = 7.0 Hz, 2H).

$^{19}\text{F-NMR}$ (282 MHz, CDCl_3): δ [ppm] = -152.66 (d, J = 17.0 Hz, 2F), -157.95 (t, J = 21.6 Hz, 1F), -161.91 – -162.66 (m, 2F).



Scheme S1. Reaction scheme illustrating synthesis of maleimidobutyryl-PFP (A), the tert-butyl ester PSMA targeting ligand ACUPA (B) and subsequent coupling of the latter two, followed by tert-butyl ester-deprotection (C).

6.6 tert-butyl ester ACUPA

Before Cbz-deprotection:

$^1\text{H-NMR}$ (300 MHz, CDCl_3): δ [ppm] = 7.44 – 7.26 (m, 5H), 5.44 – 5.14 (m, 3H), 5.13 – 4.99 (m, 2H), 4.41 – 4.25 (m, 2H), 3.28 – 3.05 (m, 2H), 2.41 – 2.17 (m, 2H), 2.13 – 1.97 (m, 1H), 1.89 – 1.66 (m, 2H), 1.67 – 1.55 (m, 1H), 1.55 – 1.47 (m, 2H), 1.44 (s, 18H), 1.42 (s, 9H), 1.38 – 1.29 (m, 2H).

$^{13}\text{C-APT-NMR}$ (75 MHz, CDCl_3): δ [ppm] = 172.57, 172.50, 172.49, 157.05, 156.73, 136.82, 128.57, 128.16, 128.10, 82.24, 81.83, 80.63, 66.66, 53.41, 53.09, 40.81, 32.77, 31.72, 29.49, 28.22, 28.14, 28.01, 22.42.

After Cbz-deprotection:

$^1\text{H-NMR}$ (300 MHz, CDCl_3): δ [ppm] = 5.18 (dd, J = 8.0, 2.2 Hz, 2H), 4.32 (td, J = 8.1, 5.0 Hz, 2H), 2.68 (t, J = 6.7 Hz, 2H), 2.42 – 2.19 (m, 2H), 2.06 (dddd, J = 13.9, 9.0, 6.7, 4.9 Hz, 1H), 1.92 – 1.68 (m, 4H), 1.68 – 1.53 (m, 1H), 1.45 (s, 18H), 1.42 (s, 9H), 1.38 – 1.26 (m, 2H).

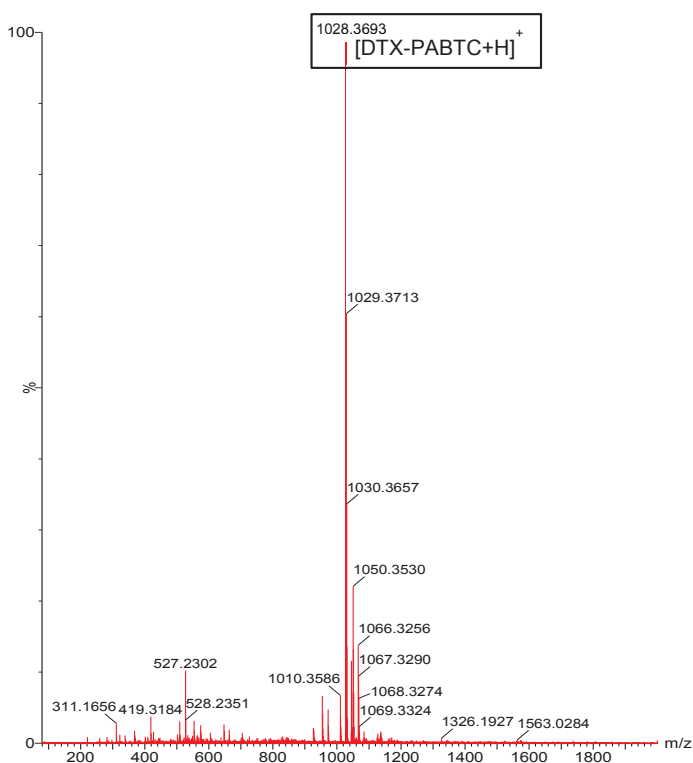


Figure S9. ESI-MS (acetonitrile) spectrum of DTX-PABTC.

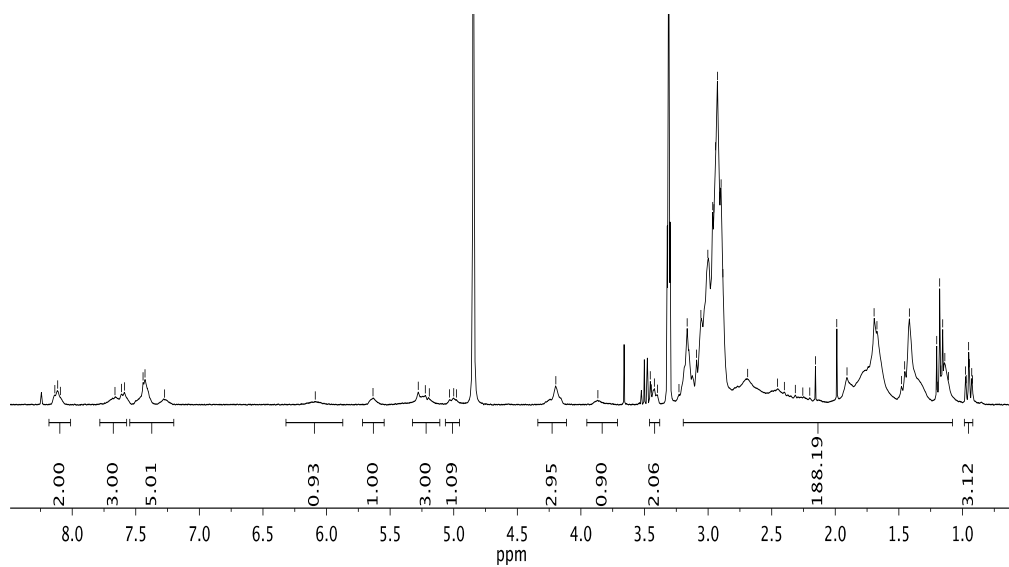


Figure S10. ¹H-NMR (300 MHz, MeOH-d₄) spectrum of DTX-pDMA₁₅.

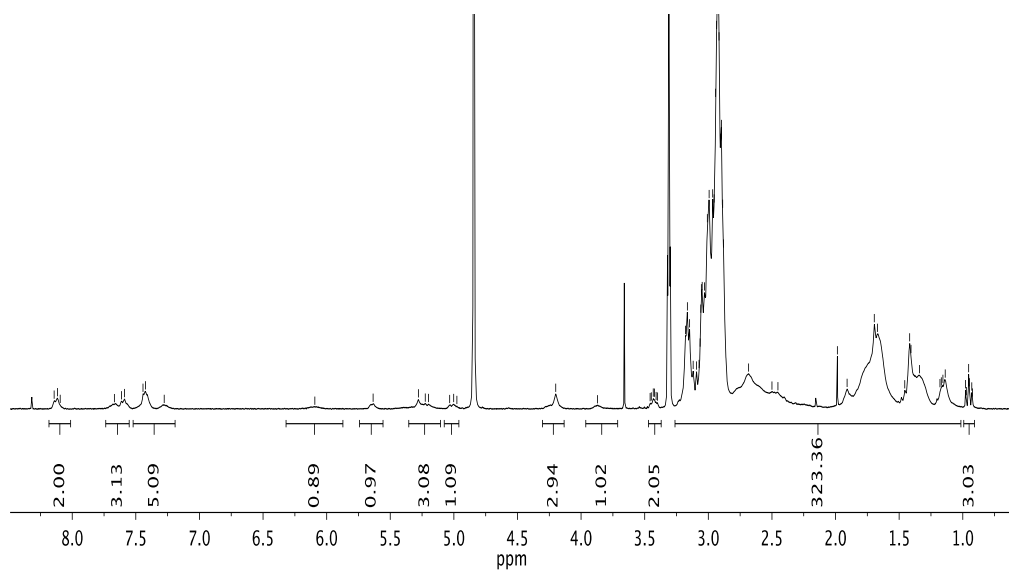


Figure S11. ¹H-NMR (300 MHz, MeOH-d₄) spectrum of DTX-pDMA₃₀.

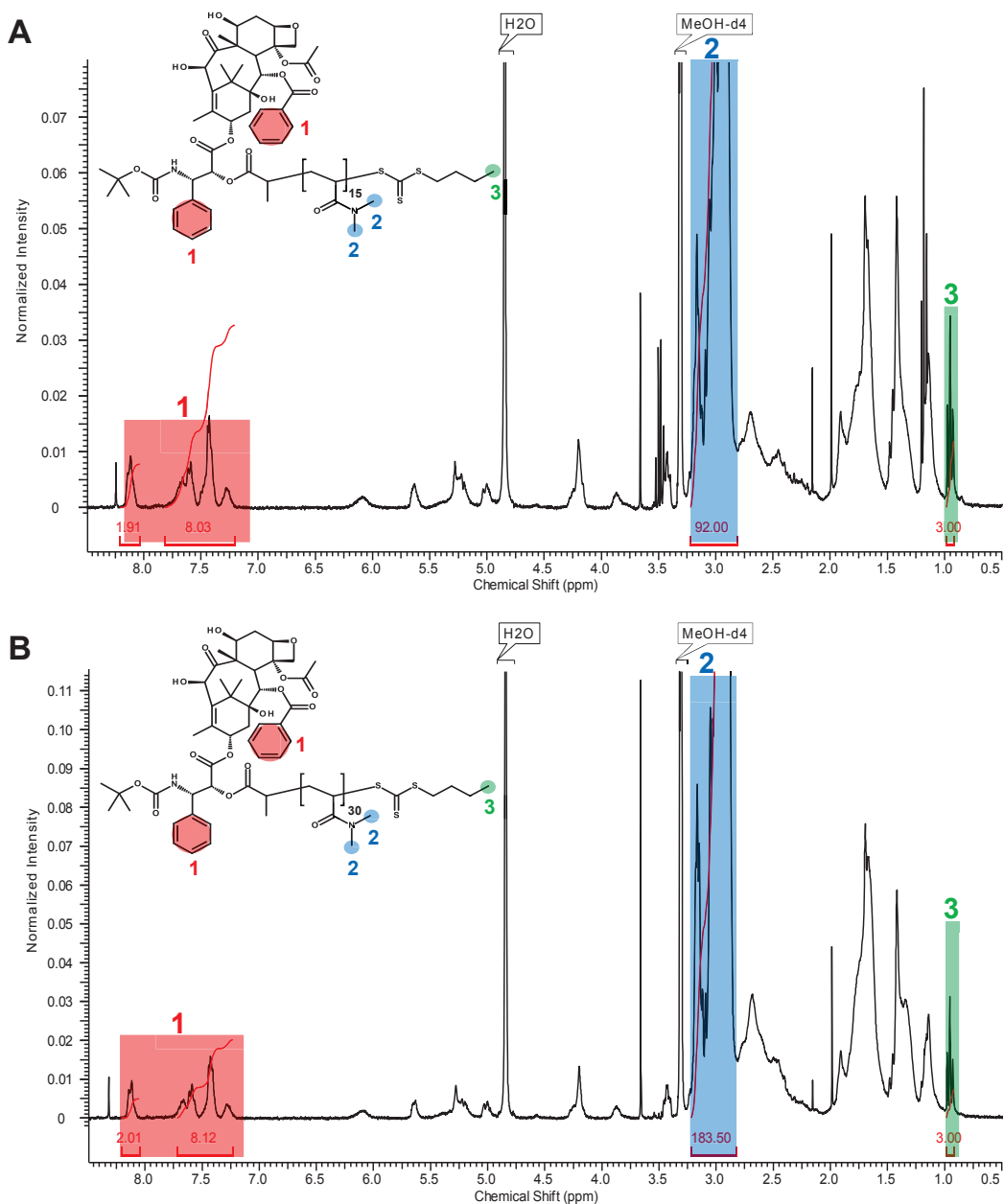


Figure S12. α,ω -endgroup fidelity confirmed by $^1\text{H-NMR}$ (300 MHz, MeOH-d_4) spectrum of DTX-pDMA₁₅ (A) and DTX-pDMA₃₀ (B).

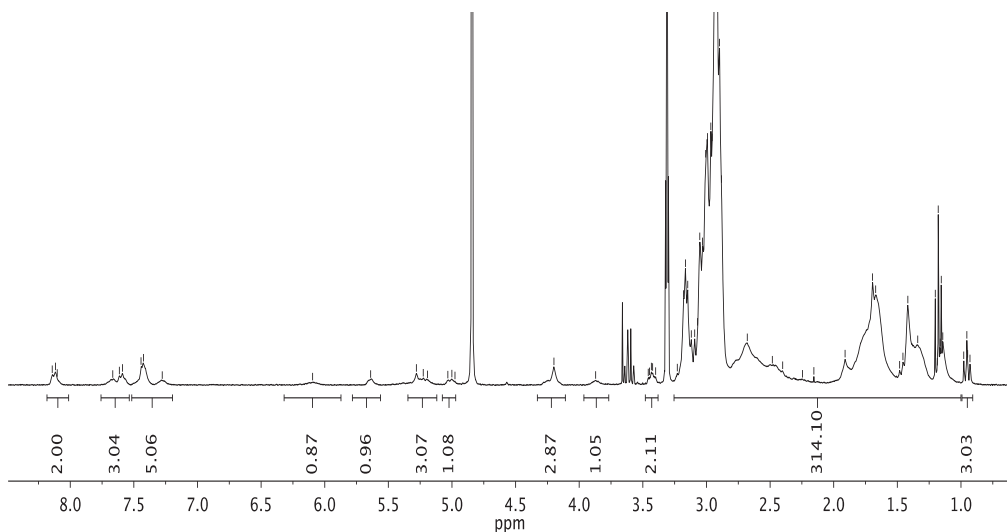


Figure S13. $^1\text{H-NMR}$ (300 MHz, MeOH-d_4) spectrum of $\text{DTX-pDMA}^{\text{Rho}}_{30}$.

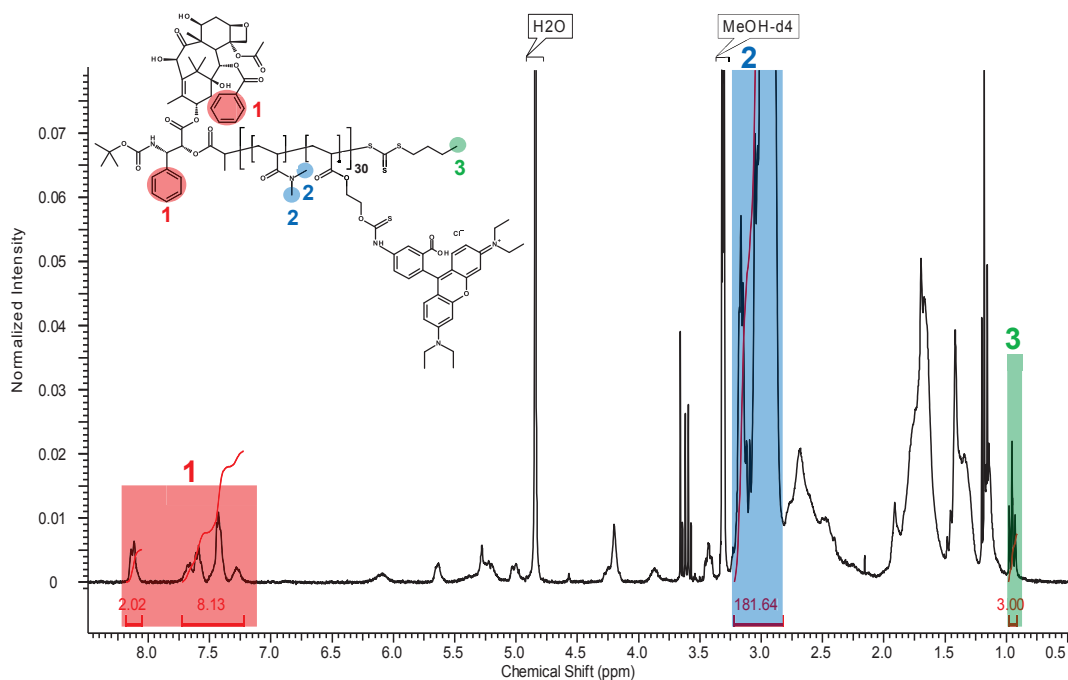


Figure S14. α,ω -endgroup fidelity confirmed by $^1\text{H-NMR}$ (300 MHz, MeOH-d_4) spectrum of $\text{DTX-pDMA}^{\text{Rho}}_{30}$.

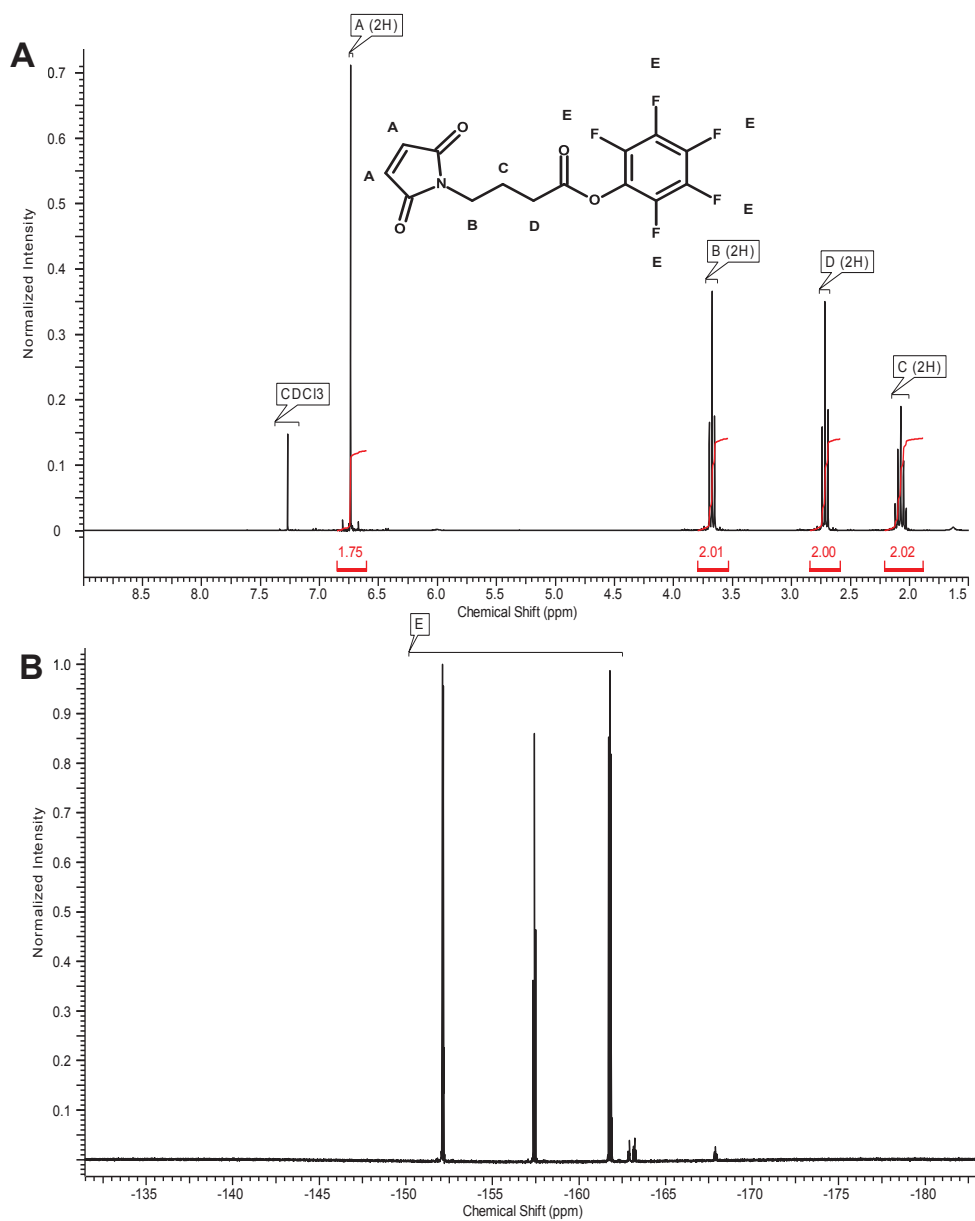


Figure S15. ^1H -NMR (A; 300 MHz, CDCl_3) and ^{19}F -NMR spectrum (B; 282 MHz, CDCl_3) of maleimidobutryl-PFP.

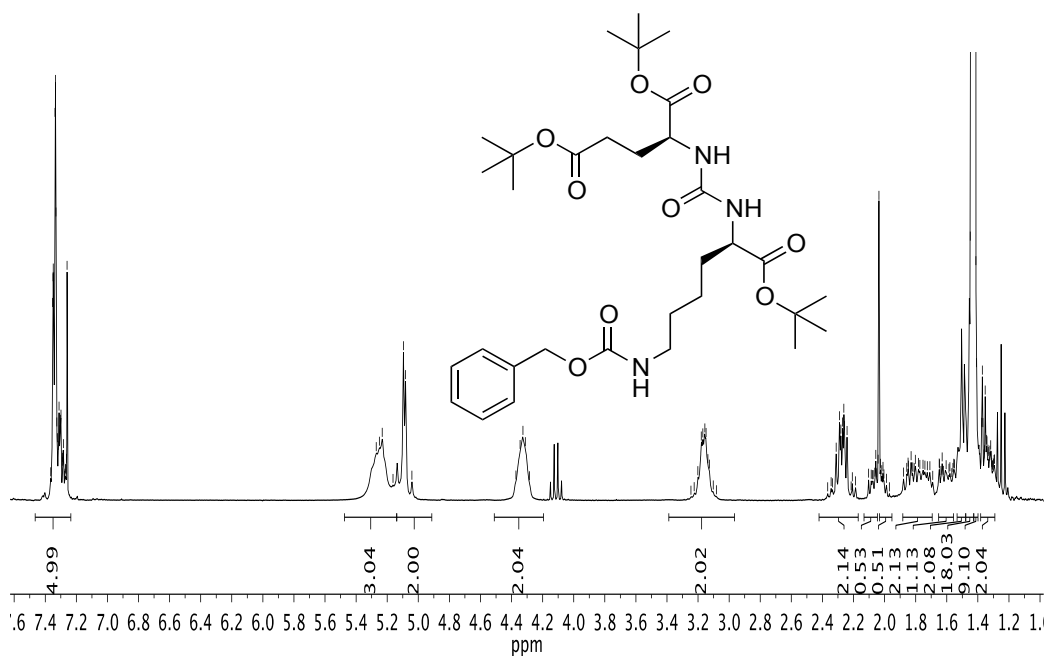


Figure S16. ¹H-NMR (300 MHz, CDCl₃) spectrum of tert-butyl ester ACUPA (Cbz-protected).

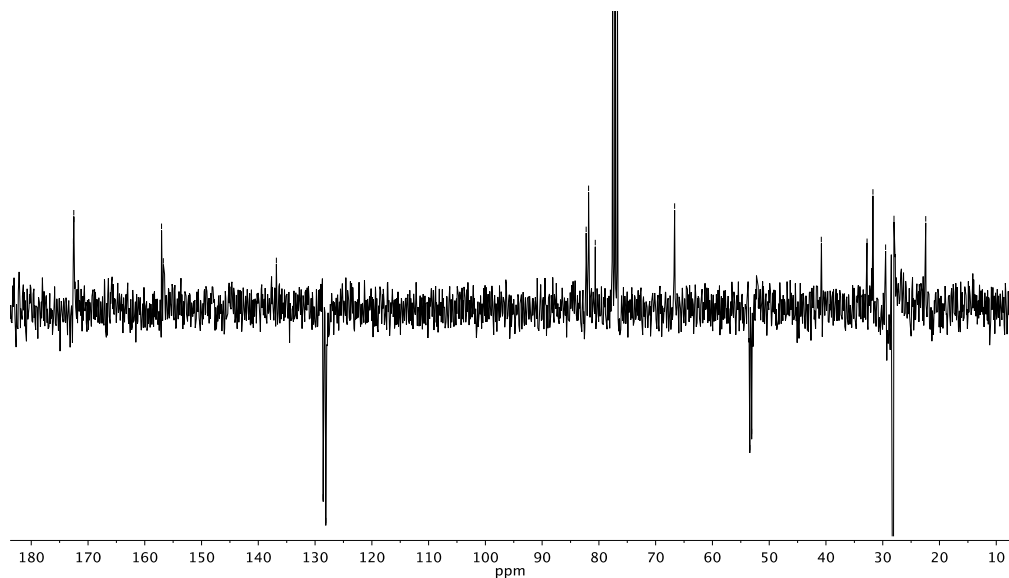


Figure S17. ¹³C-APT-NMR (75 MHz, CDCl₃) spectrum of tert-butyl ester ACUPA (Cbz-protected).

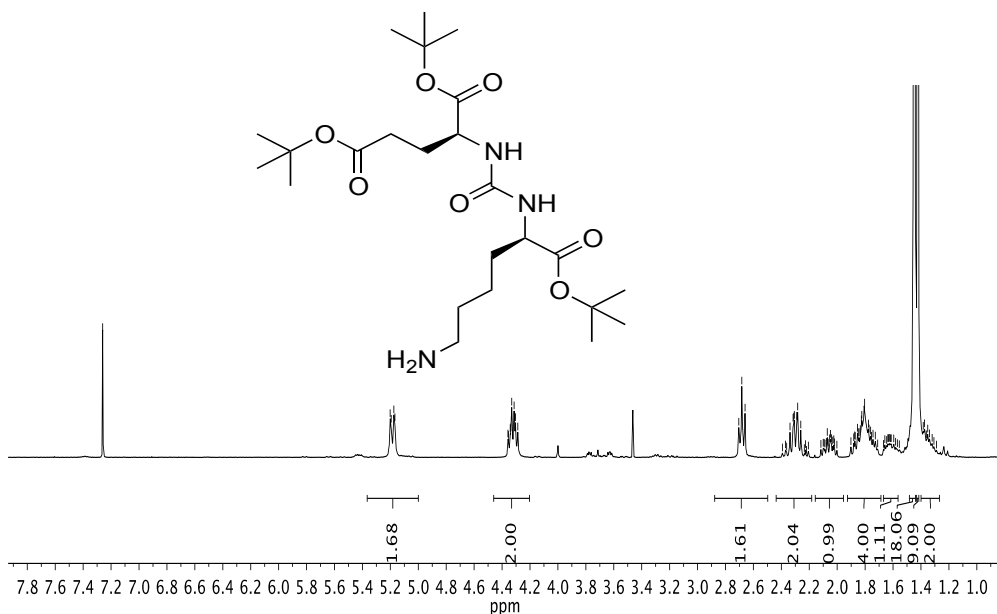


Figure S18. $^1\text{H-NMR}$ (300 MHz, CDCl_3) spectrum of tert-butyl ester ACUPA (Cbz-deprotected).

6.7 maleimidobutyl-ACUPA

Before tert-butyl ester-deprotection:

$^1\text{H-NMR}$ (300 MHz, CDCl_3): δ [ppm] = 6.72 (s, 2H), 6.31 (t, J = 5.4 Hz, 1H), 5.39 (s, 2H), 4.32 (dd, J = 4.6, 1.7 Hz, 1H), 4.30 (d, J = 5.0 Hz, 1H), 3.57 (t, J = 6.5 Hz, 2H), 3.32 (dq, J = 13.0, 6.5 Hz, 1H), 3.13 (dq, J = 12.2, 5.9 Hz, 1H), 2.45 – 2.22 (m, 2H), 2.18 (t, J = 7.0 Hz, 2H), 2.13 – 2.02 (m, 1H), 1.95 (dt, J = 11.2, 6.8 Hz, 2H), 1.89 – 1.71 (m, 2H), 1.70 – 1.58 (m, 1H), 1.56 – 1.46 (m, 2H), 1.45 (s, 9H), 1.44 (s, 9H), 1.43 (s, 9H), 1.39 – 1.29 (m, 2H).

After tert-butyl ester-deprotection:

$^1\text{H-NMR}$ (400 MHz, DMSO-d_6): δ [ppm] = 10.25 (br, 3H), 7.74 (t, J = 5.6 Hz, 1H), 6.99 (s, 2H), 6.30 (s, 2H), 4.09 (s, 1H), 4.03 (s, 1H), 3.38 (t, J = 6.9 Hz, 2H), 2.97 (q, J = 6.6 Hz, 2H), 2.28 – 2.14 (m, 2H), 2.02 (t, J = 7.5 Hz, 2H), 1.91 (dddd, J = 13.9, 9.0, 7.0, 5.2 Hz, 1H), 1.78 – 1.56 (m, 4H), 1.50 (dq, J = 14.4, 7.4 Hz, 1H), 1.43 – 1.30 (m, 2H), 1.26 (q, J = 7.9 Hz, 2H).

$^{13}\text{C-APT-NMR}$ (101 MHz, DMSO-d_6): δ [ppm] = 174.55, 174.19, 173.74, 171.06, 171.01, 157.31, 134.46, 52.27, 51.67, 38.37, 36.91, 32.61, 31.82, 29.92, 28.85, 27.54, 24.17, 22.65.

ESI-MS (acetonitrile): m/z = calcd for $\text{C}_{20}\text{H}_{28}\text{N}_4\text{O}_{10}$ 484.180, found 485.186 $[\text{M}+\text{H}]^+$

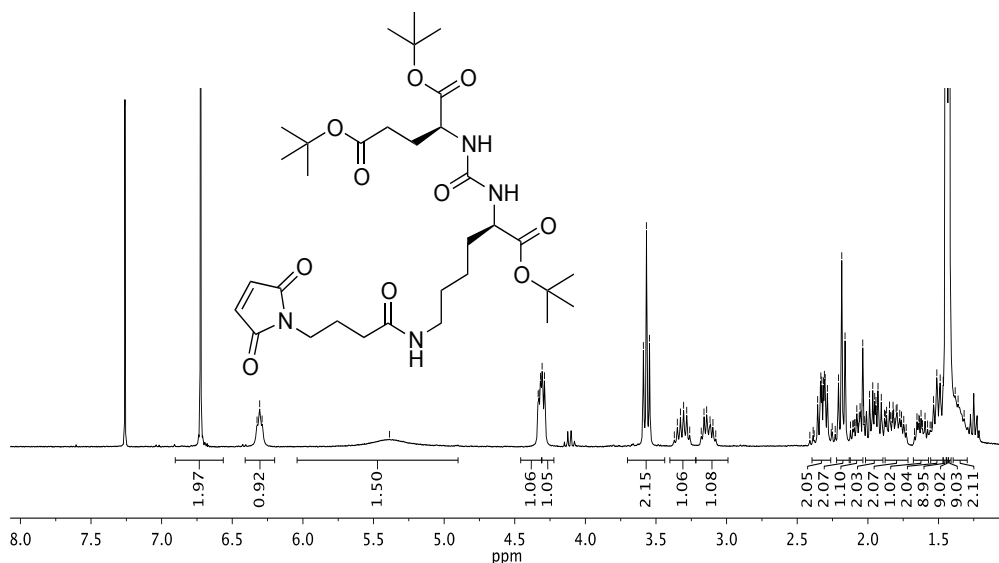


Figure S19. $^1\text{H-NMR}$ (300 MHz, CDCl_3) spectrum of tert-butyl ester maleimidobutryryl-ACUPA.

6.8 post-polymerization functionalization

SEC(DMAC, PMMA-St.):

$M_n = 4876$, PDI = 1.12 (DTX-pDMA₃₀-ACUPA) and $M_n = 5319$, PDI = 1.09 (DTX-pDMA₃₀-HA)

$M_n = 4997$, PDI = 1.13 (DTX-pDMA^{Rho}₃₀-ACUPA) and $M_n = 5222$, PDI = 1.09 (DTX-pDMA^{Rho}₃₀-HA)

DTX-pDMA₃₀-ACUPA

$^1\text{H-NMR}$ (300 MHz, MeOH-d_4): δ [ppm] = 8.11 (t, $J = 6.4\text{Hz}$, 2H), 7.68 – 7.55 (m, 3H), 7.50 – 7.14 (m, 5H), 6.09 (br, 1H), 5.63 (br, 1H), 5.45 – 5.10 (m, 3H), 5.21 (br, 1H), 5.05 – 4.92 (m, 1H), 4.50 – 3.42 (m, 4H(DTX) + 4H(ACUPA) = 8H), 3.26 – 0.80 (m, 31H DTX + 19H ACUPA + 9H x 30(DP) = 320H).

DTX-pDMA₃₀-HA

$^1\text{H-NMR}$ (300 MHz, MeOH-d_4): δ [ppm] = 8.11 (t, $J = 6.4\text{Hz}$, 2H), 7.68 – 7.55 (m, 3H), 7.50 – 7.14 (m, 5H), 6.09 (br, 1H), 5.63 (br, 1H), 5.45 – 5.10 (m, 3H), 5.21 (br, 1H), 5.05 – 4.92 (m, 1H), 4.50 – 3.42 (m, 4H(DTX) + 2H(HA) = 6H), 3.26 – 0.80 (m, 31H DTX + 9H HA + 9H x 31(DP) = 319H).

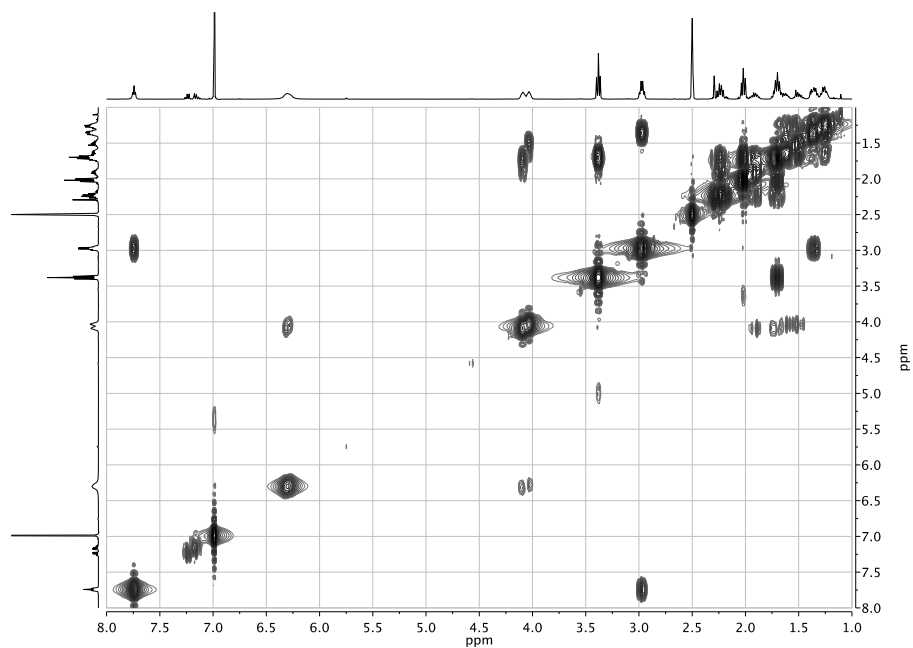


Figure S21. ^1H - ^1H -COSY spectrum of maleimidobutyryl-ACUPA (tert-butyl ester-deprotected).

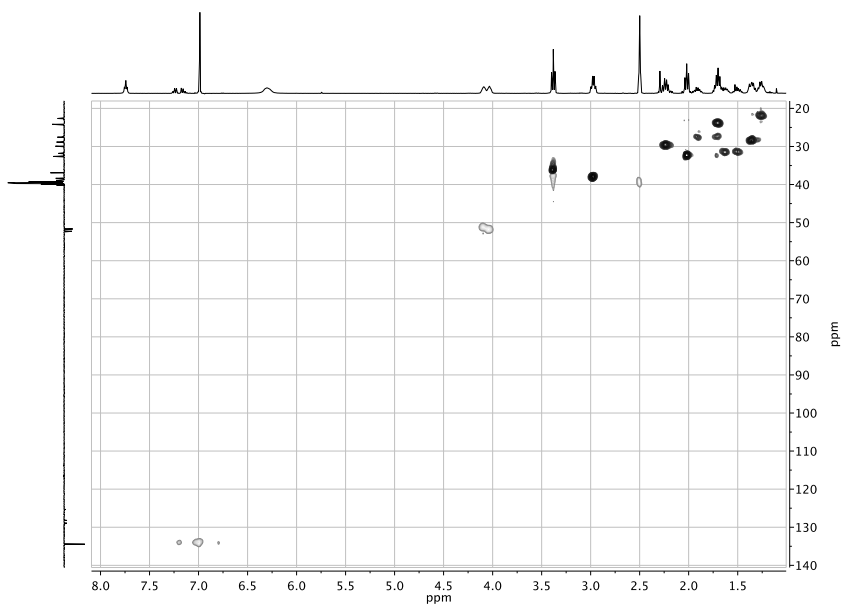


Figure S22. ^1H - ^{13}C -HSQC spectrum of maleimidobutyryl-ACUPA (tert-butyl ester-deprotected).

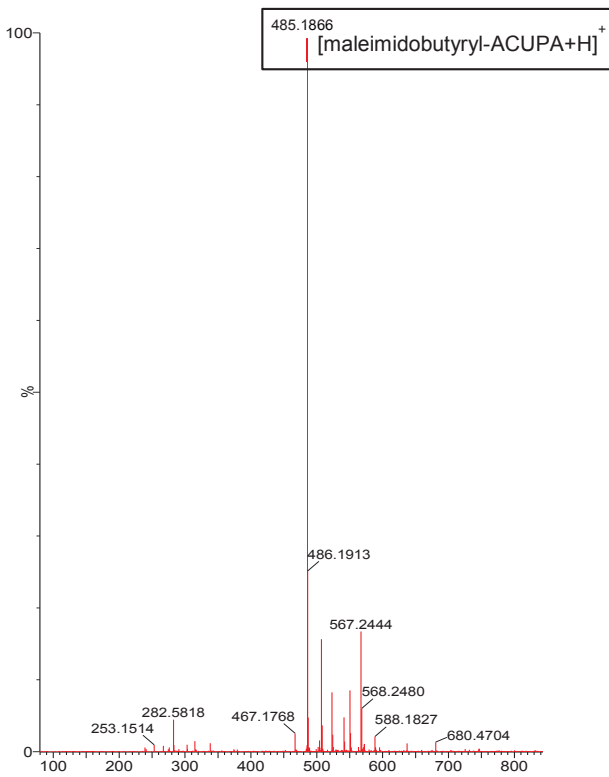


Figure S23. ESI-MS (acetonitrile) spectrum of maleimidobutyryl-ACUPA (tert-butyl ester-deprotected).

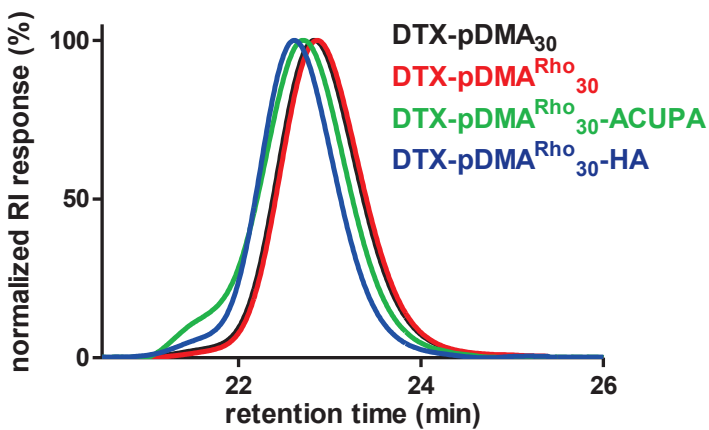


Figure S24. SEC elugrams of DTX-pDMA₃₀^{Rho}, DTX-pDMA₃₀^{Rho}-ACUPA and DTX-pDMA₃₀^{Rho}-HA, compared to DTX-pDMA₃₀.

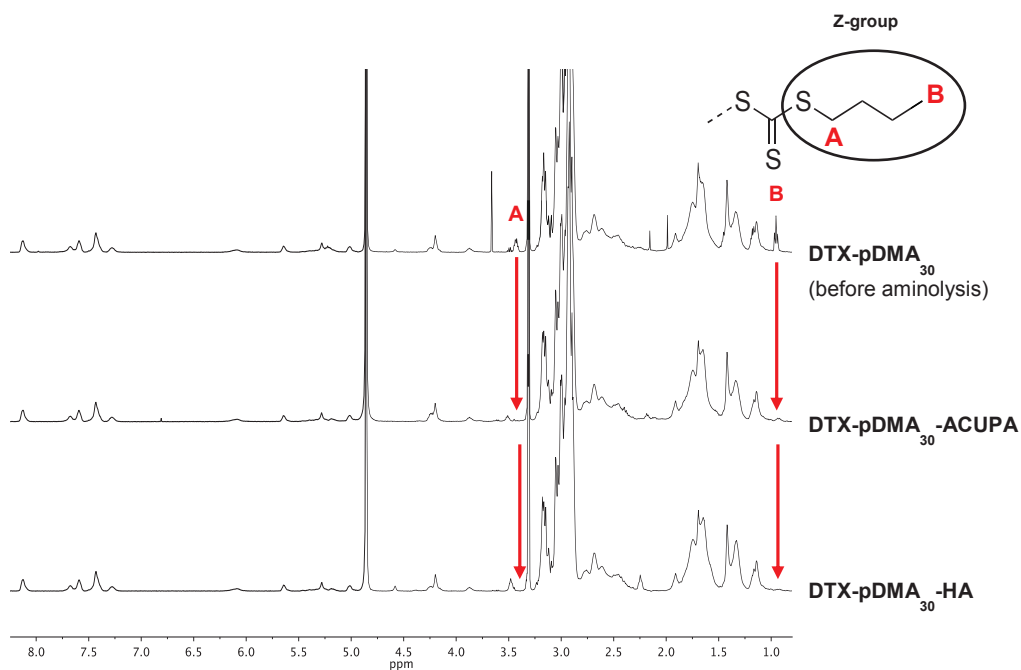


Figure S25. Absence of RAFT CTA Z-group confirmed by ¹H-NMR (300 MHz, MeOH-d₄) for DTX-pDMA₃₀-ACUPA and DTX-pDMA₃₀-HA.

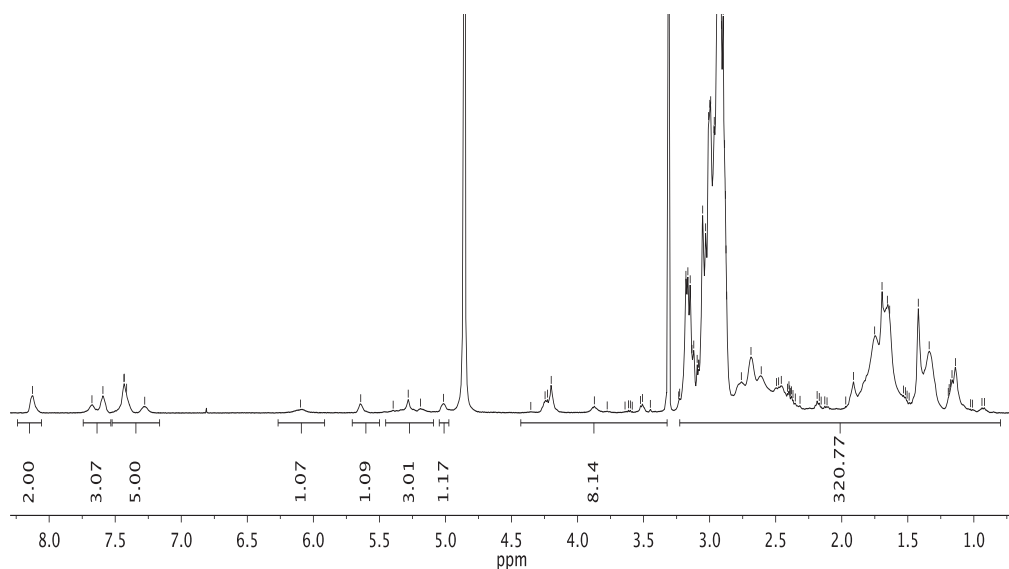


Figure S26. ¹H-NMR (300 MHz, MeOH-d₄) spectrum of DTX-pDMA₃₀-ACUPA.

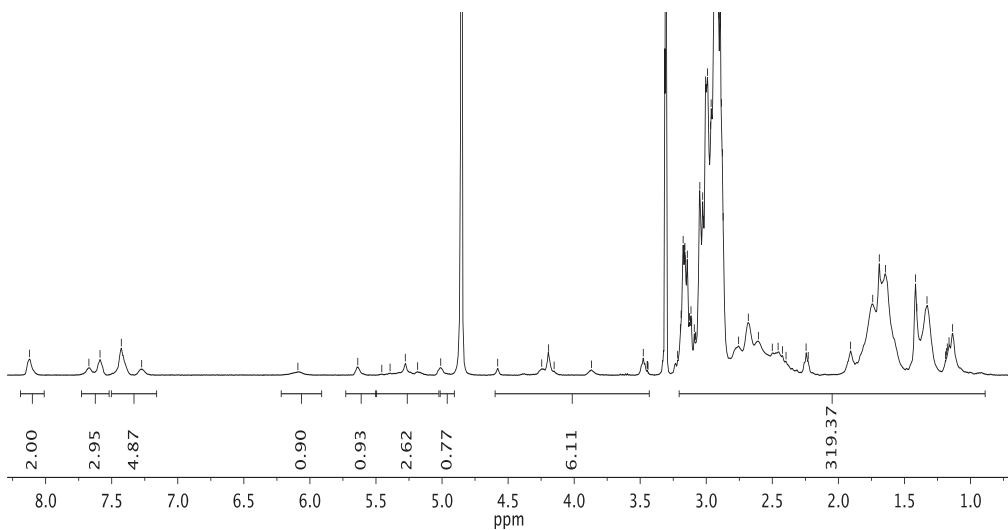


Figure S27. $^1\text{H-NMR}$ (300 MHz, MeOH-d_4) spectrum of DTX-pDMA₃₀-HA.

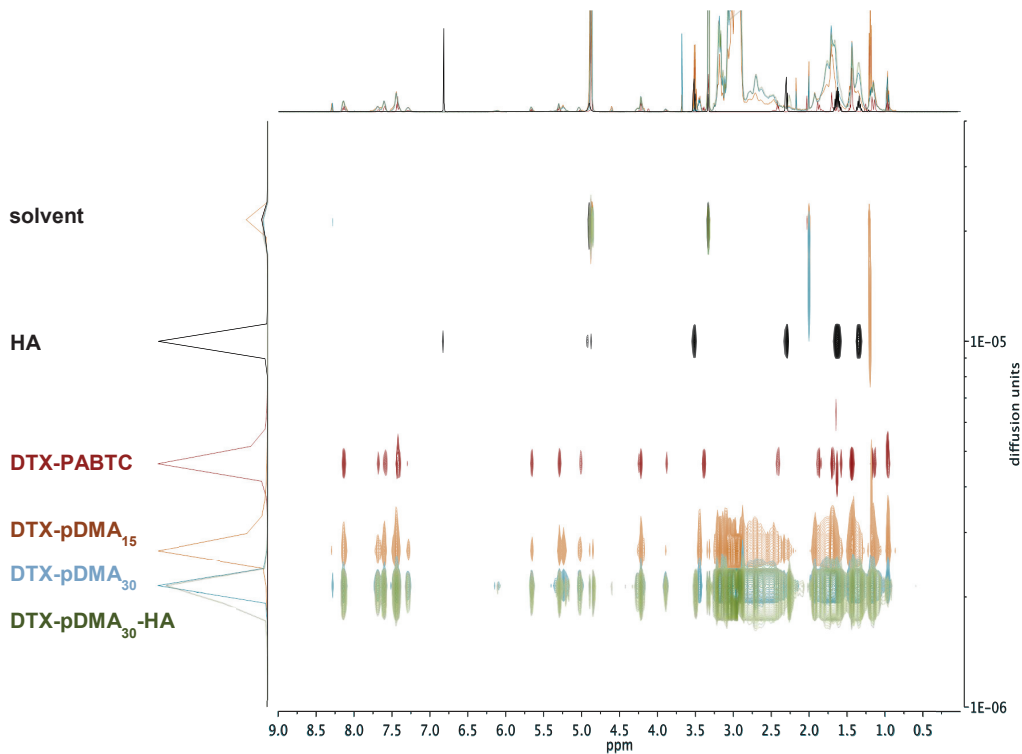


Figure S28. DOSY NMR spectra of HA, DTX-PABTC, DTX-pDMA₁₅, DTX-pDMA₃₀ and DTX-pDMA₃₀-HA.

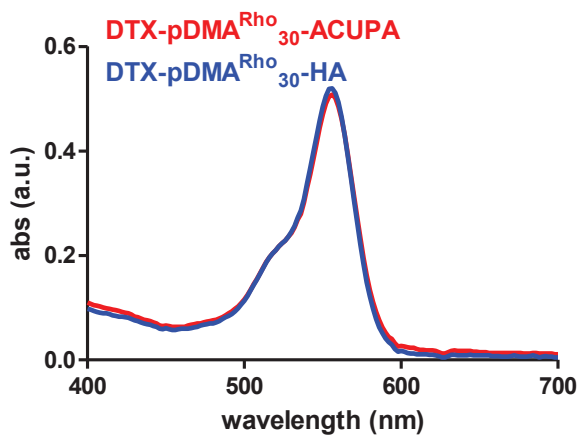


Figure S29. UV-VIS spectra of DTX-pDMA^{Rho}₃₀-ACUPA and DTX-pDMA^{Rho}₃₀-HA, both at 4 mg/mL, confirming equal rhodamine labeling.

PART IV

RELEVANCE, SUMMARY AND

GENERAL CONCLUSIONS

chapter 8

broader international context

Benoit Louage,^a Olivier De Wever,^b Wim E. Hennink,^c Bruno G De Geest^a

^a Laboratory of Pharmaceutical Technology, Department of Pharmaceutics,
Ghent University, Ottergemsesteenweg 460, 9000 Ghent, Belgium

^b Department of Radiation Oncology and Experimental Cancer Research,
Ghent University and Ghent University Hospital, De Pintelaan 185, 9000 Ghent, Belgium

^c Department of Pharmaceutics, Utrecht Institute for Pharmaceutical Sciences,
Utrecht University, Universiteitsweg 99, 3584CG Utrecht, The Netherlands

Journal of Controlled Release 2017

1 approved technologies beyond Taxol and Taxotere

1.1 Abraxane

In 2005, the first and so far only alternative PTX formulation was FDA-approved for treatment of metastatic breast cancer. It is devoid of ethanol and toxic Cremophor EL and contains human serum albumin (HSA) instead. PTX exhibits high systemic protein binding. Albumin is the most abundant plasma protein and known to function as carrier molecule for lipophilic drugs based on physical, hydrophobic interaction.^[1-4] The formulation can be prepared by dissolving 2 - 3 % of HSA in water, adding 2 to 4 % (v/v) of chloroform and finally adding PTX in a quantity between 5 - 20 % by weight relative to the weight of the albumin present in solution. The latter mixture is subjected to high pressure homogenization (i.e. between 9000 and 40 000 psi) yielding a nanoemulsion which is frozen and lyophilized. The obtained powder can be reconstituted in saline (i.e. 0.9 % NaCl), subsequently diluted in physiological solution and administered through intravenous infusion.^[5,6] Reconstitution generates 130 nm particles. Upon dilution into the bloodstream, the only modest hydrophobic interaction causes the particles to rapidly disassemble into single PTX-albumin complexes.^[7]

Phase I studies showed absence of cremophor-related toxicities which resulted in a relatively higher maximum tolerated dose (MTD; i.e. 300 mg/m² for Abraxane versus 200 - 250 mg/m² for Taxol)^[8] and greater efficacy in phase II and III trials.^[4,9-12] After FDA-approval, additional retrospective *in vitro* and *in vivo* studies showed higher tumor accumulation of Abraxane compared to Taxol at equal dose. The latter could be correlated to binding of the PTX-albumin complexes to endothelial gp60-receptors and subsequent transcytosis.^[13] Once entered in the tumor interstitium, the complex can bind the secreted protein acidic and rich in cysteine (SPARC) which could in turn facilitate the delivery of PTX into tumor cells. Even though SPARC is not a tumor specific protein, high expression has been associated with malignant transformation.^[14-17] Despite the preclinical evidence, further clinical research should be conducted to confirm whether these mechanisms also hold true in humans. It has been suggested that elevated expression of SPARC could be a positive biomarker for Abraxane efficacy, although this might apply only for specific tumor types.^[18-22] This advanced formulation is generally not considered a nanomedicine. Abraxane exhibits similar short PTX half-lives as compared to Taxol, hence EPR-mediated delivery is unlikely to occur.^[23] The success of the platform most probably lies in its ability to significantly lower the toxicity of PTX by avoiding Cremophor EL its formulation, allowing higher dosing and hence improving therapeutic effect. Recently, 2 more indications have been added for treatment with Abraxane: advanced NSCLC and late-stage

pancreatic cancer.^[24] Based on the same technology, the company (i.e. Celgene) has developed an albumin-based formulation of DTX (ABI-008) which currently undergoes phase I/II trials.

1.2 Genexol-PM

Genexol-PM was approved in South Korea in 2007 for treatment of metastatic breast cancer. The solubilizing agent in this formulation is an amphiphilic block copolymer, comprised of monomethoxy poly(ethylene-glycol)-*b*-poly(lactic acid) (PEG-PLA; **Figure 1A**) which is obtained by ring-opening polymerization (ROP).^[25,26] The formulation can be prepared by solvent diffusion. Briefly, PTX and block copolymer are dissolved in acetonitrile and stirred. After solvent evaporation, the obtained gel matrix is dispersed in water to acquire a clear micellar solution with physically entrapped PTX. The latter is filtered (0.22 μm) and subsequently lyophilized.^[27] The obtained powder is reconstituted in saline solution and diluted in 5 % dextrose before administration by intravenous infusion.^[28] Similar to Abraxane, Genexol-PM showed much lower toxicity in phase I studies compared to Taxol (MTD was more than doubled) which allowed high dose administration.^[29] However, no differences in plasma AUC were observed at equal PTX dose.^[28] This suggests the micelles rapidly disassemble after administration and/or the drug diffuses out of the particles and strongly interacts with abundant plasma proteins such as albumin. Again, the main asset of this formulation is the ability to solubilize PTX without Cremophor EL, not necessarily through acting as a nanomedicine. Genexol-PM has now also been approved in South Korea for treatment of NSCLC and ovarian cancer. No FDA-approval has yet been granted for the formulation in the US, but several clinical trials are currently ongoing.

2 advanced taxane nanomedicines

The clinical success of the aforementioned Cremophor EL-free formulations re-highlighted the great potential of taxanes. However, the rationale of these formulations was merely to solubilize these hydrophobic compounds. Even though Cremophor EL-related toxicity was avoided, high systemic drug exposure evoked by these formulations still leads to intrinsic taxane side-effects including myalgia, neutropenia and neuropathy.^[8,28] Based on the assets mentioned before, there is a great opportunity in the field of nanomedicine for further broadening the therapeutic index of taxanes. A summary of all taxane formulations in clinical trials is presented in **Table 1**. In the following paragraphs, a selection of novel, pioneering technologies will be discussed to scope the current trends in advanced taxane delivery.

2.1 physical encapsulation

As previously mentioned, PTX-encapsulated in albumin nanoparticles (i.e. Abraxane) and polymeric micelles (i.e. Genexol-PM) are likely to dissociate and/or swiftly release PTX once injected in the bloodstream.^[23] To truly be defined as nanomedicines, drug-encapsulated formulations have to ensure strong mutual hydrophobic interactions between amphiphiles intrinsically, as well as between amphiphile and drug, in order to avoid particle dissociation and premature drug release, respectively.^[30]

Kataoka and co-workers designed a micellar PTX formulation based on PEG-poly(aspartate) (i.e. NK105) in which half of the aspartate moieties are functionalized with 4-phenyl-1-butanol (PEG-p(Asp-Bz); **Figure 1B**) to yield an amphiphilic block copolymer which forms micellar structures in aqueous environment and exerts strong interaction with PTX.^[31] The block copolymer is synthesized by ring-opening polymerization of β -benzyl L-aspartate *N*-carboxy anhydride, initiated by the terminal primary amine group of a α -methoxy- ω -aminopoly(ethylene glycol) macroinitiator.^[32] After polymerization, the polymer can be dialyzed, filtered and lyophilized. Micelles are formed upon reconstitution in water. Next, PTX is dissolved in organic solvent (e.g. ethanol) and subsequently added to the micellar dispersion, allowing physical entrapment of the drug into the hydrophobic core of the micelles. The obtained formulation can be lyophilized, reconstituted in suitable iso-osmotic medium and administered through intravenous infusion.^[33] Preclinical studies showed 90-fold higher plasma AUC and 25-fold higher tumor AUC of PTX compared to the Taxol formulation.^[34,35] Phase I studies showed a significant drop in systemic neurotoxicity and clinical efficacy was proven in a phase II study.^[36] These results indicate that NK105 truly acts as a nanocarrier, avoiding premature systemic burst release of PTX and facilitating drug targeting via the EPR effect. NK105 has recently finalized a phase III trial in the US for the treatment of metastatic breast cancer. Unfortunately, the primary endpoint of the study (i.e. in terms of progression free survival (PFS)) did not meet the prespecified statistical criteria.^[37] This can put in question whether merely passively targeted nanomedicines could be used as a standard chemotherapeutic treatment modality. The latter will be further discussed in section 5.

A related block copolymer system has recently been reported by Hennink and co-workers in which the hydrophobic block consists of *N*-(2-hydroxypropyl)methacrylamide (HPMA) bearing aromatic benzoyl groups (PEG-p(HPMAm-Bz); **Figure 1C**).^[38] The formulation was evaluated in a subcutaneous xenograft mouse model and showed prolonged blood circulation kinetics, effective retention of PTX within the micellar core, low toxicity, high EPR-mediated tumor accumulation and efficient tumor regression.^[30]

Systems based on physical encapsulation are also being explored for active targeting by surface decoration with high-affinity ligands. So far, BIND-014 is the first and only active targeted polymeric taxane nanoformulation which has reached clinical trials.^[39] This system, developed by the Langer and co-workers, comprises encapsulation of DTX into nanoparticles, composed of PEG-PLA and poly(ethylene glycol)-*b*-poly(lactic-*co*-glycolic acid) (PEG-PLGA) block copolymers of which a fraction is functionalized with a small molecule high-affinity ligand for prostate specific membrane antigen (PSMA) (i.e. *S,S*-2-(3-(5-amino-1-carboxypentyl)-ureido)-pentanedioic acid (ACUPA); **Figure 1D**).^[40] Preclinical development showed superior efficacy of the PSMA-targeted DTX nanoformulation compared to the corresponding non-targeted DTX-loaded nanoparticles. BIND-014 was in clinical phase I for treatment of advanced cancer and phase II for metastatic prostate cancer and NSCLC. However, disappointing results have recently put clinical translation of BIND-014 on hold.^[41] This case study highlights the necessity for future nanomedicine development to use preclinical models providing a better predictive value towards clinical outcome and to exploit concurrent screening to enable careful patient selection for targeted nanomedicine therapy. This will be further discussed in section 5.

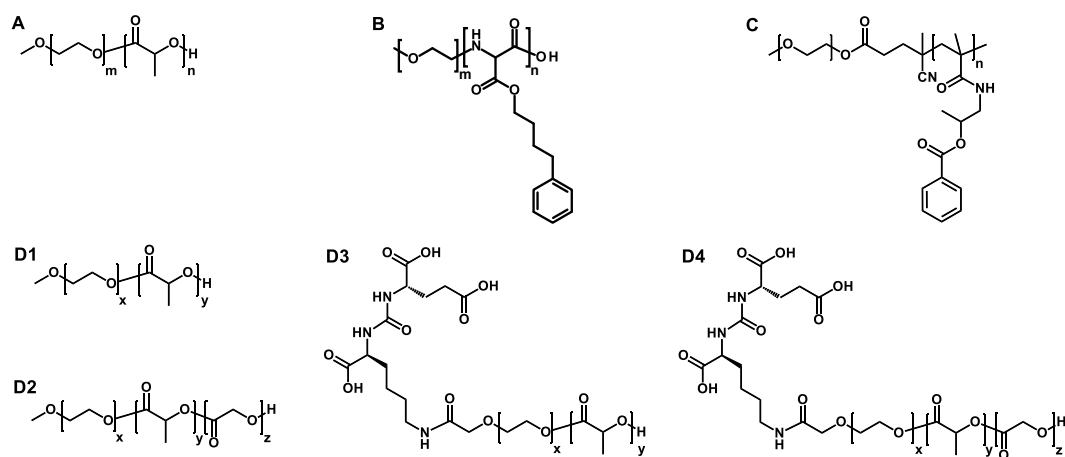


Figure 1. Molecular structures of polymeric systems used for physical encapsulation of PTX and DTX. (A) PEG-PLA, (B) PEG-p(Asp-Bz), (C) PEG-p(HPMAM-Bz), (D) BIND-014 which is composed of both PEG-PLA (D1) and PEG-PLGA (D2), and PEG-PLA (D3) / PEG-PLGA (D4) functionalized with the ACUPA targeting moiety at the hydrophilic PEG chain end.

2.2 chemical conjugation

At present, the nanomedicines with the highest approval rate are drug conjugates. These therapeutics comprise active agents, covalently attached to targeted antibodies, peptides or water-soluble polymers. Conjugating PTX to a hydrophilic polymeric carrier encompasses multiple advantages. First of all, it allows for the preparation of PTX derivatives with substantially higher aqueous solubility.^[1] Second, uncontrolled, systemic passive diffusion of drug out of the nanocarrier vehicle is limited as chemical bonds have to be cleaved first. This is a highly attractive asset for polymer-drug conjugates to compete with the numerous liposomal and polymeric micelle and nanoparticle formulations in clinical trials (**Table 1**). Third, when the polymeric carrier is of high molecular weight (HMW) and/or the polymer-drug conjugate self-assembles into a nanoparticle, renal excretion is limited and thus passive targeting is feasible. Finally, conform to the Ringsdorf model, additional ligands can be attached to the carrier vehicle for active targeting.^[42]

The approval of Oncaspar (pegylated asparaginase) in 1994 demonstrated that PEG is a highly attractive carrier molecule for bio-conjugation.^[43] Not surprisingly, only a few years after Taxol was marketed, the first linear PEG-PTX conjugates were reported by Greenwald and colleagues.^[44] A series of conjugates (PEG MW of 5 or 40 kDa) were synthesized by conjugating PEG derivatives with a terminal carboxylic acid group to PTX using carbodiimide chemistry (**Figure 2A**). Even though both low molecular weight (LMW) and HMW PTX-conjugates showed promising *in vitro* efficacy, the best *in vivo* activity was obtained with HMW PTX-conjugates.^[45] The latter showed an increased PTX half-life due to slow renal filtration. Thus, the observed *in vivo* activity most probably resulted from EPR-mediated tumor targeting, although reports have not been very clear. In 2001, Enzon Pharmaceuticals tested these PTX-conjugates in a phase I clinical trial, but decided to discontinue further development in 2003.^[46] A possible reason could be the high molecular weight and limited possibility to functionalize linear PEG which does not allow high drug loading and impedes administration to patients. Nektar Therapeutics therefore developed a 4-armed PEG structure to which 4 DTX molecules were conjugated.^[47] Improved activity and pharmacokinetics were observed in rats and dogs. This conjugate (i.e. NKTR-105) is undergoing phase I/II for treatment of several solid tumors. Other hydrophilic hyperbranched structures are now also being explored for chemical conjugation of DTX. Two of them have now entered phase I clinical trials. One is based on cyclodextrins (i.e. CRLX301), the other involves dendrimer technology (i.e. DEP DTX/DTX-SPL8783).^[48-50]

Amongst the PTX-polymer conjugates which are currently being investigated, most progress has been made by PTX poliglumex (also known as Opaxio, Xyotax, CT-2103). This is a biodegradable, HMW (i.e. 48 kDa)

conjugate of poly(L-glutamic acid) to which PTX is conjugated by esterification of its C2' hydroxyl group with the carboxylic acid side groups of the polymer (**Figure 2B**).^[51] As the C2' hydroxyl group is crucial for binding tubulin,^[52] this water-soluble nanoformulation is in fact a PTX prodrug. Preclinical evaluation showed considerably prolonged plasma half-life, higher MTD, tumor exposure and anti-tumor efficacy compared to Taxol.^[53] It has also been proposed that release of PTX predominantly occurs after cellular uptake and is mediated by lysosomal enzymes (e.g. cathepsin B).^[54,55] These features demonstrate the prodrug and passive targeting capabilities of the formulation. Although a phase III trial for first line chemotherapy of advanced NSCLC was somewhat disappointing, the formulation (in combination with platinum drugs) shows promising results in a clinical phase I/II trial for treatment of ovarian cancer and as radiosensitizers for treatment of several cancers.^[56-58]

Another conjugated system with high profile preclinical results is the CriPec platform. This core-crosslinked polymeric micelle technology is based on methoxy poly(ethylene glycol)-*b*-poly(*N*-(2-hydroxypropyl) methacrylamide-lactate) (PEG-*p*(HPMAm-Lac)_n); **Figure 2C**) block copolymers, developed by Hennink and co-workers.^[59] These polymers can self-assemble upon heating due to their lower critical solution temperature (LCST) behavior. In the CriPec platform, a fraction of the lactate side chains is reacted with methacrylic anhydride. Next, using a fast heating solvent displacement method, a methacrylated DTX-derivative is loaded into the block copolymer micelles.^[60] The micellar dispersion is then transferred to a buffer containing potassium persulfate in which the polymeric micelles are crosslinked (i.e. by mutual reaction between the pending block copolymer methacrylate moieties) and covalently loaded with DTX (i.e. by reaction between the methacrylate moieties of both the DTX-derivative and those of the block polymer).^[61] Loading capacities up to around 10 % can be achieved. The robustness of this polymer synthesis and drug formulation strategy enables to tailor the micelles in terms of size, nanocarrier degradation and drug release kinetics.^[62] This can offer opportunities in customizing DTX-formulations in function of patient-specific tumor characteristics (e.g. smaller particle sizes for tumors with more narrowly fenestrated endothelium, faster release kinetics for tumors exerting higher clearance rates^[49]) which could be assessed by imaging nanodiagnostics (e.g. iron oxide nanoparticles; section 5). A phase I study is currently recruiting patients with solid tumors for determining the highest safe dose.^[63]

No active targeted taxane-polymer conjugates are currently in clinical trials. However, the first active targeted polymeric nanoformulation ever reported was a polymer-drug conjugate, moreover a *p*(HPMA)-doxorubicin conjugate (PK2, Pfizer Inc.). This platform involves attachment of doxorubicin to the pending hydroxyl groups of *p*(HPMA), using a tetrapeptide Gly-Phe-Leu-Gly spacer.^[64] The latter was designed by Kopeček and co-workers and can be cleaved specifically by lysosomal enzymes (i.e. cathepsin B).^[65,66] Additionally, the backbone

was functionalized with galactosamine. The latter is a ligand with affinity towards lectins, present on the surface of mammalian liver cells. A phase II trial showed modest improved hepatic targeting for PK2, compared to the conjugate lacking the galactose residues (PK1).^[67] No further clinical results have been published for this system.

Table 1 gives a summary of all the aforementioned innovative taxane formulations which are currently undergoing clinical evaluation.

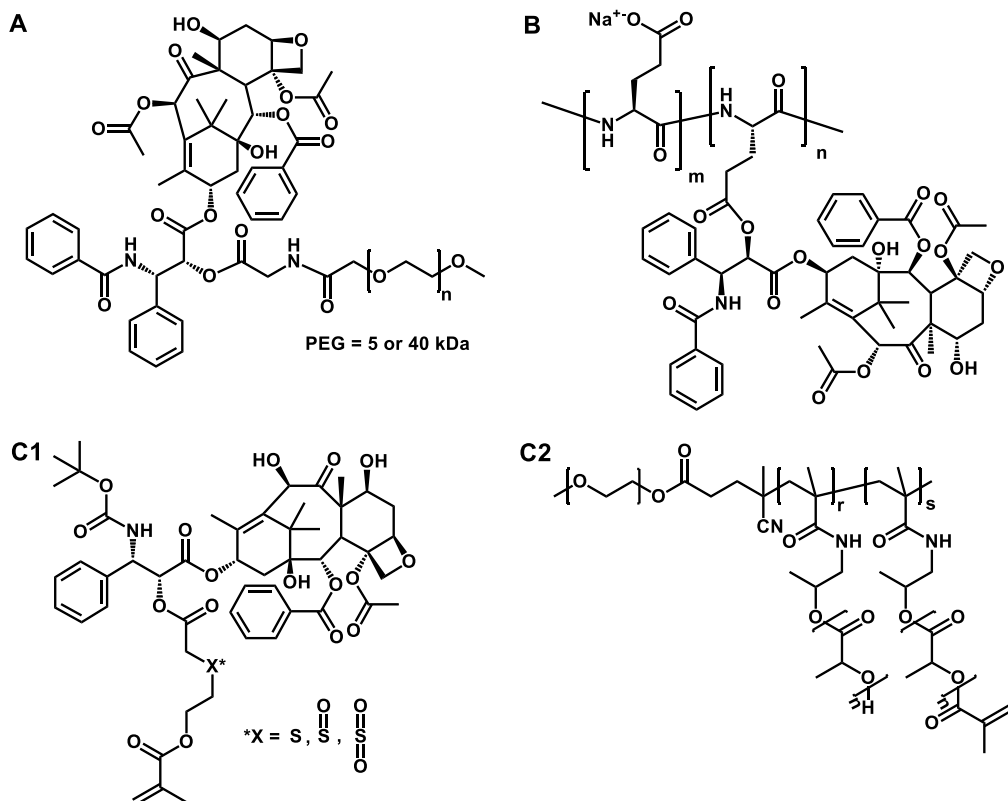


Figure 2. Molecular structures of polymeric systems used for chemical conjugation of PTX and DTX. (A) PEG-PTX, (B) poly(L-glutamic acid)-PTX, (C) Cripec, where DTX is modified with a methacrylate moiety (C1) through a hydrolysable spacer and encapsulated in core-crosslinked amphiphilic block copolymer micelles through copolymerization with methacrylate moieties on the side chain of the hydrophobic block of PEG-p(HPMAm-Lac_c) (C2).

Table 1. Summary of advanced taxane formulations in clinical trials.^[24,42,46,49,50,68–80]

product	composition	ligand (target)	indication	clinical status
LEP-ETU	PTX liposome	/	breast cancer, lung cancer, ovarian cancer	phase II
EndoTAG-1	PTX liposome	/	breast cancer, pancreatic cancer	phase II
PNU-91934	PTX liposome	/	oesophageal cancer	phase II
LE-DT	DTX liposome	/	advanced solid tumors	phase II
ATI-1123	DTX liposome	/	advanced solid tumors	phase I
Abraxane (ABI-007)	PTX albumin-bound formulation	/	breast cancer, pancreatic cancer, NSCLC	approved (US, 2005)
ABI-008	DTX albumin-bound formulation	/	metastatic breast cancer, hormone-refractory prostate cancer	phase I/II
Genexol-PM (IG-001)	PTX PEG-PLA polymeric micelle	/	breast cancer, lung cancer, ovarian cancer	phase II/III, approved (South Korea, 2007)
Paxceed	PTX PEG-PLA polymeric micelle	/	rheumatoid arthritis	phase II
Paclical	PTX retinoid XR-17 polymeric micelle	/	ovarian cancer	phase III/orphan drug (US, 2009)
NK105	PTX PEG-p(Asp-Bz) polymeric micelle	/	gastric cancer, breast cancer	phase II/III
Nanoxel	PTX polymeric micelle	/	advanced breast cancer	phase I
DTX-PM (Nanoxel-PM)	DTX polymeric micelle	/		phase I
Nanotax	PTX polymeric nanoparticle	/	peritoneal neoplasms	phase I
DTX-PNP	DTX polymeric nanoparticle	/	advanced solid malignancies	phase I
BIND-014	DTX PEG-PLGA/PEG-PLA nanoparticle	small molecule ACUPA (PSMA)	phase I: metastatic cancer phase II: metastatic castration-resistant prostate cancer, NSCLC	phase I/II
Taxoprexin	DHA-PTX conjugate	/	melanoma, liver cancer, kidney cancer, adenocarcinoma, NSCLC	phase II/III
NKTR-105	4-armed PEG-DTX conjugate	/	solid tumors, ovarian cancer	phase I/II
CRLX301	cyclodextrin-PEG-DTX conjugate	/	refractory tumors	phase I
DEP DTX (DTX-SPL8783)	dendrimer-DTX conjugate	/	advanced cancers	phase I
PTX poliglumex (Opaxio, Xyotax, CT-2103)	poly(L-glutamic acid)-PTX conjugate	/	lung cancer, ovarian cancer	phase III

Table 1 (continued)

product	composition	ligand (target)	indication	clinical status
Cripec DTX	DTX-conjugated PEG-p(HPMAM-Lac _n) core-crosslinked polymeric micelle	/	solid tumors	phase I
GRN1005 (ANG1005)	angioprep 2-PTX conjugate	low-density lipoprotein receptor- related protein 1 (LRP1)	breast cancer with brain metastases, NSCLC with brain metastases	phase II

3 antibody-drug conjugates

Although not always considered as nanomedicines, antibody-drug conjugates (ADCs) comprise the current state-of-the-art in active targeted drug delivery and are therefore mentioned in this dissertation. ADCs could also set the benchmark for novel active targeted taxane nanomedicines as the latter can compete with ADCs with regard to drug loading. Monoclonal antibodies (mAbs) bind antigens with meticulous specificity.^[81] Therefore, they have been extensively investigated over the past 20 years as carrier vehicles for targeted delivery of small molecule cytotoxic agents. To obtain an ADC, a cytotoxin is coupled to a mAb via a linker molecule. Even though stable linkers have proven to be successful, the latest trends in linker design aim at maintaining stability in the bloodstream whilst releasing drug payload at the target site. This release can be triggered either by pH-, redox- or enzyme-mediated stimuli.^[82]

The high potential of ADC-technology is reflected by its clinical track record. Over 40 ADCs are currently undergoing clinical evaluation and 2 have been FDA-approved.^[83] Brentuximab vedotin comprises the chimeric mAb cAC10, directed against CD30 and conjugated to monomethyl auristatin E (MMAE) through an cathepsin-cleavable, self-immolative dipeptide (i.e. valine-citrulline) linker (**Figure 3A**). Like taxanes, MMAE is a very potent antimetabolic agent which interferes with microtubule dynamics, but not through promotion of formation and stabilization of microtubules, but by blocking tubulin polymerization.^[84] Based on positive results obtained in single-arm multicenter clinical trials, an accelerated FDA-approval was granted in 2011 for treatment of relapsed or refractory hodgkin lymphoma and anaplastic large-cell lymphoma which are often featured by an overexpression of CD30.^[85] Trastuzumab emtansine was the first approved ADC for treatment of solid tumors. The drug consists of an anti-HER2 mAb, conjugated by its lysine residues to the cytotoxic maytansinoid emtansine through a non-cleavable thioether linker (**Figure 3B**). Emtansine (DM1) also inhibits the formation of microtubules, predominantly by binding

tubulin.^[86] Release occurs after receptor-mediated uptake and lysosomal degradation. Proved safety and effectiveness in a phase III trial involving 991 patients led to a full market approval in 2013 for treatment of HER2-positive metastatic breast cancer patients who previously received trastuzumab and a taxane. Another ADC called gemtuzumab ozogamicin was approved in 2000 but has been withdrawn in 2010 after showing lack of benefit over conventional therapy and concomitant hepatotoxicity.^[87]

The latter example along with the fact that all the approved ADCs still induce systemic toxicity (e.g. neutropenia, nausea, neuropathy, thrombocytopenia) indicate that, despite the strong ADC pipeline, the technology still needs further investigation and improvement.^[88] Lessons are to be learnt concerning linker design as several toxicities have been attributed to specific linkers.^[89–92] Next, the ability of mAbs to effectively localize at the target site can be considered a point of discussion. Even though mAbs exhibit blood half-lives > 3 days, mAbs might extravasate too slow and not efficiently penetrate in tumor tissue, leading to heterogeneous distribution with the highest concentration at the periphery.^[77,93,94] Additionally, the number of drug molecules which can be conjugated to mAbs is limited. The drug-antibody-ratio (DAR) is usually 4 mol/mol.^[95,96] As the average molecular weight of the used cytotoxins is 1000 Da and the molecular weight of an antibody is approximately 150 000 Da, loading capacities are typically even below 5 %. This explains why initially developed ADCs based on regular chemotherapeutics, including taxanes, lack therapeutic efficacy and hence novel cytotoxic agents (e.g. MMAE and DM1) with substantially higher potency (i.e. up to factor 1000) are required for obtaining sufficient therapeutic effect in spite of low drug loading.^[97,98] However, this also implies that only a small fraction of premature drug release could result in severe systemic toxicity. The final and probably biggest issue from a healthcare point of view is that the power of the technology comes at a price. ADCs rank amongst the most expensive medicines on the market (e.g. the treatment cost of trastuzumab emtansine is approximately \$ 1 400 per dose).^[82] This is not only due to the high cost of mAb manufacturing, in particular the drug conjugation and the subsequent purification are major challenges.^[99] In order to allow widespread use in clinic, these costs would have to be lowered in the future.

A lot of promising efforts are being conducted to address these issues. New linkers are being developed based on rational design. The field is currently investigating the use of smaller antibody fragments such as diabodies, miniantibodies and small immune proteins (SIPs) which could allow for more efficient distribution into tumor tissue.^[100] Novel ADCs are developed based on highly potent second-generation taxanes (**Figure 3C**).^[101] The latter show promising *in vivo* activity leading to complete tumor regression in a subcutaneous A431 xenograft mouse model.^[102] Additionally, mAb decoration with drug-functionalized polymers is being investigated to increase cytotoxic payload.^[103] For example, Mersana Therapeutics has developed an anti-HER2 ADC (XMT-1522) to which 3 to

5 hydrophilic, biodegradable polymer chains were conjugated, each bearing up to 5 auristatin molecules and an average payload of 15 molecules per mAb (**Figure 3D**).^[104] XMT-1522 showed very potent activity *in vitro* against several breast, NSCLC, gastric and ovarian cancer cell lines. Complete regression was observed *in vivo* for both high and low HER2-expressing mouse xenograft models.^[105] This could also be a viable approach for obtaining sufficiently potent taxane-based ADCs. Novel techniques including the use of algae as vector for protein expression are being explored to cut production costs.^[106] Besides these efforts, as for most biotechnological products, it is not likely that the price will dramatically drop in the very near future. This leaves opportunities open for other alternative active targeted therapies based on non-biotechnological, synthetic endeavors.

4 small molecule-drug conjugates

Besides nanomedicines and ADCs, small molecule-drug conjugates (SMDCs) have shown great promise in targeted chemotherapy and the latter could provide a complementary platform for the treatment of tumors which are less susceptible to EPR-mediated drug delivery. Similar building blocks are exploited for SMDCs as for ADCs (i.e. drug, spacer molecule and targeting moiety). The latter however is not a mAb, but a synthetic, small molecule targeting ligand. Spacer design is crucial for the construction of SMDCs. The same chemical rationale is used as for ADCs, i.e. to achieve specific drug release in the tumor environment based on (self-immolative) acid-, redox- or enzyme-sensitive properties. SMDCs preferably encompass a rigid, hydrophilic spacer molecule to avoid intramolecular interference between drug and ligand.^[107,108] Increasing hydrophilic properties also limits aspecific cellular uptake by passive diffusion which is the predominant uptake mechanism of free hydrophobic drugs.^[73,109] The molecular weight of the spacer molecule can influence the efficacy of SMDCs. For example, it was shown that folate-rhodamine conjugates with HMW PEG spacers (i.e. > 5 kDa) do not exhibit fast and adequate tumor penetration.^[110] On the other hand, SMDCs with LMW spacers (i.e. < 2 kDa) are capable of passively diffusing into the tumor tissue more thoroughly and more rapidly than macromolecular carrier molecules.^[73,110–112]

In certain respects, SMDCs have advantages over ADCs. First, the smaller size of SMDCs could allow for more effective penetration throughout the tumor mass.^[73,96] The latter can be an important asset for treating less EPR-sensitive tumors and for passing dense membrane structures such as the blood brain barrier (BBB). Second, the stepwise synthesis of SMDCs allows for a more controlled and site-specific drug conjugation.^[96] Third, the low molecular weight of SMDCs inherently results in a high drug loading capacity. Hence, beyond the conjugation of extremely potent drugs (e.g. MMAE and DM1), this technology is also suitable for conjugation of well-established

chemotherapeutic drugs including taxanes. Fourth, small hydrophilic molecules exhibit fast renal clearance.^[113] Though considered a drawback in EPR-mediated drug delivery, this property could pose advantages with regard to toxicity. Unless a technology possesses 100 % binding specificity which currently cannot even be achieved by ADCs, the longer the blood half-life, generally the higher the risk of side-effects.^[96] As SMDCs generally saturate the target receptor within 5 – 20 minutes after intravenous injection,^[110] fast excretion of the dose fraction which is not bound to the target tissue would minimize systemic side-effects.^[114,115] To compensate for the fast renal clearance, a higher dosing might be required. Hence, a prodrug approach with tumor-specific, stimuli-responsive drug release would be preferred, as this can substantially increase MTD and hence allow administration of higher doses without risking high off-site toxicity.

9 SMDCs are currently in clinical trials of which more than half in phase II or III,^[73] including GRN1005. The latter is a conjugate, composed of 3 PTX molecules linked to angiopoietin 2 by ester bonds which are cleaved in lysosomal vesicles (**Figure 4A**).^[116] Angiopoietin 2 is a peptide-based ligand, targeting low-density lipoprotein receptor-related protein 1 (LRP1), a cell-surface receptor involved in cancer metastasis. GRN1005 is currently undergoing a phase II trial for treatment of NSCLC with brain metastases and for breast cancer in combination with trastuzumab (**Table 1**).

As for nanomedicines, the hydrophobicity of anti-cancer drugs challenges the design and formulation of SMDCs. For example, a surfactant (i.e. Solutol HS15) is still required to obtain a clinically applicable formulation of GRN1005.^[117] These solubility issues could be resolved by designing spacers with sufficient hydrophilicity. Most of the spacer molecules currently used for SMDC-technology involve peptide sequences. The latter are typically synthesized by multistep solid phase peptide synthesis (SPPS). A more straightforward, alternative approach could be the one-step synthesis of a hydrophilic, LMW polymer spacer, directly onto the drug molecule. Polymerization strategies have been developed to achieve the latter. For example, degradable LMW PTX-PLA conjugates have been synthesized by direct ring-opening polymerization (ROP) of DL-lactide from PTX (**Figure 4B**).^[118] Within our own research group, we have recently developed a hybrid system in which a customized, hydrophilic LMW polymer spacer (i.e. poly(*N,N*-dimethylacrylamide) (pDMA)) can be engineered onto PTX using reversible addition-fragmentation chain transfer (RAFT) polymerization (**Figure 4C**).^[119] Additionally, the obtained highly water-soluble PTX-polymer conjugate can be post-modified by established thiol-maleimide coupling at the opposite polymer chain end. As the resulting compound meets the structural requirements of SMDCs, we are currently exploring the potential of this approach for engineering effective, water-soluble taxane-based SMDCs. Another aspect of SMDC-technology which might hamper clinical translation is the current limited availability of high-affinity small-

molecule targeting ligands. This is not an issue in the field of ADCs, as high-affinity mAbs can be raised against virtually any target antigen.^[120] The search for novel, high-affinity small-molecule ligands towards tumor-specific epitopes has indeed proven to be challenging.^[121,122] However, this can be facilitated in the future by using predictive computational modeling methods^[123] and DNA-encoded chemical library technologies which, in contrast to conventional high-throughput screening (HTS), allow for extensive parallel evaluation of chemical libraries in one reaction tube.^[124–126]

5 clinical translation of advanced taxane formulations

A broad range of taxane nanomedicines have been developed and various preclinical *in vivo* studies have demonstrated that passive and active targeting is a great tool for significantly improving drug delivery. Surprisingly, only a few of these systems survived clinical trials.^[127] This somewhat low number, along with the recent disappointing clinical results of NK105 and BIND-014, obliges the field to question the overall validity of targeted nanomedicines in clinical chemotherapy. A recently published meta-analysis on the preclinical performance of anti-cancer nanomedicines suggests that the field might have a delivery problem, as only 0.7 % (median) of the intravenously injected nanoparticle dose was claimed to accumulate in tumors.^[128] This publication triggered a major discussion amongst experts.^[129,130]

The majority of (taxane) nanomedicines currently residing in clinical trials rely on passive targeting. Their limited clinical translation thus far suggests that EPR-mediated delivery cannot always be taken for granted.^[131] Several possible limitations with regard to EPR effect have indeed been brought forward amongst experts. Two well-reported mechanisms which can counteract the EPR effect include dense stroma and high tumor interstitial fluid pressure (IFP).^[132,133] These features can impede the tumor-directed flow of nanomedicines. However, strategies have been explored to overcome these hurdles, for example by pretreatment or co-formulation with anti-stromal drugs and/or vascular endothelial growth factor (receptor) (VEGF(R)) inhibitors, respectively.^[134–136]

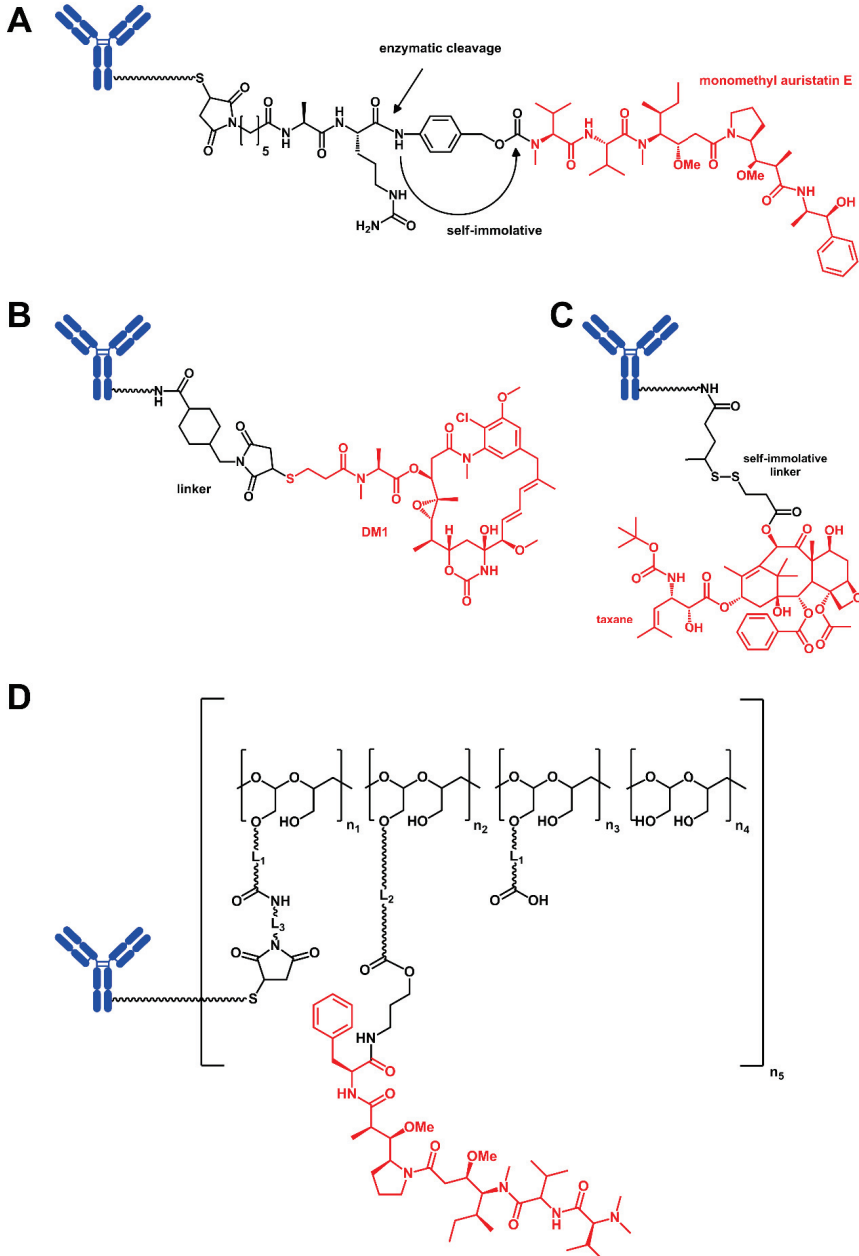


Figure 3. Molecular structures of ADCs: brentuximab vedotin (A), trastuzumab emtansine (B), a novel taxane ADC (C), XMT-1522 (D).

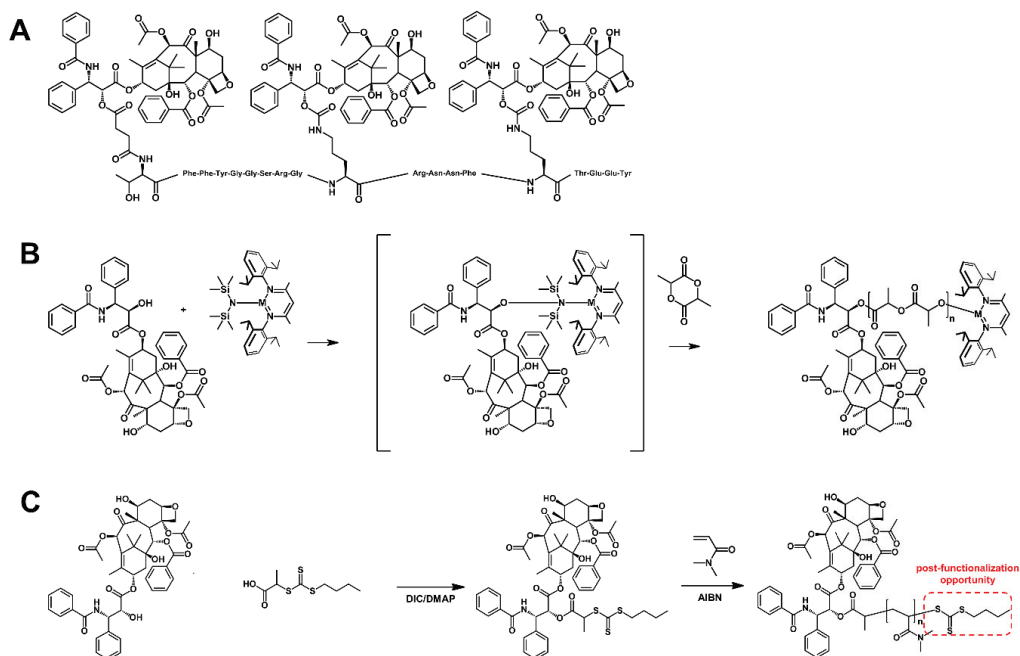


Figure 4. Molecular structures of SMDCs: GRN1005 (A) PTX-PLA (B) and PTX-pDMA (C).

The most likely reason for the limited clinical translation of nanomedicines is the overall intrinsic heterogeneity of human cancer disease which is often not accurately reflected by the current, most commonly used preclinical models.^[137–141] Due to their easy access and fast proliferation rate, *in vitro* cultured human cancer cell lines are frequently used for subcutaneous xenograft mouse models. However, extensively cultured cell lines are known to genetically adapt to their *in vitro* environment.^[142] Hence, tumors generated from these cell lines in immunodeficient mice often present pathologies *in vivo* with little resemblance to the corresponding tumors occurring in humans. For example, due to the fast proliferation rate, the tumor vasculature is often underdeveloped and fenestrated and thus very suitable for EPR-mediated drug delivery. In patients however, the immune system can drastically slow down the proliferation rate, thereby generating tumors with normal physiological vasculature. This partly explains why nanomedicines perform only moderately in clinical trials, in spite of superior preclinical efficacy. Precluding imaging techniques could determine which population would be suitable for EPR-mediated drug delivery. Indeed, besides nanomedicines, pharmaceutical companies are equally investing in nanodiagnostics. For example, Merrimack Pharmaceuticals has recently used 30 nm iron oxide nanoparticles (Feraheme, AMAG

Pharmaceuticals) in a clinical trial to screen patients on EPR effect before administration of their liposomal irinotecan formulation Onivyde (MM-398).^[41,49,143,144]

Furthermore, preclinical evaluation of anti-cancer nanomedicines typically occurs in primary tumor models. In clinical setting, however, cancer is generally treated differently. Primary tumors are preferentially removed by surgical resection and/or radiotherapy.^[140] Though occasionally conducted at presurgical stage as neoadjuvant therapy, chemotherapy is commonly applied when conditions are too delicate for the latter two techniques and for treatment of metastases.^[145] Metastatic tissues are less featured by fenestrated endothelia as compared to primary solid tumors and very small metastases are often poorly vascularized.^[146,147] It is clear that these characteristics do not allow for efficient passive targeting. Additional active targeting strategies should also be considered for more effective treatment of metastatic cancer disease and preclinical evaluation should be performed using more appropriate animal models.^[148]

Research efforts over the past 10 years resulted in development of clinically more relevant models, including the use of genetically engineered mouse (GEM) models. GEM mice can be designed to spontaneously grow orthotopic and hence anatomically relevant tumors. The latter could allow for better insights in the behavior of nanomedicines in a physiologically similar tumor environment as in patients. Furthermore, metastatic GEM models could provide an added value in identifying what features of nanomedicines are required for effective treatment of metastatic cancer disease. Another important model is the patient-derived xenograft (PDX) model.^[149,150] By extracting cancer cells directly from patients and live passaging in mice, greater concordance has been observed in terms of tumor architecture, histomorphology and global gene expression.^[151] It is likely that inter-patient variabilities in EPR susceptibility could be detected in PDX models.^[152] Expanding the patient population for PDX modelling also allows discovery of predictive biomarkers based on genomic and proteomic profiling of responders and non-responders.^[153] This could allow for a better patient screening, improve the success rate of nanomedicines in clinical trials and hence deliver a valuable contribution towards personalized medicine.^[154]

6 future perspectives

The progress towards more efficient and safer taxane anti-cancer nanomedicines has so far not been a very swift and efficient process in terms of clinical translation. Many recent ups and downs can be acknowledged. Does this imply that the assets of nanomedicines have been overestimated? Most probably not, but it would be unrealistic to expect a universal effective response in all cancer patients. Different types of nanomedicines all have their benefits and drawbacks. It is therefore useless to discuss which one is better than the other, but crucial to figure out which or which combination is best for each individual patient. Human cancer disease is highly heterogenic and should therefore be taken more into account for future design and evaluation of novel targeted anti-cancer nanomedicines. As now more and more relevant animal models (i.e. PDX, GEM) are becoming available, it will be highly recommended to expand preclinical testing beyond the well-established cell line-derived xenograft models. This will probably deliver superior predictive values and could help in deciding whether or not to proceed to evaluation in patients. These approaches will also provide biomarkers with regard to drug response which can be used in patient screening for clinical trials. Additionally, companion nanodiagnostics (e.g. imaging nanoparticles) will be complementary tools to further screen tumors in patients and evaluate their susceptibility to passive and active targeting. By careful selection of suitable patients through personalized nanomedicine, a better assessment of the full potential of targeted nanomedicine will be possible.^[355] Furthermore, the clinical response and hence approval rate of future anti-cancer (nano)medicines can be significantly improved.

7 references

- [1] J. S. Sohn, J. Il Jin, M. Hess, B. W. Jo, *Polym. Chem.* **2010**, *1*, 778–792.
- [2] F. Kratz, *J. Control. Release* **2014**, *190*, 331–336.
- [3] M. A. Lovich, C. Creel, K. Hong, C. Hwang, E. R. Edelman, *J. Pharm. Sci.* **2001**, *90*, 1324–1335.
- [4] D. A. Yardley, *J. Control. Release* **2013**, *170*, 365–372.
- [5] M. Zenoni, S. Maschio, *Process for Producing Nanoparticles of Paclitaxel and Albumin*, **2003**, US 20030185894 A1.
- [6] P. K. Paik, L. P. James, G. J. Riely, C. G. Azzoli, V. A. Miller, K. K. Ng, C. S. Sima, R. T. Heelan, M. G. Kris, E. Moore, et al., *Cancer Chemother. Pharmacol.* **2011**, *68*, 1331–1337.
- [7] A. Lluch, I. Alvarez, M. Munoz, M. A. Segui, I. Tusquets, L. Garcia-Estevez, *Crit. Rev. Oncol. Hematol.* **2014**, *89*, 62–72.
- [8] N. K. Ibrahim, N. Desai, S. Legha, P. Soon-Shiong, R. L. Theriault, E. Rivera, B. Esmaeli, S. E. Ring, A. Bedikian, G. N. Hortobagyi, et al., *Clin. Cancer Res.* **2002**, *8*, 1038–1044.
- [9] N. K. Ibrahim, B. Samuels, R. Page, D. Doval, K. M. Patel, S. C. Rao, M. K. Nair, P. Bhar, N. Desai, G. N. Hortobagyi, *J. Clin. Oncol.* **2005**, *23*, 6019–6026.
- [10] A. Moreno-Aspitia, E. A. Perez, *Clin. Breast Cancer* **2005**, *6*, 361–364.
- [11] W. J. Gradishar, S. Tjulandin, N. Davidson, H. Shaw, N. Desai, P. Bhar, M. Hawkins, J. O'Shaughnessy, *J. Clin. Oncol.* **2005**, *23*, 7794–7803.
- [12] J. O'Shaughnessy, S. Tjulandin, N. Davidson, H. Shaw, N. Desai, M. J. Hawkins, W. J. Gradishar, *Breast Cancer Res. Treat.* **2004**, *85*, 182.
- [13] N. Desai, V. Trieu, Z. W. Yao, L. Louie, S. Ci, A. Yang, C. L. Tao, T. De, B. Beals, D. Dykes, et al., *Clin. Cancer Res.* **2006**, *12*, 1317–1324.
- [14] M. J. Hawkins, P. Soon-Shiong, N. Desai, *Adv. Drug Deliv. Rev.* **2008**, *60*, 876–885.
- [15] D. Chin, G. M. Boyle, R. M. Williams, K. Ferguson, N. Pandeya, J. Pedley, C. M. Campbell, D. R. Theile, P. G. Parsons, W. B. Coman, *Int. J. Cancer* **2005**, *113*, 789–797.
- [16] M. I. Koukourakis, A. Giatromanolaki, R. A. Brekken, E. Sivridis, K. C. Gatter, A. L. Harris, E. H. Sage, *Cancer Res.* **2003**, *63*, 5376–5380.
- [17] G. Watkins, A. Douglas-Jones, R. Bryce, R. E. Mansel, W. G. Jiang, *Prostaglandins Leukot Essent Fat. Acids* **2005**, *72*, 267–272.
- [18] K. K. Frese, A. Neesse, N. Cook, T. E. Bapiro, M. P. Lolkema, D. I. Jodrell, D. A. Tuveson, *Cancer Discov.* **2012**, *2*, 260–269.
- [19] D. D. Von Hoff, R. K. Ramanathan, M. J. Borad, D. A. Laheru, L. S. Smith, T. E. Wood, R. L. Korn, N. Desai, V. Trieu, J. L. Iglesias, *J. Clin. Oncol.* **2011**, *29*, 4548–4554.
- [20] N. Desai, V. Trieu, B. Damascelli, P. Soon-Shiong, *Transl. Oncol.* **2009**, *2*, 59–64.
- [21] H. Shao, H. Tang, O. E. Salavaggione, C. Yu, B. Hylander, W. Tan, E. Repasky, A. A. Adjei, G. K. Dy, *J. Thorac. Oncol.* **2011**, *6*, 998–1005.
- [22] A. Neesse, K. K. Frese, D. S. Chan, T. E. Bapiro, W. J. Howat, F. M. Richards, V. Ellenrieder, D. I. Jodrell, D. A. Tuveson, *Gut* **2014**, *63*, 974–983.
- [23] A. Sparreboom, C. D. Scripture, V. Trieu, P. J. Williams, T. De, A. Yang, B. Beals, W. D. Figg, M. Hawkins, N. Desai, *Clin. Cancer Res.* **2005**, *11*, 4136–4143.
- [24] Y. Min, J. M. Caster, M. J. Eblan, A. Z. Wang, *Chem. Rev.* **2015**, *115*, 11147–11190.
- [25] J. Gong, M. W. Chen, Y. Zheng, S. P. Wang, Y. T. Wang, *J. Control. Release* **2012**, *159*, 312–323.
- [26] O. Dechy-Cabaret, B. Martin-Vaca, D. Bourissou, *Chem. Rev.* **2004**, *104*, 6147–6176.
- [27] S. C. Kim, D. W. Kim, Y. H. Shim, J. S. Bang, H. S. Oh, S. Wan Kim, M. H. Seo, *J. Control. Release* **2001**, *72*, 191–202.
- [28] T. Y. Kim, D. W. Kim, J. Y. Chung, S. G. Shin, S. C. Kim, D. S. Heo, N. K. Kim, Y. J. Bang, *Clin. Cancer Res.* **2004**, *10*, 3708–3716.
- [29] K. S. Lee, H. C. Chung, S. A. Im, Y. H. Park, C. S. Kim, S.-B. Kim, S. Y. Rha, M. Y. Lee, J. Ro, *Breast Cancer Res. Treat.* **2008**, *108*, 241–250.
- [30] Y. Shi, R. van der Meel, B. Theek, E. O. Blenke, E. H. E. Pieters, M. Fens, J. Ehling, R. M. Schiffelers, G. Storm, C. F. van Nostrum, et al., *ACS Nano* **2015**, *9*, 3740–3752.
- [31] N. Nishiyama, K. Kataoka, *Pharmacol. Ther.* **2006**, *112*, 630–648.

- [32] K. Kataoka, T. Matsumoto, M. Yokoyama, T. Okano, Y. Sakurai, S. Fukushima, K. Okamoto, G. S. Kwon, *J. Control. Release* **2000**, *64*, 143–153.
- [33] M. Yokoyama, Y. Sakurai, T. Okano, K. Kataoka, *Physical Trapping Type Polymeric Micelle Drug Preparation*, **1996**, US 5510103 A.
- [34] T. Negishi, F. Koizumi, H. Uchino, J. Kuroda, T. Kawaguchi, S. Naito, Y. Matsumura, *Br. J. Cancer* **2006**, *95*, 601–606.
- [35] T. Hamaguchi, Y. Matsumura, M. Suzuki, K. Shimizu, R. Goda, I. Nakamura, I. Nakatomi, M. Yokoyama, K. Kataoka, T. Kakizoe, *Br. J. Cancer* **2005**, *92*, 1240–1246.
- [36] K. Kato, K. Chin, T. Yoshikawa, K. Yamaguchi, Y. Tsuji, T. Esaki, K. Sakai, M. Kimura, T. Hamaguchi, Y. Shimada, et al., *Invest. New Drugs* **2012**, *30*, 1621–1627.
- [37] “Results of Phase III study of NK105, a novel macromolecular micelle encapsulating an anticancer drug,” can be found under https://www.nipponkayaku.co.jp/english/news/detail.php?n=20160705_78TIVWVB, **2016**.
- [38] Y. Shi, M. J. van Steenbergen, E. A. Teunissen, L. Novo, S. Gradmann, M. Baldus, C. F. van Nostrum, W. E. Hennink, *Biomacromolecules* **2013**, *14*, 1826–1837.
- [39] D. D. Von Hoff, M. M. Mita, R. K. Ramanathan, G. J. Weiss, A. C. Mita, P. M. LoRusso, H. A. Burris 3rd, L. L. Hart, S. C. Low, D. M. Parsons, et al., *Clin. Cancer Res.* **2016**, *22*, 3157–3163.
- [40] J. Hrkach, D. Von Hoff, M. M. Ali, E. Andrianova, J. Auer, T. Campbell, D. De Witt, M. Figa, M. Figueiredo, A. Horhota, et al., *Sci. Transl. Med.* **2012**, *4*, 128–139.
- [41] H. Ledford, *Nature* **2016**, *533*, 304–305.
- [42] R. Duncan, *Nat. Rev. Cancer* **2006**, *6*, 688–701.
- [43] “FDA Approves Oncaspar for Newly-Diagnosed Acute Lymphoblastic Leukemia,” can be found under <http://www.fda.gov/NewsEvents/Newsroom/PressAnnouncements/2006/ucm108700.htm>, **2006**.
- [44] R. B. Greenwald, A. Pendri, D. Bolikal, C. W. Gilbert, *Bioorg. Med. Chem. Lett.* **1994**, *4*, 2465–2470.
- [45] R. B. Greenwald, *J. Control. Release* **2001**, *74*, 159–171.
- [46] F. Dosio, B. Stella, S. Arpicco, L. Cattel, *Expert Opin. Drug Deliv.* **2011**, *8*, 33–55.
- [47] W. Li, P. Zhan, E. De Clercq, H. Lou, X. Liu, *Prog. Polym. Sci.* **2013**, *38*, 421–444.
- [48] “Going stromal with docetaxel,” can be found under <http://www.nature.com/scibx/journal/v6/n33/full/scibx.2013.881.html>, **2013**.
- [49] J. I. Hare, T. Lammers, M. B. Ashford, S. Puri, G. Storm, S. T. Barry, *Adv. Drug Deliv. Rev.* **2016**, DOI 10.1016/j.addr.2016.04.025.
- [50] J. M. Caster, A. N. Patel, T. Zhang, A. Wang, *Wiley Interdiscip. Rev. Nanomed. Nanobiotechnol.* **2016**, DOI 10.1002/wnan.1416.
- [51] S. D. Chipman, F. B. Oldham, G. Pezzoni, J. W. Singer, *Int. J. Nanomedicine* **2006**, *1*, 375–383.
- [52] D. G. I. Kingston, *Chem. Comm.* **2001**, 867–880.
- [53] C. Li, D. F. Yu, R. A. Newman, F. Cabral, L. C. Stephens, N. Hunter, L. Milas, S. Wallace, *Cancer Res.* **1998**, *58*, 2404–2409.
- [54] J. W. Singer, *J. Control. Release* **2005**, *109*, 120–126.
- [55] R. Haag, F. Kratz, *Angew. Chem. Int. Ed. Engl.* **2006**, *45*, 1198–1215.
- [56] D. A. Richards, P. Richards, D. Bodkin, M. A. Neubauer, F. Oldham, *Clin. Lung Cancer* **2005**, *7*, 215–220.
- [57] T. Dipetrillo, L. Milas, D. Evans, P. Akerman, T. Ng, T. Miner, D. Cruff, B. Chauhan, D. Iannitti, D. Harrington, et al., *Am. J. Clin. Oncol.* **2006**, *29*, 376–379.
- [58] T. Dipetrillo, M. Suntharalingam, T. Ng, J. Fontaine, N. Horiba, N. Oldenburg, K. Perez, A. Birnbaum, R. Battafarano, W. Burrows, et al., *Am. J. Clin. Oncol.* **2012**, *35*, 64–67.
- [59] O. Soga, C. F. van Nostrum, M. Fens, C. J. F. Rijcken, R. M. Schiffelers, G. Storm, W. E. Hennink, *J. Control. Release* **2005**, *103*, 341–353.
- [60] M. Talelli, C. J. F. Rijcken, C. F. van Nostrum, G. Storm, W. E. Hennink, *Adv. Drug Deliv. Rev.* **2010**, *62*, 231–239.
- [61] Q. Hu, C. J. Rijcken, R. Bansal, W. E. Hennink, G. Storm, J. Prakash, *Biomaterials* **2015**, *53*, 370–378.
- [62] Q. Hu, C. J. F. Rijcken, E. van Gaal, P. Brundel, H. Kostkova, T. Etrych, B. Weber, M. Barz, F. Kiessling, J. Prakash, et al., *J. Control. Release* **2016**.
- [63] “Cripep docetaxel clinical trial phase I,” can be found under <https://clinicaltrials.gov/ct2/show/NCT02442531>, **n.d.**
- [64] P. M. Loadman, M. C. Bibby, J. A. Double, W. M. Al-Shakhaa, R. Duncan, *Clin. Cancer Res.* **1999**, *5*, 3682–3688.

- [65] J. Kopeček, P. Kopečková, T. Minko, Z.-R. Lu, *Eur. J. Pharm. Biopharm.* **2000**, *50*, 61–81.
- [66] J. Kopeček, P. Kopečková, *Adv. Drug Deliv. Rev.* **2010**, *62*, 122–149.
- [67] L. W. Seymour, D. R. Ferry, D. J. Kerr, D. Rea, M. Whitlock, R. Poyner, C. Boivin, S. Hesselewood, C. Twelves, R. Blackie, et al., *Int. J. Oncol.* **2009**, *34*, 1629–1636.
- [68] S. Etezeadi, S. N. Ekdawi, C. Allen, *Adv. Drug Deliv. Rev.* **2015**, *91*, 7–22.
- [69] A. Wicki, D. Witzigmann, V. Balasubramanian, J. Huwyler, *J. Control. Release* **2015**, *200*, 138–157.
- [70] P. Ma, R. J. Mumper, *J. Nanomed. Nanotechnol.* **2013**, *4*, 1000164.
- [71] N. Kamaly, Z. Y. Xiao, P. M. Valencia, A. F. Radovic-Moreno, O. C. Farokhzad, *Chem. Soc. Rev.* **2012**, *41*, 2971–3010.
- [72] X. Pang, H. L. Du, H. Q. Zhang, Y. J. Zhai, G. X. Zhai, *Drug Discov. Today* **2013**, *18*, 1316–1322.
- [73] M. Srinivasarao, C. V. Galliford, P. S. Low, *Nat. Rev. Drug Discov.* **2015**, *14*, 203–219.
- [74] C. A. Schutz, L. Juillerat-Jeanneret, H. Mueller, I. Lynch, M. Riediker, *Nanomedicine* **2013**, *8*, 449–467.
- [75] K. Ulbrich, K. Hola, V. Subr, A. Bakandritsos, J. Tucek, R. Zboril, *Chem. Rev.* **2016**, *116*, 5338–5431.
- [76] R. Williams, *Expert. Opin. Investig. Drugs* **2015**, *24*, 95–110.
- [77] M. S. Dennis, H. Jin, D. Dugger, R. Yang, L. McFarland, A. Ogasawara, S. Williams, M. J. Cole, S. Ross, R. Schwall, *Cancer Res.* **2007**, *67*, 254–261.
- [78] C. von Roemeling, W. Jiang, C. K. Chan, I. L. Weissman, B. Y. S. Kim, *Trends Biotechnol.* **2016**.
- [79] J. C. Kraft, J. P. Freeling, Z. Wang, R. J. Ho, *J. Pharm. Sci.* **2014**, *103*, 29–52.
- [80] D. Mahalingam, J. J. Nemunaitis, L. Malik, J. Sarantopoulos, S. Weitman, K. Sankhala, J. Hart, A. Kousba, N. S. Gallegos, G. Anderson, et al., *Cancer Chemother. Pharmacol.* **2014**, *74*, 1241–1250.
- [81] P. D. Senter, *Curr. Opin. Chem. Biol.* **2009**, *13*, 235–244.
- [82] C. Peters, S. Brown, *Biosci. Rep.* **2015**, *35*, 1–20.
- [83] P. Polakis, *Pharmacol. Rev.* **2016**, *68*, 3–19.
- [84] L. Buckel, E. N. Savariar, J. L. Crisp, K. A. Jones, A. M. Hicks, D. J. Scanderbeg, Q. T. Nguyen, J. K. Sicklick, A. M. Lowy, R. Y. Tsien, et al., *Cancer Res.* **2015**, *75*, 1376–1387.
- [85] R. A. de Claro, K. McGinn, V. Kwitkowski, J. Bullock, A. Khandelwal, B. Habtemariam, Y. Ouyang, H. Saber, K. Lee, K. Koti, et al., *Clin. Cancer Res.* **2012**, *18*, 5845–5849.
- [86] M. Lopus, E. Oroudjev, L. Wilson, S. Wilhelm, W. Widdison, R. Chari, M. A. Jordan, *Mol. Cancer Ther.* **2010**, *9*, 2689–2699.
- [87] R. V Chari, M. L. Miller, W. C. Widdison, *Angew. Chem. Int. Ed. Engl.* **2014**, *53*, 3796–3827.
- [88] “FDA Approval for Brentuximab Vedotin,” can be found under <https://www.cancer.gov/about-cancer/treatment/drugs/fda-brentuximabvedotin>, **2016**.
- [89] L. Ducry, B. Stump, *Bioconjug. Chem.* **2010**, *21*, 5–13.
- [90] G. D. Lewis Phillips, G. Li, D. L. Dugger, L. M. Crocker, K. L. Parsons, E. Mai, W. A. Blattler, J. M. Lambert, R. V Chari, R. J. Lutz, et al., *Cancer Res.* **2008**, *68*, 9280–9290.
- [91] I. Krop, E. P. Winer, *Clin. Cancer Res.* **2014**, *20*, 15–20.
- [92] J. G. Berdeja, *Front. Biosci.* **2014**, *19*, 163–170.
- [93] P. M. LoRusso, D. Weiss, E. Guardino, S. Girish, M. X. Sliwkowski, *Clin. Cancer Res.* **2011**, *17*, 6437–6447.
- [94] A. Younes, N. L. Bartlett, J. P. Leonard, D. A. Kennedy, C. M. Lynch, E. L. Sievers, A. Forero-Torres, *N. Engl. J. Med.* **2010**, *363*, 1812–1821.
- [95] H. L. Perez, P. M. Cardarelli, S. Deshpande, S. Gangwar, G. M. Schroeder, G. D. Vite, R. M. Borzilleri, *Drug. Discov. Today* **2014**, *19*, 869–881.
- [96] G. Casi, D. Neri, *J. Med. Chem.* **2015**, *58*, 8751–8761.
- [97] G. A. Pietersz, K. Krauer, *J. Drug Target* **1994**, *2*, 183–215.
- [98] S. Panowski, S. Bhakta, H. Raab, P. Polakis, J. R. Junutula, in *MABs*, Taylor & Francis, **2014**, pp. 34–45.
- [99] N. J. Boylan, W. Zhou, R. J. Proos, T. J. Tolbert, J. L. Wolfe, J. S. Laurence, *Bioconjug. Chem.* **2013**, *24*, 1008–1016.
- [100] A. M. Wu, P. D. Senter, *Nat. Biotechnol.* **2005**, *23*, 1137–1146.
- [101] R. V Chari, *Acc. Chem. Res.* **2008**, *41*, 98–107.
- [102] X. Wu, I. Ojima, *Curr. Med. Chem.* **2004**, *11*, 429–438.
- [103] A. Mullard, *Nat. Rev. Drug Discov.* **2013**, *12*, 329–332.

- [104] D. A. Bergstrom, N. Bodyak, A. Yurkovetskiy, P. U. Park, M. DeVit, M. Yin, "A novel, highly potent HER2-targeted antibody-drug conjugate (ADC) for the treatment of low HER2-expressing tumors and combination with trastuzumab-based regimens in HER2-driven tumors," can be found under http://www.mersana.com/sites/default/files/files/XMT-1522 AACR Poster FOR DISTRIBUTION_0.PDF, **2015**.
- [105] D. A. Bergstrom, N. Bodyak, A. Yurkovetskiy, P. U. Park, M. DeVit, M. Yin, L. Poling, J. D. Thomas, D. Gumerov, D. Xiao, *Cancer Res* **2015**, *75*, LB-231-LB-231.
- [106] M. Tran, B. Zhou, P. L. Pettersson, M. J. Gonzalez, S. P. Mayfield, *Biotechnol. Bioeng* **2009**, *104*, 663–673.
- [107] Y. Nakamura, S. Inomata, M. Ebine, Y. Manabe, I. Iwakura, M. Ueda, *Org. Biomol. Chem* **2011**, *9*, 83–85.
- [108] S. Tamura, S. Inomata, M. Ebine, T. Genji, I. Iwakura, M. Mukai, M. Shoji, T. Sugai, M. Ueda, *Bioorg. Med. Chem. Lett* **2013**, *23*, 188–193.
- [109] K. Mikuni, K. Nakanishi, K. Hara, W. Iwatani, T. Amano, K. Nakamura, Y. Tsuchiya, H. Okumoto, T. Mandai, *Biol. Pharm. Bull* **2008**, *37*, 1155–1158.
- [110] E. Vlashi, L. E. Kelderhouse, J. E. Sturgis, P. S. Low, *ACS Nano* **2013**, *7*, 8573–8582.
- [111] R. K. Jain, T. Stylianopoulos, *Nat. Rev. Clin. Oncol* **2010**, *7*, 653–664.
- [112] B. Wang, C. V. Galliford, P. S. Low, *Nanomedicine* **2014**, *9*, 313–330.
- [113] M. E. Fox, F. C. Szoka, J. M. J. Frechet, *Acc. Chem. Res* **2009**, *42*, 1141–1151.
- [114] C. P. Leamon, M. A. Parker, I. R. Vlahov, L. C. Xu, J. A. Reddy, M. Vetzel, N. Douglas, *Bioconjug. Chem* **2002**, *13*, 1200–1210.
- [115] J. J. Yang, S. A. Kularatne, X. Chen, P. S. Low, E. Wang, *Mol. Pharm* **2012**, *9*, 310–317.
- [116] R. Kurzrock, N. Gabrail, C. Chandhasin, S. Moulder, C. Smith, A. Brenner, K. Sankhala, A. Mita, K. Elian, D. Bouchard, et al., *Mol. Cancer Ther* **2012**, *11*, 308–316.
- [117] A. Regina, M. Demeule, C. Che, I. Lavallee, J. Poirier, R. Gabathuler, R. Beliveau, J. P. Castaigne, *Br. J. Pharmacol* **2008**, *155*, 185–197.
- [118] R. Tong, J. Cheng, *Angew. Chem. Int. Ed. Engl* **2008**, *47*, 4830–4834.
- [119] B. Louage, L. Nuhn, M. D. Risseuw, N. Vanparijs, R. De Coen, I. Karalic, S. Van Calenbergh, B. G. De Geest, *Angew. Chem. Int. Ed. Engl* **2016**, *55*, 11791–11796.
- [120] G. Winter, A. D. Griffiths, R. E. Hawkins, H. R. Hoogenboom, *Annu. Rev. Immunol* **1994**, *12*, 433–455.
- [121] N. Krall, J. Scheuermann, D. Neri, *Angew. Chem. Int. Ed. Engl* **2013**, *52*, 1384–1402.
- [122] J.-P. Dagher, C. Zambaldo, M. Ciobanu, P. Morieux, S. Barluenga, N. Winssinger, *Chem. Sci* **2014**, *6*, 739–744.
- [123] A. F. Fullo, K. J. Fitzgerald, V. Muthusamy, M. Liu, C. Yuan, M. Huang, M. Kim, A. E. Cho, D. A. Spiegel, *Angew. Chem. Int. Ed. Engl* **2016**, *55*, 3642–3646.
- [124] A. Mullard, *Nature* **2016**, *530*, 367–369.
- [125] R. M. Franzini, D. Neri, J. Scheuermann, *Acc. Chem. Res* **2014**, *47*, 1247–1255.
- [126] A. I. Chan, L. M. McGregor, D. R. Liu, *Curr. Opin. Chem. Biol* **2015**, *26*, 55–61.
- [127] D. L. Stirland, J. W. Nichols, S. Miura, Y. H. Bae, *J. Control. Release* **2013**, *172*, 1045–1064.
- [128] S. Wilhelm, A. J. Tavares, Q. Dai, S. Ohta, J. Audet, H. F. Dvorak, W. C. W. Chan, *Nat. Rev. Mater* **2016**, *1*, 1–12.
- [129] S. E. McNeil, *Nat. Rev. Mater* **2016**, *1*, 16073.
- [130] S. Wilhelm, A. J. Tavares, W. C. W. Chan, *Nat. Rev. Mater* **2016**, *1*, 16074.
- [131] D. Brambilla, P. Luciani, J. C. Leroux, *J. Control. Release* **2014**, *190*, 9–14.
- [132] N. V. Rajeshkumar, S. Yabuuchi, S. G. Pai, Z. Tong, S. Hou, S. Bateman, D. W. Pierce, C. Heise, D. D. Von Hoff, A. Maitra, et al., *Br. J. Cancer* **2016**, *115*, 442–453.
- [133] C. H. Heldin, K. Rubin, K. Pietras, A. Ostman, *Nat. Rev. Cancer* **2004**, *4*, 806–813.
- [134] F. Gremontprez, B. Descamps, A. Izmer, C. Vanhove, F. Vanhaecke, O. De Wever, W. Ceelen, *Oncotarget* **2015**, *6*, 29889–29900.
- [135] K. P. Olive, M. A. Jacobetz, C. J. Davidson, A. Gopinathan, D. McIntyre, D. Honess, B. Madhu, M. A. Goldgraben, M. E. Caldwell, D. Allard, et al., *Science (80-.)* **2009**, *324*, 1457–1461.
- [136] K.-J. Lou, *SciBX* **2014**, *7*.
- [137] A. S. Mikhail, C. Allen, *J. Control. Release* **2009**, *138*, 214–223.
- [138] A. S. Narang, S. Varia, *Adv. Drug Deliv. Rev* **2011**, *63*, 640–658.
- [139] A. I. Minchinton, I. F. Tannock, *Nat. Rev. Cancer* **2006**, *6*, 583–592.

-
- [140] T. Lammers, F. Kiessling, W. E. Hennink, G. Storm, *J. Control. Release* **2012**, *161*, 175–187.
- [141] Y. H. Bae, K. Park, *J. Control. Release* **2011**, *153*, 198–205.
- [142] M. Hidalgo, F. Amant, A. V. Biankin, E. Budinska, A. T. Byrne, C. Caldas, R. B. Clarke, S. de Jong, J. Jonkers, G. M. Maelandsmo, et al., *Cancer Discov.* **2014**, *4*, 998–1013.
- [143] “Pilot Study to Determine Biodistribution of MM-398 and Feasibility of Ferumoxytol as a Tumor Imaging Agent,” can be found under <https://clinicaltrials.gov/ct2/show/NCT01770353>, **2012**.
- [144] “FDA Approves Onivyde Combo Regimen for Advanced Pancreatic Cancer,” can be found under <http://journals.lww.com/oncology-times/blog/fdaactionsandupdates/pages/post.aspx?PostID=124>, **2015**.
- [145] E. L. Trimble, S. Thompson, M. C. Christian, L. Minasian, *Oncologist* **2008**, *13*, 403–409.
- [146] C. Khanna, K. Hunter, *Carcinogenesis* **2005**, *26*, 513–523.
- [147] A. Schroeder, D. A. Heller, M. M. Winslow, J. E. Dahlman, G. W. Pratt, R. Langer, T. Jacks, D. G. Anderson, *Nat. Rev. Cancer* **2012**, *12*, 39–50.
- [148] O. J. Becher, E. C. Holland, *Cancer Res.* **2006**, *66*, 3355–3359.
- [149] K. K. Frese, D. A. Tuveson, *Nat. Rev. Cancer* **2007**, *7*, 645–658.
- [150] H. Gao, J. M. Korn, S. Ferretti, J. E. Monahan, Y. Wang, M. Singh, C. Zhang, C. Schnell, G. Yang, Y. Zhang, et al., *Nat. Med.* **2015**, *21*, 1318–1325.
- [151] S. Aparicio, M. Hidalgo, A. L. Kung, *Nat. Rev. Cancer* **2015**, *15*, 311–316.
- [152] R. K. Jain, *Cancer Res.* **1988**, *48*, 2641–2658.
- [153] J. J. Tentler, A. C. Tan, C. D. Weekes, A. Jimeno, S. Leong, T. M. Pitts, J. J. Arcaroli, W. A. Messersmith, S. G. Eckhardt, *Nat. Rev. Clin. Oncol.* **2012**, *9*, 338–350.
- [154] G. T. Tietjen, W. M. Saltzman, *Sci. Transl. Med.* **2015**, *7*, 314fs47.
- [155] T. Lammers, F. Kiessling, M. Ashford, W. Hennink, D. Crommelin, G. Strom, *Nat. Rev. Mater.* **2016**, *1*, 16069.

chapter 9

summary and general conclusions

This PhD dissertation focused on the design of polymer-based carrier systems to enhance both the solubility and the delivery of taxane anti-cancer drugs. **PART I** of the thesis comprises a general introduction to scope the need for advanced chemotherapy. **Chapter 1** reports on the current treatment modalities for cancer applied in clinic. In particular, anti-cancer drug treatment is described along with the issues of conventional chemotherapy, to illustrate the need for safer and more efficacious anti-cancer drug delivery. Next, the rationale and assets of nanomedicines (i.e. passive and active targeting, bioresponsive drug release) are explained, outlining a window of opportunity for the materials chemistry field to come up with alternative formulation strategies for improved anti-cancer drug delivery. **Chapter 2** provides a concise background on taxane drugs and their first approved commercial formulations. Both the discovery and early development of paclitaxel (PTX) and docetaxel (DTX) are sketched. Next, an overview is given on the sourcing and manufacturing processes of taxanes. The biological mechanism of action is covered. Finally, the physicochemical features of Taxol and Taxotere are elucidated, along with their clinical translation and toxicity issues.

PART II covers the experimental work on the design of two polymeric nanocarrier systems for physical drug entrapment. Though PTX was used within the scope of this dissertation, note that both systems could also be exploited for physical encapsulation of other hydrophobic drugs. **Chapter 3** describes the formulation of PTX-loaded poly(glycerol sebacate) (PGS) nanoparticles. To obtain the latter, a straightforward formulation procedure was developed which involves co-dissolution of PGS and PTX in ethanol (EtOH) and subsequent solvent displacement in water (H₂O). The biocompatibility of all excipients (i.e. PGS, EtOH and H₂O) is a crucial asset for biomedical applications. Dynamic light scattering (DLS) confirmed PTX/PGS particles within the 200 nm size range with narrow dispersity and high colloidal stability in physiological aqueous medium. Additionally, the critical

aggregation concentration (CAC) of the nanoparticles was very low (i.e. $< 1 \mu\text{g/mL}$), allowing substantial dilution without particle disintegration. Flow cytometry (FACS) and confocal microscopy confirmed the capability of PGS nanoparticles of delivering hydrophobic compounds into cancer cells *in vitro*. Finally, PTX/PGS nanoparticles showed equal *in vitro* biological performance compared to 2 commercial, advanced PTX formulations (i.e. Abraxane and Genexol-PM), whilst empty PGS nanoparticles confirmed the expected high cytocompatibility. These promising *in vitro* data propose key incentives for further *in vivo* evaluation. So far however, only a modest PTX concentration (i.e. 0.5 mg/mL) could be obtained in the developed formulation. Future optimization would be required to further increase the drug loading capacity of the system, allowing to formulate sufficient doses of PTX into a smaller formulation volume. The latter would render the administration (i.e. intravenous, intraperitoneal) of PTX/PGS nanoparticles more feasible in clinical setting.

Chapter 4 reports on the systematic design of amphiphilic, acid-degradable, block copolymer nanoparticles, synthesized by reversible addition-fragmentation chain transfer (RAFT) polymerization. To obtain a bioresponsive, acid-sensitive hydrophobic block, a hydrophobic, ketal-functionalized acrylate monomer (i.e. (2,2-dimethyl-1,3-dioxolane-4-yl)methyl acrylate (DMDMA)) was copolymerized with a hydrophilic monomer (i.e. hydroxyethyl acrylate (HEA)). The DMDMA:HEA molar ratio was varied to obtain 5 different block copolymers with increasing amount of DMDMA incorporated in the hydrophobic block. Next, the influence of the hydrophobic block design on the physicochemical properties was extensively investigated. A DMDMA content higher than 11 mol % results in self-assembly into nanoparticles in aqueous medium. All nanoparticles showed substantial colloidal stability in phosphate buffered saline (PBS), with sizes and CAC ranging from 23 to 338 nm and from 241 to 10 $\mu\text{g/mL}$, respectively, proportional to the block copolymer DMDMA content. Under acidic conditions, the nanoparticles decomposed into soluble unimers of which the decomposition rate was inversely proportional to the block copolymer DMDMA content. FACS and confocal microscopy confirmed *in vitro* the utility of the designed nanoparticles as carrier vehicle for the delivery of hydrophobic compounds into cancer cells. The block copolymers showed no intrinsic cytotoxicity. When loaded with PTX however, a significant decrease in cell viability was observed comparable to that of Abraxane and Genexol-PM. The main objective of this study was to deliver a proof-of-concept, demonstrating that RAFT polymerization is a valuable technique for designing well-defined, smart drug delivery carrier systems. However, this system cannot yet be reckoned suitable for further *in vivo* evaluation. Modifications in polymer design have to be considered to obtain nanoparticles with faster degradation kinetics at biologically more relevant pH-values (i.e. 5 – 6.5), to achieve higher drug loading and to ensure maintenance of

particle integrity upon substantial dilution in complex biological matrices (e.g. blood). Promising strategies to accomplish the latter include cross-linking strategies and chemically attaching the drug to the nanocarrier vehicle.

Chemical conjugation of drugs to a polymeric carrier is a highly acknowledged technique for designing advanced anti-cancer drug formulations. An important advantage of chemical conjugation over physical encapsulation is the possibility to more thoroughly restrict premature burst release and hence reduce side-effects.

PART III encompasses the second experimental section of the thesis, describing the design of taxane-polymer conjugates based on a grafting-from-drug RAFT approach. **Chapter 5** describes the first-generation of ester-based PTX-polymer prodrug conjugates developed by this approach. A RAFT chain transfer agent (CTA) was regioselectively conjugated to the C₂ hydroxyl group of PTX. The latter is crucial for the biological activity of PTX. This drug-functionalized RAFT CTA was subsequently exploited for polymerization of the hydrophilic monomer *N,N*-dimethylacrylamide (DMA), yielding well-defined, amphiphilic PTX-polymer prodrug conjugates with high drug loading (i.e. 20 wt % PTX) and water-solubility (i.e. ≥ 30 mg/mL conjugate). When dispersed in PBS, stable micellar particles were detected by DLS, 27 nm in size and with narrow dispersity. The relatively high CAC of the nanoparticles (i.e. 102 $\mu\text{g/mL}$) implicates that the conjugate will most likely switch from micellar to water-soluble state upon aqueous dilution. Additional modification of the obtained conjugate was demonstrated by ω -end post-functionalization with a fluorescent tracer molecule. *In vitro* experiments showed that this conjugate is readily taken up into endosomes where native PTX is efficiently cleaved off and subsequently reaches its subcellular target (i.e. microtubules), as confirmed by a similar cytotoxicity profile compared to Abraxane and Genexol-PM which are based on mere physical encapsulation. These results encourage further evaluation *in vivo*, especially because the high drug loading allows for the administration sufficient PTX doses. Selecting the right mouse model will be crucial. Conventional subcutaneous primary tumor models might not illustrate the full potential of this system, as the water-soluble, low molecular weight conjugates will most likely not exert significant passive targeting, mediated by the enhanced permeability and retention (EPR) effect. A clinically more relevant model (i.e. orthotopic/metastatic mouse model) might be more suitable to investigate whether, compared to nanoparticles, these small soluble conjugates can more efficiently penetrate tumor tissue, featured by poor vascularization and/or by significantly less fenestrated endothelia. For this purpose, it will be vital to collaborate with research groups, disposing of the required expertise.

Chapter 6 reports on second-generation PTX-polymer conjugates based on a similar approach as described in Chapter 5. To obtain conjugates with acid-sensitive release properties, the gained expertise on acetal/ketal synthesis in Chapter 4 was further exploited. PTX was linked to a RAFT CTA either through a cyclic or through a

linear acetal moiety. In contrast to the regioselective esterification of PTX reported in Chapter 5, direct acetalization of PTX can occur at 2 sites (i.e. either at the C₂ or at the C₇ hydroxyl group), yielding 2 regio-isomers of PTX-functionalized RAFT CTA. The isomers based on the cyclic acetal could be separated by silica gel chromatography, whilst the isomers based on the linear acetal could be used as regio-isomeric mixture for subsequent RAFT polymerization. The properties of the resulting PTX-polymer conjugates were in accordance to their first-generation counterparts in terms of polymer definition, drug loading and water-solubility. Both the first- and second-generation conjugates did not exert burst release in PBS, whether or not supplemented with 10 % fetal bovine serum (FBS). At pH 4 and 5, significant release of PTX was observed for the linear acetal-based PTX-polymer conjugate, whilst the cyclic acetal-based and first-generation conjugates showed limited and no release, respectively. Viability was decreased *in vitro* to the same extent as for the first-generation conjugates, however higher concentrations were required (i.e. roughly by factor 10² and 10³ for the linear and cyclic acetal-based conjugates, respectively). These data clearly indicate that the linear acetal-based conjugates are more acid-sensitive than their cyclic acetal-based counterparts, and that the release of PTX from the first-generation ester-based conjugates is predominantly occurring through an enzymatically catalyzed process.

As both the first- and second-generation PTX-polymer conjugates most likely form soluble unimers upon aqueous dilution, long circulation kinetics and EPR-mediated passive targeting are not to be expected *in vivo*. On the other hand, swift renal clearance of small hydrophilic molecules can be a great tool to minimize side-effects by the fraction of the dose that has not reached its target site. To still obtain efficient accumulation of short half-life PTX-conjugates in tumor tissue (less susceptible to EPR effect), active targeting strategies need to be considered. **Chapter 7** comprises the design of DTX-polymer prodrug conjugates, equipped with an active targeting ligand. Using the same approach as described in Chapter 5, a DTX-functionalized RAFT CTA was synthesized and used to obtain highly defined DTX-polymer prodrug conjugates. Additionally, S,S-2-(3-(5-amino-1-carboxypentyl)-ureido)-pentanedioic acid (ACUPA) was synthesized. The latter possesses high binding affinity towards prostate specific membrane antigen (PSMA), a surface receptor often overexpressed by malignant prostate cells. ACUPA was further modified with a maleimide moiety and subsequently used for post-modification of the DTX-polymer prodrug conjugates. Successful synthesis of DTX-polymer-ACUPA prodrug conjugates was confirmed by size exclusion chromatography (SEC) and nuclear magnetic resonance (NMR) spectroscopy. Fluorescently labeled DTX-polymer-ACUPA analogues were prepared by incorporating a small fraction of fluorescent monomer during the polymerization step. DTX-polymer prodrug conjugates, post-modified with a non-targeting moiety were prepared as control. FACS showed that the DTX-polymer-ACUPA prodrug conjugates interact to a higher extent *in vitro* with

PSMA-positive prostate cancer cells compared to the control. Complementary *in vitro* experiments (i.e. confocal microscopy, competitive binding assays, MTT) should further clarify whether DTX-polymer-ACUPA, compared to the control, can efficiently deliver higher doses of DTX to PSMA-positive prostate cancer cells by receptor-mediated endocytosis and if this translates into higher and more specific cytotoxicity.

In summary, this PhD thesis has explored various design, synthesis and formulation strategies for obtaining advanced, passively or active targeted polymeric taxane formulations. Though solvent displacement is a very simple technique that enables formulation of nanoparticles with narrow size dispersity, achieving sufficient drug loading proved to be challenging. Throughout the experimental part of this thesis, RAFT has proven its value as highly controllable and chemically versatile polymerization technique in designing well-defined, bioresponsive drug delivery systems. The grafting-from-drug approach in particular has shown great promise. This straightforward synthesis strategy results in polymeric taxane prodrug conjugates with high drug loading and limited burst release *in vitro*. The successful post-modification with an active targeting ligand further highlights the opportunities of the approach. The small size of these soluble conjugates could allow for efficient penetration into (metastatic) tumor tissue that is less susceptible to passive targeting by EPR. This can be investigated *in vivo*, though by careful selection of an appropriate and clinically relevant mouse model. Future *in vitro* and *in vivo* experiments will clarify whether this approach enables active targeted drug delivery. Overall, this thesis encompasses valuable insights for future rational design of advanced polymeric anti-cancer drug delivery systems based on physical encapsulation and chemical conjugation.

hoofdstuk 9

samenvatting en algemene conclusies

Deze thesis heeft zich gefocust op het design van polymeer-gebaseerde dragersystemen met als doel zowel de oplosbaarheid als de afgifte van taxaan anti-kankergeneesmiddelen te verbeteren. **DEEL I** van deze thesis omvat een algemene inleiding waarbij de behoefte aan geavanceerde chemotherapie in kaart wordt gebracht. **Hoofdstuk 1** beschrijft de therapieën tegen kanker die heden in de kliniek worden aangewend. De nadruk wordt vooral gelegd op conventionele chemotherapie en de problematiek met betrekking tot toxiciteit. Zo wordt ook de nood aan een veiligere en efficiëntere afgifte van anti-kankergeneesmiddelen geïllustreerd. Vervolgens worden de basisbegrippen en troeven van nanomedicijnen (bijvoorbeeld passieve en actieve 'targeting', bioresponsieve vrijstelling van geneesmiddelen) uiteengezet en aldus de mogelijkheden van dit onderzoeksveld om alternatieve formulatiestrategieën te ontwikkelen voor verbeterde afgifte van anti-kankergeneesmiddelen. In **Hoofdstuk 2** wordt de achtergrond van taxanen geschetst, samen met de eerste formulaties die hiervan op de markt werden gebracht. Eerst wordt de ontdekking en vroegtijdige ontwikkeling van paclitaxel (PTX) en docetaxel (DTX) beschreven. Vervolgens wordt een overzicht gegeven van de verschillende bronnen, grondstoffen en technieken voor de productie van taxanen. Het werkingsmechanisme wordt uitgelegd en ten slotte worden ook de fysicochemische eigenschappen van Taxol en Taxotere opgegeven, samen met het gebruik van deze formulaties in de kliniek en de gerelateerde neveneffecten.

DEEL II beschrijft het verrichte experimentele werk omtrent de ontwikkeling van twee polymeer-gebaseerde, nanoscopische dragersystemen voor fysische encapsulatie van geneesmiddelen. Hoewel in deze thesis telkens PTX werd gebruikt, kunnen beide systemen in de toekomst ook nog met andere hydrofobe geneesmiddelen getest worden. In **Hoofdstuk 3** wordt de formulatie van poly(glycerol sebacate) (PGS) nanopartikels beschreven. Hiervoor werd een eenvoudig formulatieprotocol opgesteld op basis van 'solvent displacement'. PTX en PGS

werden samen opgelost in ethanol (EtOH) en vervolgens werd deze oplossing druppelsgewijs en onder roeren toegevoegd aan water (H₂O). Een belangrijke troef van deze formulatie is de biocompatibiliteit van de gebruikte excipiëntia (PGS, EtOH en H₂O), wat cruciaal is voor systemen die bestemd zijn voor biomedische toepassing. Door middel van dynamische lichtverstrooiing (DLS) werden partikels met afmetingen niet groter dan 200 nm gedetecteerd, die gekenmerkt worden door een geringe polydispersiteit en hoge colloïdale stabiliteit in fysiologisch waterig midden. Bovendien werd een zeer lage kritische aggregatie concentratie (CAC) gemeten (< 1 µg/mL). Dit wijst erop dat de gevormde partikels niet snel uiteen zullen vallen bij substantiële verdunning. Flow cytometrie (FACS) en confocale microscopie hebben aangetoond dat hydrofobe componenten na encapsulatie in PGS nanopartikels efficiënt kunnen worden afgegeven aan kankercellen *in vitro*. Ten slotte werd via MTT assay vastgesteld dat PTX/PGS nanopartikels de viabiliteit van kankercellen in dezelfde mate kunnen inperken als 2 commerciële, geavanceerde PTX formulaties (Abraxane en Genexol-PM). Zoals verwacht werd geen intrinsieke cytotoxiciteit vastgesteld voor onbeladen PGS nanopartikels. Deze *in vitro* data vormen een goed onderbouwde basis voor verdere *in vivo* evaluatie. Echter, tot op heden kon enkel een matige PTX concentratie (0.5 mg/mL) verkregen worden in de ontwikkelde formulatie. Het systeem vereist dus nog verdere optimalisatie om de geneesmiddelbelading te verhogen. Op die manier kan een klein volume formulatie over een adequate dosis PTX beschikken, wat de formulatie toegankelijker maakt voor toediening (intraveneus, intraperitoneaal) aan patiënten.

Hoofdstuk 4 beschrijft het systematische design van amfifiele, zuur-degradeerbare, blok copolymeer nanopartikels, gesynthetiseerd via 'reversible addition-fragmentation chain transfer' (RAFT) polymerisatie. Om een bioresponsief, zuurgevoelig hydrofoob blok te verkrijgen, werd een hydrofoob, ketal-gefunctionaliseerd acrylaat monomeer ((2,2-dimethyl-1,3-dioxolane-4-yl)methyl acrylaat (DMDMA)) gecopolymeriseerd met een hydrofiel monomeer (hydroxyethyl acrylaat (HEA)). Door de DMDMA:HEA molaire ratio te variëren, werden 5 verschillende blok copolymeren gesynthetiseerd met een toenemende fractie DMDMA in het hydrofobe blok. Vervolgens werd de invloed van de samenstelling van het hydrofobe blok op de fysicochemische eigenschappen van het polymeer onderzocht. Polymeren met een DMDMA fractie hoger dan 11 mol % vormen spontaan nanopartikels in waterig midden. De nanopartikels vertoonden hoge colloïdale stabiliteit in fosfaat gebufferde zoutoplossing (PBS). De grootte en de CAC van de partikels varieerde respectievelijk van 23 tot 338 nm en van 241 tot 10 µg/mL, evenredig met de molaire fractie DMDMA. Onder zure condities degradeerden de nanopartikels tot wateroplosbare unimeren. De degradatiesnelheid was omgekeerd evenredig met de molaire fractie DMDMA. FACS en confocale microscopie hebben *in vitro* aangetoond dat de ontwikkelde nanopartikels kunnen aangewend worden als dragersysteem voor efficiënte afgifte van hydrofobe geneesmiddelen aan kankercellen. De blok copolymeren zelf vertoonden geen

intrinsieke cytotoxiciteit. Echter, wanneer de nanopartikels werden beladen met PTX, kon de viabiliteit van kankercellen in dezelfde mate gereduceerd worden als met Abraxane en Genexol-PM. Het doel van deze studie was vooral om na te gaan of RAFT toelaat om gedefinieerde, responsieve dragersystemen voor geneesmiddelafgifte te ontwikkelen. In dit opzet werd geslaagd. Echter, in dit stadium is het systeem nog niet geschikt voor verdere *in vivo* evaluatie. Aanpassingen in polymeerdesign moeten worden overwogen om nanopartikels te verkrijgen met een snellere degradatiekinetiek bij fysiologisch relevantere pH-waarden (5 – 6.5), met een hogere geneesmiddelbelading en met behoud van partikelintegriteit bij substantiële verdunning. Dit zou kunnen worden verwezenlijkt door de nanopartikels te crosslinken enerzijds en anderzijds door het geneesmiddel chemisch te koppelen aan het dragersysteem.

Chemische conjugatie van geneesmiddelen aan polymere dragers is een erkende techniek voor de ontwikkeling van geavanceerde formulaties voor anti-kankergeneesmiddelen. Door middel van chemische conjugatie kan versnelde geneesmiddelvrijstelling in de bloedbaan in grotere mate ingeperkt worden in vergelijking met fysische encapsulatie, wat toelaat om ongewenste neveneffecten verder te onderdrukken. **DEEL III** omvat het tweede experimentele luik van deze thesis en beschrijft een nieuwe designstrategie voor de aanmaak van taxaan-polymeer conjugaten op basis van een 'grafting-from-drug' RAFT approach. In **Hoofdstuk 5** wordt de synthese en evaluatie van de 'eerste-generatie', ester-gebaseerde PTX-polymeer prodrug conjugaten beschreven. Een RAFT 'chain transfer agent' (CTA) werd regioselectief gekoppeld aan de C₂ hydroxyl groep van PTX. Deze is cruciaal voor de biologische activiteit van PTX. De PTX-gefunctionaliseerde RAFT CTA werd vervolgens aangewend voor de polymerisatie van het hydrofiële monomeer *N,N*-dimethylacrylamide (DMA). Gedefinieerde, amfifiele PTX-polymeer conjugaten werden verkregen met een hoge geneesmiddelbelading (20 wt % PTX) en wateroplosbaarheid (≥ 30 mg/mL conjugaat). Na dispergeren in PBS werden via DLS stabiele micellen gedetecteerd, met een grootte van 27 nm en een lage polydispersiteit. De relatief hoge CAC (102 μ g/mL) van de conjugaten impliceert dat deze micellen bij substantiële verdunning in waterig midden zullen uiteenvallen. Aanvullende modificatie werd verricht door ω -eindgroep post-functionaliseren met een fluorescente 'tracer' molecuul. *In vitro* experimenten hebben aangetoond dat de conjugaten snel door kankercellen worden opgenomen via endocytose. Vanuit deze endosomen kan PTX vrijgesteld worden en vervolgens zijn subcellulair doelwit (microtubuli) bereiken. De conjugaten vertoonden een gelijkaardig cytotoxiciteitsprofiel in vergelijking met systemen, gebaseerd op louter fysische encapsulatie (Abraxane en Genexol-PM). Deze resultaten vormen een goede basis voor verdere *in vivo* evaluatie, vooral omdat de hoge geneesmiddelbelading toelaat om een adequate dosis PTX toe te dienen. De keuze van een geschikt *in vivo* muismodel zal hierbij wel cruciaal zijn. Conventionele

muismodellen op basis van een primaire subcutane tumor kunnen mogelijks niet ten volle het potentieel van dit systeem vaststellen, omdat deze wateroplosbare conjugaten met laag molecuulgewicht niet in grote mate passief zullen accumuleren in tumorweefsel door middel van het 'enhanced permeability and retention' ('EPR') effect. Een klinisch relevanter model (orthotopisch/metastatisch muismodel) is mogelijks geschikter om te onderzoeken of deze kleine conjugaten in vergelijking met nanopartikels efficiënter zijn in het doordringen van tumorweefsel, dat gekenmerkt wordt door een beperkte doorbloeding en/of door fysiologisch normaal afgelijnd endotheel. Om deze proeven te kunnen verrichten zal het essentieel zijn om samen te werken met onderzoeksgroepen die beschikken over de nodige expertise.

Hoofdstuk 6 handelt over de ontwikkeling van 'tweede-generatie' PTX-polymeer conjugaten, gebaseerd op dezelfde approach zoals beschreven in Hoofdstuk 5. Er werd hiervoor gebruik gemaakt van de opgebouwde expertise omtrent acetal/ketal synthese, beschreven in Hoofdstuk 4, om conjugaten te verkrijgen met zuurgevoelige vrijstellingseigenschappen. PTX werd gekoppeld aan een RAFT CTA, zowel via een cyclische als via een lineaire acetalgroep. In tegenstelling tot de regioselectieve estervorming met PTX, beschreven in Hoofdstuk 5, kan rechtstreekse acetalisatie gebeuren op 2 posities van PTX: ofwel op de C₂ of op de C₇ hydroxyl groep. Deze chemische koppelingsreactie geeft dus aanleiding tot 2 regio-isomeren van PTX-gefunctionaliseerde RAFT CTA. De isomeren op basis van het cyclische acetal konden van elkaar gescheiden worden via silica gel chromatografie. De isomeren op basis van het lineaire acetal konden als regio-isomeer mengsel worden gebruikt in de daaropvolgende polymerisatiestap. De eigenschappen van de verkregen PTX-polymeer conjugaten waren in overeenstemming met deze van de 'eerste-generatie' conjugaten met betrekking tot polymeerdefinitie, geneesmiddelbelading en wateroplosbaarheid. Zowel de 'eerste-' als de 'tweede-generatie' conjugaten vertoonden geen versnelde vrijstelling in PBS, zowel in aan- als in afwezigheid van 10 % foetaal kalfsserum (FBS). Bij pH 4 en 5 werd een significante vrijstelling van PTX vastgesteld voor de conjugaten op basis van het lineaire acetal. Vrijstelling was beperkt en afwezig bij pH 4 en 5 voor de conjugaten op basis van het cyclische acetal en de 'eerste-generatie' conjugaten, respectievelijk. De celviabiliteit kon in dezelfde mate worden teruggedrongen als met de 'eerste-generatie' conjugaten, echter hogere concentraties waren vereist. Een concentratie, hoger met ongeveer factor 10² en 10³ was vereist voor de conjugaten op basis van het lineaire en cyclische acetal, respectievelijk. Deze data tonen duidelijk aan dat het lineaire acetal zuurgevoeliger is dan het cyclische acetal, en dat de vrijstelling van PTX uit de 'eerste-generatie' conjugaten, op basis van esterkoppeling, hoogst waarschijnlijk via een enzymatisch proces verloopt.

Wegens de kleine afmeting en hoge wateroplosbaarheid van deze conjugaten is het onwaarschijnlijk dat deze *in vivo* lang in de bloedbaan zullen circuleren en efficiënt via 'EPR' zullen accumuleren in tumorweefsel. Echter, vlotte renale klaring van de fractie geneesmiddel die het tumorweefsel niet bereikt, kan een belangrijke troef zijn voor reduceren van systemische neveneffecten. Om toch een adequate dosis van deze PTX-conjugaten met korte halfwaardetijd ter hoogte van tumorweefsel (minder onderhevig aan 'EPR' effect) te kunnen afgeven, moeten actieve 'targeting' strategieën overwogen worden. **Hoofdstuk 7** omvat het design van DTX-polymeer prodrug conjugaten, uitgerust met een ligand voor actieve 'targeting'. Door gebruik te maken van de designstrategie beschreven in Hoofdstuk 5, werd een DTX-gefunctionaliseerde RAFT CTA gesynthetiseerd en verder gebruikt voor de aanmaak van gedefinieerde DTX-polymeer prodrug conjugaten. Bovendien werd *S,S*-2-(3-(5-amino-1-carboxypentyl)-ureido)-pentanedioic acid (ACUPA) gesynthetiseerd. Dit ligand heeft een hoge bindingsaffiniteit voor prostaat specifiek membraan antigeen (PSMA), een receptor die tot overexpressie wordt gebracht door maligne prostaat kankercellen. ACUPA werd verder gemodificeerd met een maleimide eindgroep en vervolgens gebruikt voor de post-modificatie van de DTX-polymeer prodrug conjugaten. De synthese van ACUPA-gefunctionaliseerde DTX-polymeer prodrug conjugaten kon worden bevestigd via 'size exclusion' chromatografie (SEC) en nucleaire magnetische resonantie (NMR) spectroscopie. Fluorescent gelabelde analogen konden worden aangemaakt door een kleine fractie fluorescent monomeer mee te laten reageren tijdens de polymerisatiestap. Als controle werden DTX-polymeer prodrug conjugaten aangemaakt, gefunctionaliseerd met een eindgroep die niet specifiek bindt met PSMA. FACS heeft aangetoond dat de DTX-polymeer-ACUPA prodrug conjugaten in grotere mate interageren *in vitro* met PSMA-positieve prostaat kankercellen in vergelijking met de controle. Aanvullende *in vitro* experimenten (confocale microscopie, competitieve bindingsexperimenten, MTT) zullen moeten aantonen of DTX-polymeer-ACUPA, in vergelijking met de controle, al dan niet op efficiënte wijze hogere dosissen DTX kan afgeven aan PSMA-positieve prostaat kankercellen via receptor-gemedieerde endocytose en of dit leidt tot hogere en selectievere cytotoxiciteit.

Samengevat werden gedurende deze thesisperiode meerdere design-, synthese- en formulatiestrategieën onderzocht en uitgewerkt, met als doel geavanceerde polymere formulaties te ontwikkelen voor zowel passieve als actieve 'targeting' van taxaan anti-kankergeneesmiddelen. Ondanks de eenvoud van 'solvent displacement' en de hoge definitie van de partikels die met deze techniek werd verkregen, kon tot nu toe nog geen adequate geneesmiddelbelading worden verwezenlijkt. Er werd aangetoond dat RAFT een controleerbare en chemische veelzijdige polymerisatietechniek is voor het ontwerpen van gedefinieerde, bioresponsieve dragersystemen voor geneesmiddelen. De 'grafting-from-drug' approach blijkt veelbelovend te zijn. Deze eenvoudige synthese strategie

geeft aanleiding tot polymere taxaan prodrug conjugaten met hoge geneesmiddelbelading en beperkte versnelde vrijstelling *in vitro*. De succesvolle post-modificatie met een ligand voor actieve 'targeting' benadrukt verder de veelzijdigheid van deze syntheseroute. De kleine afmeting van deze wateroplosbare conjugaten kan ertoe leiden dat deze efficiënter kunnen binnendringen in (metastatisch) tumorweefsel dat minder onderhevig is aan passieve 'targeting' door 'EPR'. Dit kan worden nagegaan *in vivo*, op voorwaarde dat hiervoor een geschikt en klinisch relevant muismodel wordt gebruikt. Toekomstige *in vitro* en *in vivo* experimenten zullen verder moeten uitmaken of deze approach ook geneesmiddelen selectiever kan afgeven via actieve 'targeting'. Kortom, in deze thesis werden waardevolle inzichten verschaft die van belang kunnen zijn voor toekomstig rationeel design van geavanceerde polymere dragersystemen voor fysische encapsulatie en chemische conjugatie van anti-kankergeneesmiddelen.

curriculum vitae

personal information

surname	Louage
first names	Benoit Claude Noël
nationality	Belgian
date/place of birth	June 22 nd 1989/Kortrijk
domicile	Vinkestraat 77, 8560 Wevelgem, Belgium benoit.louage@gmail.com http://linkedin.com/in/benoit-louage-859a4711a +32 494 68 23 43
work address	Faculty of Pharmaceutical Sciences Ottergemsesteenweg 460, 9000 Ghent, Belgium benoit.louage@UGent.be +32 9 264 80 82
hobbies/interests	travel, gastronomy, design, architecture, history, culture, art, music, movies, sports (fitness, swimming, golf)

secondary education

2001 – 2005	Latin – Maths (6 h) Sint-Pauluscollege, Wevelgem, Belgium
2005 – 2007	Maths (8 h) - Sciences Sint-Aloysiuscollege, Menen, Belgium

higher education

2007 – 2010

Bachelor in Pharmaceutical Sciences

Graduated magna cum laude

Faculty of Pharmaceutical Sciences, Ghent University, Belgium

2010 – 2012

Master in Drug Development

Graduated magna cum laude

Faculty of Pharmaceutical Sciences, Ghent University, Belgium

January – May 2011: master thesis

*Sample preparation development for LC-MS/MS folate analysis
in plasma and red blood cells*

Promotor: Prof. Dr. PharmD. W. Lambert

January – May 2012: pharmacy internship

Apotheek Crocodile/AZ Groeninge, Kortrijk, Belgium

PhD experience

2012 – present

Design, synthesis and evaluation of advanced polymeric taxane formulations

Promotor: Prof. Dr. Ir. B. G. De Geest

June/August 2016: research visit at Utrecht University

Department of Pharmaceutics (Utrecht Institute for Pharmaceutical
Sciences), The Netherlands

Research collaborators: Prof. Dr. W. E. (Wim) Hennink, M. J. (Mies) van
Steenbergen

May 2016: research visit at University of Oslo

Department of Radiation Biology (Institute for Cancer Research),
Norway

Research collaborators: Prof. Dr. Kristian Berg,
Dr. Theodossis A. Theodossiou

July 2015: research visit at Eindhoven University of Technology

Department of Chemical Engineering and Chemistry (Physical
Chemistry), The Netherlands

Research collaborator: Prof. Dr. I.K. (Ilja) Voets

Teaching practical courses pharmaceutical preparations (3rd bachelor and 2nd
master students)

Thesis supervising (1st master students)

honors and awards

Agency for Innovation by Science and Technology (IWT) grant for Strategic Basic Research

specialist courses

Training: BD ACCURI™ C6 operator course, BD Biosciences European training and education center, Erembodegem (Belgium), October 16-18, 2012

language skills

Dutch: native language

English: excellent

French: good

Italian: level 2

publications in peer reviewed journals

Louage, B.; De Wever, O.; Hennink, W. E.; De Geest, B. G.

Developments and future clinical outlook of taxane nanomedicines

Journal of Controlled Release **2017**

IF 2016: 7.441

Louage, B.; van Steenberghe, M. J.; Nuhn, L.; Risseeuw, M. D. P.; Karalic, I.; Winne, J.; Van Calenbergh, S.; Hennink, W. E.; De Geest, B. G.

Micellar paclitaxel-initiated RAFT polymer conjugates with acid-sensitive behavior

ACS Macro Letters **2017**, DOI: 10.1021/acsmacrolett.6b00977

IF 2016: 5.766

Louage, B.; Tack, L.; Wang, Y.; De Geest, B. G.

Poly(glycerol sebacate) nanoparticles for encapsulation of hydrophobic anti-cancer drugs

Polymer Chemistry **2017**, DOI: 10.1039/C6PY02192A

IF 2016: 5.687

Alkan, A.; Wald, S.; Louage, B.; De Geest, B. G.; Landfester, K.; Wurm, F. R.

Amphiphilic ferrocene-containing PEG block copolymers as micellar nanocarriers and smart surfactants

Langmuir : the ACS journal of surfaces and colloids **2016**, DOI: 10.1021/acs.langmuir.6b03917

IF 2016: 3.993

Louage, B.; Nuhn, L.; Risseeuw, M. D.; Vanparijs, N.; De Coen, R.; Karalic, I.; Van Calenbergh, S.; De Geest, B. G.

Well-Defined Polymer-Paclitaxel Prodrugs by a Grafting-from-Drug Approach

Angewandte Chemie International Edition **2016**, *55* (39), 11791-6

IF 2016: 11.709

De Coen, R.; Vanparijs, N.; Risseeuw, M. D.; Lybaert, L.; Louage, B.; De Koker, S.; Kumar, V.; Grooten, J.; Taylor, L.; Ayres, N.; Van Calenbergh, S.; Nuhn, L.; De Geest, B. G.

pH-Degradable Mannosylated Nanogels for Dendritic Cell Targeting

Biomacromolecules **2016**, *17*(7), 2479-88

IF 2016: 5.583

Kasmi, S.; Louage, B.; Nuhn, L.; Van Driessche, A.; Van Deun, J.; Karalic, I.; Risseeuw, M.; Van Calenbergh, S.; Hoogenboom, R.; De Rycke, R.; De Wever, O.; Hennink, W. E.; De Geest, B. G.

Transiently Responsive Block Copolymer Micelles Based on N-(2-Hydroxypropyl)methacrylamide Engineered with Hydrolyzable Ethylcarbonate Side Chains

Biomacromolecules **2016**, *17*(1), 119-27

IF 2016: 5.583

Louage, B.; Zhang, Q.; Vanparijs, N.; Voorhaar, L.; Vande Castelee, S.; Shi, Y.; Hennink, W. E.; Van Bocxlaer, J.; Hoogenboom, R.; De Geest, B. G.

Degradable ketal-based block copolymer nanoparticles for anticancer drug delivery: a systematic evaluation

Biomacromolecules **2015**, *16*(1), 336-50

IF 2015: 5.583

Zhang, Q.; Hou, Z.; Louage, B.; Zhou, D.; Vanparijs, N.; De Geest, B. G.; Hoogenboom, R.

Acid-Labile Thermo-responsive Copolymers That Combine Fast pH-Triggered Hydrolysis and High Stability under Neutral Conditions

Angewandte Chemie International Edition **2015**, *54*(37), 10879-83

IF 2015: 11.709

Ruiz Garcia, Y.; Iyer, A.; Van Lysebetten, D.; Pabon, Y. V.; Louage, B.; Honcharenko, M.; De Geest, B. G.; Smith, C. I.; Stromberg, R.; Madder, A.

Sequence-selective DNA recognition and enhanced cellular up-take by peptide-steroid conjugates

Chemical Communications **2015**, *51*(99), 17552-5

IF 2015: 6.567

Vanparijs, N.; De Coen, R.; Laplace, D.; [Louage, B.](#); Maji, S.; Lybaert, L.; Hoogenboom, R.; De Geest, B. G.

Transiently responsive protein-polymer conjugates via a 'grafting-from' RAFT approach for intracellular co-delivery of proteins and immune-modulators

Chemical Communications **2015**, *51*(73), 13972-5

IF 2015: 6.567

Vanparijs, N.; Maji, S.; [Louage, B.](#); Voorhaar, L.; Laplace, D.; Zhang, Q.; Shi, Y.; Hennink, W.E.; Hoogenboom, R.; De Geest, B.G.

Polymer-protein conjugation via a 'grafting to' approach - a comparative study of the performance of protein-reactive RAFT chain transfer agents

Polymer Chemistry **2015**, *6*(31), 5602-14

IF 2015: 5.687

Iyer, A.; Van Lysebetten, D.; Ruiz Garcia, Y.; [Louage, B.](#); De Geest, B. G.; Madder, A.

Stapling monomeric GCN4 peptides allows for DNA binding and enhanced cellular uptake

Organic & biomolecular chemistry **2015**, *13*(13), 3856-62

IF 2015: 3.559

Fernandes Stefanello, T.; Szarpak-Jankowska, A.; Appaix, F.; [Louage, B.](#); Hamard, L.; De Geest, B. G.; van der Sanden, B.; Nakamura, C. V.; Auzely-Velty, R.

Thermoresponsive hyaluronic acid nanogels as hydrophobic drug carrier to macrophages

Acta biomaterialia **2014**, *10*(11), 4750-8

IF 2014: 6.025

Zhang, Q.; Vanparijs, N.; [Louage, B.](#); De Geest, B.G.; Hoogenboom, R.

Dual pH- and temperature-responsive RAFT-based block co-polymer micelles and polymer-protein conjugates with transient solubility

Polymer Chemistry **2014**, *5*(4), 1140-4

IF 2014: 5.520

Pavlov, A. M.; De Geest, B. G.; Louage, B.; Lybaert, L.; De Koker, S.; Koudelka, Z.; Sapelkin, A.; Sukhorukov, G. B.

Magnetically engineered microcapsules as intracellular anchors for remote control over cellular mobility

Advanced Materials **2013**, *25*(48), 6945-50

IF 2013: 15.409

attended conferences

Well-Defined Polymer–Paclitaxel Prodrugs by a Grafting-from-Drug Approach

B. Louage, B. G. De Geest

253rd American Chemical Society (ACS) National Meeting – San Francisco, California – April 2-6, 2017 - oral presentation

11th International Symposium on Polymers Therapeutics From Laboratory to Clinical Practice – Valencia, Spain – Centro de Investigación Príncipe Felipe - May 23–25, 2016

Acid-cleavable acetal-linked paclitaxel-polymer conjugates via a drug-functionalized RAFT CTA approach

B. Louage, B. G. De Geest

251st American Chemical Society (ACS) National Meeting – San Diego, California – March 13-17, 2016 - oral presentation

Ketal-containing polyacrylates and polyacrylamides as building blocks for multi-responsive nanomedicines

B. Louage, B. G. De Geest

249th American Chemical Society (ACS) National Meeting – Denver, Colorado – March 22-26, 2015 - poster presentation

Degradable ketal-based block copolymer nanoparticles for anti-cancer drug delivery: a systematic evaluation

B. Louage, B. G. De Geest

Meeting of the Belgian-Dutch Biopharmaceutical Society – Vlaardingen, The Netherlands – December 12th, 2014 - poster presentation

Stimuli-responsive block copolymers aiming for micellar anti-cancer drug formulations

B. Louage, B. G. De Geest

248th American Chemical Society (ACS) National Meeting – San Francisco, California – August 10-14, 2014 - poster presentation

13th European Symposium on Controlled Drug Delivery (ESCDD) – Egmond aan Zee, The Netherlands – April 16-18, 2014

Meeting of the Belgian-Dutch Biopharmaceutical Society – Ghent, Belgium – December 18th, 2013

pH degradable thermoresponsive polymers

Q. Zhang, N. Vanparijs, B. Louage, B. G. De Geest, R. Hoogenboom

European Science Foundation (ESF) Research Networking Programme, 2nd Precision Polymer Materials (P2M) Conference – Ghent, Belgium – August 25-28, 2013 – poster presentation

Meeting of the Belgian-Dutch Biopharmaceutical Society – Utrecht, The Netherlands – November 9th, 2012

